

Bio-inspired Transformations for Late Stage Molecular Diversification

William Givan Shuler  
Columbia, South Carolina

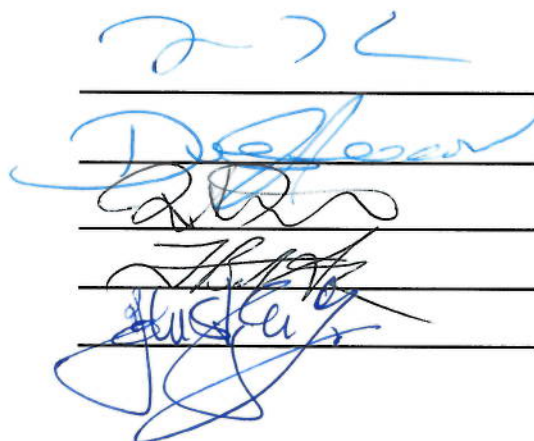
B.S., Chemistry and Biochemistry, College of Charleston, 2013

A Dissertation presented to the Graduate Faculty of the University of Virginia in  
Candidacy for the Degree of Doctor of Philosophy

Department of Chemistry

University of Virginia

July 2018



Four handwritten signatures in blue ink are written over four horizontal lines. The signatures are stylized and appear to be in blue ink.

## Copyright Information

Chapters 2, 3, and 4 contain data from previously published works.

Chapter 2: Shuler, W. G.; Combee, L. A.; Falk, I. D.; Hilinski, M. K.; *Eur. J. Org. Chem.* **2016**, 3335–3338.

Chapter 3: Shuler, W. G.; Johnson, S. L.; Hilinski, M. K.; *Org. Lett.*, **2017**, 19, 4790-4793.

Chapter 4: Wang, D.; Shuler, W. G.; Pierce, C. J.; Hilinski, M. K.; *Org Lett.*, **2016**, 18, 3825-3829.

## Abstract

Billions of years of evolutionary pressure have fueled the development of highly selective enzyme-catalyzed reactions that deliver densely functionalized bioactive compounds through step economical and high yielding processes. One such highly efficient pathway commonly used in the biosynthesis of natural products involves a two-phase process. In the first phase, simple precursors are combined to form the core structure of the molecule. In the second phase, selective modifications of this core scaffold produce the natural product.<sup>1</sup>

This approach to natural product synthesis has been difficult to translate into a laboratory setting due to a lack of synthetic techniques that mimic enzymatic selectivity.<sup>2</sup> To address this deficiency, we have pursued bio-inspired transformations that capture enzymatic reactions.

We have introduced a Lewis acid catalyzed (3+2) cyclization of epoxides and alkenes. The reaction conditions employed allow modestly diastereoselective cyclizations of aryl epoxides with styrenes, dienes, and alkynes in modest to good yields using low catalyst loading of metal triflate salts. This methodology generates stereodefined natural product cores from petrochemical feedstock on decagram scale in under 10 minutes.

We have developed new organocatalytic strategies for the hydroxylation of aliphatic C–H bonds. Reactive substrates using this methodology include C–H bonds present in naturally occurring motifs that are commonly oxidized *in vivo* with enzymatic catalysis. Initial exploration of organocatalysts derived from natural

products has been conducted, in search of catalysts that capture the catalyst-controlled site- and stereo-selectivity observed in enzymatic systems.

1. Chen, K.; Baran, P. S.; *Nature*, **2009**, 459, 824–828.

2. Kamil Godula, D. S; *Science*, **2006**, 312, 67–73.



## Acknowledgements

**Chapter 2** contains contributions made by Logan A. Combee. Much of the reaction optimization and exploration experiments reported in this dissertation were conducted by him. I'm glad we stuck it out together, even when we faced 15% yields for an entire summer.

**Chapter 3** contains contributions made by Shea "Freddie" L. Johnson. For every substrate we hydroxylated, you tried five that didn't end up working (though did you try gibberellic acid?). Your enthusiasm for the project made it all so much more enjoyable.

**Chapter 4** contains contributions from Daoyong Wang and Conor Pierce. Daoyong and Conor performed all the optimization experiments- I was very fortunate to come on board when I did. Thank you both for teaching me first-hand how to be a chemist.

All of this would not have been possible without the leadership and guidance of Michael Hilinski. You have pushed me to be the best I can be and have set me on a great track for success. I've been fortunate to work on your projects, and I'm excited to see where your ideas lead.

To my committee members, Professors W. Dean Harman, Timothy Macdonald, Glenn McGarvey, Lin Pu, T. Brent Gunnoe, and John Lazo: thank you for the courses you have taught, the conversations we have had, and all the help you have given me over the years.

To all my friends I've made along the way-thank you all for your incredible support. Through all the ups and downs, you have been there every step of the way.

To Joseph, Matthew, Mom, grandparents, and the family- your unwavering love and encouragement is the only reason I'm writing this. Who woulda thought the basement lab would lead here?

To Bobby and Al- I would've had a nervous breakdown without you. Y'all mean the world to me.

### List of Abbreviations

BAr <sup>F</sup> <sub>4</sub>	Tetrakis[3,5-bis(trifluoromethyl)phenyl]borate
BINAP	2,2'-Bis(diphenylphosphino)-1,1'-binaphthyl
BINOL	1,1'-Bi-2-naphthol
BOX	Methylenebis(oxazoline)
br	Broad
Cp	Cyclopentadienyl
CSA	Camphorsulfonic acid
d	doublet
DBU	1,8-Diazabicyclo[5.4.0]undec-7-ene
DCE	Dichloroethane
DCM	Dichloromethane
DFT	Density functional theory
DIBAL	Diisobutylaluminum hydride
DMDO	Dimethyldioxirane
DMF	N,N-Dimethylformamide
DMP	Dimethylphosphonyl
Dtbp <sub>y</sub>	4,4'-Di-tert-butyl-2,2'-dipyridyl
EDTA	Ethylenediaminetetraacetic acid
EtOAc	Ethyl acetate
HFIP	1,1,1,3,3,3-hexafluoroisopropan-2-ol
<i>i</i> Pr	Isopropyl
LAH	Lithium aluminum hydride
LDA	Lithium diisopropylamide
LUMO	Lowest unoccupied molecular orbital
m	Multiplet
<i>m</i> -CPBA	<i>meta</i> -Chloroperbenzoic acid

Me	Methyl
Me <sub>ax</sub>	Axial methyl group
MsCl	Mesityl chloride
<i>n</i> Bu	<i>n</i> -Butyl
NPhth:	Phthalimide
<i>n</i> Pr	<i>n</i> -Propyl
[O]	Oxidant
O. A.	Oxidative addition
OAc	Acetate
OBz	Benzoate
OTf	Trifluoromethylsulfonate
OTFA	Trifluoroacetate
OTs	Tosylate
PDP	1,1'-Bis(2-pyridinylmethyl)-2,2'-bipyrrolidine
Ph	Phenyl
Pyr	Pyridine
q	Quartet
R. E.	Reductive elimination
s	Singlet
SDS	Sodium dodecylsulfate
t	Triplet
<i>t</i> Bu	<i>tert</i> -Butyl
TBS	<i>tert</i> -Butyldimethylsilyl
TFAA	Trifluoroacetic anhydride
TFDO	Methyl(trifluoromethyl)dioxirane
TFE	2,2,2-Trifluoroethanol
TfOH	Trifluoromethanesulfonic acid
THF	Tetrahydrofuran

TIPS	Triisopropylsilyl
TMS	Trimethylsilyl
TPPP	Tetraphenylphosphonium persulfate
Ts	Tosyl

## Table of Contents

<b>Copyright Information</b>	<b>I</b>
<b>Abstract</b>	<b>II</b>
<b>Acknowledgements</b>	<b>IV</b>
<b>List of Abbreviations</b>	<b>V</b>
<b>Table of Contents</b>	<b>VII</b>
<b>List of Figures</b>	<b>XIII</b>
<b>List of Schemes</b>	<b>XIV</b>
<b>List of Tables</b>	<b>XVII</b>
<b>1: Catalytic C–H Bond Hydroxylation Methods for Use in Synthesis</b>	<b>1</b>
1.1 Utility of Aliphatic C–H Bond Hydroxylation	1
1.1.1 Introduction	1
1.1.2 Pursuit of the ideal synthesis	2
1.1.3 Late stage functionalization	3
1.2 C–H Bond Activation Systems for Hydroxylation	6
1.2.1 Overview	6
1.2.2 Platinum based systems	7
1.2.3 Palladium based systems	9
1.3 Concerted Metal-based Hydroxylation	14
1.3.1 Ruthenium based systems	14
1.4 Radical Rebound Hydroxylation	16
1.4.1 Iron catalysts	16
1.4.2 Manganese catalysts	19
1.5 Organocatalytic Approaches to Hydroxylation	21
1.5.1 Oxaziridine mediated catalysis	22
1.6 Conclusions	24
1.7 References	25

<b>2: Reactivity of C–O Cleaved Epoxide Zwitterions</b>	<b>30</b>
2.1 Introduction	30
2.1.1 C–C bond formation using C–O cleaved epoxide zwitterions	30
2.1.2 Ring opened epoxides as dipolar intermediates	33
2.1.3 Epoxide (3+2) cyclizations as a retrosynthetic disconnection	35
2.1.4 Product distribution of epoxide zwitterions reacting with alkenes	37
2.1.5 Circumvention of instability via homolytic C–O bond cleavage	39
2.2 Styrene and Styrene Oxide (3+2) Cyclizations	42
2.2.1 Initial reaction conditions	42
2.2.2 Lewis acid screening	44
2.2.3 Increasing the stability of the dipolar intermediate	45
2.2.4 Suppression of epoxide oligomerization through addition rate	47
2.3 $\alpha$ -Methylstyrene and Styrene Oxide (3+2) Cyclizations	48
2.3.1 Selection of optimal C–C $\pi$ reaction partners	48
2.3.2 Lewis acid screening for $\alpha$ -methylstyrene cyclizations	49
2.3.3 Additional optimization of conditions	51
2.4 Scope of Reaction Partners	53
2.4.1 Alkene reactivity	53
2.4.2 Alkene substitution impact on diastereoselectivity	55
2.4.3 Scope of epoxide cyclization partners	57
2.5 Exploration of Chiral Catalysts	58
2.6 Conclusions	59
2.7 Experimental Details	60

2.7.1 General methods	60
2.7.2 General procedure for Lewis acid catalyzed [3+2] cyclizations	60
2.7.3 Characterization of reaction products	61
2.7.4 HPLC chromatograms	100
2.8 References	103
<b>3: Catalytic Dioxirane-Mediated Aliphatic C–H Bond Hydroxylation</b>	<b>105</b>
3.1 Introduction	105
3.1.1 Discovery of dioxiranes	105
3.1.2 Use of dioxirane oxidations in total synthesis	108
3.1.3 Use of dioxirane oxidations in natural product diversification	108
3.1.4 Development of in situ protocols for dioxirane oxidations	109
3.1.5 Catalytic dioxirane epoxidation	110
3.1.6 Catalytic dioxirane C–H hydroxylation	111
3.2 Reaction Optimization	112
3.2.1 Selection of initial reaction conditions	112
3.2.2 Further development of reaction parameters	114
3.2.3 Recovery experiments	117
3.2.4 Steady state approximation	121
3.3 Scope of Reaction Partners	124
3.3.1 Cyclic substrates	124
3.3.2 Acyclic substrates	127
3.3.3 Complimentary selectivity between dioxirane catalysts	129
3.3.4 Comparison of methods	130
3.3.5 Incompatible substrates	132
3.4 Exploration of Chiral Catalysts	134

3.5 Conclusions	135
3.6 Experimental Details	136
3.6.1 General methods	136
3.6.2 General procedure for hydroxylation	136
3.6.3 Characterization of reaction products	137
3.7 References	166
<b>4: Iminium Salt Catalyzed C–H Functionalization</b>	<b>169</b>
4.1 Introduction	169
4.2 Reaction Discovery and Optimization	171
4.2.1 Selection of reaction conditions	171
4.2.2 Exploration of electronic effects on catalyst activity	174
4.3 Catalytic C–H Bond Hydroxylation	178
4.3.1 Hydroxylation of tertiary C–H bonds	178
4.3.2 Chemoselective aliphatic C–H hydroxylation	181
4.4 Investigation of Chemoselectivity in C–H Bond Hydroxylations	183
4.4.1 Hydrophobic rate enhancement	183
4.4.2 Solvent effects	187
4.5 In situ Formation of Iminiums	190
4.5.1 General approach and methods	190
4.5.2 Identification of suitable carbonyl components	194
4.5.3 Identification of suitable amine catalysts	195
4.5.4 Future directions for development of a C–H bond hydroxylation reaction	196
4.6 Chiral Iminium Salt Catalysts	198
4.6.1 Introduction to asymmetric iminium salt atom transfer catalysis	198
4.6.2 Norepinephrine derived iminium catalysts	199
4.6.3 Iminium salts from chiral amines	201



4.6.4 Acetonide substituted dihydroisoquinoliniums	203
4.6.5 Binaphthyl or biphenyl azepinium catalysts: structure and reactivity	205
4.6.6 Impact of oxidant on enantioselectivity	208
4.6.7 Design of a chiral atom transfer catalyst	208
4.6.8 Transition states and mechanistic concerns	210
4.6.9 Synthetic route to catalysts	213
4.6.10 NMR experiments to probe diastereoselective diaziridinium formation	214
4.6.11 Initial reactivity in C–H functionalization	216
4.6.12 Low temperature aziridinations	218
4.7 Conclusions	220
4.8 Experimental Details	220
4.8.1 General methods	220
4.8.2 General procedure for iminium catalyzed hydroxylations	221
4.8.3 General procedure for iminium catalyzed aminations	221
4.8.4 General procedure for iminium catalyzed aziridinations	222
4.8.5 Characterization of reaction products	222
4.9 References	278

## List of Figures

<b>Figure 1.1:</b> Natural product analogs generated through C–H hydroxylation	5
<b>Figure 3.1:</b> Reactivity of dimethyldioxirane and trifluoromethyl(methyl)dioxirane	106
<b>Figure 3.2:</b> Dioxirane oxidations of natural products	107
<b>Figure 3.3:</b> Recovery experiments; <i>cis</i> -decalin hydroxylation	119
<b>Figure 3.4:</b> Comparison of efficiency of oxidant consumption	123
<b>Figure 3.5:</b> Chiral catalysts that fail to promote hydroxylation	134
<b>Figure 3.6:</b> Miller type epoxidation catalysts	135
<b>Figure 4.1:</b> Stoichiometric organic reagents for C–H bond hydroxylation	169
<b>Figure 4.2:</b> Hypothesis for catalyst design	171
<b>Figure 4.3:</b> NMR monitoring of oxaziridinium degradation	177
<b>Figure 4.4:</b> Modulation of bond strength through hydrogen bonding	188
<b>Figure 4.5:</b> Impact of HFIP on $^1\text{H}$ chemical shift in $\text{CDCl}_3$	188
<b>Figure 4.6:</b> Impact of HFIP on $^1\text{H}$ chemical shift in $\text{C}_6\text{D}_6$	189
<b>Figure 4.7:</b> Calculated LUMO energies of various oxaziridiniums	197
<b>Figure 4.8:</b> Library synthesis of chiral iminium salts	202
<b>Figure 4.9:</b> Impact of ion coordination and solvent on enantioselectivity	203
<b>Figure 4.10:</b> High enantioselectivity in dihydroisoquinolinium catalyzed epoxidation	204
<b>Figure 4.11:</b> General trend for dihedral angle impact on enantioselectivity	207
<b>Figure 4.12:</b> Effect of dihedral angle on blocking ability	210
<b>Figure 4.13:</b> Transition states for asymmetric aziridination	211
<b>Figure 4.14:</b> Reaction of iminium salts and PhINTs	215
<b>Figure 4.15:</b> PhINTs incorporation in <b>4.17</b> and <b>4.130</b>	216
<b>Figure 4.16:</b> Steric interactions of facially blocked diaziridiniums	218

## List of Schemes

<b>Scheme 1.1:</b> Biosynthesis of paclitaxel	1
<b>Scheme 1.2:</b> Subsection of Heathcock's dihydro-protodaphniphylline synthesis	2
<b>Scheme 1.3:</b> An idealized synthesis	3
<b>Scheme 1.4:</b> C–H bond activation for catalytic hydroxylation	7
<b>Scheme 1.5:</b> Sen platinum catalyzed hydroxylation	7
<b>Scheme 1.6:</b> Sames platinum catalyzed hydroxylation	8
<b>Scheme 1.7:</b> Sanford platinum catalyzed hydroxylation	9
<b>Scheme 1.8:</b> Baldwin cyclopalladation-hydroxylation	10
<b>Scheme 1.9:</b> Sanford palladium catalyzed acetoxylation	11
<b>Scheme 1.10:</b> Palladium catalyzed acetoxylation in total synthesis	12
<b>Scheme 1.11:</b> Nonideality of palladium catalyzed acetoxylation	13
<b>Scheme 1.12:</b> Ruthenium tetroxide catalyzed hydroxylation	14
<b>Scheme 1.13:</b> Du Bois ruthenium catalyzed hydroxylation	15
<b>Scheme 1.14:</b> Radical rebound hydroxylation	16
<b>Scheme 1.15:</b> Early examples of iron catalyzed hydroxylation	17
<b>Scheme 1.16:</b> White iron catalyzed hydroxylation	17
<b>Scheme 1.17:</b> Directed iron catalyzed hydroxylation	18
<b>Scheme 1.18:</b> Catalyst controlled site selectivity in hydroxylation	19
<b>Scheme 1.19:</b> Asymmetric manganese catalyzed hydroxylation	20
<b>Scheme 1.20:</b> Asymmetric hydroxylation of linear alkanes	21
<b>Scheme 1.21:</b> Organic oxidants for hydroxylation	21
<b>Scheme 1.22:</b> Organocatalytic hydroxylation	22

<b>Scheme 1.23:</b> Third generation organocatalytic hydroxylation of natural products	24
<b>Scheme 2.1:</b> Reactions of activated epoxides with alkenes	30
<b>Scheme 2.2:</b> Reactions of activated epoxides with polyenes	32
<b>Scheme 2.3:</b> Activated epoxides as dipolar intermediates	34
<b>Scheme 2.4A:</b> Linear synthesis of tetrahydrofurans	36
<b>Scheme 2.4B:</b> Convergent synthesis of tetrahydrofurans from aldehydes	36
<b>Scheme 2.4C:</b> Convergent synthesis of tetrahydrofurans from cyclization	36
<b>Scheme 2.5A:</b> Titanium catalyzed epoxide (3+2) cyclization	40
<b>Scheme 2.5B:</b> Iron catalyzed epoxide (3+2) cyclization	40
<b>Scheme 2.6:</b> Epoxy-alkene (3+2) cyclizations in synthesis	41
<b>Scheme 2.7A:</b> Product distribution of intermolecular (3+2) cyclization	43
<b>Scheme 2.7B:</b> Requirements for carbocation stability	43
<b>Scheme 3.1:</b> (+)-Zerumin B end game	108
<b>Scheme 3.2:</b> Protecting group free Bryostatin diversification	109
<b>Scheme 3.3:</b> <i>In situ</i> dioxirane formation	110
<b>Scheme 3.4:</b> Structure-dependent selectivity	111
<b>Scheme 3.5:</b> Catalytic C-H hydroxylation under unoptimized conditions	113
<b>Scheme 3.6:</b> Routes of potassium persulfate consumption	121
<b>Scheme 3.7:</b> Catalyst controlled selectivity	130
<b>Scheme 4.1:</b> Oxaziridine mediated hydroxylation of complex molecules	170
<b>Scheme 4.2:</b> Organocatalytic oxaziridine mediated hydroxylation of C–H bonds	170
<b>Scheme 4.3:</b> Oxaziridinium degradation	176
<b>Scheme 4.4:</b> Hydrophobic interactions driving oxidative selectivity	184
<b>Scheme 4.5:</b> Proposed catalytic cycle for intramolecular hydroxylation	191
<b>Scheme 4.6:</b> Yang <i>in situ</i> oxaziridinium formation	192

<b>Scheme 4.7:</b> Attempted intramolecular C–H bond hydroxylation	193
<b>Scheme 4.8:</b> Iminium salt catalyzed functionalization of prochiral substrates	198
<b>Scheme 4.9:</b> The first chiral epoxidation organocatalyst	200
<b>Scheme 4.10:</b> Routes for catalyst degradation	201
<b>Scheme 4.11:</b> Dihydroisoquinolinium catalysis in total synthesis	205
<b>Scheme 4.12:</b> Binaphthalene azepinium catalyst	206
<b>Scheme 4.13:</b> Proposed catalyst structures for asymmetric transformations	209
<b>Scheme 4.14:</b> Carbocation rearrangement products from aziridinations	212
<b>Scheme 4.15:</b> Testing for racemization under reaction conditions	213
<b>Scheme 4.16:</b> Synthesis of chiral catalysts	214
<b>Scheme 4.17:</b> Partially optimized low temperature aziridination	220

### List of Tables

<b>Table 1.1:</b> Second generation organocatalytic hydroxylation	23
<b>Table 2.1:</b> Impact of conditions on product distribution	38
<b>Table 2.2:</b> Lewis acid screening	45
<b>Table 2.3:</b> Solvent screening	46
<b>Table 2.4:</b> Lewis acid screening	49
<b>Table 2.5:</b> Screening of triflic acid loading	51
<b>Table 2.6:</b> Screening of solvents	52
<b>Table 2.7:</b> Scope of alkene reaction partners	54
<b>Table 2.8:</b> Impact of alkene substitution on diastereoselectivity	56
<b>Table 2.9:</b> Scope of epoxide reaction partners	57
<b>Table 3.1:</b> First reported catalytic dioxirane mediated C–H hydroxylation reaction	112
<b>Table 3.2:</b> Investigation of phase transfer catalysts	115
<b>Table 3.3:</b> Investigation of catalysts	116
<b>Table 3.4:</b> Investigation of solvents	117
<b>Table 3.5:</b> Optimized oxidant addition protocol	124
<b>Table 3.6:</b> Scope of cyclic hydroxylation substrates	126
<b>Table 3.7:</b> Scope of acyclic hydroxylation substrates	128
<b>Table 3.8:</b> Comparison of hydroxylation methods	131
<b>Table 3.9:</b> Unreactive substrates	133
<b>Table 4.1:</b> Impact of catalyst structure on reactivity	172
<b>Table 4.2:</b> Impact of reaction conditions on conversion and yield	174
<b>Table 4.3:</b> Electronic effects on catalyst activity	175
<b>Table 4.4:</b> Activity comparison of catalyst and degraded catalyst	176
<b>Table 4.5:</b> Half-life of substituted oxaziridiniums	178
<b>Table 4.6:</b> Hydroxylation of tertiary aliphatic C–H bonds	180
<b>Table 4.7:</b> Selective aliphatic C–H bond oxidation	182

<b>Table 4.8:</b> Salt effects on chemoselectivity	185
<b>Table 4.9:</b> Effect of dispersing agents on chemoselectivity	186
<b>Table 4.10:</b> Effect of cyclodextrins on chemoselectivity	187
<b>Table 4.11:</b> Impact of carbonyl component on oxaziridinium formation	194
<b>Table 4.12:</b> Impact of amine catalyst on oxaziridinium formation	196
<b>Table 4.13:</b> Impact of oxidant on enantioselectivity	208
<b>Table 4.14:</b> C–H bond amination	217
<b>Table 4.15:</b> Unsuccessful low temperature aziridinations	219

## Chapter One

### Catalytic C–H Bond Hydroxylation Methods for Use in Synthesis

#### 1.1 Utility of Aliphatic C–H Bond Hydroxylation

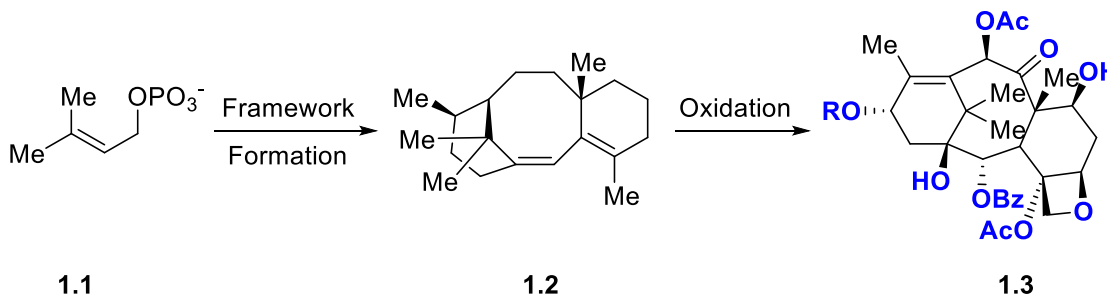
##### *1.1.1 Introduction*

In recent years, a number of methods have been introduced that can convert aliphatic alkanes into hydroxylated alkanes (vide infra). Spanning transition metal catalysts and stoichiometric organic reagents, these methods allow new retrosynthetic disconnections to be drawn in the planning of complex molecule total synthesis.

Use of these methods allows synthetic chemists to mimic a common synthetic strategy present in nature.<sup>1</sup> For example, in the biosynthesis of the paclitaxel— a top selling breast cancer therapeutic— enzymatic transformations first establish taxane core **1.2** of the molecule.<sup>2</sup> Selective oxidation transformations then elaborate this core, forming the anticancer natural product **1.3** (Scheme 1.1).



---

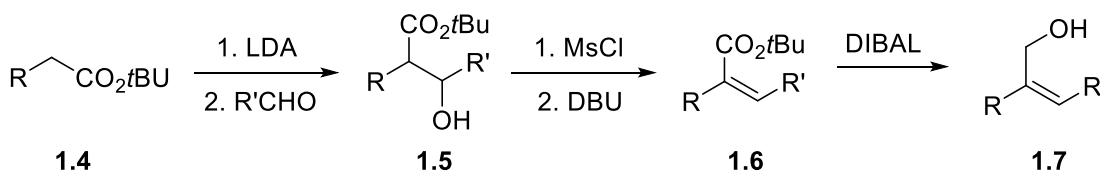
**Scheme 1.1: Biosynthesis of paclitaxel**


Mimicking this blueprint of framework establishment and selective oxidation by use of C–H bond hydroxylation reagents has allowed the total synthesis of several molecules to be reenvisioned, providing new, highly efficient routes for their syntheses.<sup>1,3</sup>

### 1.1.2 Pursuit of the ideal synthesis

In general, an ideal synthesis of a natural product compound would allow affordable access to large quantities of the synthetic material. For this strategy to be economically sound, syntheses would need to feature routes with low step count and low waste production.<sup>4</sup> Typically employed synthetic routes, though, often fall short of this target. A portion of Heathcock's bioinspired synthesis of dihydro-protodaphniphylline exemplifies these shortcomings (**Scheme 1.2**).<sup>5</sup>

---

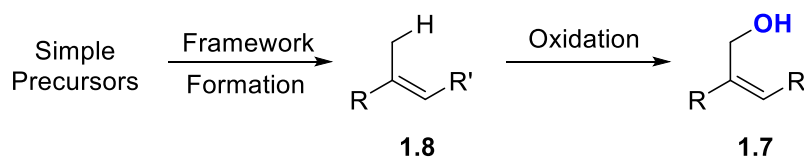
**Scheme 1.2: Subsection of Heathcock's dihydro-protodaphniphylline synthesis**


In this example, an initial aldol reaction requires stoichiometric lithiation of **1.4** for carbon-carbon bond formation followed by a subsequent two step reaction to give aldol condensation product **1.6**. Finally, stoichiometric reduction forms desired allylic alcohol **1.7**. Overall, most atoms used for the transformation do not appear in the final product and are instead converted into waste byproducts. The reliance on oxidation state interconversions, functional group interconversions, and protecting group interconversions highlight the current inefficiency of synthetic chemistry.

In an ideal synthesis, the carbon framework would be initially established followed by incorporation of oxygenation, eliminating unnecessary transformations (**Scheme 1.3**). Use of catalytic methods for these steps would eliminate stoichiometric waste.

---

**Scheme 1.3:** An idealized synthesis




---

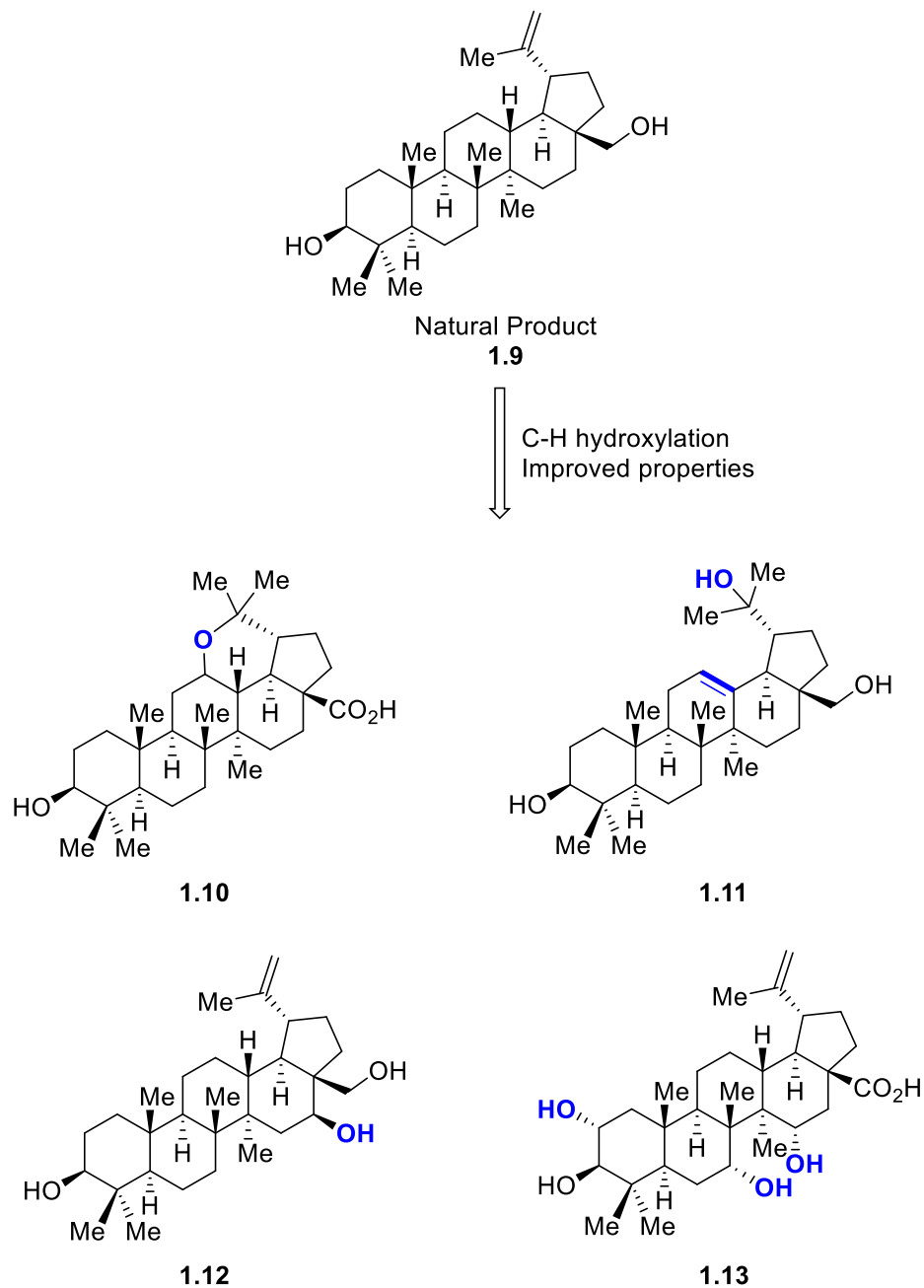
### 1.1.3 Late stage functionalization

The enormous cost of drug discovery is exacerbated by the number of drug candidates that fail due to poor efficacy, poor side effect profiles, and poor bioavailability.<sup>6</sup> Although synthetic small molecule drug candidates can be easily modulated to include molecular features to combat these issues, drugs derived

from complex natural products are less easily modified. As natural occurring compounds constitute or inspire upwards of 60% of FDA approved anticancer drugs and half of drugs in clinical trials,<sup>7</sup> the development of methods that can selectively functionalize natural products and address poor therapeutic properties is of utmost importance.

C–H bond hydroxylation reagents often proceed with a high degree of selectivity (*vide infra*) and operate on typically unreactive chemical space, making them ideal candidates for structural elaboration of natural products. The utility of these methods was exemplified by Baran and coworkers, who generated a series of analogs from an easily isolated natural product with potent *in vitro* activity but poor *in vivo* activity due to low bioavailability (**Figure 1.1**).<sup>8</sup> The variety of stoichiometric, catalytic, and enzymatic C–H bond hydroxylation methods available allowed the synthesis of diverse analogs with improved pharmacological properties.

**Figure 1.1:** Natural product analogs generated through C–H hydroxylation



Although able to generate diverse analogs directly from the natural product, many of these transformations required multistep synthetic sequences

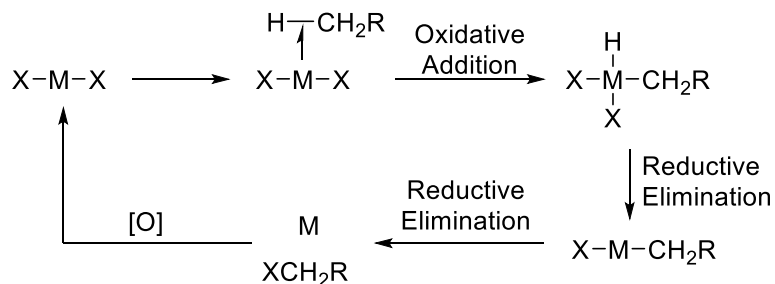
and provided products in low overall yield. Additionally, most of the C–H bonds present in the molecule cannot be targeted for hydroxylation using existing methods. There is a clear need for the development of new methodologies that unlock new modes of reactivity.

## 1.2 C–H Bond Activation Systems for Hydroxylation

### 1.2.1 Overview

Some of the earliest examples of aliphatic C–H bond activation for hydroxylation involve stoichiometric platinum reagents developed by Shilov.<sup>9</sup> Since these initial reports, this chemistry has received considerable attention for use in the functionalization of light alkanes with a focus on industrial processes. Additional investigation revealed new metal complexes and conditions that led to the development of catalytic oxygenation of light alkanes. In a typical reaction, an oxidative addition of the C–H bond by the metal center is followed by reductive eliminations of acid and the functionalized alkanes (**Scheme 1.4**)<sup>9</sup>. A stoichiometric oxidant completes the cycle through regeneration of the active metal catalyst. The exact nature of the intermediates and mechanism is dependent on the metal complex and conditions used (vide infra).

---

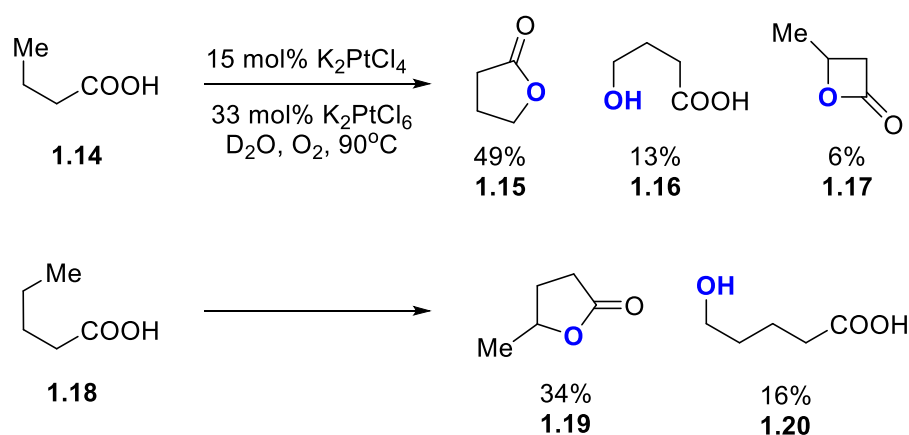
**Scheme 1.4:** C–H bond activation for catalytic hydroxylation



---

**1.2.2 Platinum based systems**

Sen introduced one of the first examples of a platinum catalyst that expands the scope of Shilov platinum chemistry from light alkane functionalization to organic synthesis (**Scheme 1.5**).<sup>10</sup> Lactonization of primary and secondary C–H bonds was accomplished using high (ca. 50 mol%) catalyst loading of mixed platinum salts using oxygen as the stoichiometric oxidant.

---

**Scheme 1.5:** Sen platinum catalyzed hydroxylation


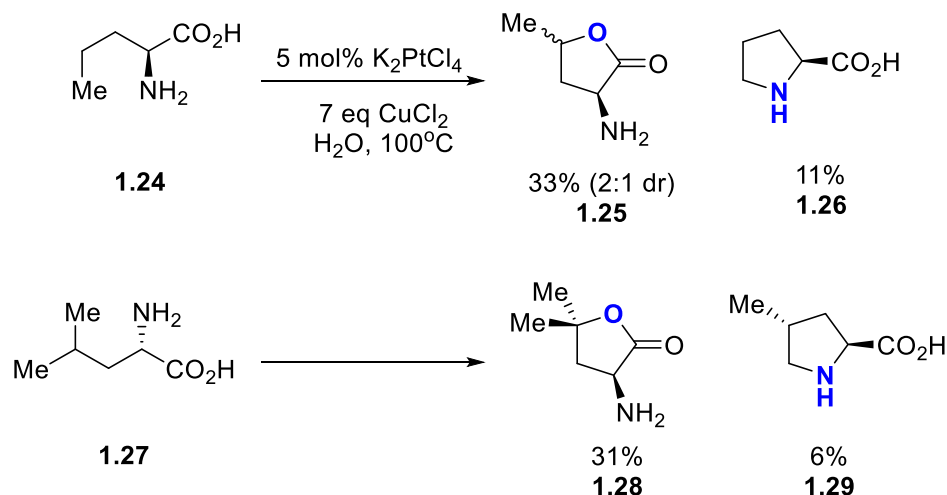

---

Lactonization selectivity was governed by the ability of substrate-coordinated platinum to insert into the C–H bond. In most cases, a mixture of

possible mono and di-oxygenation products was obtained. Reactivity was limited to water soluble substrates.

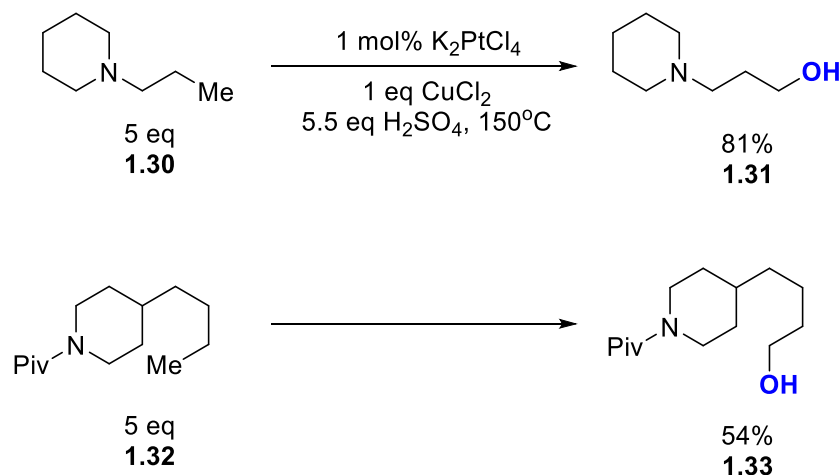
Sames et al. introduced a new platinum catalyst system that uses  $\text{CuCl}_2$  as the stoichiometric oxidant (**Scheme 1.6**).<sup>11</sup> Although selectivity for five membered ring formation was high, the reaction provided products in low yields as a mixture of lactone diastereomers. The formation of C–N bonds was an additional confounding factor. High product selectivity was obtained in only a limited set of substrates.

**Scheme 1.6:** Sames platinum catalyzed hydroxylation



In 2015, the Sanford group introduced a new strategy for improving the selectivity of Sames-type catalytic oxygenations in which amine protonation directs the C–H activation event to occur at the most remote C–H bond in the molecule (**Scheme 1.7**).<sup>12</sup> A significant decrease in selectivity occurs when multiple C–H bonds are present at sites remote from the protonated amine.

---

**Scheme 1.7:** Sanford platinum catalyzed hydroxylation

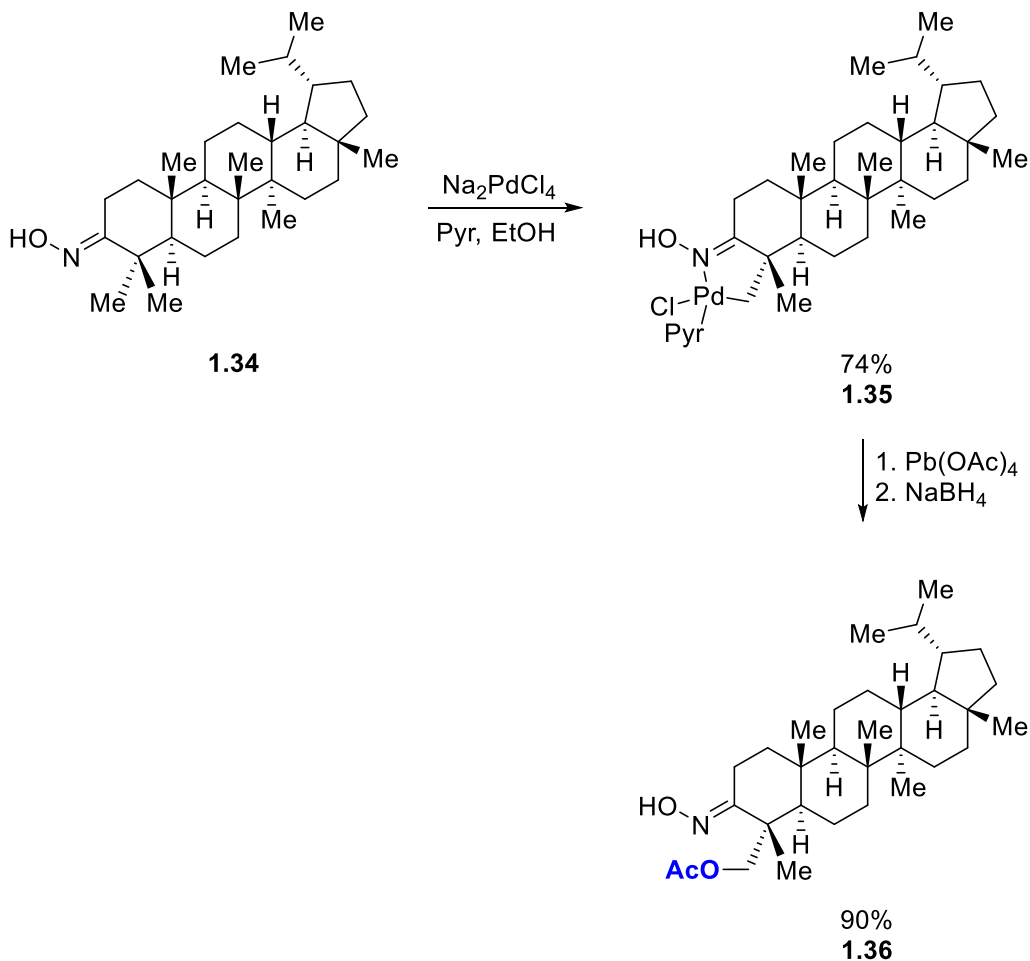
---

The harsh conditions employed and lower selectivity observed in large molecules limit the utility of this method in the functionalization of complex or acid sensitive molecules.

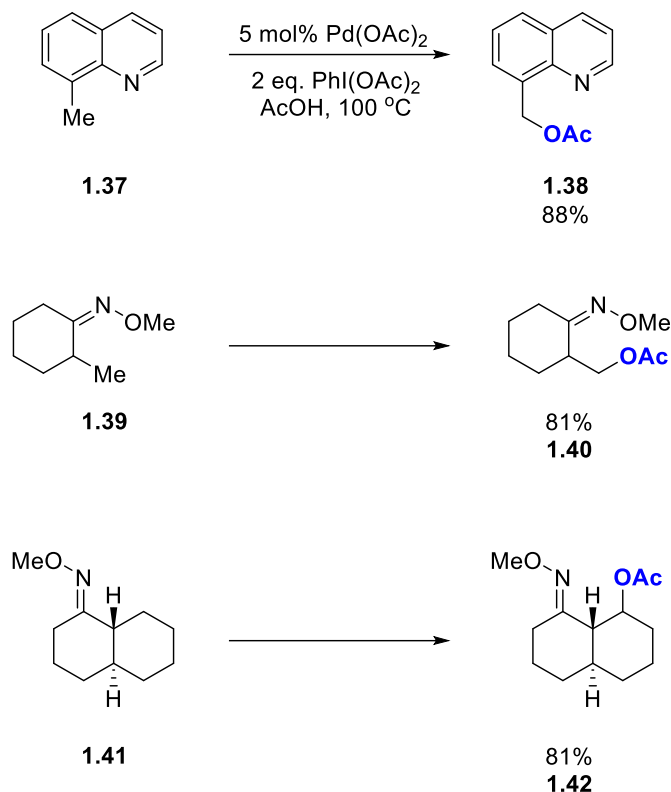
### 1.2.3 Palladium based systems

Related palladium catalyzed C–H activation strategies for hydroxylation have seen more substantial use in synthetic chemistry. Early use of this chemistry was reported by Baldwin using stoichiometric palladium for C–H activation (**Scheme 1.8**).<sup>13</sup> Treatment of  $\beta$ -methyloximes with  $Na_2PdCl_4$  afforded isolable palladacycles. These palladacycles can undergo functionalization reactions, including acetoxylation using lead tetraacetate and sodium borohydride. In the case of lupane, the oxidation is selective for the equatorial methyl group based on geometric constraints.

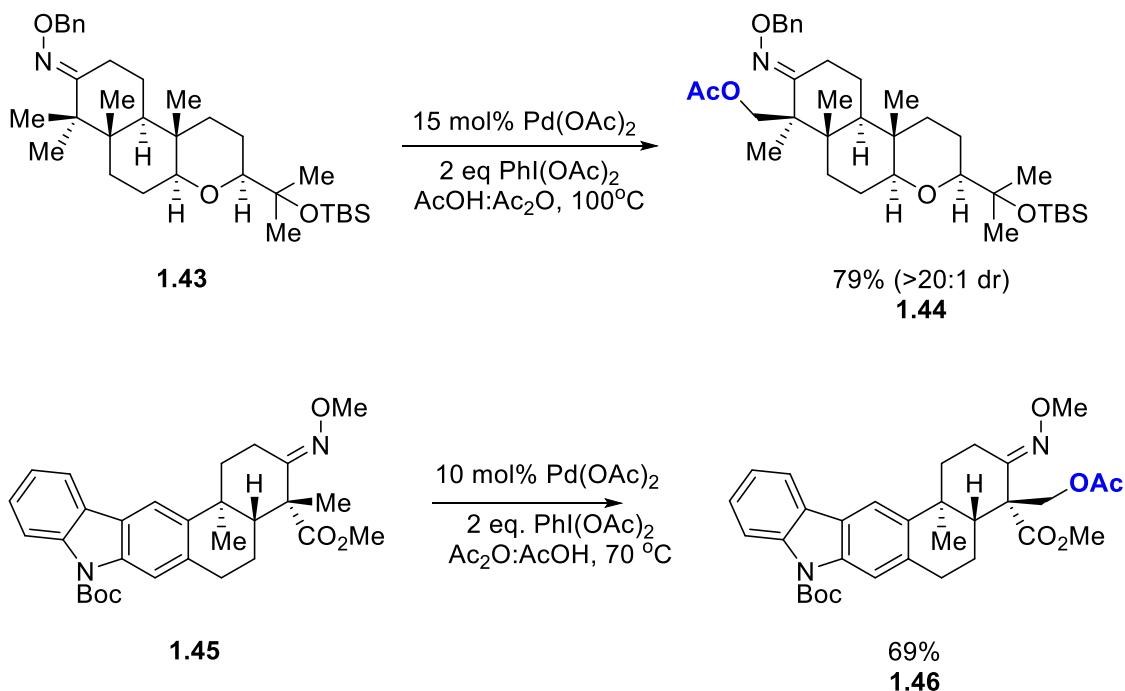


**Scheme 1.8:** Baldwin cyclopalladation-hydroxylation

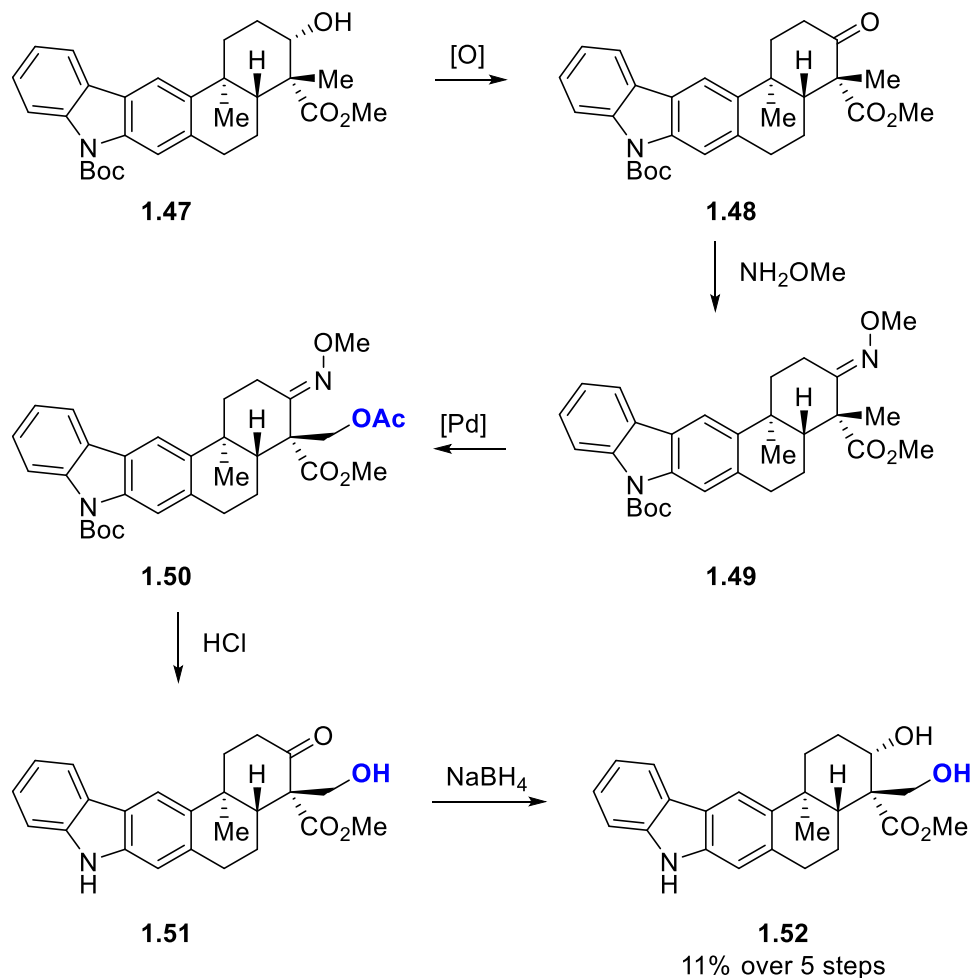
The high yields and selectivity observed in these oxidations spurred the development of catalytic methods by Sanford and coworkers (**Scheme 1.9**).<sup>14</sup> In a series of two papers, they demonstrated that substituted quinolines and *O*-methyloximes can be stereospecifically acetoxyated using  $\text{PhI}(\text{OAc})_2$  as the stoichiometric oxidant. Both primary and secondary C–H bonds can be converted to their acetoxyated derivatives in high yields.

**Scheme 1.9:** Sanford palladium catalyzed acetoxylation

Sanford's catalytic system has since been used in total synthesis efforts (**Scheme 1.10**). In Johnson's synthesis of Paspaline, O-Bn oxime **1.43** directs oxidation of the desired methyl group, affording the product as a single diastereomer in 79% yield.<sup>15</sup> In Trotta's synthesis of Oridamycin B, acid sensitive Boc-protected carbazole **1.45** was selectively acetoxyated in 79% yield.<sup>16</sup>

**Scheme 1.10: Palladium catalyzed acetoxylation in total synthesis**


Although capable of providing products in high yields, this strategy requires the installation of the directing groups which increase overall step count and lowers total yield of the final natural product. In the case of Ordamycin B, use of this strategy requires five total steps in 11% overall yield for the formation of a single C–O bond (**Scheme 1.11**).

**Scheme 1.11: Nonideality of palladium catalyzed acetoxylation**

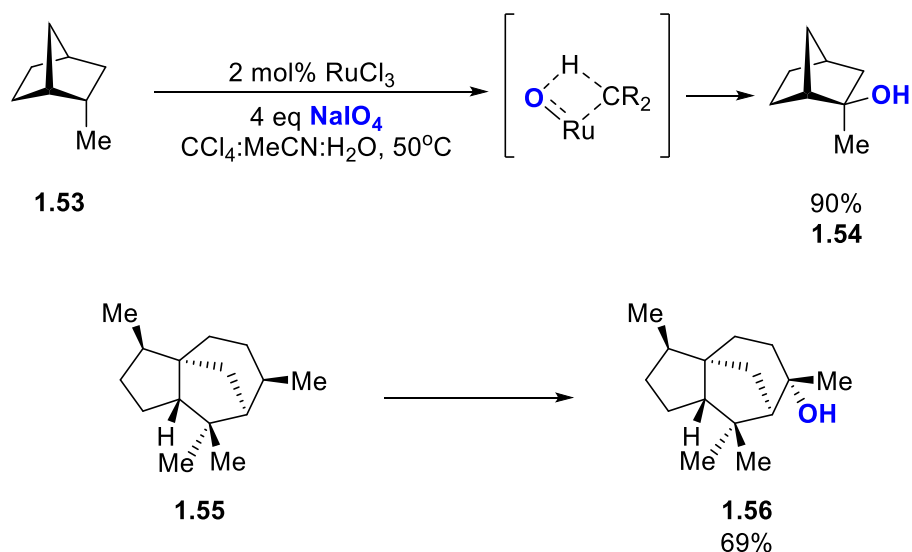
While palladium catalyzed C–H acetoxylation provides a valuable retrosynthetic disconnection, in practice the prerequisites for reactivity are not ideal for use in synthesis.

### 1.3 Concerted metal-based hydroxylation

#### 1.3.1 Ruthenium based systems

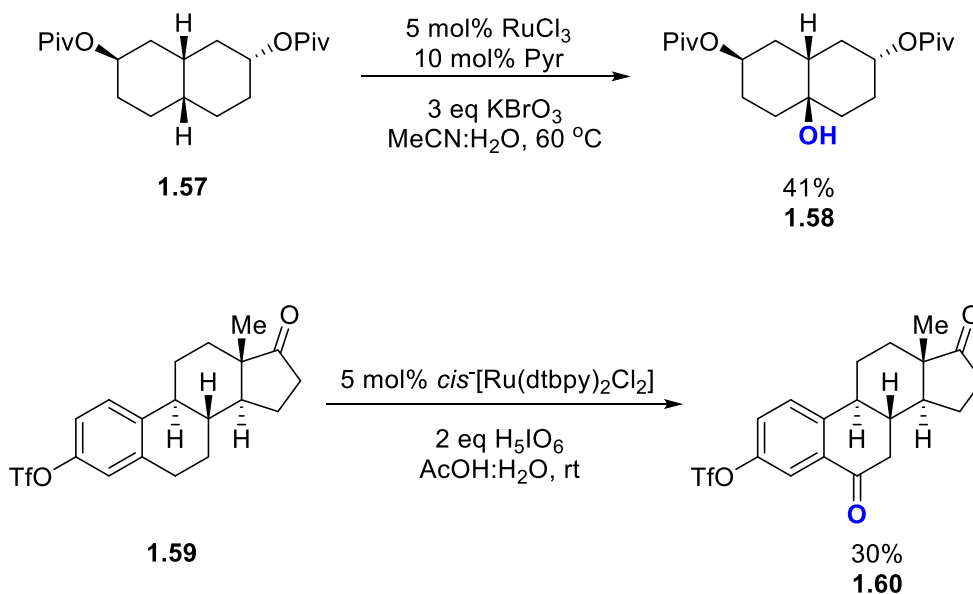
The need for directing groups in transition metal catalyzed oxidations can be circumvented through use of metals such as ruthenium tetroxide that operate by a sigma metathesis-reductive elimination C–O bond formation mechanism.<sup>17</sup> In the case of these concerted reactions selectivity is often governed by the electron richness and steric accessibility of the C–H bond, taking advantage of the innate oxidative propensity present within a molecule. As ruthenium tetroxide is unstable, a typical reaction utilizes a catalytic amount of ruthenium trichloride that forms the tetroxide on exposure to a stoichiometric oxidant. Several natural product scaffolds can be stereo- and site-selectively hydroxylated using this strategy (**Scheme 1.12**).

**Scheme 1.12:** Ruthenium tetroxide catalyzed hydroxylation



The significant oxidizing power of ruthenium tetroxide can provide nonselective oxidation in some cases, limiting its utility in the synthesis of complex molecules. Du Bois and coworkers identified a new ruthenium-oxo complex that tempers the nonselective reactivity observed in early examples by modulation of metal center electrophilicity through ligand effects (**Scheme 1.13**).<sup>18</sup> In most cases under Du Bois conditions, a singly hydroxylated product and unreacted starting material constitute the bulk of the crude reaction mixture. In a follow up investigation, they identified a bipyridyl ruthenium-oxo catalyst with increased stability that selectively hydroxylates natural products and pharmaceuticals.<sup>19</sup>

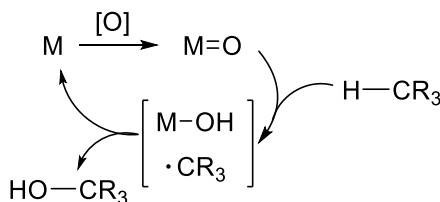
**Scheme 1.13:** Du Bois ruthenium catalyzed hydroxylation



## 1.4 Radical rebound hydroxylation

A series of biologically inspired iron and manganese catalysts that display similar selectivity to ruthenium-based systems have also been investigated. These catalysts are based on enzyme porphyrin cofactors and effect C–H bond hydroxylation through a radical abstraction-radical rebound mechanism (**Scheme 1.14**).<sup>20</sup> In a typical catalytic cycle, a metal-oxo species is formed from a stoichiometric oxidant. The metal-oxo abstracts a hydrogen atom to form a carbon centered radical and a hydroxido-bound metal. Recombination gives the hydroxylated product and regenerates the metal catalyst. The radical intermediates involved are short lived, allowing stereospecific transformations.

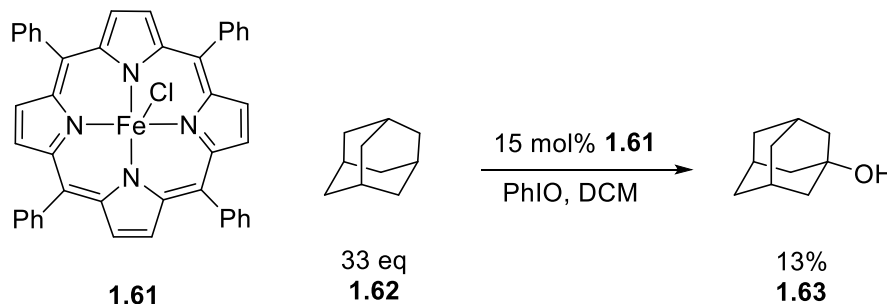
**Scheme 1.14:** Radical rebound hydroxylation



### 1.4.1 Iron catalysts

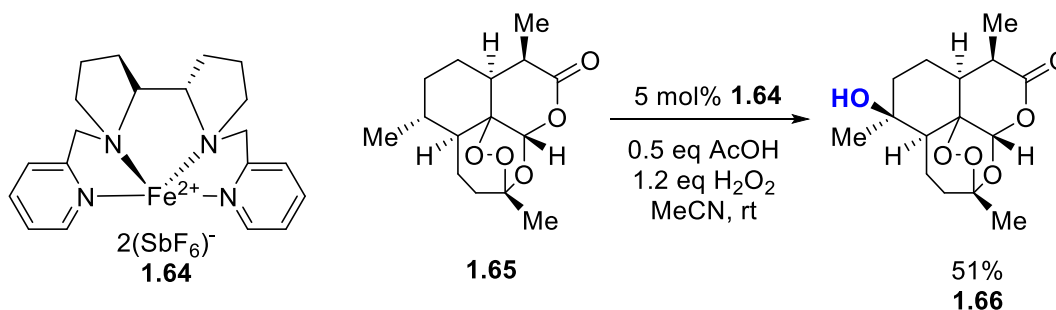
Early examples of radical rebound catalysis required high catalyst loading and an excess of substrate to produce hydroxylated products due to rapid catalyst degradation (**Scheme 1.15**).<sup>20</sup> Considerable research efforts eventually led to iron-porphyrin and related catalysts that could hydroxylate complex molecules in synthetically useful yields.<sup>21</sup>

---

**Scheme 1.15:** Early examples of iron catalyzed hydroxylation


A major advancement in the field of iron-catalyzed hydroxylation was contributed by White and coworkers.<sup>22</sup> Utilizing a cationic Fe(PDP) catalyst and hydrogen peroxide as the stoichiometric oxidant, hydroxylation of natural products and pharmaceuticals occurred predictably and selectively on complex molecules. In one such example, the highly functionalized antimalarial drug artemisinin was hydroxylated at a single position in 51% yield (**Scheme 1.16**). Notably, the reaction proceeded with complete diastereocontrol despite the intermediacy of a carbon centered radical.

---

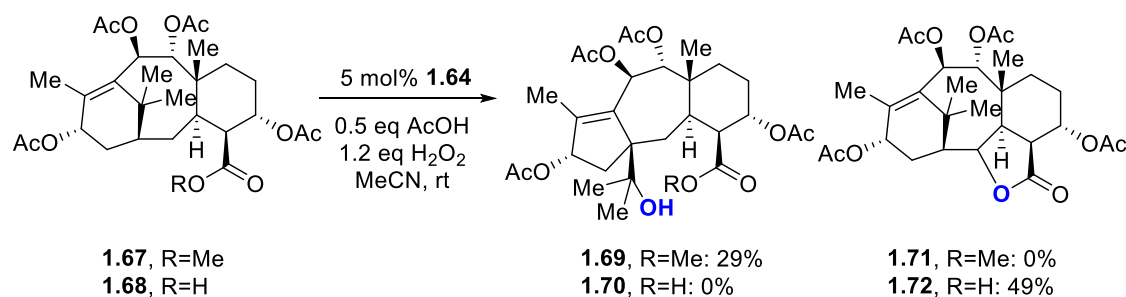
**Scheme 1.16:** White iron catalyzed hydroxylation


In a follow up paper, White and coworkers demonstrated that the open coordination site present in the Fe(PDP) catalyst can be leveraged to perform



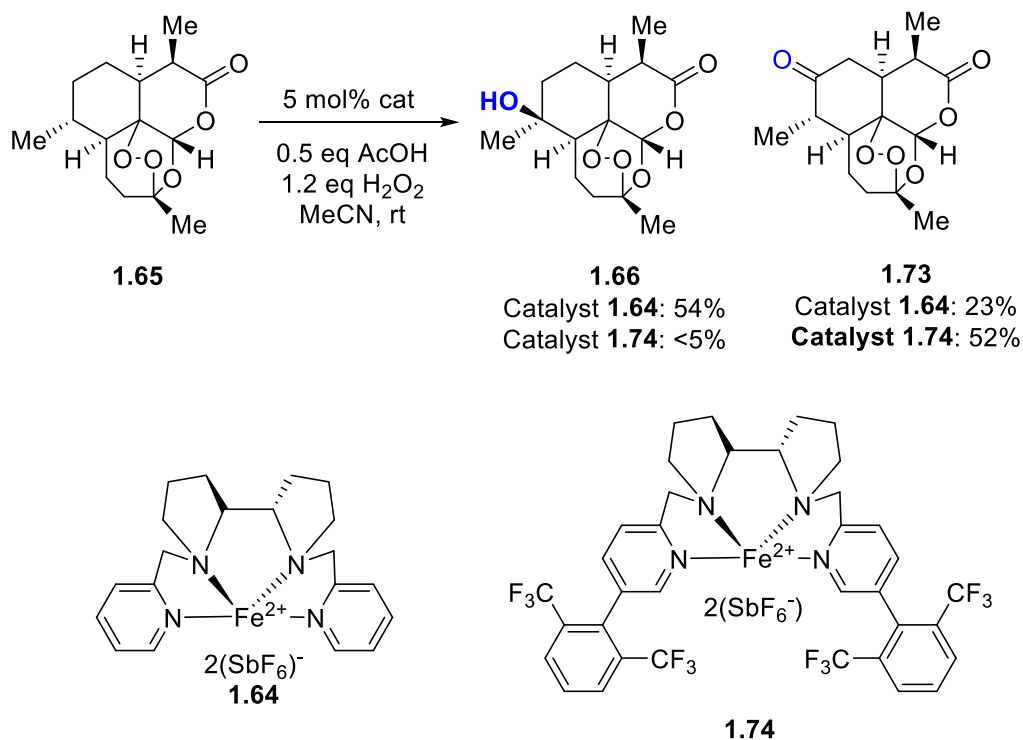
directed oxidations.<sup>23</sup> In doing so, they were able to override the inherent selectivity presented by the substrate using preexisting directing groups contained within the molecule (**Scheme 1.17**).

**Scheme 1.17:** Directed iron catalyzed hydroxylation

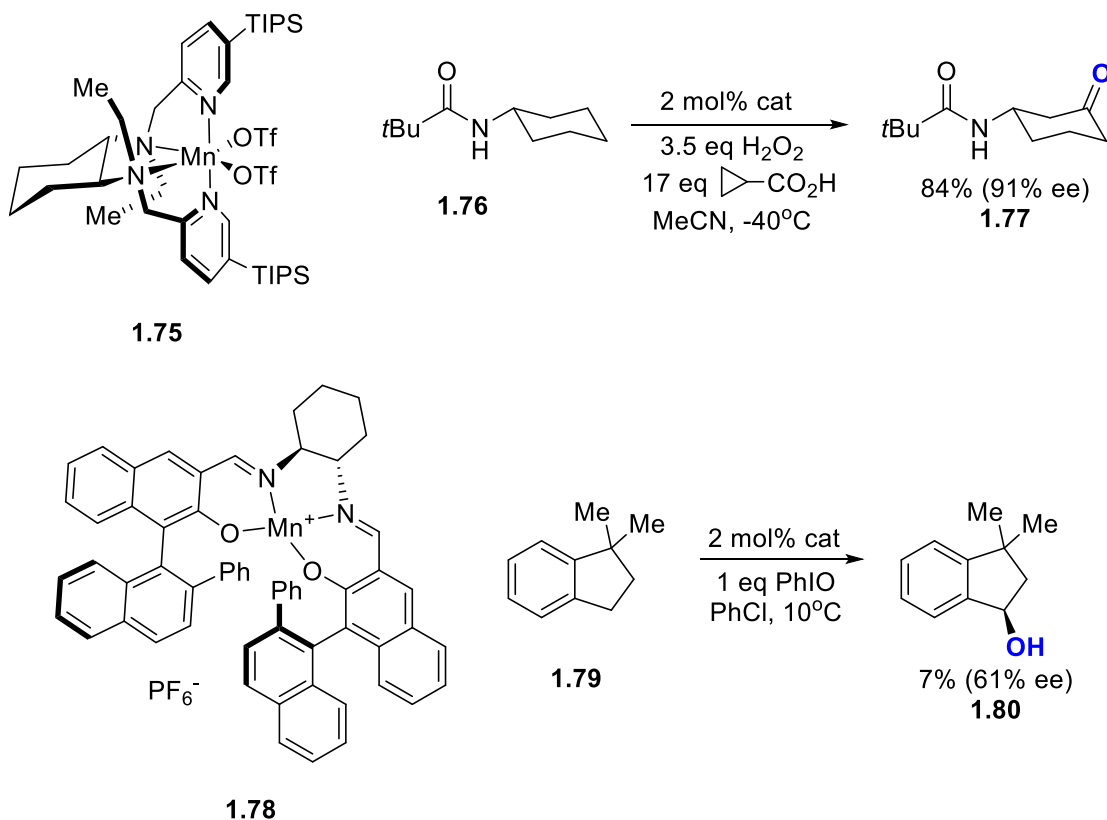


When the coordinating carboxyl group is protected as its methyl ester, hydroxylation proceeds with typical selectivity. However, in this example rearrangement of the intermediate radical outcompetes radical rebound. In the presence of an unprotected carboxyl group, the inherent C–H bond selectivity is overridden, allowing access to a new site for hydroxylation. In each case, the product isolated is the sole major constituent of the crude reaction mixture.

White and coworkers have also demonstrated that inherent selectivity can be overridden by tuning the steric bulk of the PDP ligand.<sup>24</sup> When using aryl substituted Fe(PDP) catalyst **1.74** the trajectory of substrate approach to the catalyst is restricted, directing reactivity towards a more accessible C–H bond. In the case of artemisinin, a more encumbered catalyst favors secondary C–H bond hydroxylation (**Scheme 1.18**).

**Scheme 1.18: Catalyst controlled site selectivity in hydroxylation**

**1.4.2 Manganese catalysts**

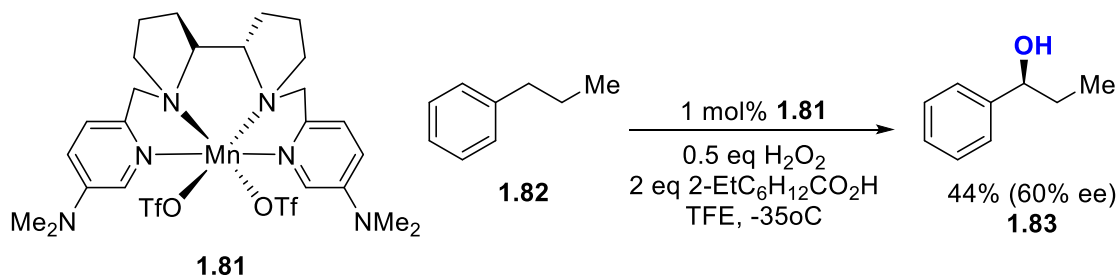
The use of catalyst dictated selectivity has seen impressive use in mechanistically analogous manganese catalysts. For example, bulky, chiral Mn(<sup>TIPS</sup>ecp) catalyst **1.75** was capable of enantioselective C–H hydroxylation of methylene carbons (**Scheme 1.19**).<sup>25</sup> Several additional chiral scaffolds for manganese catalyzed asymmetric C–H bond hydroxylation have also been developed.<sup>20</sup>

**Scheme 1.19: Asymmetric manganese catalyzed hydroxylation**


Schiff-base ligated manganese catalyst **1.78** is one of few examples that allow direct installment of an enantioenriched alcohol onto a prochiral framework.<sup>26</sup> In this case, overoxidation to the ketone is prevented by geometric constraints of the substrate and is not general for all secondary C–H bond oxidations.

A more general solution has been recently developed using Mn(PDP) catalyst **1.81**, in which solvent effects prevent exhaustive oxidation of prochiral centers to achiral ketones (**Scheme 1.20**).<sup>27</sup>

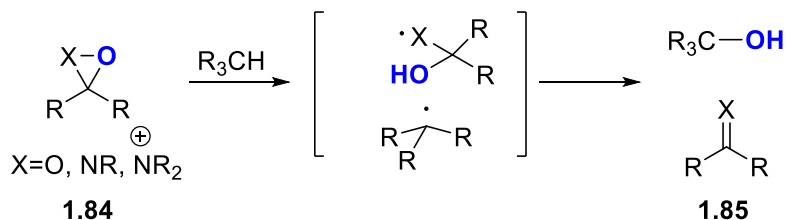
---

**Scheme 1.20:** Asymmetric hydroxylation of linear alkanes


The tunable site-selectivity and enantiocontrol offered by radical rebound based metal catalysts have solidified their place in the literature for the functionalization of C–H bonds.

**1.5 Organocatalytic approaches to hydroxylation**

Stoichiometric organic C–H bond hydroxylation reagents have a long history of use in synthetic chemistry due to their ability to selectively operate on complex molecules.<sup>28</sup> These hydroxylation reagents feature a strained heteronuclear ring that hydroxylate C–H bonds through a radical pair-radical rebound mechanism<sup>29</sup> (**Scheme 1.21**).

**Scheme 1.21:** Organic oxidants for hydroxylation


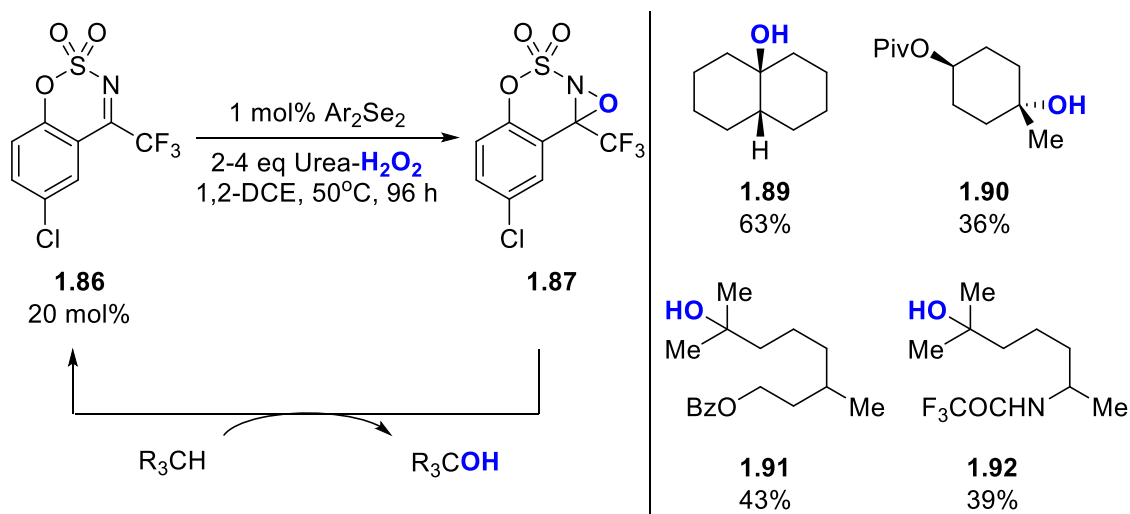
The abundance of organic compounds in nature allows affordable and rapid synthesis of organic reagents containing considerable complexity. As such,

employment of organocatalysts can allow use of complex, chiral catalyst scaffolds at low cost. Additional benefits of these reagents include low toxicity and low costs of disposal.<sup>30</sup> Despite these possible advantages, catalytic variants of organic C–H bond hydroxylation reagents have only recently been explored.

### 1.5.1 Oxaziridine mediated catalysis

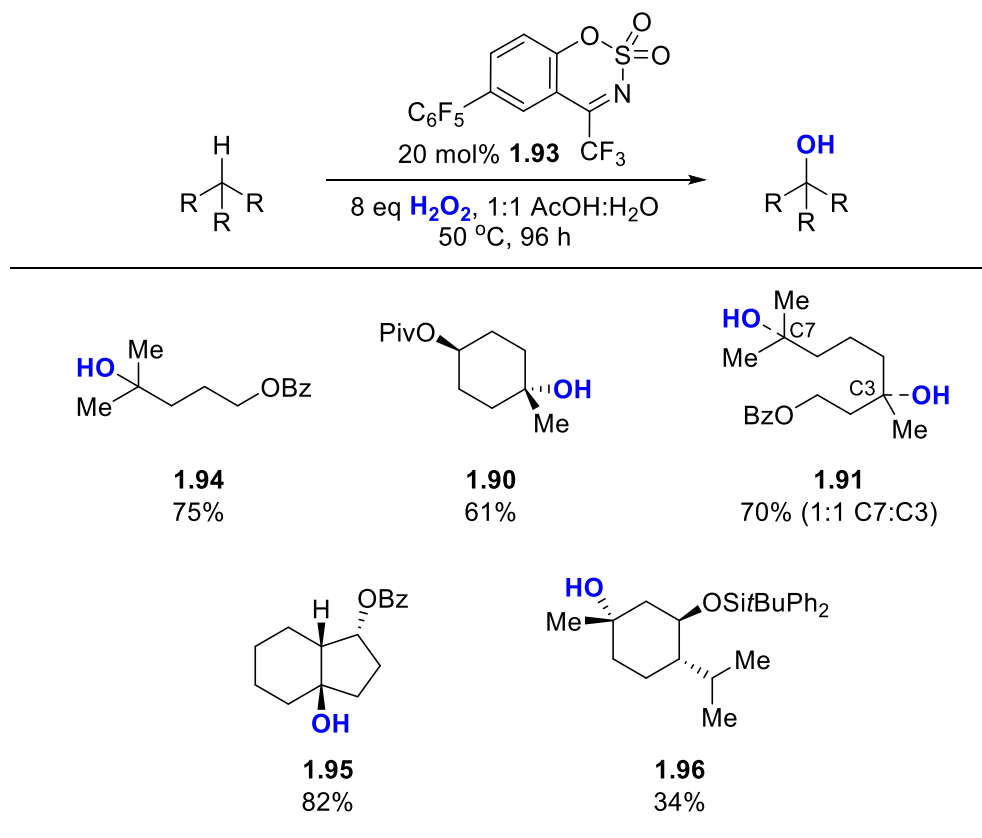
The first example of an organocatalytic C–H bond hydroxylation reaction was reported by Du Bois and coworkers in 2005.<sup>31</sup> Use of 20 mol% benzoxathiazine catalyst **1.86**, converted to its corresponding oxaziridine **1.87** by exposure to in situ generated perselenic acid, was able to hydroxylate tertiary C–H bonds in modest (typically <50%) yield (**Scheme 1.22**). Substrate scope (**1.89-1.92**) was limited to four substrates due to poor catalyst activity.

**Scheme 1.22:** Organocatalytic hydroxylation



Additional investigation revealed a new set of aqueous conditions that expanded substrate scope by increasing the reaction rate of hydroxylation relative to catalyst degradation.<sup>32</sup> Through the introduction of hydrophobic clustering between catalyst and substrate, reactivity was biased towards C–H bond hydroxylation (**Table 1.1**). Additional investigation revealed that electron deficient benzoxathiazine **1.93** further increased catalytic activity, although at the expense of site selectivity (**Table 1.1, 1.91**).

**Table 1.1:** Second generation organocatalytic hydroxylation

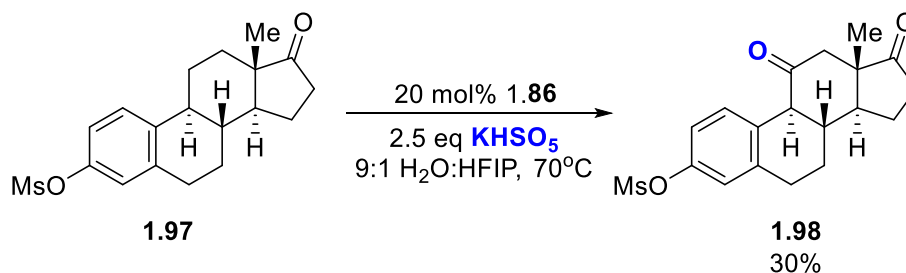


In their final report on benzoxathiazine catalyzed C–H bond hydroxylation, Du Bois and coworkers explored solvent effects on the stability of oxaziridinium

**1.87.**<sup>33</sup> When using 1:1 AcOH:H<sub>2</sub>O, the observed a half-life of less than 4 h, however, with use of 1,1,1,3,3,3-hexafluoroisopropanol (HFIP), the half-life is extended beyond 30 h. With this information in hand, they were able to develop conditions using more selective catalyst **1.86** that afforded considerable improvement in yield, substrate scope, reaction time, and reaction mildness. Under these new conditions, the first examples of organocatalytic hydroxylation of complex natural product derivatives was reported (**Scheme 1.23**).

---

**Scheme 1.23:** Third generation organocatalytic hydroxylation of natural products




---

## 1.6 Conclusions

Considerable effort has been lent to the development of methods that are capable of selectively reacting with aliphatic C–H bonds. These methods allow new retrosynthetic disconnections to be drawn and allow for the functionalization of typically unreactive chemical space. Recent investigations have continued to unlock previously inaccessible synthetic transformations, allowing increased efficiency in the synthesis of complex molecules.

## 1.7 References

1. Chen, K.; Baran, P. S.; *Nature*, **2009**, *459*, 824–828.
2. Croteau, R.; Ketchum, R. E. B.; Long, R. M.; Kaspera, R.; Wildung, M. R.; *Phytochem Rev.*, **2010**, *5*, 75-97.
3. Kawamura, S.; Chu, H.; Felding, J.; Baran, P. S., *Nature*, **2016**, *532*, 90–93.
4. For perspectives on ideal syntheses, see: Hendrickson, J. B.; *J. Am. Chem. Soc.* **1975**, *97*, 5784. Trost, B. M. *Science*, **1991**, *254*, 1471. Trost, B. M.; *Angew. Chem., Int. Ed.*, **1995**, *34*, 259. Wender, P.A.; Croatt, M. P.; Witulski, B.; *Tetrahedron*, **2006**, *62*, 7505. Wender, P. A.; Verma, V. A.; Paxton, T. J.; Pillow, T. H.; *Acc. Chem. Res.*, **2008**, *41*, 40. Wender, P. A.; Miller, B. L.; *Nature*, **2009**, *460*, 197. Richter, J. M.; Ishihara, Y.; Masuda, T.; Whitefield, B. W.; Llamas, T.; Pohjakallio, A.; Baran, P. S.; *J. Am. Chem. Soc.*, **2008**, *130*, 17938. Burns, N. Z.; Baran, P. S.; Hoffmann, R. W. *Angew. Chem., Int. Ed.*, **2009**, *48*, 2854. Gaich, T.; Baran, P. S.; *J. Org. Chem.*, **2010**, *75*, 4657.
5. Piettre, S.; Heathcock, C. H.; *Science*, **1990**, *248*, 1532-1534.
6. Kola, I.; Landis, J.; *Nat. Rev. Drug Discovery*, **2004**, *3*, 711-715. Meanwell, N. A.; *Chem. Res. Toxicol.*, **2011**, *24*, 1420-1456.



7. Cragg, G. M.; Newman, D. J.; *J. Ethnopharmacology*, **2005**, 100, 72–79.  
Cragg, G. M.; Newman, D. J.; *Expert Opinion Investigational Drugs*, **2000**, 9, 2783–97.
8. Michaudel, Q.; Journot, G.; Regueiro-ren, A.; Goswami, A.; Guo, Z.; Tully, T. P.; Baran, P. S.; *Angew. Chem. Int. Ed.*, **2014**, 126, 12091–12096.
9. For a review of initial reports and further development, see: Shilov, A. E.; Shul'pin, G. B.; *Chem. Rev.*, **1997**, 97, 2879–2932.
10. Kao, L.; Sen, A.; *J. Chem. Soc., Chem. Commun.*, **1991**, 1–2.
11. Dangel, B. D.; Johnson, J. A.; Sames, D.; *J. Am. Chem. Soc.*, **2001**, 123, 8149–8150.
12. Lee, M.; Sanford, M. S.; *J. Am. Chem. Soc.*, **2015**, 137, 12796–12799.
13. Baldwin, J. E.; Jones, R. H.; Najera, C.; Yus, M.; *Tetrahedron*, **1985**, 41, 699–711.
14. Dick, A. R.; Hull, K. L.; Sanford, M. S.; *J. Am. Chem. Soc.*, **2004**, 126, 2300–2301. Desai, L. V.; Hull, K. L.; Sanford, M. S.; *J. Am. Chem. Soc.*, **2004**, 126, 9542–9543.
15. Sharpe, R. J.; Johnson, J. S.; *J. Org. Chem.*, **2015**, 80, 9740–9766.
16. Trotta, A. H.; *Org. Lett.*, **2015**, 17, 3358–3361.

17. Tenaglia, A.; Terranova, E.; Waegell, B. *Tetrahedron Lett.*, **1989**, 30, 5271–5274.
18. McNeill, E.; Du Bois, J.; *J. Am. Chem. Soc.*, **2010**, 132, 10202–10204.
19. Mack, J. B. C.; Gipson, J. D.; Du Bois, J.; Sigman, M. S.; *J. Am. Chem. Soc.*, **2017**, 139, 9503–9506.
20. For reviews and key examples of iron catalyzed hydroxylations with use in synthetic chemistry, see: Talsi, E. P.; Bryliakov, K. P.; *Coord. Chem. Rev.*, **2012**, 256, 1418-1434. Correa, A.; Mancheo, O. G.; Bolm, C.; *Chem. Soc. Rev.*, **2008**, 37, 1108-1117. Costas, M.; Chen, K.; Que, L.; *Coord. Chem. Rev.*, **2000**, 200-202. Que, L.; Tolman, W. B.; *Nature*, **2008**, 455, 333-340. England, J.; Davies, C. R.; Banaru, M.; White, A. J. P.; Britovsek, G. J. P.; *Adv. Synth. Catal.*, **2008**, 350, 883-897. Company, A.; Gomez, L.; Fontrodona, X.; Ribas, X.; Costas, M.; *Chem. Eur. J.*, **2008**, 14, 5727-5731. England, J.; Britovsek, G. J. P.; Rabadia, N.; White, A. J. P.; *Inorg. Chem.*, **2007**, 46, 3752-3767. Company, A.; Gomez, L.; Giell, M.; Ribas, X.; Luis, J. M.; Que, L.; Costas, M.; *J. Am. Chem. Soc.*, **2007**, 129, 15766-15767. Romakh, V. B.; Therrien, B.; Suss-Fink, B.; Shul'pin, G. B.; *Inorg. Chem.*, **2007**, 46, 3166-3175. Chen, K.; Que, L.; *J. Am. Chem. Soc.* **2001**, 123, 6327-6337. Roelfes, F.; Lubben, M.; Hage, R.; Que, L.; Feringa, B. L.; *Chem. Eur. J.*, **2000**, 6, 2152-2159.

21. Groves, J. T.; McClusky, G. A.; *J. Am. Chem. Soc.*, **1976**, *98*, 859–861.  
Groves, J. T.; Nemo, T. E.; Myers, R. S.; *J. Am. Chem. Soc.*, **1979**, *101*, 1032–1033.
22. Chen, M. S.; White, M. C.; *Science*, **2007**, *318*, 783–787. Vermeulen, N. A.;  
Chen, M. S.; Christina White, M. *Tetrahedron*, **2009**, *65*, 3078–3084.
23. Bigi, M. A.; Reed, S. A.; White, M. C.; *J. Am. Chem. Soc.*, **2012**, *134*, 9721–9726.
24. Gormisky, P. E.; White, M. C.; *J. Am. Chem. Soc.*, **2013**, *135*, 14052–14055.
25. Milan, M.; Bietti, M.; Costas, M.; *ACS Central Science*, **2017**, *3*, 196–204.
26. Hamada, T.; Irie, R.; Mihara, J.; Hamachi, K.; Katsuki, T.; *Tetrahedron*, **1998**, *54*, 10017–10028.
27. Dantignana, V.; Milan, M.; Cussó, O.; Company, A.; Bietti, M.; Costas, M.;  
*ACS Central Science*, **2017**, *3*, 1350–1358.
28. Newhouse, T.; Baran, P. S.; *Angew. Chem. Int. Ed.*, **2011**, *50*, 3362–3374.
29. Simakov, P. A.; Choi, S. Y.; Newcomb, M.; *Tet. Lett.*, **1998**, *39*, 8187–8190.  
Yang, Z.; Yu, P.; Houk, K. N.; *J. Am. Chem. Soc.*, **2016**, *138*, 4237–4232.
30. MacMillan, D. W. C.; *Nature*, **2008**, *455*, 304–308.

31. Brodsky, B. H.; Du Bois, J.; *J. Am. Chem. Soc.*, **2005**, 127, 15391–15393.
32. Litvinas, N. D.; Brodsky, B. H.; Du Bois, J. *Angew. Chem. Int. Ed.*, **2009**, 48, 4513–4516.
33. Adams, A. M.; Du Bois, J.; *Chem. Sci.*, **2014**, 5, 656–659.

## Chapter Two

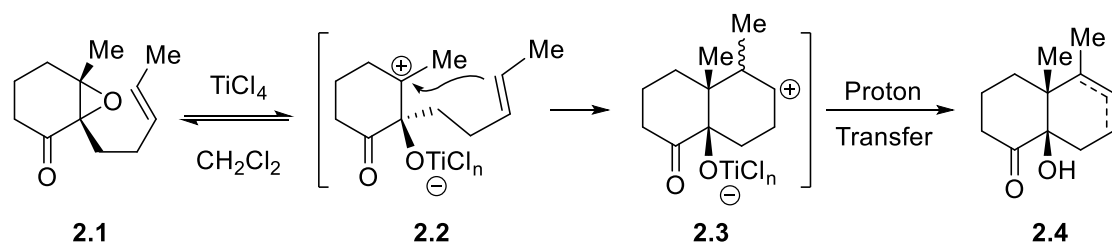
### Reactivity of C–O Cleaved Epoxide Zwitterions

#### 2.1 Introduction

##### 2.1.1 C–C bond formation using C–O cleaved epoxide zwitterions

The synthetic utility of Lewis or Brønsted acid mediated activation of epoxides towards nucleophilic attack was advanced beyond classical heteroatomic or carbanionic nucleophiles with the observation by Goldsmith that carbon-carbon  $\pi$ -bonds are also competent nucleophiles.<sup>1</sup> This precludes the need for premetallated carbon nucleophiles in the formation of carbon-carbon bonds and ring systems.

**Scheme 2.1:** Reactions of activated epoxides with alkenes

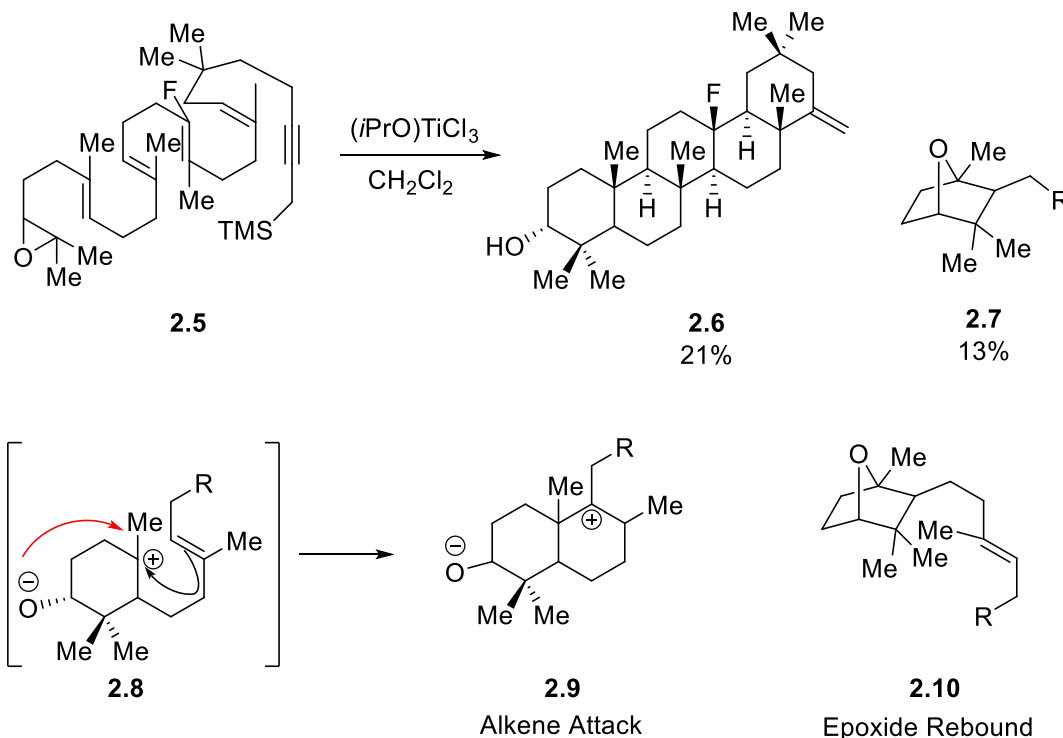


In a typical reaction setup (**Scheme 2.1**), activation of epoxide **2.1** is accomplished through Lewis acid coordination.<sup>2</sup> The weakened C–O bond of the epoxide heterolytically dissociates to form long-lived zwitterion **2.2**. Epimerization of the  $\alpha$ -keto stereocenter (between **2.1** and **2.2**) observed in this reaction

suggests that ring opening is a reversible process. Nucleophilic attack by the tethered carbon-carbon  $\pi$  bond on carbocation **2.2** forms a carbon-carbon  $\sigma$  bond and carbocation **2.3**, which upon proton transfer generates transposed alkene **2.4** as a mixture of regioisomers.

The true power of these transformations is revealed in reactions between epoxides and polyunsaturated frameworks. In the initial report by Goldsmith and coworkers the reaction is terminated after a single carbon-carbon  $\sigma$  bond formation step by proton transfer. However, with a sufficiently long-lived carbocation additional carbon-carbon  $\pi$  bonds can participate, allowing multiple successive nucleophilic attack-carbocation forming steps to occur.

The rapid increase in molecular complexity generated by epoxy-polyene cascade cyclizations has led to widespread use in total synthesis of polycyclic hydrocarbon containing natural products. In Johnson's landmark syntheses of the oleanane triterpenes, they were able to cascade the nucleophilic attack of multiple unsaturated carbon-carbon bonds using a Lewis acid activated epoxide (**Scheme 2.2**).<sup>3</sup> In a single step, this epoxy-polyene cascade formed five carbon-carbon bonds with eight contiguous stereocenters, five of which are stereodefined quaternary carbons.

**Scheme 2.2:** Reactions of activated epoxides with polyenes


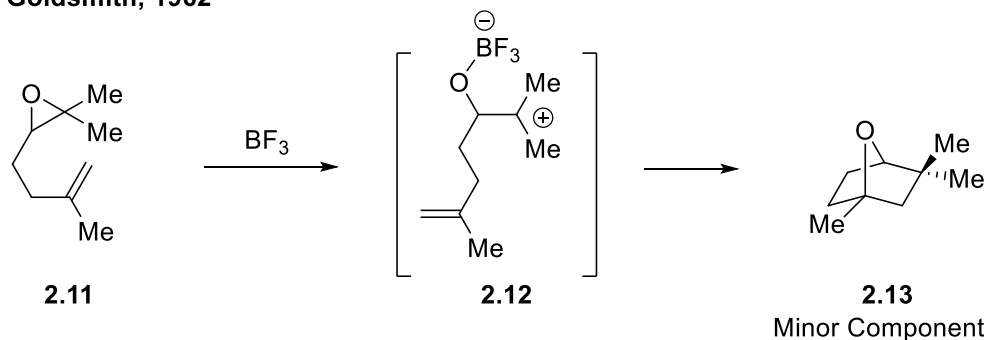
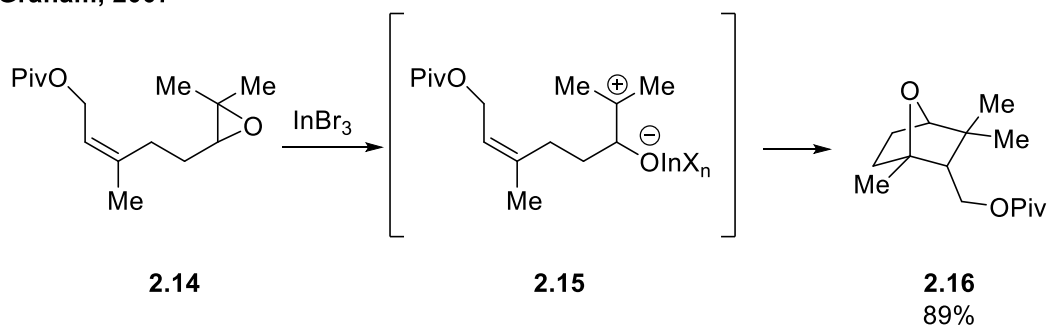
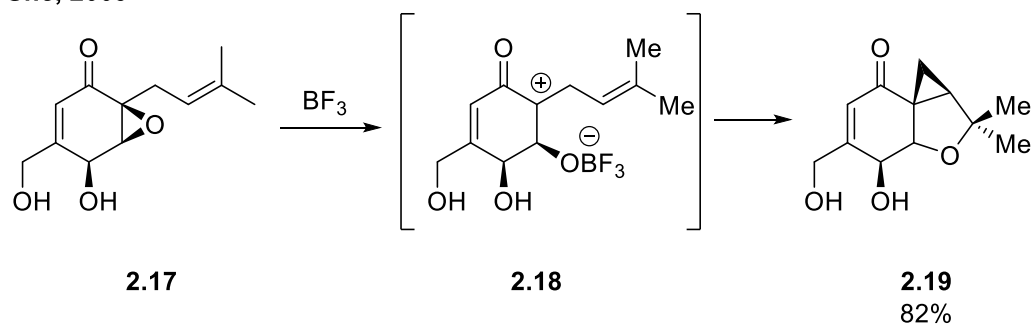
In addition to the desired pentacyclic hydrocarbon **2.6**, the reaction produced a nearly equivalent amount of bicyclic tetrahydrofuran product **2.7**. Johnson and coworkers suggested that this product formation occurs through an interruption of the desired mechanistic pathway wherein the rate of nucleophilic attack of the alkoxide on cationic intermediates **2.8** outcompetes the remaining alkenes present in the polyene tail. Although this constitutes an undesired mechanistic pathway for their purposes it demonstrates a powerful alternative reaction manifold for C–O cleaved epoxide zwitterions. In many examples of alkene-epoxide reactions the ring opened epoxide as a monofunctional electrophilic cation; however, they can also function as electrophilic-nucleophilic

zwitterions. In acting as such, the C–O cleaved epoxide zwitterion can participate in formal (3+2) cyclizations en route to small and medium ring heterocycles.

#### *2.1.2 Ring opened epoxides as dipolar intermediates*

Considerably fewer examples utilizing the dipolar nature of ring-opened epoxides have been reported in the literature despite its concurrent discovery with monopolar epoxy-alkene reactivity. While the initial report cited (3+2) dipolar cyclizations as a minor constituent of the reaction mass, subsequent reports have demonstrated the preference for monopolar and dipolar reactivity is highly substrate and catalyst dependent (**Scheme 2.3**).



**Scheme 2.3: Activated epoxides as dipolar intermediates**
**Goldsmith, 1962**

**Graham, 2007**

**She, 2009**


Whereas dipolar reactivity was an insubstantial pathway with activated geraniolene epoxide **2.11**, the closely related citronellal derived epoxide **2.14** provided dipolar (3+2) cyclization product **2.16** in 89% yield as a mixture of diastereomers.<sup>4</sup> She and coworkers identified that a stereospecific (3+2) epoxy-

alkene cyclization allows single step establishment of the core scaffold of the fungal metabolite Mycorrhizin A.<sup>5</sup> Despite the early realization that zwitterionic reactivity can only be achieved in a narrow cross-section of reaction partners, intramolecular (3+2) reactions of C–O cleaved epoxides and alkenes have seen sporadic development and use.

### *2.1.3 Epoxide (3+2) cyclizations as a retrosynthetic disconnection*

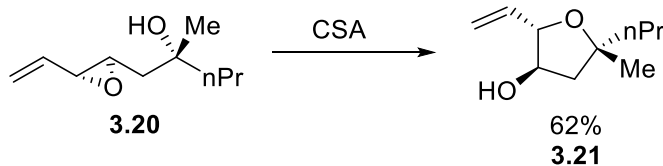
Despite the rapid increase in molecular complexity demonstrated by use of zwitterionic epoxide (3+2) cyclizations for tetrahydrofuran synthesis, the most common approaches typically rely on S<sub>N</sub>2 type or related radical ring closing processes (**Scheme 2.4A**). Reliance on these techniques requires that the relative stereochemistry of the ring system to be established in an acyclic molecule. This typically involves a linear, stepwise introduction of functionality, greatly increasing the total step count required to generate these small heterocyclic rings.

**Scheme 2.4A:** Linear synthesis of tetrahydrofurans<sup>6</sup>

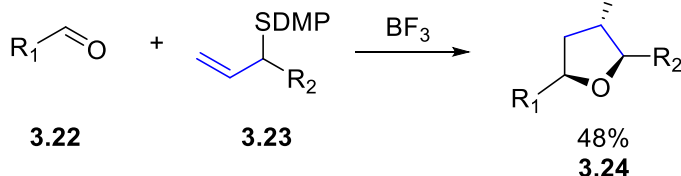
C-O Bond Formation



Frequently Employed

**Scheme 2.4B:** Convergent synthesis of tetrahydrofurans from aldehydes<sup>7</sup>C-O Bond Formation  
C-C Bond Formation

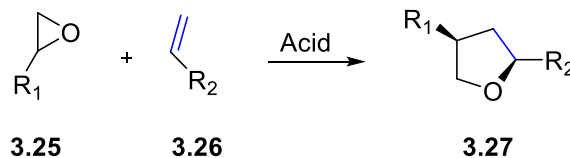
Limited Utility

**Scheme 2.4C:** Convergent synthesis of tetrahydrofurans from cyclization

(3+2) Cyclization



Unknown Reaction



In contrast, a dipolar epoxide (3+2) cyclization divides the tetrahydrofuran ring into two modular fragments that can be conjoined at a late stage in the synthesis. This approach increases the convergence of the synthetic strategy, thereby allowing shorter synthetic routes, higher overall yields, and facile formation of analogs. Recent reports have discovered annulation reactions which share the bond disconnections made possible by epoxide (3+2) cyclizations, but these strategies are mechanistically limited to a small subset of reaction partners

(**Scheme 2.4B**). The use of an epoxide (3+2) cyclizations (**Scheme 2.4C**) for ring formation represents an efficient but underdeveloped method for the generation of natural product core scaffolds.

#### *2.1.4 Product distribution of epoxide zwitterions reacting with alkenes*

Despite the possible advantages of a dipolar epoxide (3+2) cyclization, the development and adoption of this strategy for tetrahydrofuran formation has been hampered by the instability of C–O cleaved epoxide zwitterions and concurrently limited scope of reaction partners. Additional research into Goldsmith's original 1962 report conducted by Mohan and coworkers illustrates the difficulty faced in achieving a modestly yielding (3+2) cyclization.<sup>8</sup> Despite extensive screening of solvents, temperatures, concentrations, and epoxide activating reagents, they found that the predominant products across all conditions are derived from epoxide zwitterion degradation pathways (**Table 2.1**). In each case, the desired cyclization product was only a minor component of the crude reaction mixture.

**Table 2.1:** Impact of conditions on product distribution

	Conditions →			
<b>2.11</b>				
	<b>2.28</b>	<b>2.29</b>	<b>2.30</b>	<b>2.13</b>
Conditions	[1,2] Shift	E <sub>1</sub>	Interrupted (3+2)	(3+2)
TfOH / DCM	21%	33%	36%	10%
Bi(OTf) <sub>3</sub> / DCM	22%	29%	13%	13%
Bi(OTf) <sub>3</sub> / Pentane	27%	20%	17%	6%
Bi(OTf) <sub>3</sub> / THF	55%	39%	6%	0%

The major products of epoxide zwitterion reactivity result from nonproductive quenching of the carbocation. The primary mechanism of carbocation quenching is a unimolecular [1,2]-sigmatropic shift of the  $\alpha$ -hydrogen to form **2.28**. This sigmatropic rearrangement, known as the Meinwald rearrangement, has a low kinetic barrier due to the excellent orbital overlap present. Due to its rapid rate, Meinwald rearrangement products of C–O cleaved epoxide zwitterions comprise a major portion of the reaction mix and limit dipolar (3+2) cyclizations to intramolecular reactions. The carbonyl formed through carbocation rearrangement is typically more nucleophilic than alkenes, further reducing yields of the desired tetrahydrofuran product.<sup>9</sup> Epoxides bearing  $\alpha$ -protons are also highly susceptible to  $E_1$  eliminations, further reducing yields and limiting scope of reaction partners.

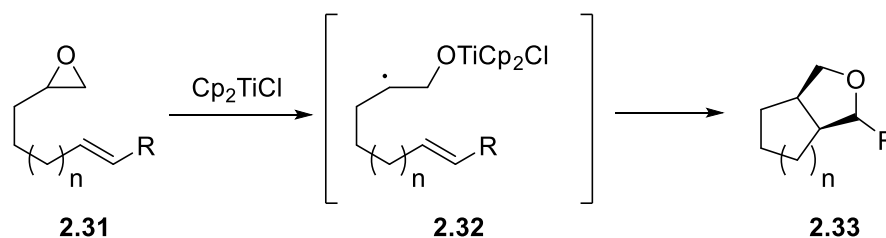
Additional factors hindering the development of dipolar epoxide reactivity include high energy transition state geometries preventing oxygen-carbocation

ring closure, leading to arrested cyclization products commonly associated with epoxide-alkene reactions. Although not observed in the reaction of geraniolene epoxide, unhindered epoxide zwitterions are also prone to head to tail dimerization and oligomerization reactions.<sup>10</sup> Interestingly, these oligomerization events are known to encourage ring opening polymerization of tetrahydrofuran, further confounding the formation of cyclized products in useful yields.<sup>11</sup> In conjunction, these competing reactions have thus far rendered epoxide (3+2) cyclizations an unattractive option for synthetic transformations.

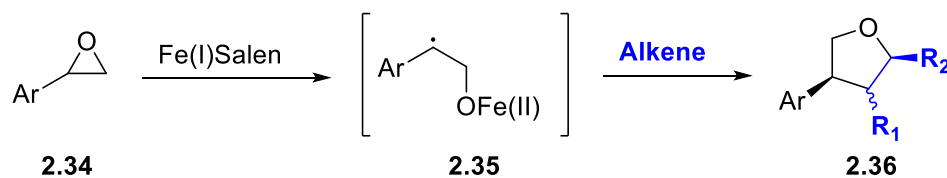
#### *2.1.5 Circumvention of instability via homolytic C-O bond cleavage*

While heterolytically cleaved epoxide zwitterions have limited applicability due to these instability issues, others have found *homolytic* C–O bond cleavage allows access to the same cyclization products through more stabilized reaction intermediates. In these reactions a low valent transition metal acts as a one electron acceptor, homolytically cleaving the weakest C–O bond present in the epoxide to form a  $\beta$ -metalalkoxy radical. The resulting radical reacts with alkenes to induce cyclization. As the reaction still proceeds through electron deficient intermediates, trends for reaction partners and selectivity closely match those observed in two-electron catalytic processes.

---

**Scheme 2.5A:** Titanium catalyzed epoxide (3+2) cyclization


For R=H: <10% Yield; For R=Me: 50-60% Yield; For R=Ar: 80-90% Yield

**Scheme 2.5B:** Iron catalyzed epoxide (3+2) cyclization


30-60% Yield; d.r. < 2:1

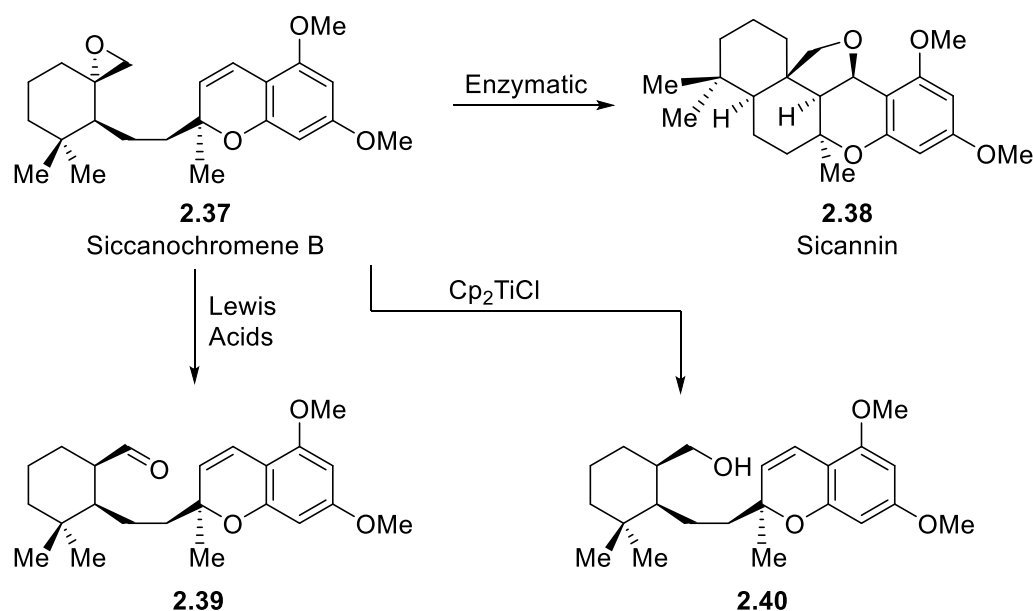
---

In the first reported demonstration of this one-electron approach, a Ti(III) metal center heterolytically cleaves alkyl epoxides which undergo intramolecular cyclizations to form the bicyclic tetrahydrofurans (**Scheme 2.5A**).<sup>12</sup> The stability of radical intermediates proved critical for reaction success: substrates lacking stabilized radicals engage exclusively in nonproductive reaction pathways.

Hilt and coworkers have identified an Fe(I) based catalyst that expands the scope of Ti(III) chemistry and allows the first examples of high yielding *intermolecular* (3+2) cyclizations between epoxides and alkenes (**Scheme 2.5B**).<sup>13</sup> This approach allows the intermolecular cyclization of styrene oxide with a broad range of alkene reaction partners including styrenes, dienes, enynes, and enones. Additionally, these intermolecular reactions proceed with modest (typically 2:1) diastereoselectivity.

Although one electron catalytic cycles have offered substantial improvements over the initial reports of Lewis acid mediated transformations, all existing methods still suffer a lack of broad applicability. Trost and coworkers highlighted this drawback in their biomimetic synthesis of the sicannin terpene family.<sup>14</sup> Their key retrosynthetic disconnection to be employed in the final step of their synthetic route relied on an epoxy-alkene (3+2) cyclization to form sicannin **2.38** (Scheme 2.6). However, even with ideal reaction partners and extensive reaction optimization, both radical and cationic cyclization conditions produced the desired product in only trace quantities.

**Scheme 2.6:** Epoxy-alkene (3+2) cyclizations in synthesis



Despite the potential utility of an epoxy-alkene (3+2) cyclization, to date they remain limited in their ability to deliver diverse scaffolds and lack wide spread

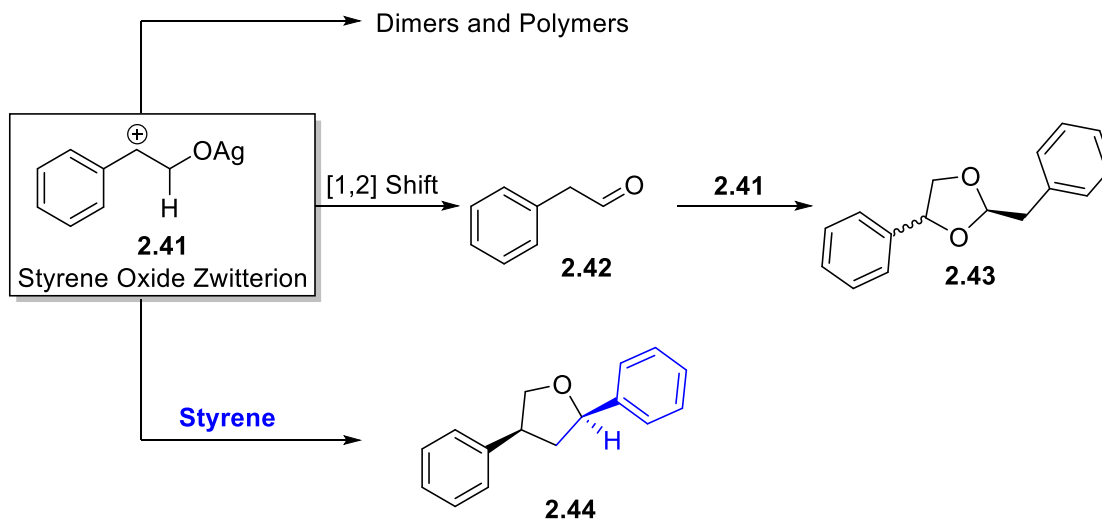
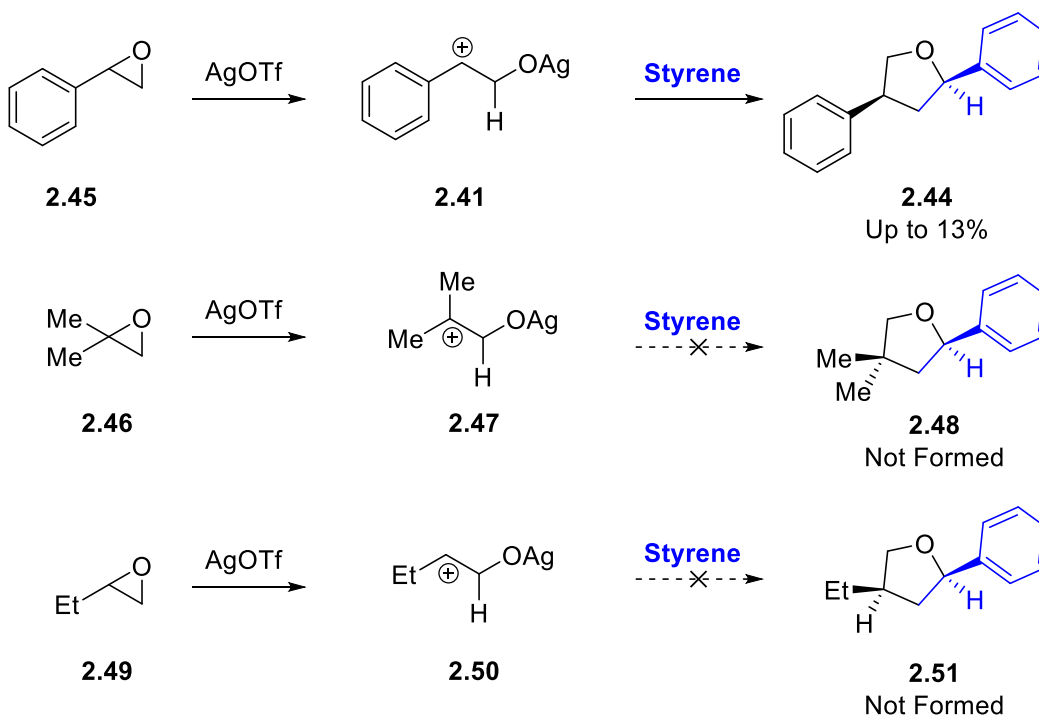


tolerance for reaction partners. Additional investigation is required to harness the power of this synthetic strategy.

## 2.2 Styrene and Styrene Oxide (3+2) Cyclizations

### 2.2.1 Initial reaction conditions

Inspired by the potential synthetic value of a high yielding epoxide (3+2) cyclization, we undertook a systematic investigation of conditions to probe if the known nonproductive epoxide consumption mechanisms could be overcome. Ultimately, we endeavored to discover a broadly applicable intermolecular cyclization reaction. Initial conditions employed styrene and styrene oxide in hopes that the stabilized benzylic cation intermediates would be sufficiently long-lived to engage in cyclizations with minimal degradation of intermediates. Rapid addition of styrene oxide to a solution of 2 mol% silver triflate in 2 equiv. styrene afforded epoxy-alkene (3+2) cyclization product **2.44** in low yields (<10%). Control experiments revealed that the major reaction products observed include aldehyde **2.42** generated from Meinwald rearrangement, diphenyldioxilane **2.43** derived from the (3+2) cyclization of zwitterionic epoxide with **2.41**, and several unidentified products arising from nucleophilic attack of styrene on phenylacetaldehyde (**Scheme 2.7A**). Our initial intermolecular cyclization conditions closely replicated product distributions previously reported in intramolecular cyclizations.

**Scheme 2.7A:** Product distribution of intermolecular (3+2) cyclization

**Scheme 2.7B:** Requirements for carbocation stability


As all routes identified for nonproductive reactivity were ultimately derived from the Meinwald rearrangement product the emphasis of further exploration was

therefore to suppress the rate of 1,2-hydride shift. The importance of addressing this mode of zwitterion degradation was reinforced by reactions conducted with epoxides that generate zwitterions less stable than that of styrene oxide: both 1,1-dimethyloxirane (tertiary carbocation intermediate **2.47**) and 1-ethyloxirane (secondary carbocation intermediate **2.50**) are rapidly consumed under the initial conditions but afford no cyclized products.

### 2.2.2 Lewis acid screening

Our first approach to extending the lifetime of the dipolar intermediate was to investigate metals with varying Lewis acidity (**Table 2.2**). We envisioned that reducing the effective electron density centered on the ring opened epoxide oxygen by using more electrophilic or oxophilic metals could raise the activation energy of the Meinwald rearrangement. Investigation of a series of silver salts revealed a strong correlation between reactivity and counterion coordination ability. Silver salts with coordinating counterions (e.g.: nitrate, *para*-tolylsulfonate, trifluoroacetate) showed limited epoxide consumption and no product formation (**Table 2.2, Entries 1-3**). Other metals possessing moderately to strongly coordinating counterions behaved similarly (**Table 2.2, Entries 6-10**).

**Table 2.2:** Lewis acid screening

c1ccccc1C1OC1 (2.45) + c1ccccc1C=O (2.52)  $\xrightarrow{2 \text{ mol\% Catalyst}}$  c1ccccc1C1OC(C1)c2ccccc2 (2.44)

Entry	Lewis Acid	<b>2.44</b> (%)	Entry	Lewis Acid	<b>2.44</b> (%)
1	AgOTFA	trace	8	TaCl <sub>5</sub>	trace
2	AgNO <sub>3</sub>	trace	9	YbCl <sub>3</sub>	trace
3	AgOTs	trace	10	Et <sub>3</sub> PAuCl	trace
4	AgOTf	10	11	In(OTf) <sub>3</sub>	9
5	AgSbF <sub>6</sub>	13	12	Sc(OTf) <sub>3</sub>	12
6	Tl(OTFA) <sub>3</sub>	trace	13	Yb(OTf) <sub>3</sub>	13
7	Hg(OTFA) <sub>2</sub>	trace	14	NaOTf	trace

Reactions performed on 2 mmol scale, using 2:1 styrene:styrene oxide with 2 mol% Lewis acid catalyst. Yields reported as corrected GC yields.

A screening of several metal triflates with varying electrophilicity showed minimal difference in reactivity under our conditions (**Table 2.2, Entries 11-13**). Despite our hypothesis that metal electrophilicity may alter the rate of hydride shift, no effective control of product distribution was obtainable by varying the Lewis acid catalyst.

### 2.2.3 Increasing the Stability of the Dipolar Intermediate

An alternative strategy to extend the life-time of the ring opened epoxide zwitterion is to stabilize the benzylic carbocation through solvent effects (**Table 2.3**). The initial screenings employed neat reaction mixtures to maximize the concentration of styrene relative to epoxide. We maintained high concentration of styrene (4 M) in solvent screening to preserve this effect.

**Table 2.3:** Solvent screening

c1ccccc1C1OC1 (2.45) + c1ccccc1C=C (2.52)  $\xrightarrow{2 \text{ mol\% Catalyst}}$  c1ccccc1C2OC(C1)CC2 (2.44)

Entry	Solvent	<b>2.44</b> (%)	Entry	Solvent	<b>2.44</b> (%)
1	-	10	6	DCM	13
2	benzene	6	7	1,2-DCE	12
3	DMF	trace	8	CHCl <sub>3</sub>	10
4	1,4-dioxane	4	9	CCl <sub>4</sub>	11
5	THF	6			

Reactions performed on 2 mmol scale [4 M] in solvent, using 2:1 styrene:styrene oxide with 2 mol% silver triflate. Yields reported as corrected GC yields.

We observed that the Lewis basic solvents ideal for carbocation stability significantly decrease catalytic activity, with strongly coordinating solvents such as DMF halting epoxide consumption. More weakly coordinating solvents such as dioxane and THF required longer reaction times for full consumption of styrene oxide but led to slightly lower yield of the desired cyclization product. Although inclusion of a mild Lewis basic solvents did not have the desired effect on zwitterion longevity, it suggests that our active catalyst is not a Brønsted acid. Similar reaction performance when using THF also suggested that product-level inhibition of catalyst activity is likely only a minor contributor to reaction inefficiency.

Use of the moderately polar chlorinated solvents DCM ( $\epsilon$  8.93) and 1,2-DCE ( $\epsilon$  10.36) provided a minor improvement in yields whereas less polar solvents such as chloroform ( $\epsilon$  4.81) and carbon tetrachloride ( $\epsilon$  2.24) gave no enhancement.

These trends in solvent impact on yield hold true over a range of dilution (8 M to 2 M). No solvents were identified that substantially improved reactivity.

#### *2.2.4 Suppression of epoxide oligomerization through addition rate*

It seemed unlikely that modifying conditions would lead to substantial reduction in the rate of Meinwald rearrangement based on Lewis acid and solvent screening. Although suppression of the 1,2-hydride shift was not feasible, we attempted to prevent the reaction of the epoxide zwitterion with phenylacetaldehyde by keeping the relative concentration of epoxide low. The epoxide was added in a single portion under our initial conditions, leading to substantial formation of dimers and higher order oligomers. Under modified conditions, a portionwise addition protocol tested to minimize undesired reactions. Unfortunately, the rate of epoxide activation is fast enough that portionwise addition did not impact product distribution. Addition of styrene oxide as a DCM solution did not impact product distribution either. A slow overnight addition of styrene oxide to the solution was able to suppress the formation of higher order epoxide oligomers, leaving all epoxide reactivity funneled towards (3+2) cyclization, Meinwald rearrangement, and dimerization. Fortunately, these benefits were maintained with a 10 minute dropwise addition of epoxide. As such, a syringe pump controlled dropwise addition protocol was employed in further studies.

## 2.3 $\alpha$ -Methylstyrene and Styrene Oxide (3+2) Cyclizations

### 2.3.1 Selection of optimal C–C $\pi$ reaction partners

The difficulty faced in extending the lifetime of styrene oxide zwitterions spurred a search for more nucleophilic carbon-carbon  $\pi$ -bond coupling partners. Alkynes that cyclize with related ring opened aziridine zwitterions in excellent yields failed to provide any cyclization product on subjection to our reaction mixture. Allyl silanes, also competent reaction partners with aziridine zwitterions, gave a complex mixture of products with no determinable cyclization occurring. Substitution of styrene's aromatic ring gave the first improvement in yield: while *meta*-bromostyrene gave comparable yields to unsubstituted styrene (12 %), use of *meta*-chlorostyrene doubled the yield of the (3+2) cyclization product (17 %). Unfortunately, highly nucleophilic alkenes that would be expected to greatly outcompete epoxide degradation (e.g.: *para*-methoxystyrene and enols) polymerized immediately on exposure to competent Lewis acids. Although strong  $\pi$ -donor substituents failed to produce cyclized products,  $\sigma$ -donating substituents such as  $\alpha$ -methylstyrene offered a slight improvement in the yield of the desired (3+2) adduct without rapid alkene polymerization.

Although polymerization was slow, the amount of polymerization that did occur led to difficulty in stirring and generated widely varying yields for identical reactions. As DCM was previously determined to have negligible effect on the reaction, a small amount was added to aid in reaction homogeneity and stirring.

We determined that an 8 M solution of styrene in DCM was an appropriate dilution to maintain high styrene concentration while preventing solidification of the reaction mass.

### 2.3.2 Lewis acid screening for $\alpha$ -methylstyrene cyclizations

The Lewis acid catalysts determined to be effective for styrene-styrene oxide cyclization were rescreened using  $\alpha$ -methylstyrene and styrene oxide (**Table 2.4**). Interestingly, the higher conversion led to discernable differences in catalytic activity between metal triflates not previously observed in styrene-styrene oxide or intramolecular cyclizations.

**Table 2.4:** Lewis acid screening

Entry	Catalyst	<b>2.42</b> (%)	<b>2.43</b> (%)	<b>2.54</b> (%)
1	AgBF <sub>4</sub>	trace	20	2
2	AgPF <sub>6</sub>	trace	26	trace
3	AgSbF <sub>6</sub>	9	15	47
4	AgOTf	3	23	16
5	Cu(OTf) <sub>2</sub>	14	19	62
6	In(OTf) <sub>3</sub>	19	12	60
7	Yb(OTf) <sub>3</sub>	13	26	57
8	HOTf	28	13	trace
<b>9</b>	<b>Sc(OTf)<sub>3</sub></b>	<b>16</b>	<b>8</b>	<b>69</b>

Reactions performed on 2 mmol scale [8 M] in solvent, using 2:1 styrene:styrene oxide with 2 mol% Lewis acid catalyst. Room temp, 10 minute epoxide addition. Yields reported as corrected GC yields.



Although silver triflate was a competent catalyst for styrene-styrene oxide (3+2) cyclizations, it was a poor catalyst for generation of cycloadduct **2.54**. Interestingly, silver hexafluoroantimonate was alone amongst silver salts in its ability to promote (3+2) cyclization (**Table 2.4, Entries 1-4**). These unexpected trends may be due to variations in silver salt solubility or introduction of non-silver mediated reaction mechanisms. As previously predicted, more electrophilic metal triflates in +2 or +3 oxidation states gave cycloadduct **2.54** in highest yields (**Table 2.4, Entries 5-9**). Sc(OTf)<sub>3</sub> was selected as the Lewis acid of choice for further investigation.

To further probe the active catalytic species in our reaction, several control reactions were run with decreased loading of triflic acid. At the highest catalyst loadings, styrene polymerization occurs along with substantial decomposition of the epoxide. At lower triflic acid loading, formation of epoxide zwitterions outcompetes styrene polymerization but still does not reproduce the yields of **2.54** observed when using metal triflates. At the lowest loading triflic acid appears to lose catalytic ability. Triflic acid loadings over several orders of magnitude failed to reproduce the reactivity observed with metal triflates, further confirming a Lewis acid mediated process as the major contributor to product formation.

**Table 2.5:** Screening of triflic acid loading

Entry	mol% HOTf	<b>2.42</b> (%)	<b>2.43</b> (%)	<b>2.54</b> (%)
1	2	13	28	trace
2	0.1	n.d.	n.d.	19
3	0.01	n.d.	n.d.	3
4	0.001	trace	trace	trace

Reactions performed on 2 mmol scale [8 M] in DCM, using 2:1 styrene:styrene oxide with varying amounts of HOTf. Room temp, 10 minute epoxide addition. Yields reported as corrected GC yields.

### 2.3.3 Additional optimization of conditions

Exploration of additional reaction parameters such as solvent largely matched the results observed during screening of styrene-styrene oxide cyclizations (**Table 2.6**). Reactions performed in strongly coordinating solvents such as DMF and MeCN quenched the Lewis acidity of  $\text{Sc}(\text{OTf})_3$  leading to no consumption of epoxide. Interestingly, ethereal solvents such as THF and diethyl ether failed to give **2.54** despite full consumption of styrene oxide. This remains unexplained but has been observed in intramolecular (3+2) cyclizations. Chlorinated solvents were determined to perform best under these conditions.

**Table 2.6:** Screening of solvents

Entry	Solvent	<b>2.42</b> (%)	<b>2.43</b> (%)	<b>2.54</b> (%)
1	DMF	8	trace	trace
2	MeCN	14	trace	trace
3	THF	48	3	trace
4	Et <sub>2</sub> O	43	6	trace
5	DCM	14	9	29
6	1,2-DCE	14	12	23

Reactions performed on 2 mmol scale [4 M] in solvent, using 2:1 styrene:styrene oxide with 2 mol% Sc(OTf)<sub>3</sub>. Room temp, 10 minute epoxide addition. Yields reported as corrected GC yields.

As anticipated, the yield of cycloadduct **2.54** was heavily dependent on the relative concentration of  $\alpha$ -methylstyrene. In reactions run under high dilution (0.2 M styrene in DCM) only 10 % formation of the desired cyclization product was observed compared to 69 % obtained with 8 M styrene in DCM.

Increasing the number of equivalents of  $\alpha$ -methylstyrene employed was met with diminishing returns: whereas yields double between use of one and two equivalents of  $\alpha$ -methylstyrene, exceeding two equivalents affords no improvement in yield.

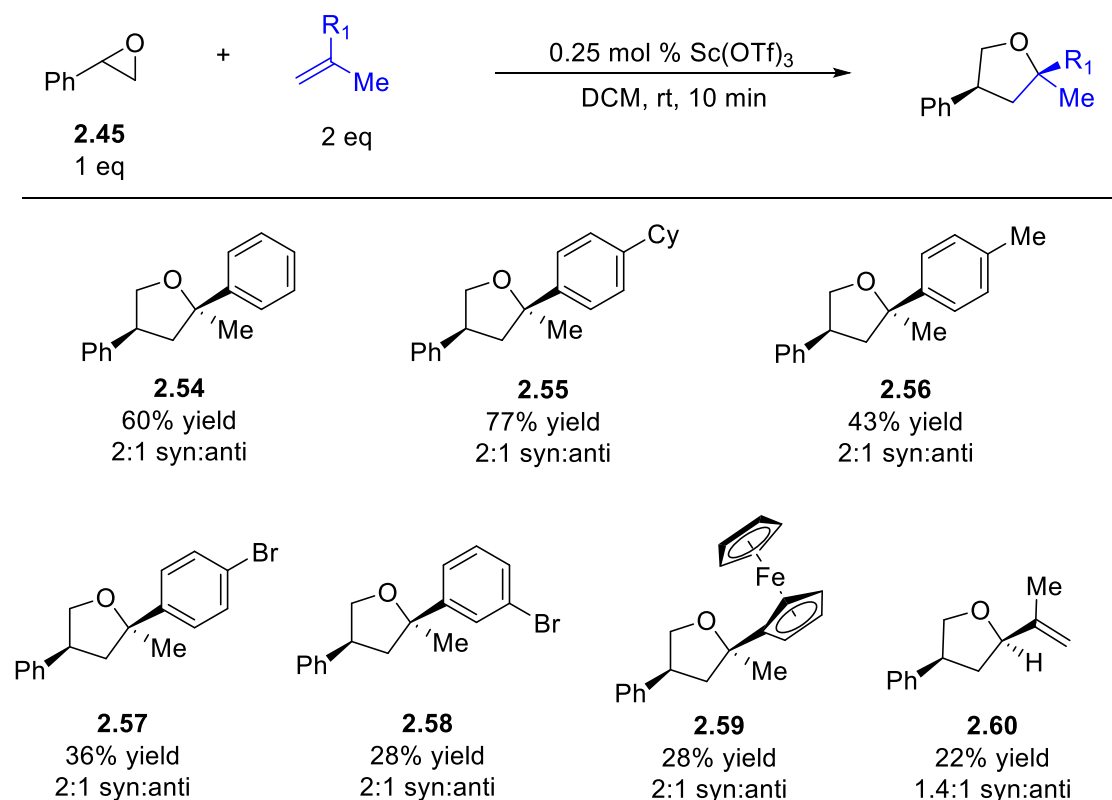
Several temperatures were screened in a final attempt to better control the fate of the epoxide zwitterion. While decreasing temperatures may have had a positive effect on the lifetime of the intermediate, this was offset by decreased

alkene nucleophilicity. The yield of the (3+2) cycloadduct is decreased to 53% at -15 °C and less than 5% at -40 °C. The decrease in yield observed below -20 °C is concurrent with a decrease in styrene oxide consumption, suggesting that Sc(OTf)<sub>3</sub> may be insoluble at lower temperatures. Elevated temperatures led to polymerization of both  $\alpha$ -methylstyrene and styrene oxide. Ultimately, we determined that dropwise addition of styrene oxide to a room temperature, 8 M solution of  $\alpha$ -methylstyrene in DCM containing 2 mol% Sc(OTf)<sub>3</sub> was optimal for biasing epoxide zwitterion reactivity towards cyclization products.

## 2.4 Scope of Reaction Partners

### 2.4.1 Alkene reactivity

With optimized conditions in hand, we examined the scope of alkene partners capable of engaging in epoxy-alkene (3+2) cyclizations (**Table 2.7**). Although several halogenated and alkylated  $\alpha$ -methylstyrenes generated tetrahydrofuran products in modest to good yields, the yields do not consistently match anticipated trends in nucleophilicity. *Para*-cyclohexyl substituted  $\alpha$ -methylstyrene gave 77% yield of the cycloadduct whereas *para*-methyl substituted  $\alpha$ -methylstyrene provided only 43% yield, despite similar predicted nucleophilicity. The substitution patterns present on the aryl ring may impart substantial changes to the colligative properties of the reaction due to the high concentrations employed.

**Table 2.7:** Scope of alkene reaction partners

Reactions performed on 2 mmol scale [8 M] in solvent, using 2:1 styrene:styrene oxide with 0.25 mol%  $\text{Sc(OTf)}_3$ . Room temp, 10 minute epoxide addition. Yields reported are of isolated material after purification. Diastereoselectivity was assessed by crude  $^1\text{H-NMR}$ .

Unlike alkyl substituted  $\alpha$ -methylstyrenes, brominated styrenes match well with predicted trends. Ferrocene derived  $\alpha$ -methylstyrene gave substantially lower yields likely due to additional dilution required to fully solubilize the material- again highlighting the importance of high reaction concentration. Overall, the tetrahydrofuran products formed were obtained in modest 2:1 diastereoselectivity with a similar preference for *syn* ring geometry as observed in Fe(I) catalyzed radical (3+2) cyclizations.

The scope of tolerated alkenes was largely limited to electron-neutral substitutions due to limitations observed in optimization studies. Under optimized conditions, highly nucleophilic alkenes such as *para*-methoxy- $\alpha$ -methylstyrene and *para*-dimethylamino- $\alpha$ -methylstyrene polymerized on exposure to Sc(OTf)<sub>3</sub> across a range of temperatures from -40 °C to room temperature. Alkenes possessing strongly coordinating substituents (e.g.: vinyl pyridine) halted catalytic activity of Sc(OTf)<sub>3</sub> from loadings between 2 and 10 mol%.

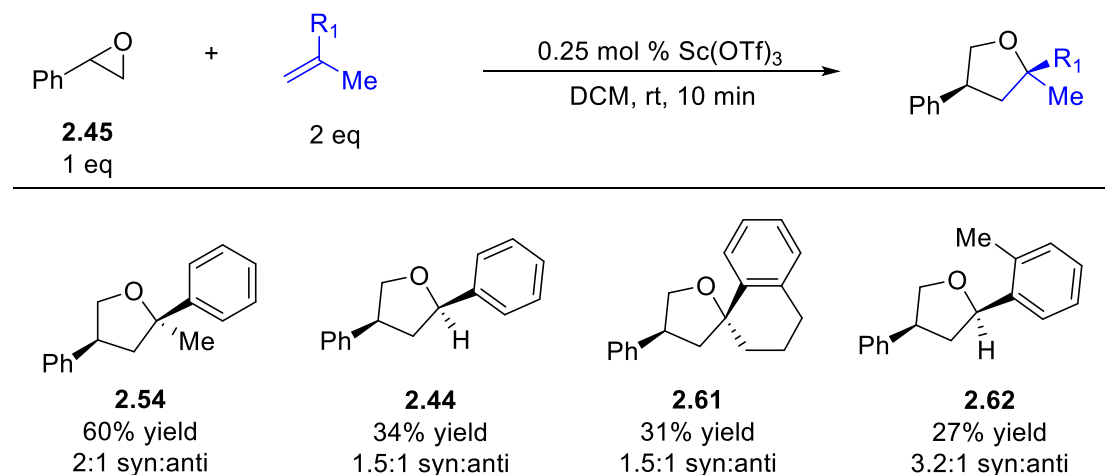
Resonance stabilization of the alkene-based carbocation proved to be essential for reactivity. Alkenes with tertiary allylic resonance stabilization such as 2,3-dimethylbutadiene afforded tetrahydrofuran product **2.60** in 22% yield. Alkenes lacking aryl or allylic stabilization gave tetrahydrofurans in trace quantities. For example, both methylenecyclopentane and methylenecyclohexane afforded THF products in less than 10% yield. Additional limitations include a lack of tolerance for 1,2-disubstituted styrenes which formed tetrahydrofurans as a low yielding complex mixture of diastereomers.

#### 2.4.2 Alkene substitution impact on diastereoselectivity

Alkenes with substitution remote from the reaction site showed a consistent preference for the formation of *syn* ring geometry in the THF ring (2:1 *d.r.*). This distribution was confirmed to be under kinetic control by exposing diastereomerically enriched product to the reaction conditions. Due to the small energy differences between conformers, likely less than 1 kcal/mol, a predictive

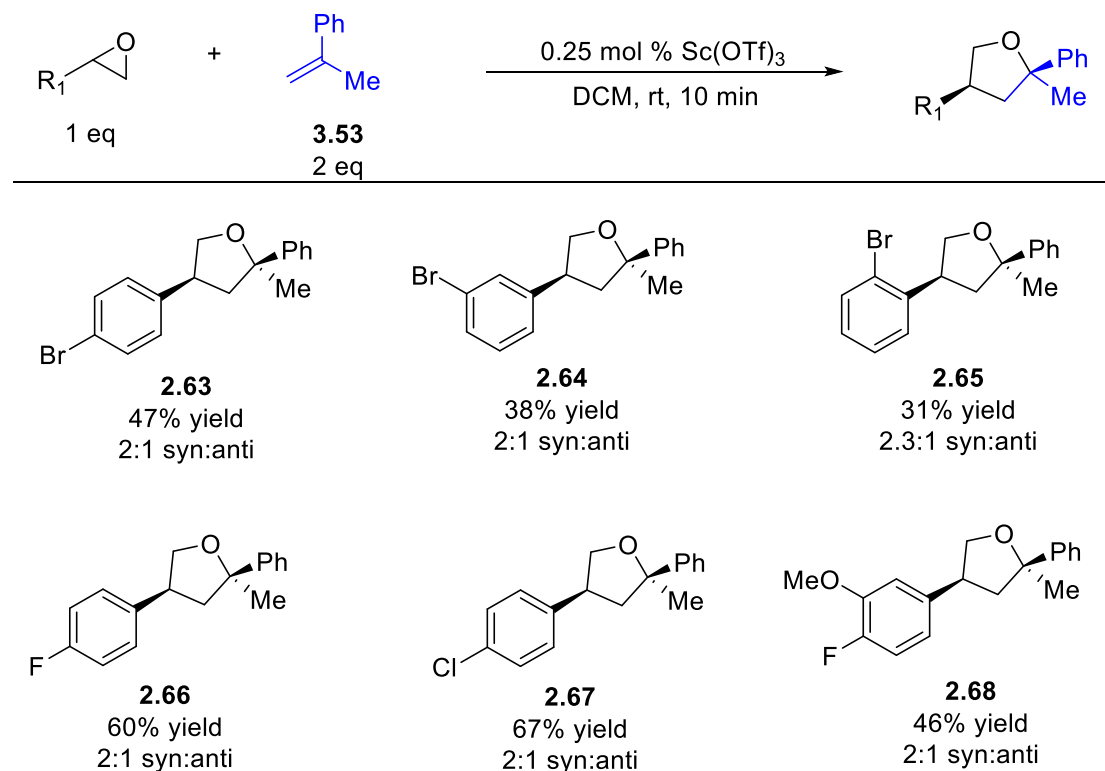
transition state model was unable to be developed. Diastereoselectivity of the reaction can be modulated by use of sterically encumbered alkenes (**Table 2.8**).

**Table 2.8:** Impact of alkene substitution on diastereoselectivity



Reactions performed on 2 mmol scale [8 M] in solvent, using 2:1 styrene:styrene oxide with 0.25 mol% Sc(OTf)<sub>3</sub>. Room temp, 10 minute epoxide addition. Yields reported are of isolated material after purification. Diastereoselectivity was assessed by crude <sup>1</sup>H-NMR.

## 2.4.3 Scope of epoxide cyclization partners

**Table 2.9:** Scope of epoxide reaction partners

Reactions performed on 2 mmol scale [8 M] in solvent, using 2:1 styrene:styrene oxide with 0.25 mol% Sc(OTf)<sub>3</sub>. Room temp, 10 minute epoxide addition. Yields reported are of isolated material after purification. Diastereoselectivity was assessed by crude <sup>1</sup>H-NMR.

A variety of substituted aryl epoxides provided isolable quantities of (3+2) cyclization products on exposure to the reaction conditions (**Table 2.9**). Epoxides with stronger carbocation destabilizing groups such as *meta*-halogenation provided lower yields likely due to C–O cleaved epoxide zwitterion instability. In a series of brominated epoxides, *para*-bromostyrene oxide gave tetrahydrofuran **2.63** in 47% yield followed by *meta*-bromostyrene oxide giving tetrahydrofuran **2.64** in 38% yield. *Ortho*-bromostyrene oxide provided (3+2) adduct **2.65** in low yields



due to a combination of electronic and steric effects as evidenced by the altered diastereoselectivity of the transformation. Electron rich epoxides, including  $\alpha$ -substituted epoxides, failed to provide tetrahydrofuran products. Additionally, epoxides with non-aryl resonance stabilization such as vinyl oxirane failed to provide products.

We probed whether complete C–O bond scission occurs by subjecting enantiopure (*R*)-styrene oxide to a cyclization reaction with *meta*-bromo- $\alpha$ -methylstyrene. Upon conclusion of the reaction, a racemic tetrahydrofuran product was obtained, supporting the intermediacy of a carbocation. No racemization was observed when enantioenriched products were exposed to the reaction conditions, further confirming this hypothesis.

## 2.5 Exploration of chiral catalysts

Strong literature precedence exists for related *enantioselective* dipolar (3+2) cycloadditions.<sup>17</sup> As there was substantially more literature precedent surrounding L<sup>\*</sup>Cu(OTf)<sub>2</sub> catalyzed reactions, screening of ligands was conducted with both Cu(OTf)<sub>2</sub> and Sc(OTf)<sub>3</sub>.

Unfortunately, initial screening of  $\alpha$ -methylstyrene-styrene oxide cyclizations using (*R*)-BINAP or (*S,S*)-diphenylBOX with either Sc(OTf)<sub>3</sub> or Cu(OTf)<sub>2</sub> failed to produce enantioenriched products. Additionally, investigation of Jacobsen's catalyst- known to catalyze asymmetric addition of alkenes to epoxides<sup>18</sup>- failed to provide any desired tetrahydrofuran product.

This lack of enantioselectivity could be explained by the reaction partners chosen for investigation: unfortunately, partners that operate well under our reaction conditions lack the chelation sites necessary for introducing rigidity in the transition state of the enantiomer determining step. Without these structural features, freely rotating bonds make it more unlikely that an enantioselective transformation will occur.

## 2.6 Conclusions

We have discovered the first example of a (3+2) intermolecular cyclization reaction between carbon-carbon  $\pi$  systems and C–O bond cleaved epoxide zwitterions. The conditions employed utilize high concentrations of reaction partners, slow addition of epoxides, and low catalyst loading to circumvent the known instability of epoxide zwitterions.

Investigation into additional reaction partners should be undertaken to truly capitalize on the reactivity of these with the ultimate goal of identifying reaction partners with nucleophilicity sufficient to outcompete the rapid degradation of unstabilized zwitterions, allowing for broad reactivity across multiple classes of reaction partners likely to be present in natural product total synthesis efforts. Additionally, efforts should be focused on identifying reaction partners with chelation sites, which should allow enantioselective transformations to take place.

## 2.7 Experimental Details

### 2.7.1 General methods

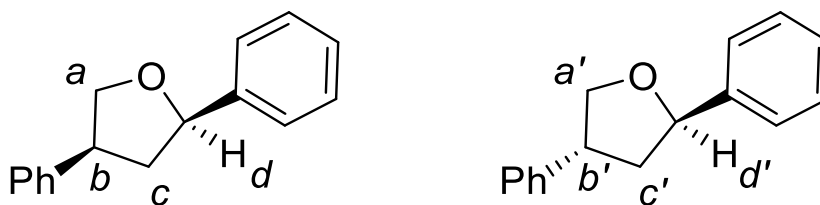
All commercially obtained reagents were obtained in the highest grade and used as received. Dichloromethane was purified by degassing with argon and drying through alumina columns. Flash column chromatography was conducted with 230-400 mesh silica gel purchased from Fisher Scientific.  $^1\text{H}$ ,  $^{13}\text{C}$ , and  $^{19}\text{F}$  NMR spectra were acquired at 300 K on Bruker or Varian spectrometers at 600 Mhz. Chemical shifts are reported in parts per million (ppm  $\delta$ ) referenced to the residual  $^1\text{H}$  peak of the solvent. The following abbreviations are used to indicate signal multiplicity: s - singlet, d - doublet, t - triplet, q - quartet, m - multiplet and br - broad. Gas chromatography was performed using an Agilent 7820A GC with FID detector, using *n*-dodecane as an internal standard for GC yield calculations. Normal phase chiral HPLC was performed using an Agilent 1260 HPLC equipped with a diode-array detector. IR spectra were recorded on a Thermo Scientific Nicolet iS5 with iD5 ATR attachment. High resolution mass spectrometry was performed by the University of Illinois at Urbana-Champaign Mass Spectrometry Lab using Waters Q-TOF ESI or Waters oa-TOF EI spectrometers.

### 2.7.2 General procedure for Lewis acid catalyzed [3+2] cyclizations

To a 5 mL round bottom flask containing  $\text{Sc}(\text{OTf})_3$  under  $\text{N}_2$  atmosphere was added 2 eq. styrene (8 M in DCM). Styrene oxide was added dropwise over 10 minutes via syringe pump with vigorous stirring. Upon completion the crude

product was loaded directly onto a silica column and eluted with EtOAc/hexanes. Diastereoselectivity was assessed by  $^1\text{H}$  NMR of the purified product. Diastereomeric assignment was conducted based on previous literature reports or by analogy.

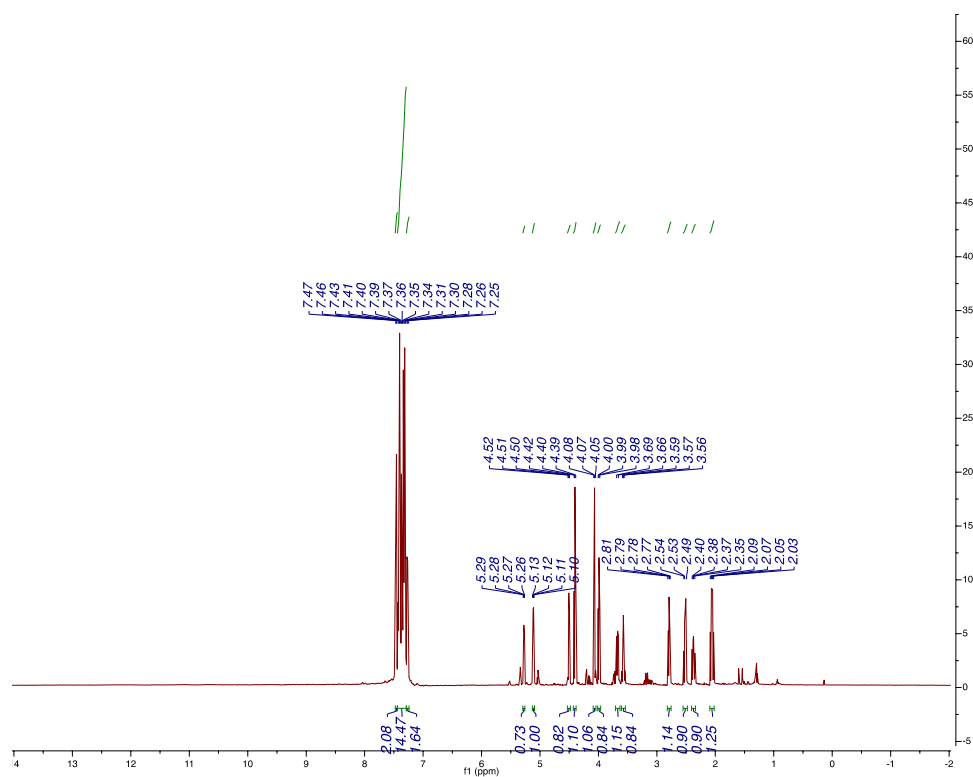
### 2.7.3 Characterization of reaction products

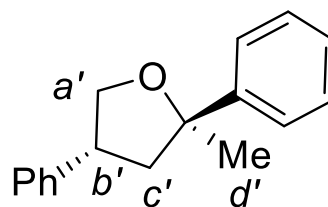
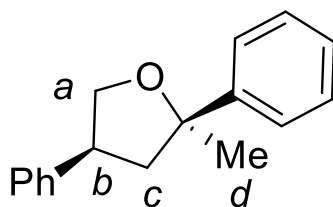
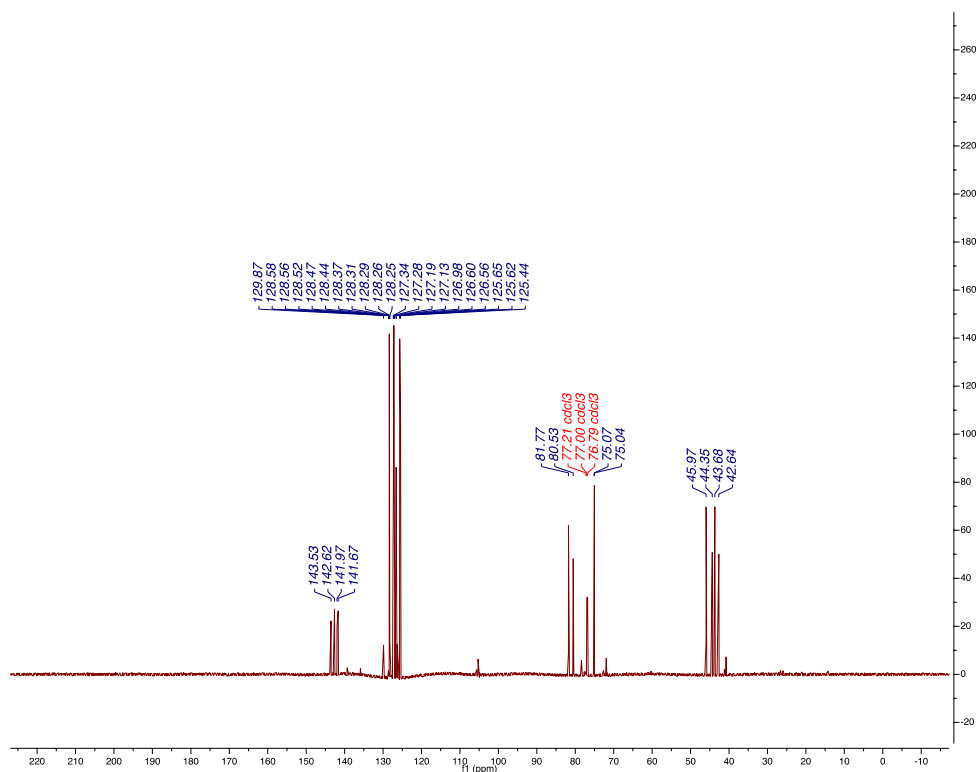


#### 2,4-Diphenyltetrahydrofuran (2.44)

Following the general procedure, a RBF was loaded with  $\text{Sc}(\text{OTf})_3$  (0.01 mmol, 5.2 mg), DCM (0.5 mL), and styrene (4 mmol, 0.46 mL). 2-Phenyloxirane (2 mmol, 0.23 mL) was added dropwise by syringe over 10 min. After addition was complete, the crude reaction mixture was loaded onto a silica column and eluted with ethyl acetate:hexanes (hexanes to 2 % EtOAc/hexanes) to afford product as a colorless oil in 34 % yield (0.68 mmol, 153 mg, crude dr: 1.5:1 syn:anti, isolated dr: 1.4:1 syn:anti). All spectral data were consistent with literature values.<sup>13</sup>).  $^1\text{H}$  NMR (598 MHz,  $\text{CDCl}_3$ ): *syn* diastereomer:  $\delta$  7.46 (d,  $J = 7.3$  Hz, 2H), 7.44 – 7.29 (m, 14H), 7.29 – 7.24 (m, 2H), 5.11 ( $\text{H}_d$ , dd,  $J = 10.2, 5.7$  Hz, 1H), 4.40 ( $\text{H}_a$ , t,  $J = 8.2$  Hz, 1H), 4.07 ( $\text{H}_a$ , t,  $J = 8.5$  Hz, 1H), 3.61 – 3.54 ( $\text{H}_b$ , m, 1H), 2.82 – 2.76 ( $\text{H}_c$ , m, 1H), 2.09 – 2.02 ( $\text{H}_c$ , m, 1H).; further signals for the *anti* diastereomer:  $\delta$  5.28 ( $\text{H}_{d'}$ , dd,  $J = 7.6, 5.9$  Hz, 1H), 4.53 – 4.48 ( $\text{H}_{a'}$ , m, 1H), 3.99 ( $\text{H}_{a'}$ , t,  $J = 8.2$  Hz, 1H), 3.67 ( $\text{H}_{b'}$ ,

d,  $J = 18.4$  Hz, 1H), 2.41 – 2.34 (H<sub>c</sub>, m, 1H), 2.55 – 2.48 (H<sub>c</sub>, m, 1H). <sup>13</sup>C NMR (150 MHz, CDCl<sub>3</sub>)  $\delta$  142.62, 141.67, 128.56, 128.31, 127.28, 127.19, 126.60, 125.65, 81.77, 77.21, 77.00, 76.79, 75.04, 45.97, 43.68; further signals for the *anti* diastereomer:  $\delta$  143.53, 141.97, 128.58, 128.37, 127.34, 127.13, 126.56, 125.44, 80.53, 75.07, 44.35, 42.64.



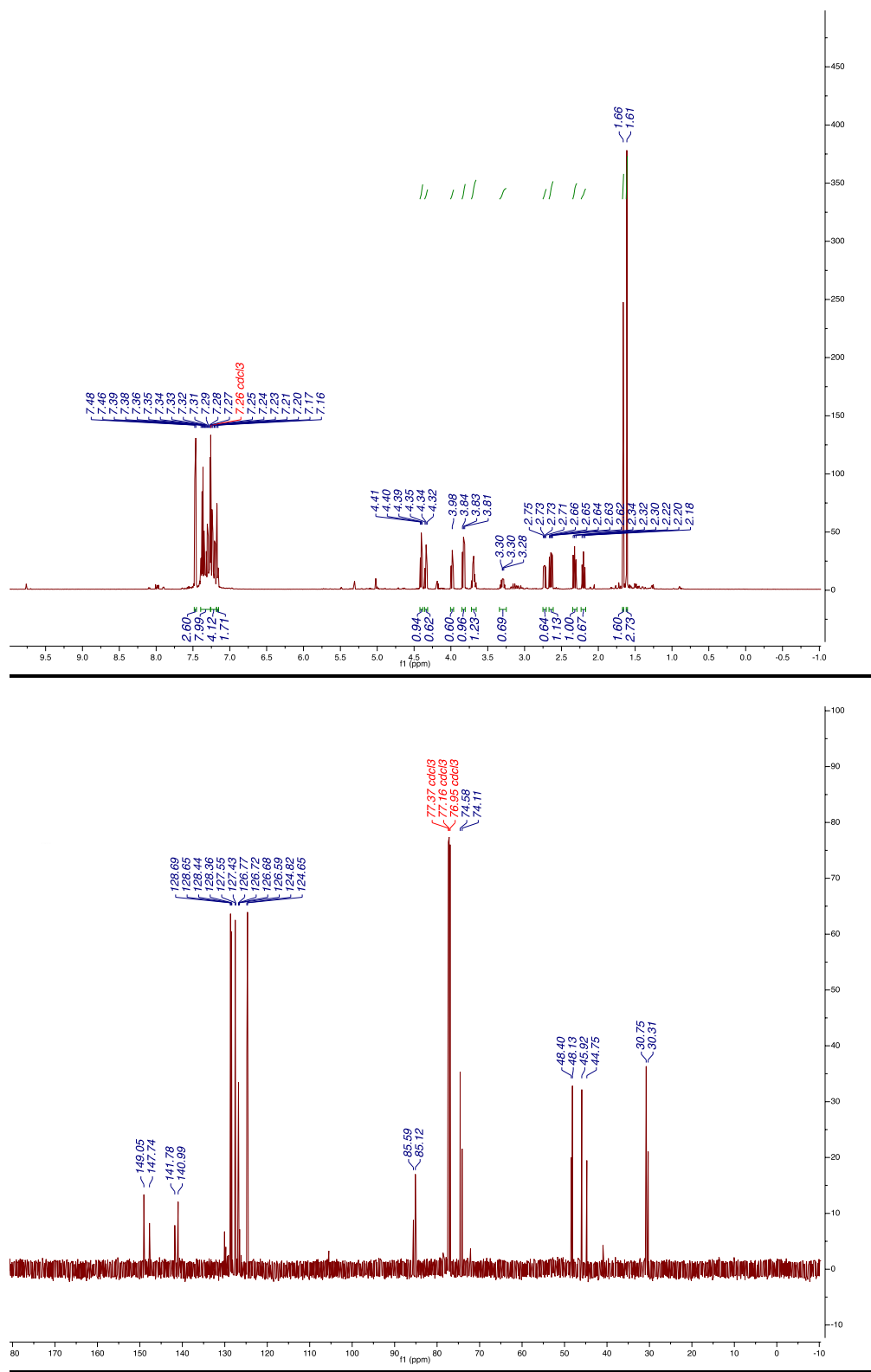


### 2-Methyl-2,4-diphenyltetrahydrofuran (2.54)

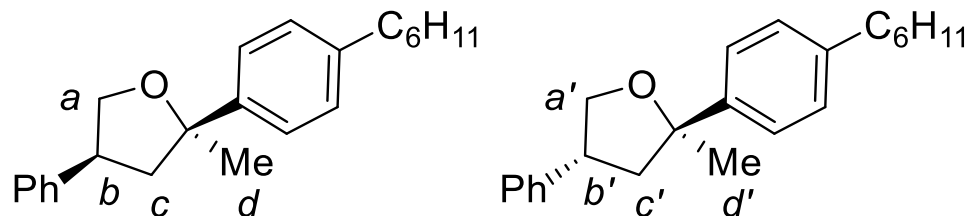
Following the general procedure, a RBF was loaded with Sc(OTf)<sub>3</sub> (0.005 mmol, 2.5 mg), DCM (0.5 mL), and 1-methyl-1-phenylethene (4 mmol, 0.52 mL). 1-Phenyloxirane (2 mmol, 0.23 mL) was added dropwise by syringe over 10 min. After addition was complete, the crude reaction mixture was loaded onto a silica column and eluted with ethyl acetate:hexanes (hexanes to 5 % EtOAc/hexanes) to afford

product as a colorless oil in 60 % yield (1.2 mmol, 286 mg, crude dr: 2:1 syn:anti, isolated dr: 1.5:1 syn:anti). All spectral data were consistent with literature values.<sup>13</sup>

<sup>1</sup>H NMR (598 MHz, CDCl<sub>3</sub>): *syn* diastereomer:  $\delta$  7.47 (d,  $J$  = 9.0 Hz, 3H), 7.40 – 7.26 (m, 8H), 7.26 – 7.18 (m, 4H), 7.17 (d,  $J$  = 7.5 Hz, 2H), 4.40 (H<sub>a</sub>, t,  $J$  = 8.0 Hz, 1H), 3.85 – 3.81 (H<sub>a</sub>, m, 1H), 3.72 – 3.66 (H<sub>b</sub>, m, 1H), 2.67 – 2.61 (H<sub>c</sub>, m, 1H), 2.35 – 2.29 (H<sub>c</sub>, m, 1H), 1.61 (H<sub>d</sub>, s, 3H).; further signals for the *anti* diastereomer:  $\delta$  4.34 (H<sub>a'</sub>, t,  $J$  = 8.4 Hz, 1H), 3.98 (H<sub>a'</sub>, t,  $J$  = 8.7 Hz, 1H), 3.30 (H<sub>b'</sub>, dd,  $J$  = 11.2, 7.8 Hz, 1H), 2.73 (H<sub>c'</sub>, dd,  $J$  = 12.2, 7.1 Hz, 1H), 2.20 (H<sub>c'</sub>, t,  $J$  = 11.8 Hz, 1H), 1.66 (H<sub>d'</sub>, s, 3H). <sup>13</sup>C NMR (150 MHz, CDCl<sub>3</sub>)  $\delta$  149.05, 141.78, 128.65, 128.44, 127.55, 126.77, 126.59, 124.65, 85.12, 77.37, 77.16, 76.95, 74.58, 48.13, 45.92, 30.75; further signals for the *anti* diastereomer:  $\delta$  147.74, 140.99, 128.69, 128.36, 127.43, 126.72, 126.68, 124.82, 85.59, 74.11, 48.40, 44.75, 30.31.



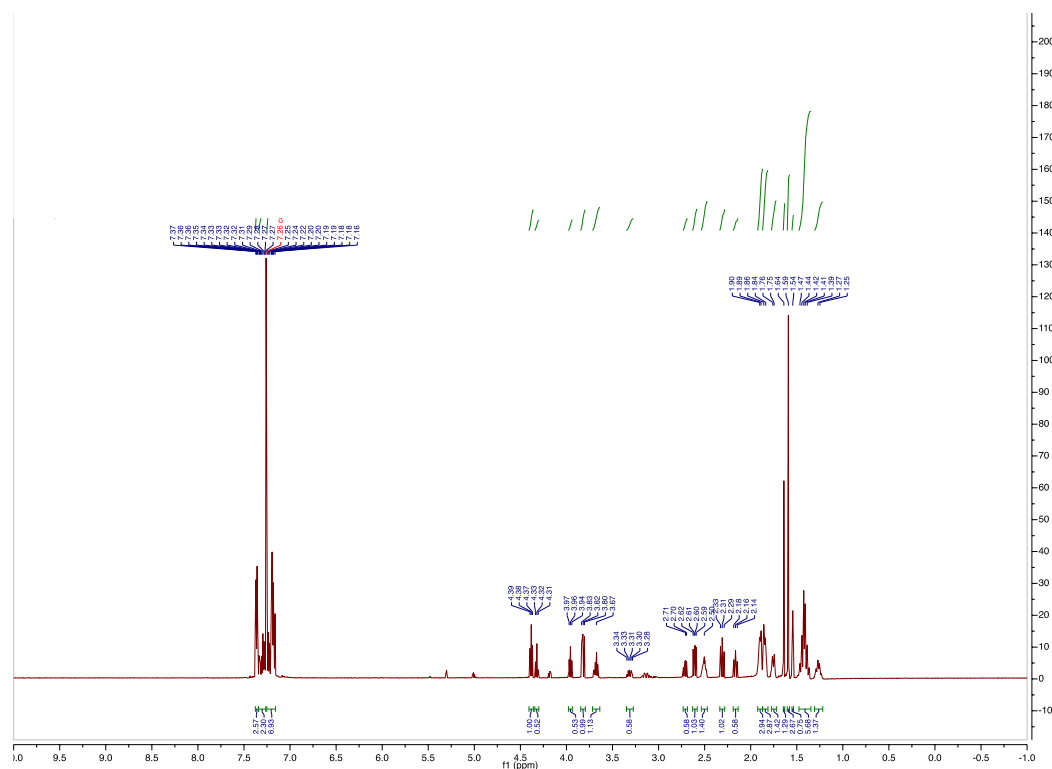


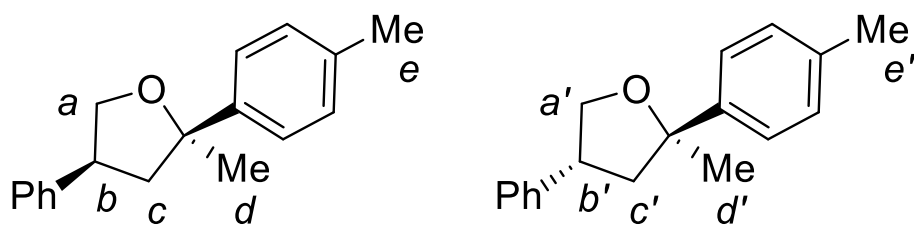
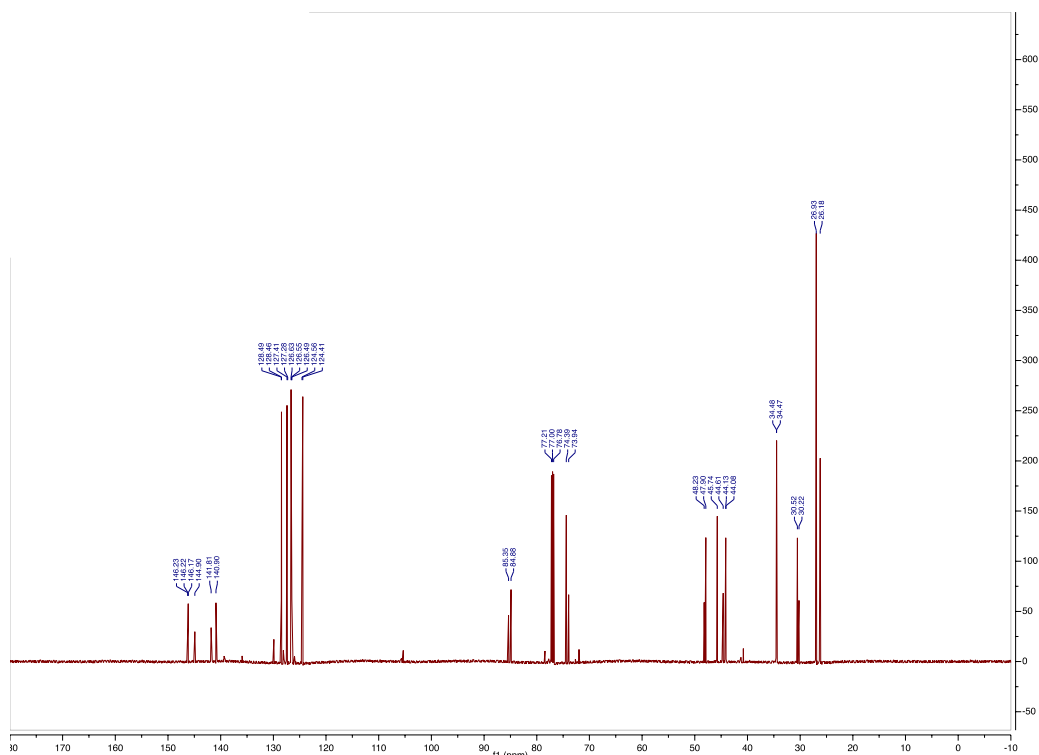


### 2-(4-Cyclohexylphenyl)-2-methyl-4-phenyltetrahydrofuran (2.55)

Following the general procedure, a RBF was loaded with  $\text{Sc}(\text{OTf})_3$  (0.0044 mmol, 2.2 mg), DCM (0.44 mL), and 1-methyl-1-(4-cyclohexylphenyl)ethene (3.5 mmol, 0.76 mL). 1-Phenyloxirane (1.8 mmol, 0.21 mL) was added dropwise by syringe over 10 min. After addition was complete, the crude reaction mixture was loaded onto a silica column and eluted with DCM:hexanes (1:3 to 1:1) to afford product as a colorless oil in 77 % yield (1.5 mmol, 492 mg, crude dr: 2:1 syn:anti, isolated dr: 1.8:1 syn:anti).  $^1\text{H}$  NMR (598 MHz,  $\text{CDCl}_3$ ): *syn* diastereomer:  $\delta$  7.39 – 7.16 (ArH, m, 9H), 4.39 ( $\text{H}_a$ , t,  $J$  = 8.0 Hz, 1H), 3.86 – 3.80 ( $\text{H}_a$ , m, 1H), 3.72 – 3.64 ( $\text{H}_b$ , m, 1H), 2.61 ( $\text{H}_c$ , dd,  $J$  = 12.4, 7.9 Hz, 1H), 2.32 ( $\text{H}_c$ , dd,  $J$  = 12.3, 10.8 Hz, 1H), 1.94 – 1.83 (CyH, m, 5H), 1.60 ( $\text{H}_d$ , s, 3H), 1.49 – 1.35 (CyH, m, 6H); further signals for the *anti* diastereomer:  $\delta$  7.38 – 7.19 (ArH, m, 9H), 4.33 ( $\text{H}_{a'}$ , t,  $J$  = 8.3 Hz, 1H), 3.96 ( $\text{H}_{a'}$ , t,  $J$  = 8.6 Hz, 1H), 3.32 ( $\text{H}_{b'}$ , dq,  $J$  = 11.3, 8.3 Hz, 1H), 2.72 ( $\text{H}_{c'}$ , dd,  $J$  = 12.1, 7.2 Hz, 1H), 2.51 ( $\text{H}_{c'}$ , tdd,  $J$  = 11.8, 5.5, 3.2 Hz, 2H), 2.20 – 2.14 (m, 1H), 1.79 – 1.72 (m, 3H), 1.33 – 1.22 (m, 4H).  $^{13}\text{C}$  NMR (150 MHz,  $\text{CDCl}_3$ )  $\delta$  146.38, 146.33, 141.07, 128.62, 127.57, 126.80, 126.72, 124.57, 85.04, 74.56, 48.06, 45.90, 44.29, 34.64, 30.68, 27.10; further signals for the *anti* diastereomer:  $\delta$  146.40, 145.06, 141.97, 128.65, 127.44, 126.65, 126.51, 124.72, 85.51, 74.10, 48.39,

44.78, 44.25, 34.65, 30.38, 26.35. IR (film):  $\bar{\nu}$  = 2844 (w), 2787 (w), 1508 (m), 1050 (m), 826 (s)  $\text{cm}^{-1}$ . HRMS (EI):  $m/z$  calcd for  $[\text{C}_{23}\text{H}_{28}\text{O}]^+$ : 320.2140; found: 320.2141.

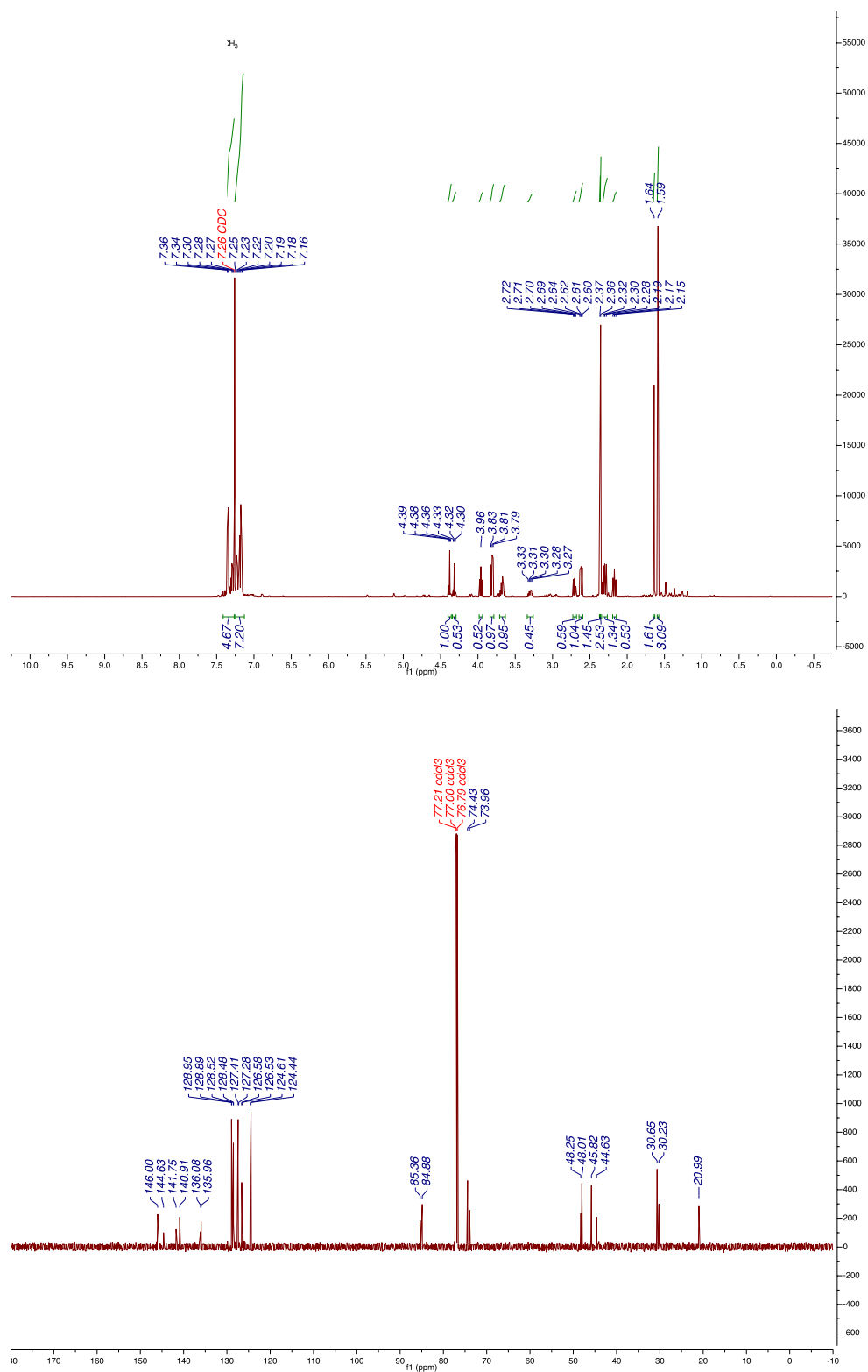


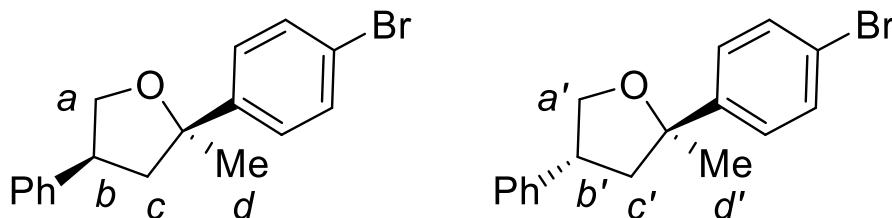


### 2-Methyl-4-phenyl-2-(*p*-tolyl)tetrahydrofuran (2.56)

Following the general procedure, a RBF was loaded with  $\text{Sc}(\text{OTf})_3$  (0.005 mmol, 2.9 mg), DCM (0.5 mL), and 1-methyl-4-(prop-1-en-2-yl)benzene (4 mmol, 527 mg). 1-Phenyloxirane (2 mmol, 0.23 ml) was added dropwise by syringe over 10 min. After addition was complete, the crude reaction mixture was loaded onto a silica column and eluted with ethyl acetate:hexanes (hexanes to 3 %

EtoAc/hexanes) to afford product as a colorless oil in 43 % yield (0.86 mmol, 217 mg, crude dr: 2:1 *syn*:*anti*, isolated dr: 1.9:1 *syn*:*anti*).  $^1\text{H}$  NMR (600 MHz,  $\text{CDCl}_3$ ) *syn* diastereomer  $\delta$  7.41 – 7.27 (ArH, m, 5H), 7.26 – 7.13 (ArH, m, 7H), 4.38 ( $\text{H}_a$ , t,  $J$  = 8.0 Hz, 1H), 3.84 – 3.79 ( $\text{H}_a$ , m, 1H), 3.71 – 3.63 ( $\text{H}_b$ , m, 1H), 2.62 ( $\text{H}_c$ , dd,  $J$  = 12.4, 8.0 Hz, 1H), 2.36 ( $\text{H}_e$ , s, 3H), 2.33 – 2.27 ( $\text{H}_c$ , m, 1H), 1.59 ( $\text{H}_d$ , s, 3H); further signals for the *anti* diastereomer:  $\delta$  4.32 ( $\text{H}_a'$ , t,  $J$  = 8.4 Hz, 1H), 3.96 ( $\text{H}_a'$ , t,  $J$  = 8.7 Hz, 1H), 3.34 – 3.26 ( $\text{H}_b'$ , m, 1H), 2.70 ( $\text{H}_c'$ , dd,  $J$  = 12.1, 7.1 Hz, 1H), 2.37 ( $\text{H}_e'$ , s, 3H), 2.17 ( $\text{H}_c'$ , t,  $J$  = 11.7 Hz, 1H), 1.64 ( $\text{H}_d'$ , s, 3H).  $^{13}\text{C}$  NMR (151 MHz,  $\text{CDCl}_3$ ): *syn* diastereomer:  $\delta$  146.00, 140.91, 135.96, 128.95, 128.48, 127.41, 126.58, 124.44, 84.88, 74.43, 48.01, 45.82, 30.65, 20.99; further signals for the *anti* diastereomer:  $\delta$  144.63, 141.75, 136.08, 128.89, 128.52, 127.28, 126.53, 124.61, 85.36, 73.96, 48.25, 44.63, 30.23. IR (film):  $\bar{\nu}$  = 3029 (w), 2971 (w), 2867 (w), 817 (m), 698 (s)  $\text{cm}^{-1}$ . HRMS (EI):  $m/z$  calcd for  $[\text{C}_{18}\text{H}_{20}\text{O}]^+$ : 252.1514; found: 252.1516.

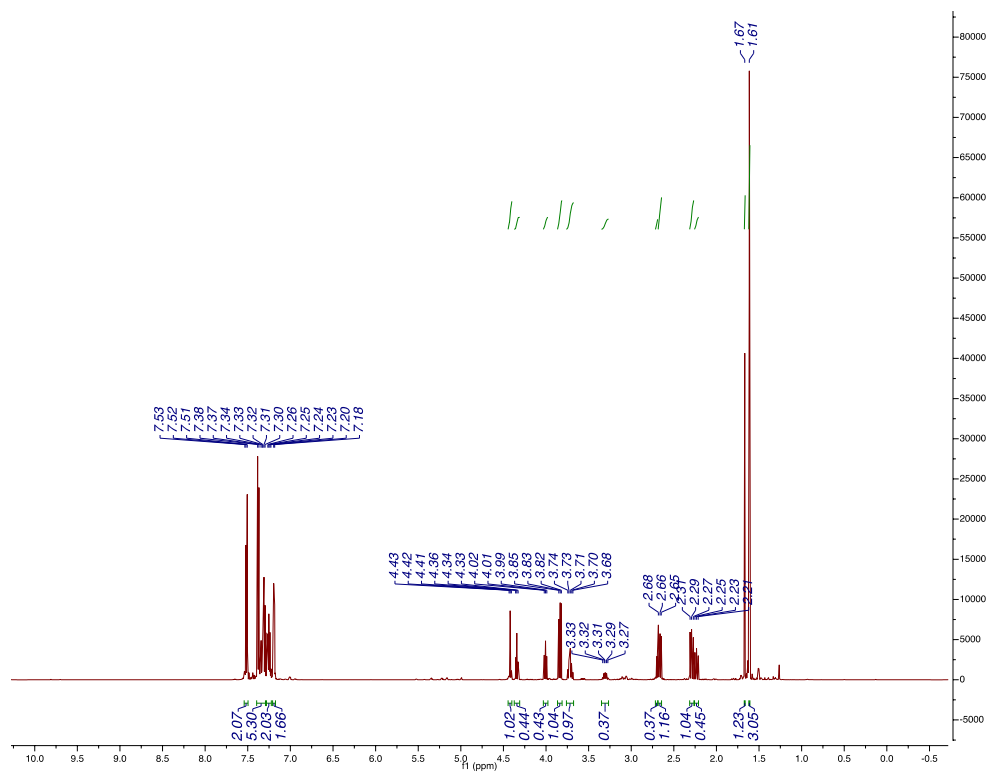


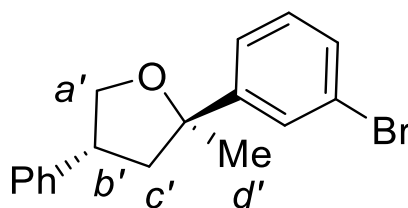
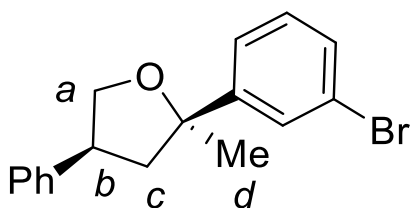
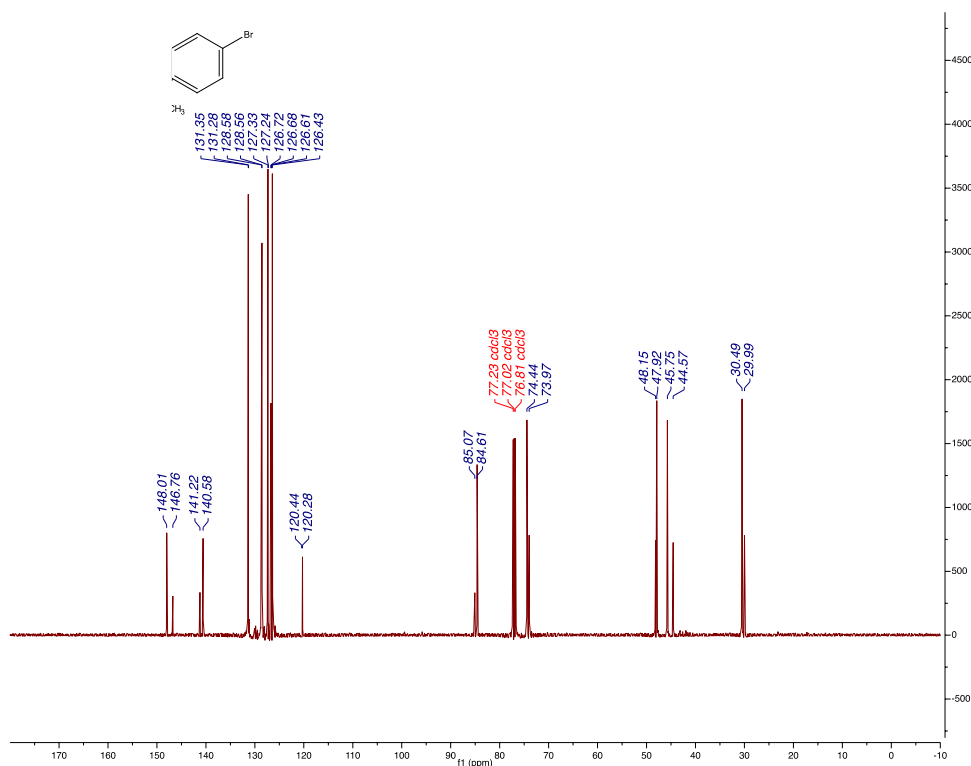


### 2-(4-Bromophenyl)-2-methyl-4-phenyltetrahydrofuran (2.57)

Following the general procedure, a RBF was loaded with  $\text{Sc}(\text{OTf})_3$  (0.005 mmol, 2.5 mg), DCM (0.5 mL), and 1-methyl-1-(4-bromophenyl)ethene (4 mmol, 781 mg). 1-Phenyloxirane (2 mmol, 0.23 ml) was added dropwise by syringe over 10 min. After addition was complete, the crude reaction mixture was loaded onto a silica column and eluted with ethyl acetate:hexanes (hexanes to 2 % EtOAc/hexanes) to afford product as a colorless oil in 36 % yield (0.72 mmol, 228 mg, crude dr: 2:1 syn:anti, isolated dr: 2.5:1 syn:anti).  $^1\text{H}$  NMR (600 MHz,  $\text{CDCl}_3$ ): *syn* diastereomer:  $\delta$  7.51 – 7.47 (ArH, m, 2H), 7.37 – 7.26 (ArH, m, 5H), 7.25 – 7.19 (ArH, m, 2H), 7.16 (ArH, dd,  $J$  = 8.3, 1.2 Hz, 2H), 4.39 ( $\text{H}_a$ , t,  $J$  = 8.0 Hz, 1H), 3.81 ( $\text{H}_a$ , dd,  $J$  = 9.9, 8.5 Hz, 1H), 3.72 – 3.65 ( $\text{H}_b$ , m, 1H), 2.64 ( $\text{H}_c$ , dd,  $J$  = 12.3, 7.8 Hz, 1H), 2.26 ( $\text{H}_c$ , dd,  $J$  = 12.4, 10.6 Hz, 1H), 1.59 ( $\text{H}_d$ , s, 3H); further signals for the *anti* diastereomer:  $\delta$  4.31 ( $\text{H}_{a'}$ , t,  $J$  = 8.4 Hz, 1H), 3.98 ( $\text{H}_{a'}$ , t,  $J$  = 8.8 Hz, 1H), 3.31 – 3.25 ( $\text{H}_{b'}$ , m, 1H), 2.69 – 2.66 ( $\text{H}_{c'}$ , m, 1H), 2.21 ( $\text{H}_{c'}$ , dd,  $J$  = 12.2, 11.5 Hz, 1H), 1.64 ( $\text{H}_{d'}$ , s, 3H).  $^{13}\text{C}$  NMR (151 MHz,  $\text{CDCl}_3$ ): *syn* diastereomer:  $\delta$  148.15, 140.72, 131.49, 128.70, 127.47, 126.85, 126.57, 120.42, 84.75, 74.58, 48.06, 45.89, 30.63; further signals for the *anti* diastereomer:  $\delta$  146.90, 141.36, 131.42, 128.72, 127.38, 126.82, 126.75, 120.58, 85.21, 74.11, 48.29, 44.71, 30.13. IR (film):  $\bar{\nu}$  =

3028 (w), 2975 (w), 2865 (w), 785 (m), 697 (s)  $\text{cm}^{-1}$ . HRMS (EI):  $m/z$  calcd for  $[\text{C}_{17}\text{H}_{17}\text{OBr}]^+$ : 316.0463; found: 316.0468.



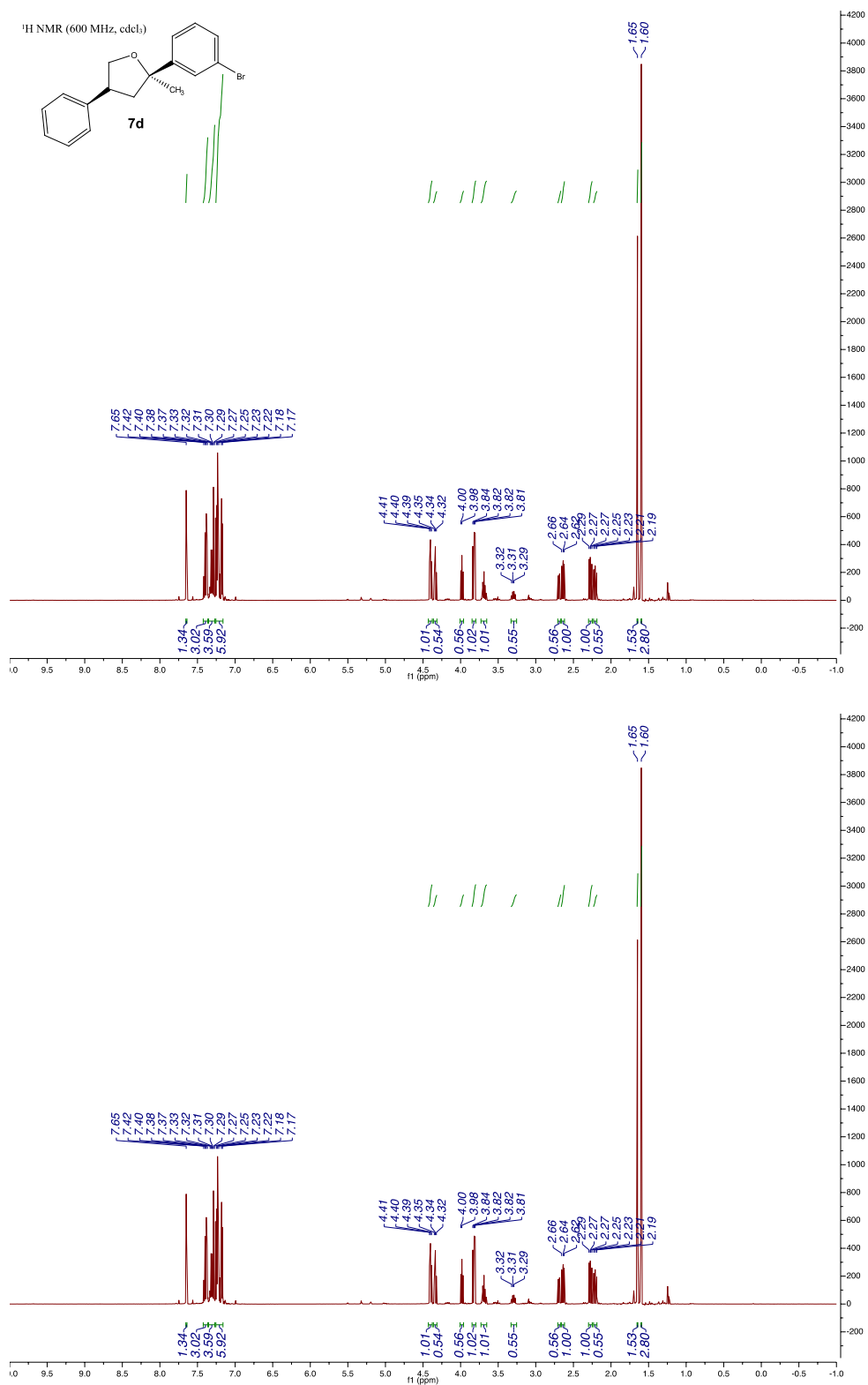


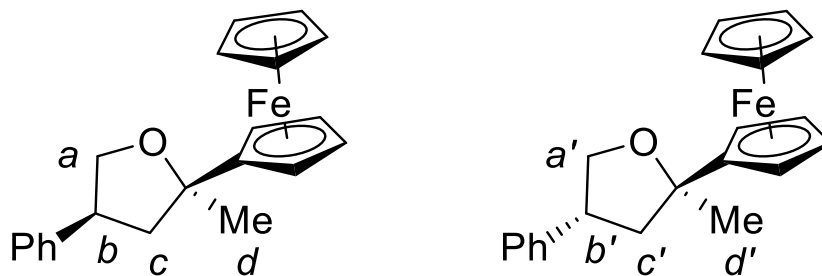
### 2-(3-Bromophenyl)-2-methyl-4-phenyltetrahydrofuran (2.58)

Following the general procedure, a RBF was loaded with  $\text{Sc}(\text{OTf})_3$  (0.005 mmol, 3.8 mg), DCM (0.5 mL), and 1-methyl-1-(3-bromophenyl)ethene (4 mmol, 835 mg). 1-Phenyloxirane (2 mmol, 0.23 mL) was added dropwise by syringe over 10 min. After addition was complete, the crude reaction mixture was loaded onto a silica column and eluted with ethyl acetate:hexanes (gradient, hexanes to 2 % EtOAc in hexanes) to afford product as a colorless oil in 28 % yield (0.56 mmol, 177 mg,



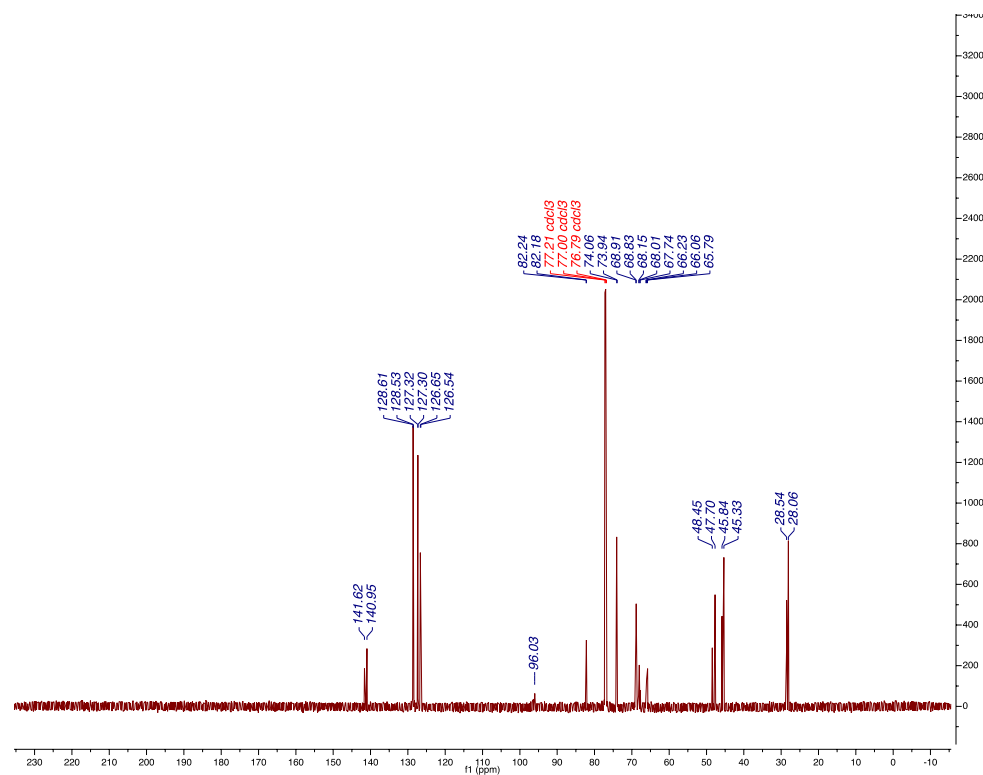
crude dr: 2:1 *syn*:*anti*, isolated dr: 1.8:1 *syn*:*anti*). When (*R*)-1-phenyloxirane was used the enantiopurity of the product was assessed using a Chiralpak AD-H column eluted with a 1:99 *i*-PrOH:hexanes mixture.  $^1\text{H}$  NMR (600 MHz,  $\text{CDCl}_3$ ): *syn* diastereomer:  $\delta$  7.65 (ArH, dt,  $J$  = 3.9, 1.8 Hz, 1H), 7.42 – 7.36 (ArH, m, 3H), 7.30 (ArH, dt,  $J$  = 18.9, 7.6 Hz, 4H), 7.25 – 7.20 (ArH, m, 4H), 7.19 – 7.16 (ArH, m, 2H), 4.40 ( $\text{H}_a$ , t,  $J$  = 8.0 Hz, 1H), 3.82 ( $\text{H}_a$ , dd,  $J$  = 10.0, 8.5 Hz, 1H), 3.73 – 3.65 ( $\text{H}_b$ , m, 1H), 2.64 ( $\text{H}_c$ , dd,  $J$  = 12.4, 7.9 Hz, 1H), 2.27 ( $\text{H}_c$ , dd,  $J$  = 12.4, 10.8 Hz, 1H), 1.60 ( $\text{H}_d$ , s, 3H); further signals for the *anti* diastereomer: 4.34 ( $\text{H}_a'$ , t,  $J$  = 8.4 Hz, 1H), 3.98 ( $\text{H}_a'$ , t,  $J$  = 8.8 Hz, 1H), 3.33 – 3.25 ( $\text{H}_b'$ , m, 1H), 2.69 ( $\text{H}_c'$ , dd,  $J$  = 12.3, 7.1 Hz, 1H), 2.24 – 2.18 ( $\text{H}_c'$ , m, 1H), 1.65 ( $\text{H}_d'$ , s, 3H).  $^{13}\text{C}$  NMR (151 MHz,  $\text{CDCl}_3$ ): *syn* diastereomer:  $\delta$  148.01, 140.58, 131.35, 128.56, 127.34, 126.72, 126.43, 120.28, 84.62, 74.45, 47.92, 45.76, 30.49; further signals for the *anti* diastereomer:  $\delta$  146.75, 141.22, 131.28, 128.58, 127.24, 126.68, 126.61, 120.44, 85.08, 73.97, 48.15, 44.57, 29.88. IR (film):  $\tilde{\nu}$  = 3023 (w), 2964 (w), 2865 (w), 1007 (m), 823 (s), 697 (s)  $\text{cm}^{-1}$ . HRMS (EI):  $m/z$  calcd for  $[\text{C}_{17}\text{H}_{17}\text{OBr}]^+$ : 316.0463; found: 316.0459.

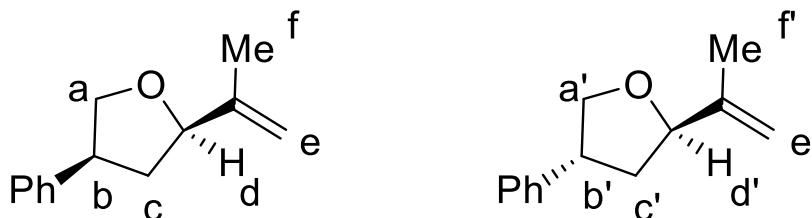




### 2-Ferrocenyl-2-methyl-4-phenyltetrahydrofuran (2.59)

Following the general procedure, a RBF was loaded with  $\text{Sc}(\text{OTf})_3$  (0.02 mmol, 9.1 mg), DCM (1.0 mL), and prop-1-en-2-ylferrocene (4 mmol, 901 mg). 1-Phenyloxirane (2 mmol, 0.23 mL) was added dropwise by syringe over 10 min. After addition was complete, the crude reaction mixture was loaded onto a silica column and eluted with dichloromethane:hexanes (25% DCM/hexanes) to afford product as an orange oil in 28 % yield (0.56 mmol, 194 mg, crude dr: 2:1 syn:anti, isolated dr: 1.7:1 syn:anti).  $^1\text{H}$  NMR (600 MHz,  $\text{CDCl}_3$ ): *syn* diastereomer:  $\delta$  7.32 (ArH, ddd,  $J = 29.7, 15.2, 7.9$  Hz, 6H), 7.24 (ArH, dd,  $J = 13.1, 7.2$  Hz, 1H), 4.31 – 4.26 (m, 2H), 4.24 (s, 1H), 4.20 (d,  $J = 8.2$  Hz, 13H), 4.14 (s, 1H), 3.92 – 3.84 (m, 2H), 3.67 – 3.57 (m, 2H), 2.46 ( $\text{H}_c$ , dd,  $J = 12.4, 7.7$  Hz, 1H), 2.39 ( $\text{H}_c$ , t,  $J = 11.9$  Hz, 1H), 1.66 ( $\text{H}_d$ , s, 3H); further signals for the *anti* diastereomer: 2.67 – 2.62 ( $\text{H}_{c'}$ , m, 1H), 2.13 ( $\text{H}_{c'}$ , dd,  $J = 12.6, 10.4$  Hz, 1H), 1.77 ( $\text{H}_{d'}$ , s, 3H).  $^{13}\text{C}$  NMR (151 MHz,  $\text{CDCl}_3$ ): *syn* diastereomer:  $\delta$  140.95, 128.61, 127.32, 126.65, 82.18, 74.06, 68.83, 68.01, 67.74, 66.24, 66.06, 65.85, 65.79, 47.70, 45.33, 28.06; further signals for the *anti* diastereomer: 141.62, 128.54, 127.30, 126.54, 82.24, 73.94, 68.91, 68.15, 48.45, 45.84, 28.55. IR (film):  $\bar{\nu} = 3099$  (w), 2982 (w), 1020 (m), 726 (s)  $\text{cm}^{-1}$ . HRMS (EI):  $m/z$  calcd for  $[\text{C}_{21}\text{H}_{22}\text{FeO}]^+$ : 346.1020; found: 346.1019.

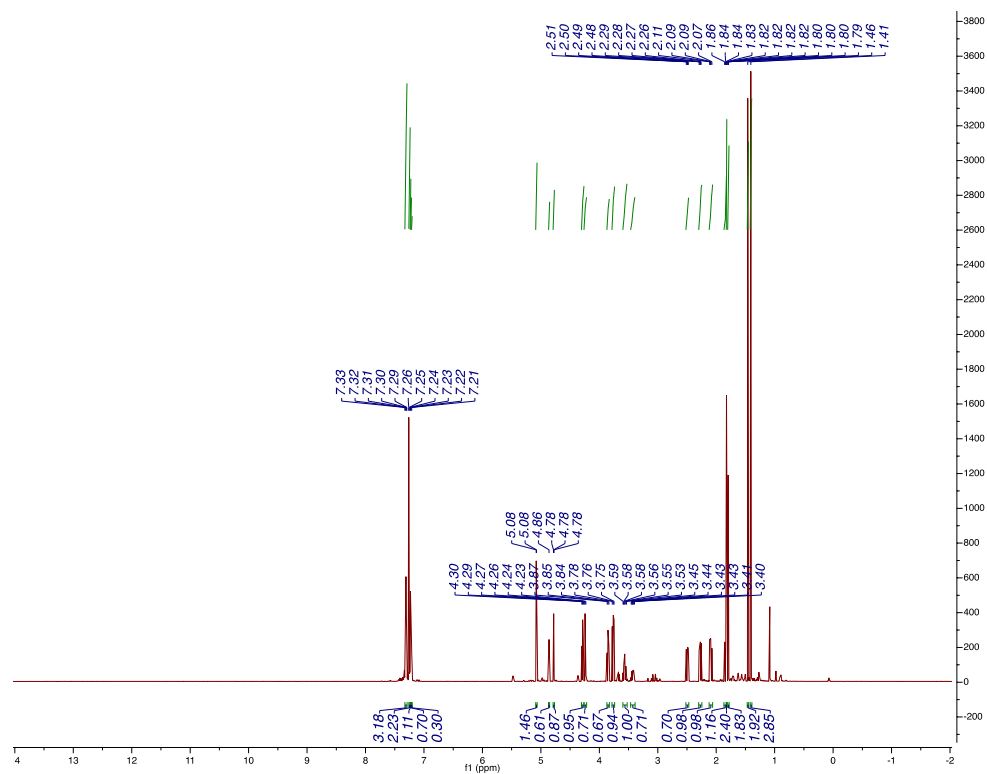


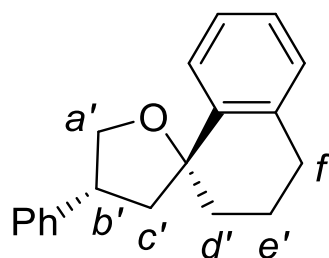
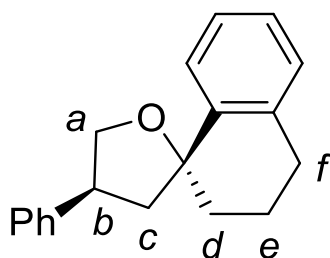
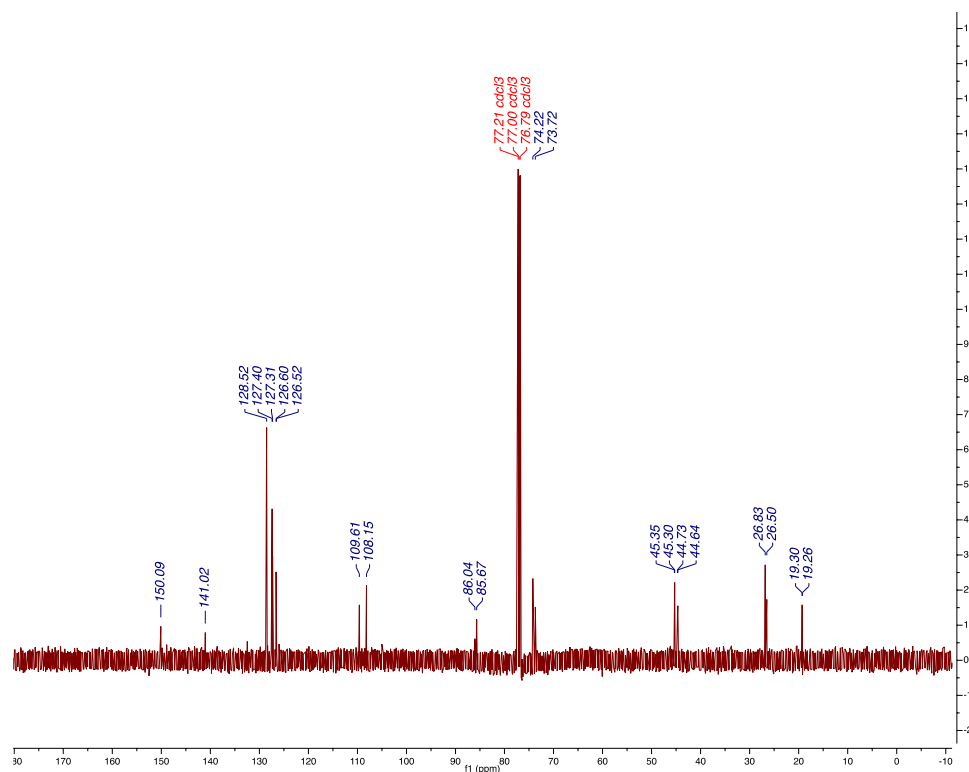


### 2-Methyl-4-phenyl-2-(prop-1-en-2-yl)tetrahydrofuran (2.60)

Following the general procedure, a RBF was loaded with  $\text{Sc}(\text{OTf})_3$  (0.004 mmol, 4.0 mg), DCM (0.5 mL), and 2,3-dimethylbutadiene (4 mmol, 0.45 mL). 2-Phenyloxirane (2 mmol, 0.23 mL) was added dropwise by syringe over 10 min. After addition was complete, the crude reaction mixture was loaded onto a silica column and eluted with ethyl acetate:hexanes (1 % EtOAc/hexanes to 2 % EtOAc/hexanes) to afford product as a colorless oil in 22 % yield (0.44 mmol, 88 mg, crude dr: 1.4:1 syn:anti, isolated dr: 2:1 syn:anti). All spectral data were consistent with literature values.  $^{13}\text{C}$   $^1\text{H}$  NMR (600 MHz,  $\text{CDCl}_3$ ): *syn* diastereomer:  $\delta$  7.33 – 7.29 (m, 3H), 7.25 (d,  $J$  = 7.4 Hz, 2H), 7.23 (s, 1H), 7.22 (s, 1H), 5.08 (He, d,  $J$  = 2.0 Hz, 2H), 4.79 – 4.77 (Ha, m, 1H), 4.29 (Ha, t,  $J$  = 7.9 Hz, 1H), 3.78 – 3.74 (Hb, m, 1H), 3.60 – 3.52 (m, 1H), 2.27 (dd,  $J$  = 12.4, 7.9 Hz, 1H), 2.09 (dd,  $J$  = 12.3, 10.9 Hz, 1H), 1.87 – 1.83 (m, 1H), 1.83 – 1.82 (Hf, m, 3H), 1.41 (Hd, s, 3H); further signals for the *anti* diastereomer: 4.86 (He', s, 1H), 4.24 (Ha', t,  $J$  = 8.3 Hz, 1H), 3.87 – 3.83 (Ha', m, 1H), 3.47 – 3.39 (Hb', m, 1H), 2.49 (dd,  $J$  = 12.3, 7.3 Hz, 1H), 1.80 (Hf', dd,  $J$  = 1.4, 0.7 Hz, 3H), 1.46 (Hd', s, 3H),  $^{13}\text{C}$  NMR (151 MHz,  $\text{CDCl}_3$ ): *syn* diastereomer:  $\delta$  150.09, 128.52, 127.40, 126.60, 108.15, 85.67, 77.21, 77.00, 76.79, 74.22, 45.30, 44.64, 26.83, 19.30; further signals for

the *anti* diastereomer: 141.02, 127.31, 126.52, 109.61, 86.04, 73.72, 45.35, 44.73, 26.50, 19.26.



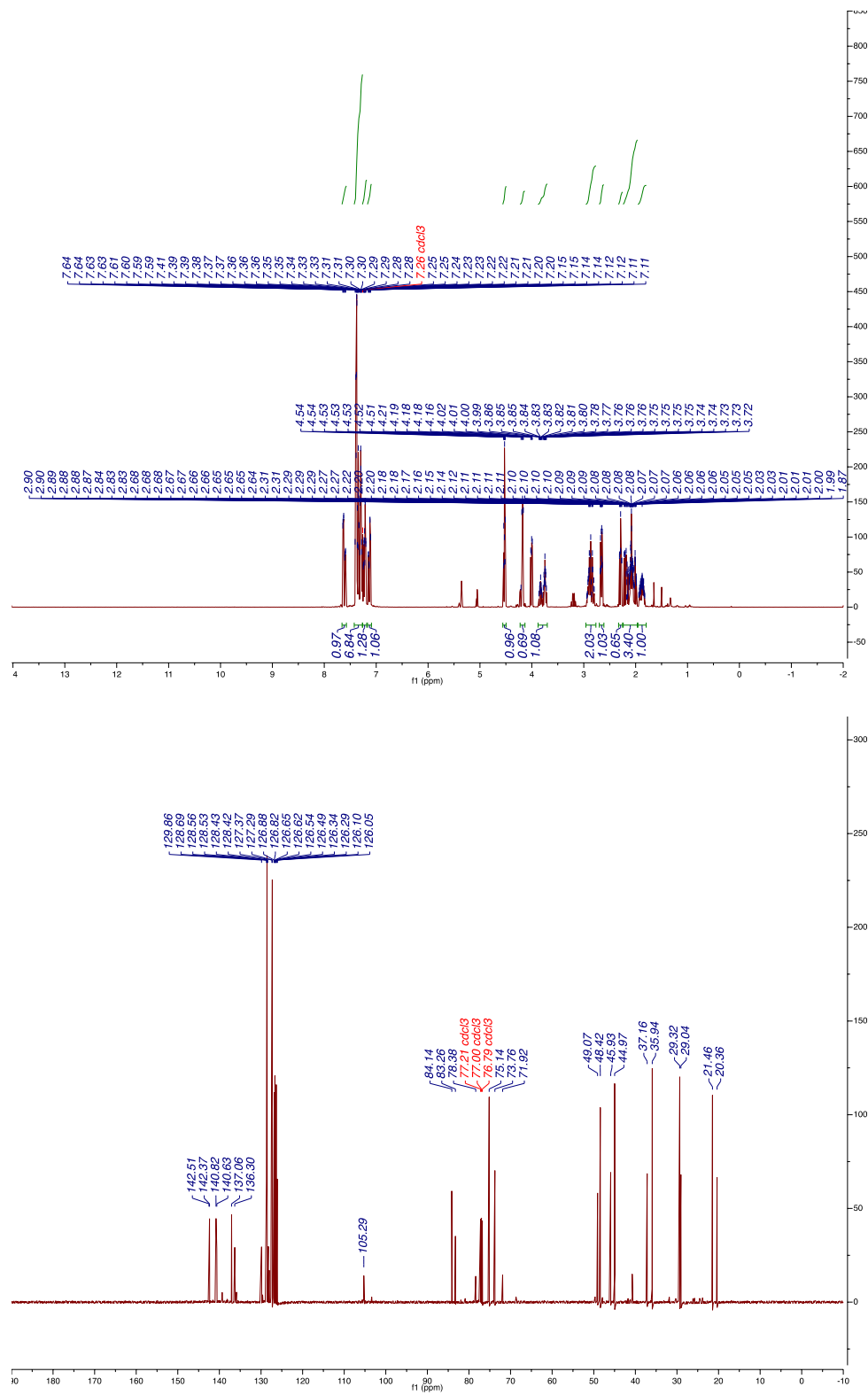


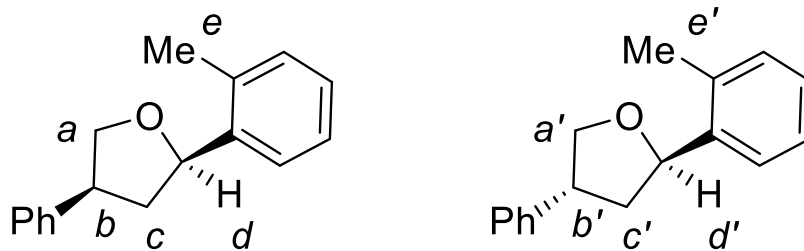
#### 4-Phenyl-3',4,4',5-tetrahydro-2'*H*,3'*H*-spiro[furan-2,1'-naphthalene] (2.61)

Following the general procedure, a RBF was loaded with  $\text{Sc}(\text{OTf})_3$  (0.005 mmol, 2.6 mg), DCM (0.5 mL), and 1-methylene-1,2,3,4-tetrahydronaphthalene (4 mmol, 580 mg). 1-Phenyloxirane (2 mmol, 0.23 mL) was added dropwise by syringe over 10 min. After addition was complete, the crude reaction mixture was loaded onto a silica column and eluted with ethyl acetate:hexanes (hexanes to 4 %

EtOAc/hexanes) to afford product as a pale yellow oil in 31 % yield (0.62 mmol, 164 mg, crude dr: 1.5:1 *syn*:*anti*, isolated dr: 1.4:1 *syn*:*anti*).  $^1\text{H}$  NMR (600 MHz,  $\text{CDCl}_3$ ): *syn* diastereomer:  $\delta$  7.63 (ArH, d,  $J = 7.9$  Hz, 1H), 7.60 (ArH, d,  $J = 8.9$  Hz, 1H), 7.41 – 7.32 (ArH, m, 8H), 7.32 – 7.27 (ArH, m, 3H), 7.22 (ArH, dt,  $J = 14.7, 7.4$  Hz, 2H), 7.14 (ArH, d,  $J = 7.6$  Hz, 1H), 7.11 (ArH, d,  $J = 7.6$  Hz, 1H), 4.53 ( $\text{H}_a$ , t,  $J = 8.2$  Hz, 2H), 4.18 ( $\text{H}_a$ , dd,  $J = 9.8, 8.4$  Hz, 1H), 3.79 – 3.71 (m, 1H), 3.24 – 3.14 (m, 1H), 2.95 – 2.79 (m, 3H), 2.70 – 2.64 (m, 2H), 2.29 (t,  $J = 12.2$  Hz, 1H), 2.23 – 2.13 (m, 1H), 2.13 – 1.98 (m, 4H), 1.95 – 1.81 (m, 2H); further signals for the *anti* diastereomer: 4.01 ( $\text{H}_a$ , dd,  $J = 10.6, 8.6$  Hz, 1H), 3.87 – 3.79 ( $\text{H}_a$ , m, 1H).  $^{13}\text{C}$  NMR (150 MHz,  $\text{CDCl}_3$ ): *syn* diastereomer:  $\delta$  142.37, 140.82, 137.06, 128.56, 128.53, 127.29, 126.82, 126.65, 126.34, 126.10, 84.14, 75.14, 48.42, 44.97, 35.94, 29.32, 21.46; further signals for the *anti* diastereomer:  $\delta$  142.51, 140.63, 136.30, 128.69, 128.42, 127.37, 126.88, 126.62, 126.49, 126.05, 83.26, 73.76, 49.07, 45.93, 37.16, 29.04, 20.36. IR (film):  $\bar{\nu} = 2969$  (w), 2862 (w), 1495 (w), 790 (s), 787 (s)  $\text{cm}^{-1}$ . HRMS (EI):  $m/z$  calcd for  $[\text{C}_{19}\text{H}_{20}\text{O}]^+$ : 264.1514; found: 264.1517.





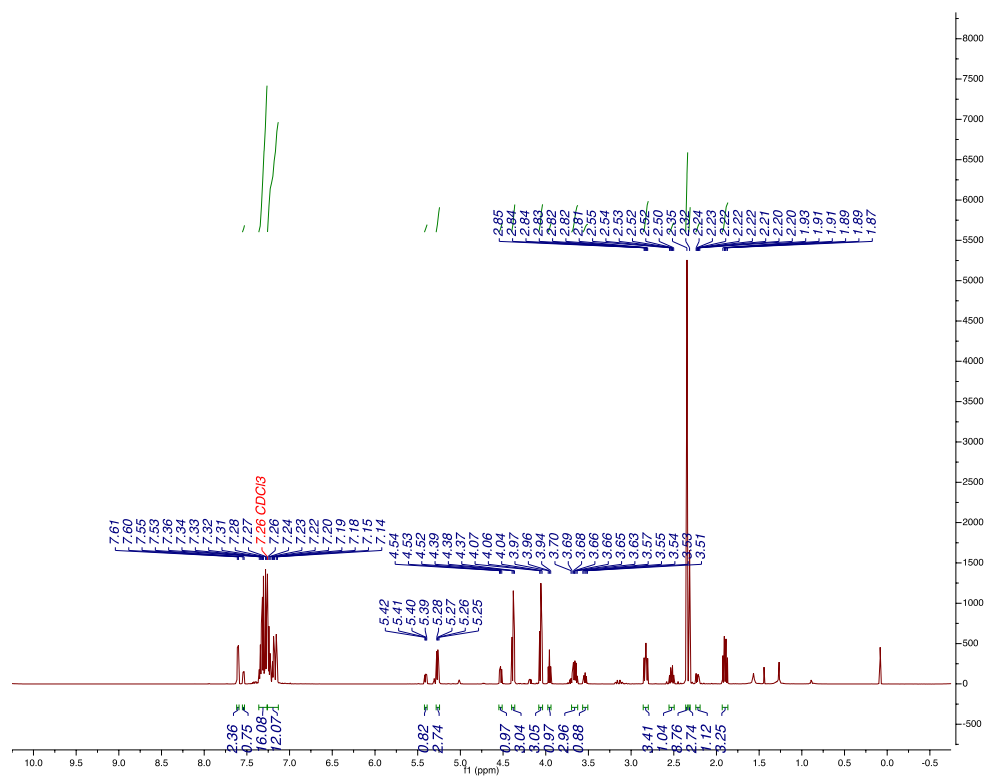


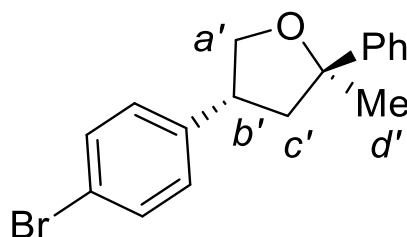
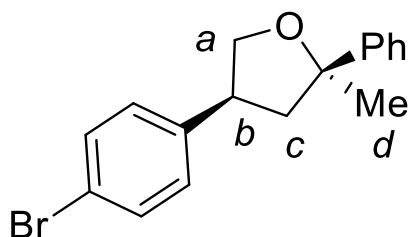
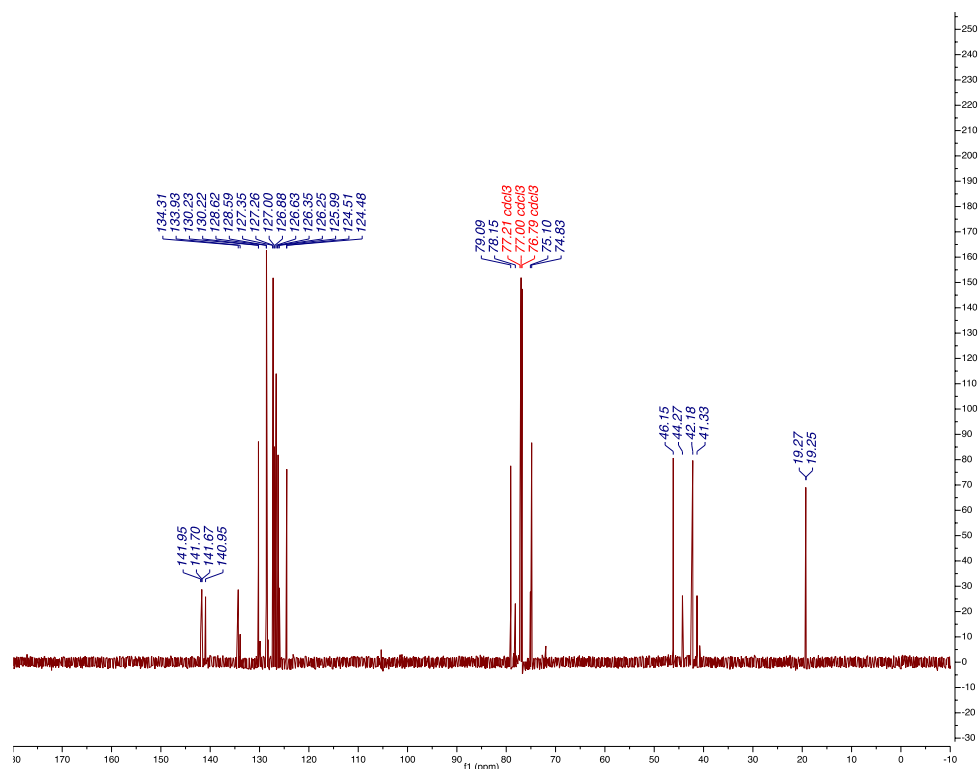
#### 4-Phenyl-2-(*o*-tolyl)tetrahydrofuran (2.62)

Following the general procedure, a RBF was loaded with  $\text{Sc}(\text{OTf})_3$  (0.007 mmol, 3.5 mg), DCM (0.5 mL), and 1-methyl-2-vinylbenzene (4 mmol, 0.52 mL). 2-Phenyloxirane (2 mmol, 0.23 mL) was added dropwise by syringe over 10 min. After addition was complete, the crude reaction mixture was loaded onto a silica column and eluted with ethyl acetate:hexanes (hexanes to 2 % EtOAc/hexanes) to afford product as a colorless oil in 27 % yield (0.54 mmol, 129 mg, crude dr: 3.2:1 *syn*:*anti*, isolated dr: 3.2:1 *syn*:*anti*).  $^1\text{H}$  NMR (600 MHz,  $\text{CDCl}_3$ ): *syn* diastereomer:  $\delta$  7.61 (ArH, d,  $J = 7.6$  Hz, 1H), 7.54 (ArH, d,  $J = 7.5$  Hz, 0H), 7.36 – 7.26 (ArH, m, 6H), 7.26 – 7.13 (ArH, m, 4H), 5.26 ( $\text{H}_d$ , dd,  $J = 10.1, 5.8$  Hz, 1H), 4.38 ( $\text{H}_a$ , t,  $J = 8.2$  Hz, 1H), 4.06 ( $\text{H}_a$ , t,  $J = 8.5$  Hz, 1H), 3.70 – 3.63 ( $\text{H}_b$ , m, 1H), 2.83 ( $\text{H}_c$ , ddd,  $J = 12.9, 7.3, 5.9$  Hz, 1H), 2.35 ( $\text{H}_e$ , s, 3H), 1.90 ( $\text{H}_c$ , dt,  $J = 12.4, 10.4$  Hz, 1H); further signals for the *anti* diastereomer: 5.40 ( $\text{H}_{d'}$ , dd,  $J = 8.1, 5.4$  Hz, 1H), 4.55 – 4.51 ( $\text{H}_{a'}$ , m, 1H), 3.96 ( $\text{H}_{a'}$ , t,  $J = 8.5$  Hz, 1H), 3.54 ( $\text{H}_{b'}$ , p,  $J = 8.2$  Hz, 1H), 2.53 ( $\text{H}_{c'}$ , dt,  $J = 12.4, 8.2$  Hz, 1H), 2.32 ( $\text{H}_{e'}$ , s, 3H), 2.22 ( $\text{H}_{c'}$ , ddd,  $J = 12.5, 8.3, 5.4$  Hz, 1H).  $^{13}\text{C}$  NMR (150 MHz,  $\text{CDCl}_3$ ): *syn* diastereomer:  $\delta$  141.70, 140.95, 134.31, 130.23, 128.59, 127.26, 127.00, 126.63, 126.25, 124.48, 79.09, 74.83, 46.15, 42.18, 19.27; further signals for the *anti* diastereomer:  $\delta$  141.95, 141.67, 133.93,

130.22, 128.62, 127.35, 126.88, 126.35, 125.99, 124.51, 78.15, 75.10, 44.27, 41.33, 19.25. IR (film):  $\bar{\nu}$  = 3035 (w), 2861 (w), 1489 (w), 1067 (m), 700 (s)  $\text{cm}^{-1}$ .

HRMS (EI):  $m/z$  calcd for  $[\text{C}_{17}\text{H}_{18}\text{O}]^+$ : 238.1358; found: 238.1350.

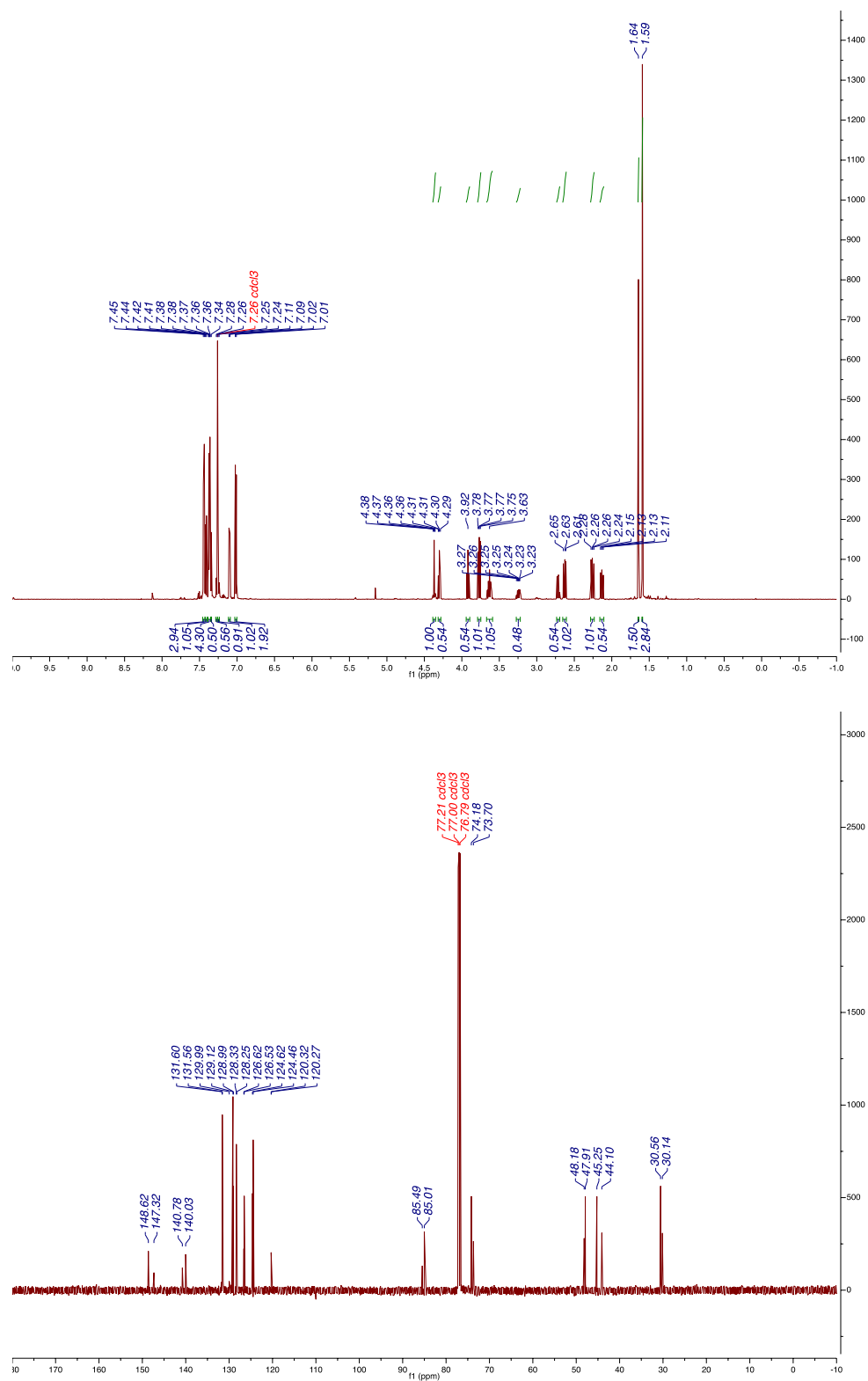


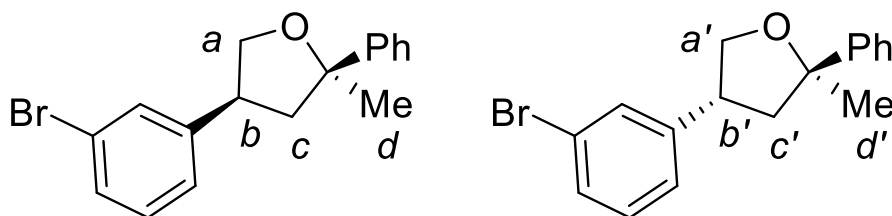


#### 4-(4-Bromophenyl)-2-methyl-2-phenyltetrahydrofuran (2.63)

Following the general procedure, a RBF was loaded with  $\text{Sc}(\text{OTf})_3$  (.02 mmol, 9.4 mg), DCM (0.5 mL), and 1-methyl-1-phenylethene (4 mmol, 0.52 mL). 2-(4-Bromophenyl)oxirane (2 mmol, 0.26 mL) was added dropwise by syringe over 10 min. After addition was complete, the crude reaction mixture was loaded onto a silica column and eluted with ethyl acetate:hexanes (hexanes to 2 % EtOAc/hexanes) to afford product as a colorless oil in 47% yield (0.94 mmol, 297

mg, crude dr: 2:1 *syn*:*anti*, isolated dr: 1.9:1 *syn*:*anti*).  $^1\text{H}$  NMR (600 MHz,  $\text{CDCl}_3$ ): *syn* diastereomer:  $\delta$  7.44 (ArH, d,  $J = 8.3$  Hz, 3H), 7.41 (ArH, d,  $J = 8.4$  Hz, 1H), 7.39 – 7.35 (ArH, m, 4H), 7.34 (ArH, s, 1H), 7.27 (ArH, d,  $J = 7.4$  Hz, 1H), 7.25 (ArH, d,  $J = 7.4$  Hz, 1H), 7.10 (ArH, d,  $J = 8.4$  Hz, 1H), 7.02 (ArH, d,  $J = 8.4$  Hz, 2H), 4.37 ( $\text{H}_a$ , t,  $J = 8.0$  Hz, 1H), 3.77 ( $\text{H}_a$ , dd,  $J = 9.7, 8.5$  Hz, 1H), 3.63 ( $\text{H}_b$ , tt,  $J = 9.9, 7.8$  Hz, 1H), 2.63 ( $\text{H}_c$ , dd,  $J = 12.5, 8.1$  Hz, 1H), 2.26 ( $\text{H}_c$ , dd,  $J = 12.5, 10.3$  Hz, 1H), 1.59 ( $\text{H}_d$ , s, 3H); further signals for the *anti* diastereomer: 4.30 ( $\text{H}_a'$ , t,  $J = 8.4$  Hz, 1H), 3.92 ( $\text{H}_a'$ , t,  $J = 8.6$  Hz, 1H), 3.27 – 3.22 ( $\text{H}_b'$ , m, 1H), 2.71 ( $\text{H}_c'$ , dd,  $J = 12.2, 7.2$  Hz, 1H), 2.13 ( $\text{H}_c'$ , dd,  $J = 12.1, 11.3$  Hz, 1H), 1.64 ( $\text{H}_d'$ , s, 3H).  $^{13}\text{C}$  NMR (150 MHz,  $\text{CDCl}_3$ ): *syn* diastereomer:  $\delta$  148.62, 140.02, 131.56, 129.12, 128.33, 126.53, 124.46, 120.32, 85.01, 74.18, 47.19, 45.25, 30.56; further signals for the *anti* diastereomer:  $\delta$  147.32, 140.78, 131.60, 128.99, 128.25, 126.62, 124.62, 120.27, 85.49, 73.70, 48.18, 44.10, 30.14. IR (film):  $\bar{\nu} = 2854$  (w), 1490 (m), 1009 (m), 765 (s)  $\text{cm}^{-1}$ . HRMS (EI):  $m/z$  calcd for  $[\text{C}_{17}\text{H}_{17}\text{BrO}]^+$ : 316.0463; found: 316.0452.

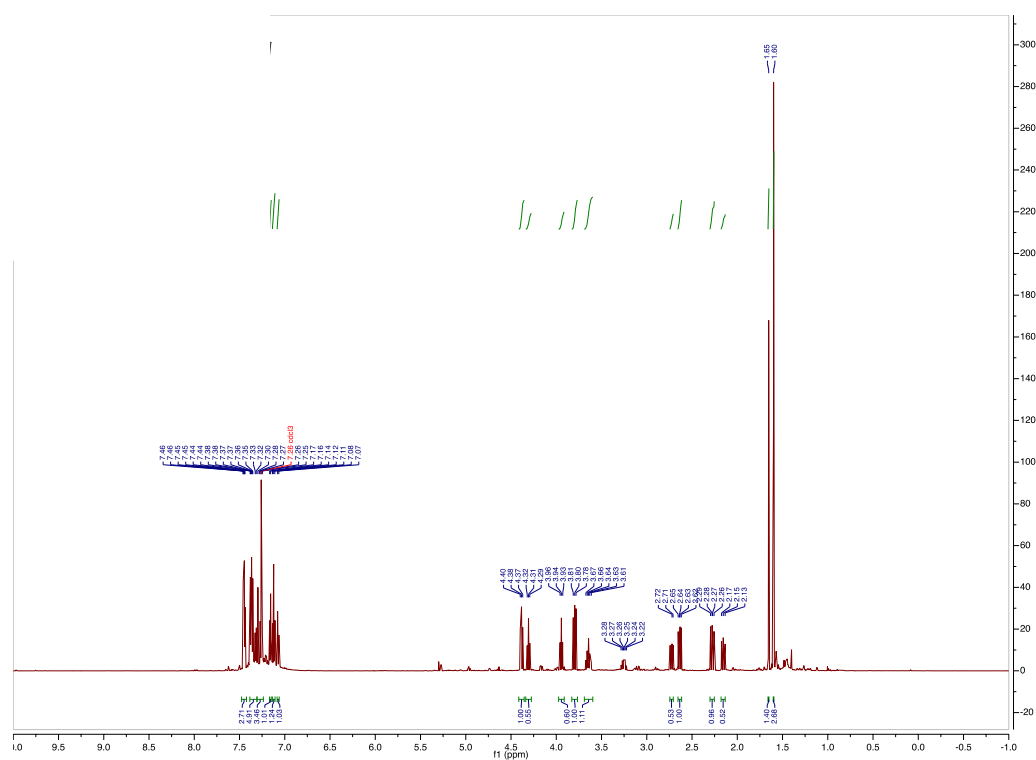




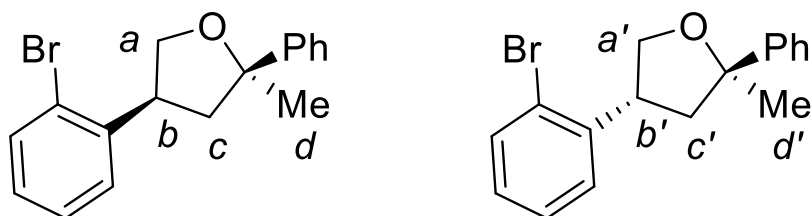
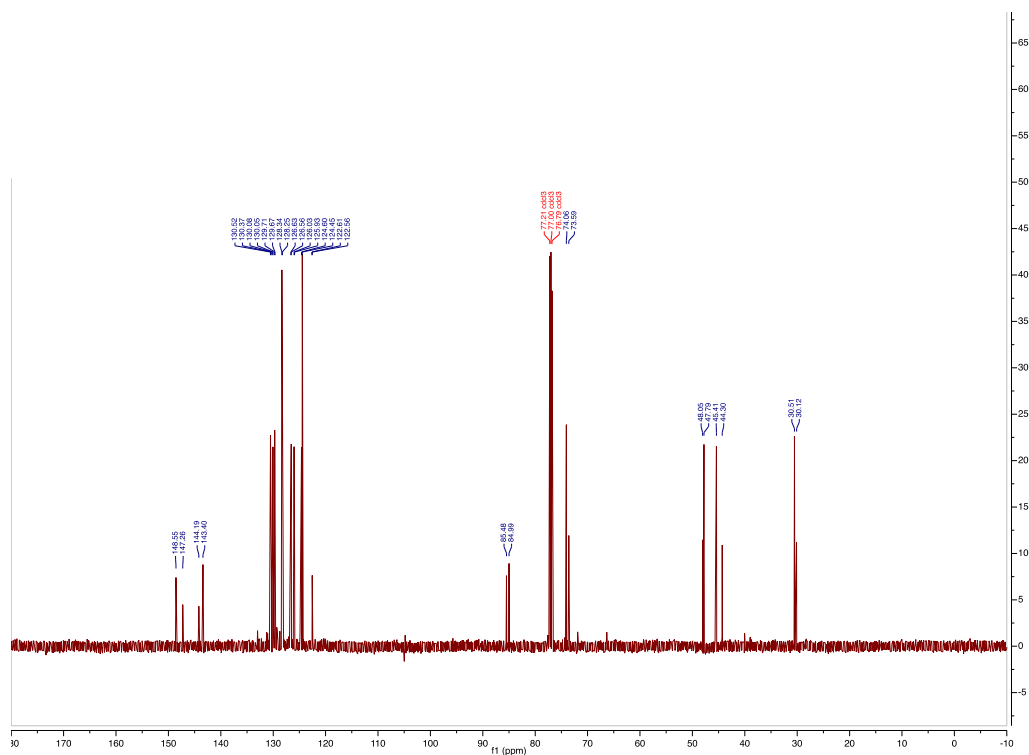
#### 4-(3-Bromophenyl)-2-methyl-2-phenyltetrahydrofuran (2.64)

Following the general procedure, a RBF was loaded with  $\text{Sc}(\text{OTf})_3$  (0.005 mmol, 2.5 mg), DCM (0.5 mL), and 1-methyl-1-phenylethene (3.5 mmol, 0.46 mL). 2-(3-Bromophenyl)oxirane (1.8 mmol, 0.22 mL) was added dropwise by syringe over 10 min. After addition was complete, the crude reaction mixture was loaded onto a silica column and eluted with DCM:hexanes (hexanes to 50 % DCM/hexanes) to afford product as a colorless oil in 38 % yield (0.66 mmol, 210 mg, crude dr: 2:1 syn:anti, isolated dr: 1.9:1 syn:anti).  $^1\text{H}$  NMR (598 MHz,  $\text{CDCl}_3$ ): *syn* diastereomer:  $\delta$  7.44 (ArH, ddt,  $J = 7.4, 4.2, 1.2$  Hz, 3H), 7.39 – 7.35 (ArH, m, 3H), 7.29 (ArH, t,  $J = 1.9$  Hz, 1H), 7.28 – 7.24 (ArH, m, 2H), 4.38 ( $\text{H}_a$ , dd,  $J = 8.4, 7.6$  Hz, 1H), 3.79 ( $\text{H}_a$ , dd,  $J = 9.7, 8.5$  Hz, 1H), 3.67 – 3.60 ( $\text{H}_b$ , m, 1H), 2.63 ( $\text{H}_c$ , dd,  $J = 12.4, 8.0$  Hz, 1H), 2.27 ( $\text{H}_c$ , dd,  $J = 12.4, 10.4$  Hz, 1H), 1.59 ( $\text{H}_d$ , s, 3H); further signals for the *anti* diastereomer:  $\delta$  7.36 – 7.33 (ArH, m, 2H), 7.32 (ArH, ddd,  $J = 7.8, 2.0, 1.2$  Hz, 2H), 7.22 – 7.18 (ArH, m, 1H), 7.17 – 7.14 (ArH, m, 2H), 7.08 – 7.06 (ArH, m, 2H), 4.30 ( $\text{H}_{a'}$ , t,  $J = 8.4$  Hz, 1H), 3.94 ( $\text{H}_{a'}$ , t,  $J = 8.6$  Hz, 1H), 3.28 – 3.21 ( $\text{H}_{b'}$ , m, 1H), 2.72 ( $\text{H}_{c'}$ , dd,  $J = 12.2, 7.2$  Hz, 1H), 2.15 ( $\text{H}_{c'}$ , dd,  $J = 12.2, 11.1$  Hz, 1H), 1.65 ( $\text{H}_{d'}$ , s, 3H).  $^{13}\text{C}$  NMR (150 MHz,  $\text{CDCl}_3$ )  $\delta$  148.55, 143.40, 130.52, 130.05, 129.71, 128.34, 126.56, 126.03, 124.45, 122.56, 84.99, 74.06, 47.79, 45.41, 30.51; further signals for the *anti* diastereomer:  $\delta$  147.26, 144.19, 130.37, 130.09, 129.67,

128.25, 126.63, 125.93, 124.60, 122.61, 85.48, 73.59, 48.05, 44.30, 30.11. IR (film):  $\bar{\nu}$  = 3049 (w), 2718 (w), 785 (m), 750 (s)  $\text{cm}^{-1}$ . HRMS (ESI):  $m/z$  calcd for  $[\text{C}_{17}\text{H}_{17}\text{BrO}+\text{H}]^+$ : 317.04628; found: 317.0458.



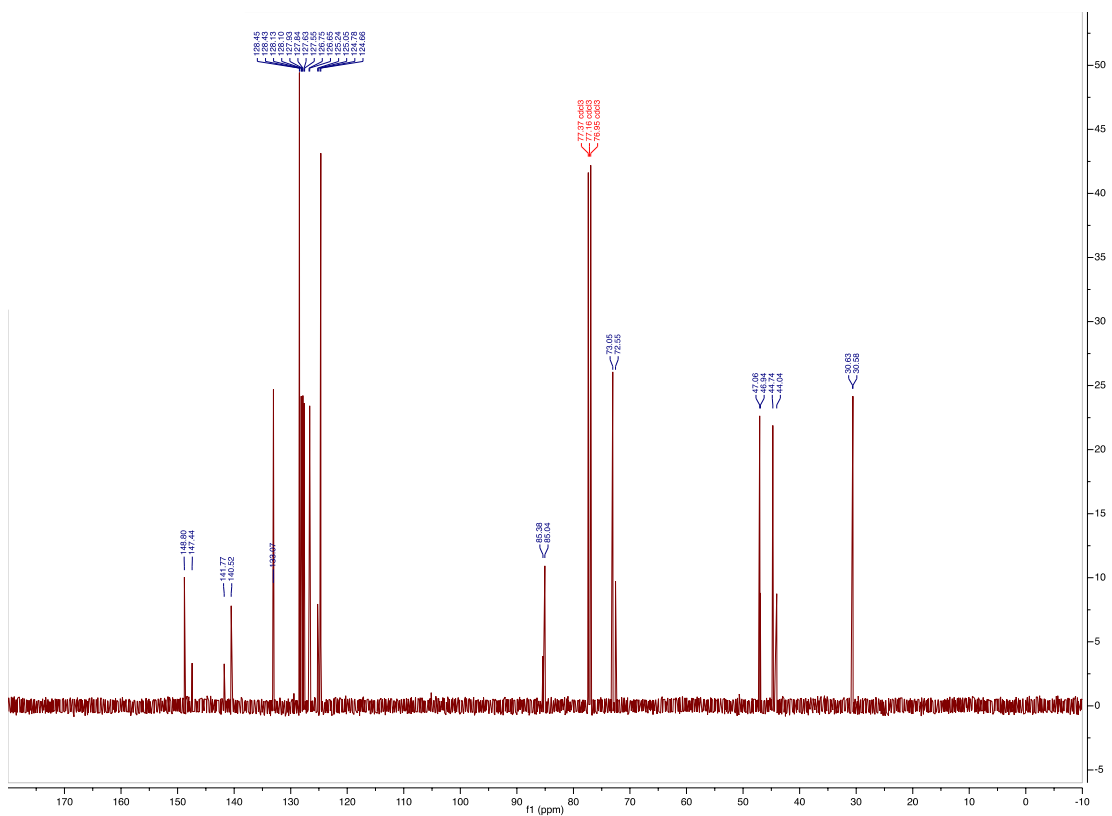


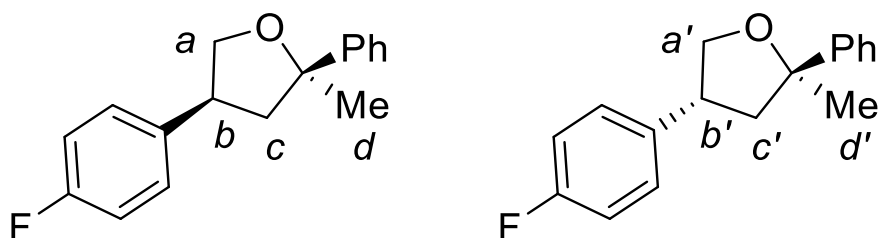


#### 4-(2-Bromophenyl)-2-methyl-2-phenyltetrahydrofuran (2.65)

Following the general procedure, a RBF was loaded with  $\text{Sc}(\text{OTf})_3$  (.005 mmol, 25 mg), DCM (0.5 mL), and 1-methyl-1-phenylethene (4 mmol, 0.52 mL). 2-(2-Bromophenyl)oxirane (2 mmol, 0.25 mL) was added dropwise by syringe over 10 min. After addition was complete, the crude reaction mixture was loaded onto a silica column and eluted with ethyl acetate:hexanes (2:98) to afford product as a colorless oil in 31 % yield (0.62 mmol, 197 mg, crude dr: 2.33:1 syn:anti, isolated

dr: 2.6:1 syn:anti).  $^1\text{H}$  NMR (600 MHz,  $\text{CDCl}_3$ )  $\delta$  7.53 (ArH, dd,  $J = 8.0, 1.3$  Hz, 1H), 7.46 – 7.44 (ArH, m, 2H), 7.36 – 7.33 (ArH, m, 2H), 7.24 (ArH, ddt,  $J = 7.6, 6.8, 1.3$  Hz, 1H), 7.16 (ArH, td,  $J = 7.6, 1.3$  Hz, 1H), 7.10 (ArH, dd,  $J = 7.9, 1.8$  Hz, 1H), 7.02 (ArH, ddd,  $J = 7.9, 7.2, 1.8$  Hz, 1H), 4.45 – 4.40 ( $\text{H}_a$ , m, 1H), 4.13 ( $\text{H}_a$ , tt,  $J = 9.5, 7.9$  Hz, 1H), 3.82 ( $\text{H}_b$ , t,  $J = 8.8$  Hz, 1H), 2.68 ( $\text{H}_c$ , dd,  $J = 12.4, 8.2$  Hz, 1H), 2.24 ( $\text{H}_c$ , dd,  $J = 12.4, 9.9$  Hz, 1H), 1.61 ( $\text{H}_d$ , s, 3H); further signals for the *anti* diastereomer:  $\delta$  7.52 – 7.49 (ArH, m, 1H), 7.46 – 7.45 (ArH, m, 2H), 7.38 – 7.34 (ArH, m, 2H), 7.31 – 7.28 (ArH, m, 1H), 7.27 – 7.24 (ArH, m, 2H), 7.06 (ArH, td,  $J = 7.7, 1.5$  Hz, 1H), 3.95 ( $\text{H}_a'$ , ddd,  $J = 8.7, 7.2, 1.2$  Hz, 1H), 3.74 ( $\text{H}_a'$ , dq,  $J = 10.4, 7.8$  Hz, 1H), 2.80 ( $\text{H}_c'$ , ddd,  $J = 12.3, 7.6, 1.1$  Hz, 1H), 2.14 ( $\text{H}_c'$ , ddd,  $J = 12.2, 9.8, 1.2$  Hz, 1H), 1.62 ( $\text{H}_d'$ , s, 3H).  $^{13}\text{C}$  NMR (150 MHz,  $\text{CDCl}_3$ )  $\delta$  148.64, 140.36, 132.88, 128.29, 127.97, 127.68, 127.47, 126.49, 125.07, 124.50, 84.88, 72.89, 46.90, 44.58, 30.42; further signals for the *anti* diastereomer:  $\delta$  147.28, 141.60, 132.91, 128.27, 127.94, 127.77, 127.38, 126.59, 124.89, 124.62, 85.22, 72.39, 46.78, 43.88, 30.46. IR (film):  $\bar{\nu} = 3029$  (w), 2722 (w), 1437 (m), 1020 (s), 913 (m), 701 (s)  $\text{cm}^{-1}$ . HRMS (ESI):  $m/z$  calcd for  $[\text{C}_{17}\text{H}_{17}\text{BrO}+\text{H}]^+$ : 317.0541; found: 317.0528.

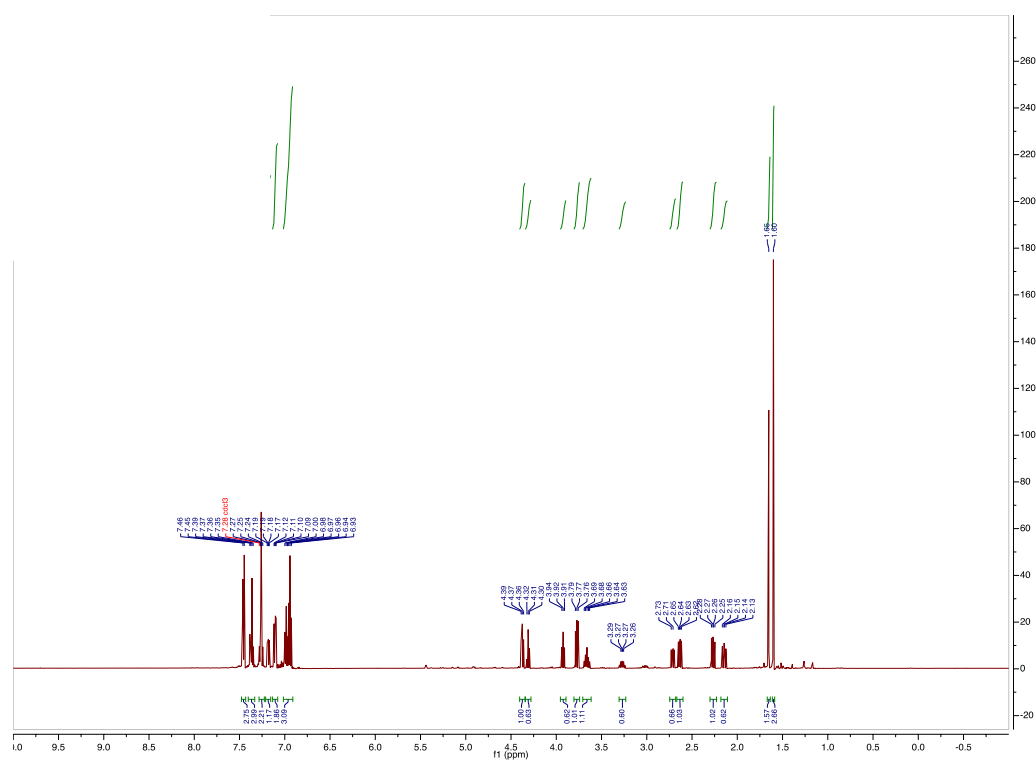


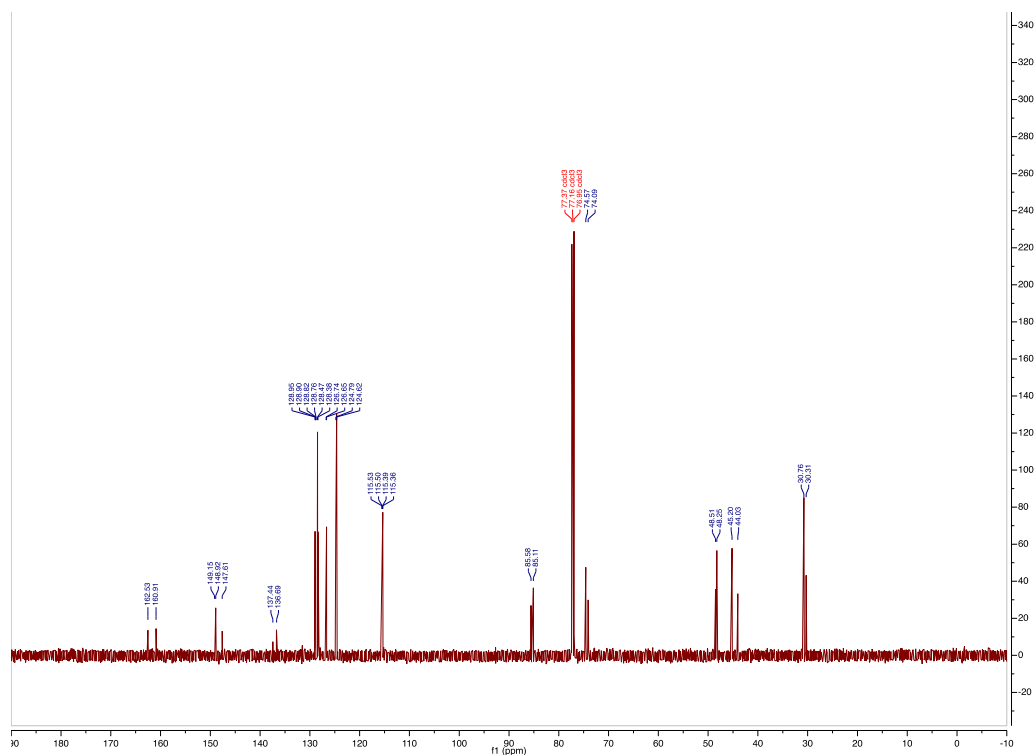


#### 4-(4-Fluorophenyl)-2-methyl-2-phenyltetrahydrofuran (2.66)

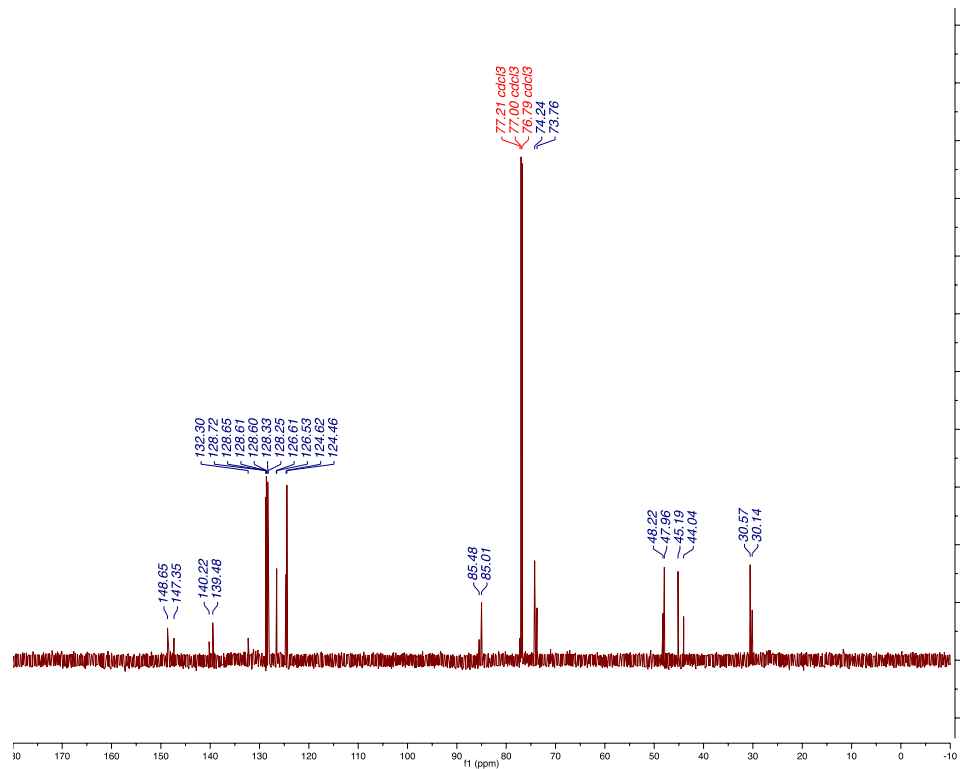
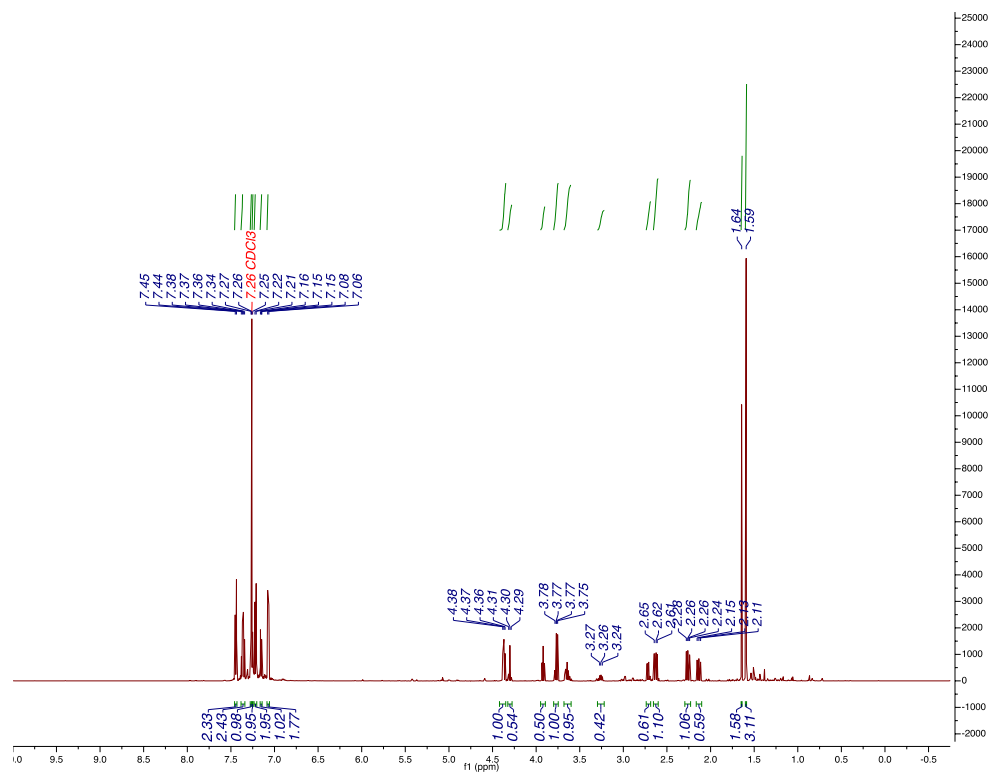
Following the general procedure, a RBF was loaded with  $\text{Sc}(\text{OTf})_3$  (0.005 mmol, 2.5 mg) and 1-methyl-1-phenylethene (4 mmol, 0.52 mL). 2-(4-Fluorophenyl)oxirane (2 mmol, 0.24 mL) was added dropwise by syringe over 10 min. After addition was complete, the crude reaction mixture was loaded onto a silica column and eluted with a gradient of ethyl acetate in hexanes (0 to 10%) to afford product as a colorless oil in 60 % yield (1.24 mmol, 317 mg, crude dr: 2:1 syn:anti, isolated dr: 1.6:1 syn:anti).  $^1\text{H}$  NMR (600 MHz,  $\text{CDCl}_3$ ): *syn* diastereomer:  $\delta$  7.45-6.94 (ArH, m, 9H), 4.37 ( $\text{H}_a$ , t,  $J = 8.0$  Hz, 1H), 3.80 – 3.75 ( $\text{H}_a$ , m, 1H), 3.66 ( $\text{H}_b$ , t,  $J = 7.8$  Hz, 1H), 2.63 ( $\text{H}_c$ , dd,  $J = 12.4, 8.0$  Hz, 1H), 2.29 – 2.24 ( $\text{H}_c$ , m, 1H), 1.60 ( $\text{H}_d$ , s, 3H); further signals for the *anti* diastereomer:  $\delta$  4.31 ( $\text{H}_{a'}$ , t,  $J = 8.4$  Hz, 1H), 3.92 ( $\text{H}_{a'}$ , t,  $J = 8.7$  Hz, 1H), 3.31 – 3.23 ( $\text{H}_{b'}$ , m, 1H), 2.71 ( $\text{H}_{c'}$ , dd,  $J = 12.2, 7.1$  Hz, 1H), 2.14 ( $\text{H}_{c'}$ , dd,  $J = 12.2, 11.3$  Hz, 1H), 1.65 ( $\text{H}_{d'}$ , s, 3H).  $^{13}\text{C}$  NMR (151 MHz,  $\text{CDCl}_3$ )  $\delta$  148.75, 128.78, 128.75 (d,  $J = 8.1$  Hz), 126.48, 124.45, 115.26 (d,  $J = 20.9$  Hz), 84.94, 74.39, 48.08, 45.03, 30.59; further signals for the *anti* diastereomer:  $\delta$  162.36, 147.44, 137.27, 128.73, 128.62 (d,  $J = 8.0$  Hz), 126.56, 124.62, 115.29 (d,  $J = 21.4$  Hz), 85.41, 73.92, 48.34, 43.86, 30.14.  $^{19}\text{F}$  NMR (564 MHz,  $\text{CDCl}_3$ ): *syn* diastereomer:  $\delta$  -116.48 (tt,  $J = 8.6, 5.3$  Hz); further signals for

the *anti* diastereomer:  $\delta$  -116.55 (tt,  $J = 8.7, 5.4$  Hz). IR (film):  $\bar{\nu} = 2857$  (w), 1510 (m) 764 (s), 700 (s)  $\text{cm}^{-1}$ . HRMS (EI):  $m/z$  calcd for  $[\text{C}_{17}\text{H}_{17}\text{OF}]^+$ : 256.1263; found: 256.1266.

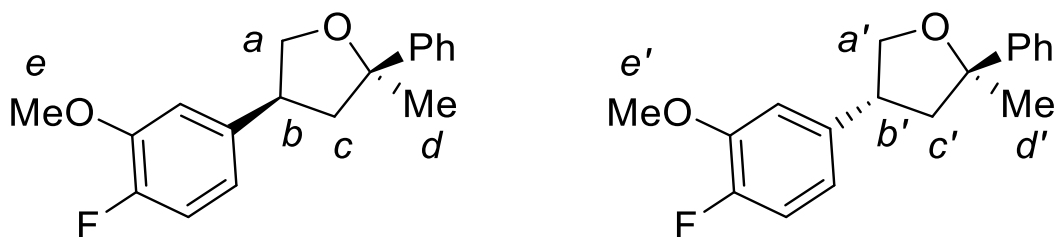




*syn* diastereomer:  $\delta$  7.44 (ArH, d,  $J$  = 8.4 Hz, 2H), 7.38 – 7.34 (ArH, m, 2H), 7.27 (ArH, d,  $J$  = 3.7 Hz, 1H), 7.25 (ArH, s, 1H), 7.22 (ArH, d,  $J$  = 8.5 Hz, 2H), 7.16 – 7.14 (ArH, m, 1H), 7.07 (ArH, d,  $J$  = 8.7 Hz, 2H), 4.37 (H<sub>a</sub>, t,  $J$  = 8.0 Hz, 1H), 3.77 (H<sub>a</sub>, dd,  $J$  = 9.7, 8.5 Hz, 1H), 3.68 – 3.60 (H<sub>b</sub>, m, 1H), 2.63 (H<sub>c</sub>, dd,  $J$  = 12.5, 8.1 Hz, 1H), 2.26 (H<sub>c</sub>, dd,  $J$  = 12.5, 10.3 Hz, 1H), 1.59 (H<sub>d</sub>, s, 3H); further signals for the *anti* diastereomer: 4.30 (H<sub>a'</sub>, t,  $J$  = 8.4 Hz, 1H), 3.92 (H<sub>a'</sub>, t,  $J$  = 8.6 Hz, 1H), 3.30 – 3.22 (H<sub>b'</sub>, m, 1H), 2.71 (H<sub>c'</sub>, dd,  $J$  = 12.2, 7.2 Hz, 1H), 2.16 – 2.10 (H<sub>c'</sub>, m, 1H), 1.64 (H<sub>d'</sub>, s, 3H). <sup>13</sup>C NMR (150 MHz, CDCl<sub>3</sub>): *syn* diastereomer:  $\delta$  148.65, 139.48, 132.30, 128.72, 128.61, 128.33, 126.53, 124.46, 85.01, 74.24, 47.96, 45.19, 30.57; further signals for the *anti* diastereomer:  $\delta$  147.35, 140.22, 128.65, 128.60, 128.25, 126.61, 124.62, 85.48, 73.76, 48.22, 44.04, 30.14. IR (film):  $\bar{\nu}$  = 2866 (w), 1493 (m), 824 (s), 736 (s) cm<sup>-1</sup>. HRMS (EI):  $m/z$  calcd for [C<sub>17</sub>H<sub>17</sub>ClO]<sup>+</sup>: 272.0968; found: 272.0968.



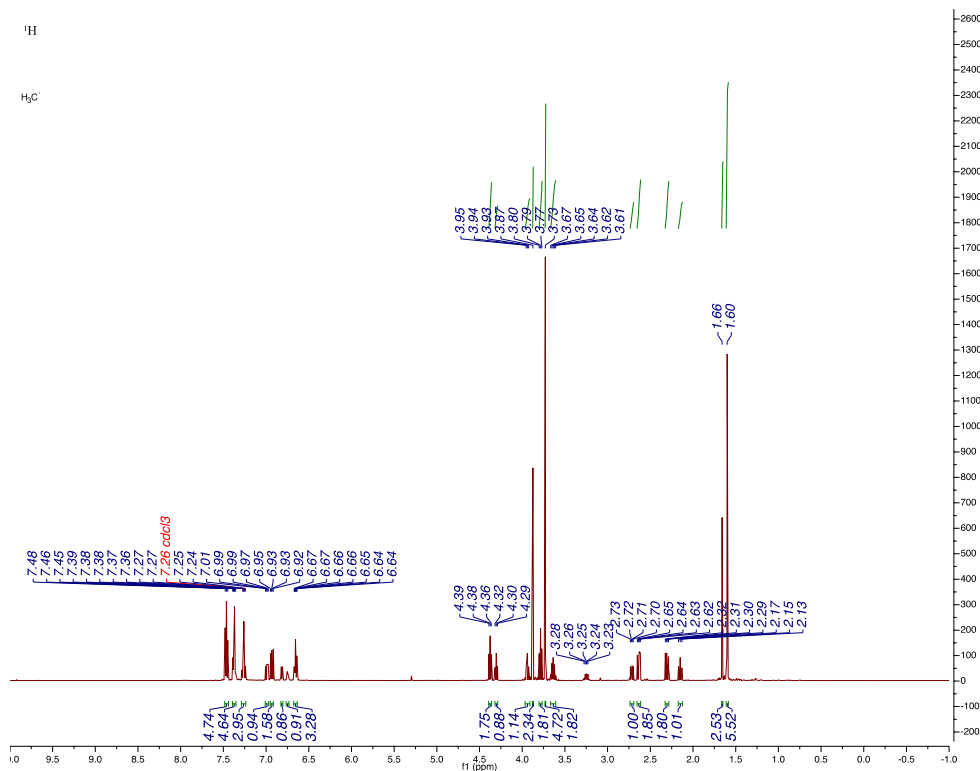




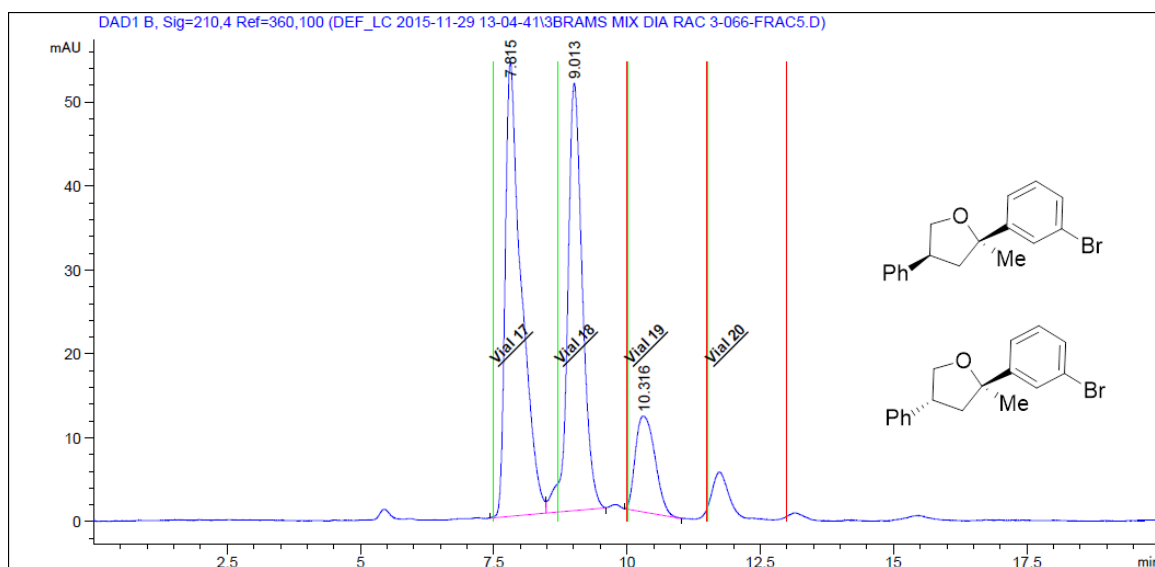
#### 4-(3-Methoxy-4-fluorophenyl)-2-methyl-2-phenyltetrahydrofuran (2.68)

Following the general procedure, a RBF was loaded with  $\text{Sc}(\text{OTf})_3$  (0.005 mmol, 2.5 mg), DCM (0.5 mL), and 1-methyl-1-phenylethene (4 mmol, 0.52 mL). 2-(3-methoxy-4-fluorophenyl)oxirane (2 mmol, 0.27 mL) was added dropwise by syringe over 10 min. After addition was complete, the crude reaction mixture was loaded onto a silica column and eluted with ethyl acetate:hexanes (hexanes to 20 % EtOAc/hexanes) to afford product as a colorless oil in 46 % yield (0.92 mmol, 262 mg, crude dr: 2:1 syn:anti, isolated dr: 1.8:1 syn:anti).  $^1\text{H}$  NMR (600 MHz,  $\text{CDCl}_3$ ): *syn* diastereomer:  $\delta$  7.47 – 7.42 (ArH, m, 2H), 7.38 – 7.33 (ArH, m, 2H), 7.27 – 7.22 (ArH, m, 2H), 6.92 (ArH, dd,  $J$  = 11.2, 8.2 Hz, 1H), 6.66 – 6.62 (ArH, m, 1H), 4.38 – 4.34 ( $\text{H}_a$ , m, 1H), 3.86 ( $\text{H}_a$ , s, 1H), 3.77 ( $\text{H}_b$ , dd,  $J$  = 9.3, 8.6 Hz, 1H), 3.71 ( $\text{H}_e$ , s, 3H), 2.62 ( $\text{H}_c$ , dd,  $J$  = 12.5, 8.4 Hz, 1H), 2.29 ( $\text{H}_c$ , dd,  $J$  = 12.5, 9.5 Hz, 1H), 1.58 ( $\text{H}_d$ , s, 3H); further signals for the *anti* diastereomer: 4.29 ( $\text{H}_{a'}$ , t,  $J$  = 8.4 Hz, 1H), 3.86 ( $\text{H}_{e'}$ , s, 3H), 3.62 ( $\text{H}_{b'}$ , ddd,  $J$  = 17.7, 9.3, 7.9 Hz, 1H), 2.70 ( $\text{H}_{c'}$ , dd,  $J$  = 12.2, 7.1 Hz, 1H), 2.13 ( $\text{H}_{c'}$ , dd,  $J$  = 12.2, 11.2 Hz, 1H), 1.64 ( $\text{H}_{d'}$ , s, 3H).  $^{13}\text{C}$  NMR (150 MHz,  $\text{CDCl}_3$ )  $\delta$  151.97, 148.60, 138.02, 137.74, 128.34, 126.51, 124.58, 119.56 (d,  $J$  = 6.7 Hz), 115.69 (d,  $J$  = 18.2 Hz), 112.41, 85.01, 74.41, 56.10, 48.05, 45.51, 30.72; further signals for the *anti* diastereomer:  $\delta$  150.34, 147.38, 138.00, 137.77, 128.23, 126.59, 124.62, 119.22 (d,  $J$  = 6.7 Hz), 115.88 (d,  $J$  = 18.2 Hz),

112.61, 85.44, 73.86, 56.27, 48.34, 44.35, 30.14.  $^{19}\text{F}$  NMR (564 MHz,  $\text{CDCl}_3$ ): *syn* diastereomer:  $\delta$  -138.40 (ddd,  $J = 12.0, 8.1, 4.3$  Hz); further signals for the *anti* diastereomer:  $\delta$  -138.33 (ddd,  $J = 11.8, 8.1, 4.2$  Hz). IR (film):  $\bar{\nu} = 2872$  (w), 1463 (s), 736 (s), 701 (s)  $\text{cm}^{-1}$ . HRMS (EI):  $m/z$  calcd for  $[\text{C}_{18}\text{H}_{19}\text{O}_2\text{F}]^+$ : 286.1369; found: 286.1369.



2.7.4a: (3+2) between *meta*-bromo- $\alpha$ -methylstyrene and (*R*)-styrene oxide  
(Racemic mixture of diastereomers)



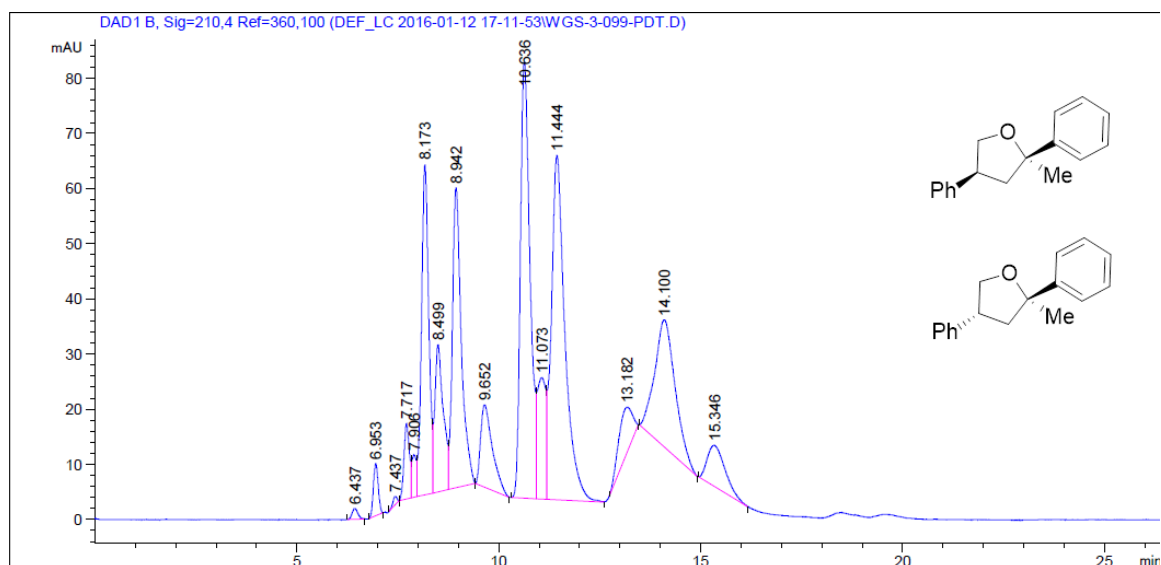
Signal 1: DAD1 B, Sig=210,4 Ref=360,100

Peak #	RetTime [min]	Type	Width [min]	Area [mAU*s]	Height [mAU]	Area %
1	7.815	BV	0.2958	1146.74561	54.09262	47.3098
2	9.013	VB	0.2746	984.60870	50.91247	40.6207
3	10.316	BB	0.3011	292.55429	11.42876	12.0695

Totals : 2423.90860 116.43385

2.7.4b: (3+2) between  $\alpha$ -methylstyrene and styrene oxide using Cu(BOX)

(Racemic mixture of diastereomers. Representative of other chiral catalysts)



Peak #	RetTime [min]	Type	Width [min]	Area [mAU*s]	Height [mAU]	Area %
1	6.437	BB	0.1181	19.68154	1.97731	0.2841
2	6.953	BB	0.1193	78.79197	9.44872	1.1375
3	7.437	BB	0.0862	10.85044	1.54088	0.1566
4	7.717	BV	0.1355	127.12829	13.67107	1.8353
5	7.906	VV	0.0974	58.96226	7.69742	0.8512
6	8.173	VV	0.1862	753.54443	59.91893	10.8789
7	8.499	VV	0.2021	389.49472	26.70762	5.6231
8	8.942	VB	0.2247	837.84137	54.41017	12.0959
9	9.652	BB	0.2419	302.74921	14.93871	4.3708
10	10.636	BV	0.2455	1307.69080	79.06905	18.8791
11	11.073	VV	0.1764	324.29486	22.00491	4.6818
12	11.444	VB	0.3251	1467.90784	62.47383	21.1921
13	13.182	BB	0.2928	202.84497	8.16576	2.9285
14	14.100	BB	0.4160	813.69891	23.01543	11.7473
15	15.346	BB	0.3626	231.17906	7.49000	3.3375

Totals : 6926.66067 392.52982

## 2.8 References

1. Goldsmith, David J.; *J. Am. Chem. Soc.*, **1962**, *84*, 3913-3918.
2. Huq, E.; Mellor, M.; Scovell, E. G.; Sutherland, J. K.; *J. Chem. Soc., Chem. Commun.*, **1978**, 526-528.
3. Fish, P. V.; Sudhakar, A. R.; Johnson, W. S.; *Tet. Lett.*, **1993**, *34*, 7849-7852.
4. Smith, B. M.; Skellam, E. J.; Oxley, S. J.; Graham, A. E.; *Org. Biomol. Chem.*, **2007**, *5*, 1979-1982.
5. Yu, B.; Jiang, T.; Quan, W.; Li, J.; Pan, X.; She, X.; *Org. Lett.*, **2009**, *11*, 629-632.
6. Jin, J.; Chen, Y.; Li, Y.; Wu, J.; Dai, W. M.; *Org. Lett.*, **2007**, *9*, 2585-2588.
7. Va, P.; Roush, W. R.; *J. Am. Chem. Soc.*, **2006**, *128*, 15960-15961.
8. Lacey, J. R.; Anzalone, P. W.; Duncan, C. M.; Hackert, M. J.; Mohan, R. S.; *Tet. Lett.*, **2005**, *46*, 8507-8511.
9. Krasik, P.; Bohemier-Bernard, M.; Yu, Q.; *Synlett*, **2005**, *5*, 854-856.
- 10a. Ling, J.; You, L.; Wang, Y.; Shen, Z.; *J. App. Polymer Sci.*, **2012**, *124*, 2537-2540. b. Cabrera, A.; Peon, J.; Velasco, L.; Miranda, R.; Salmon, A.; Salmon, M.; *J. Mol. Cat. A: Chem.*, **1995**, *104*, L5-L7. c. Mazimba, O.; Majinda, R.; Masesane, I. B.; *Bull. Chem. Soc. Ethiop.*, **2011**, *25*, 299-304.

11. You, L. Hogen-Esch, T. E.; Zhu, Y.; Ling, J.; Shen, Z.; *Polymer*, **2012**, *53*, 4112-4118.
- 12a. Roy, S. C.; Rana, K. K.; Guin, C.; *J. Org. Chem.*, **2002**, *67*, 3242-3248. b. Banerjee, B. Roy, S. C.; *Synthesis*, **2005**, *17*, 2913-2919.
13. Hilt, G.; Bolze, P.; Harms, K.; *Chem. Eur. J.*, **2007**, 4312-4325
14. Trost, B. M.; Shen, H. C.; Survivet, J.; *J. Am. Chem. Soc.*, **2004**, *126*, 12565-12579.
- 15a. Tschan, M. K. L.; Thomas, C. M.; Strub, H.; Carpentier, J. F.; *Adv. Synth. Catal.*, **2009**, *351*, 2496-2504. b. Dang, T. T.; Boeck, F.; Hintermann, L. *J. Org. Chem.*, **2011**, *76*, 9353-9361.
16. For example, see: Chen, J.; Goforth, S. K.; McKeown, B. A.; Gunnoe, T. B.; *Dalton Trans.*, **2017**, *46*, 2884-2891.
17. For lead reviews, see: Gothelf, K. V.; Jorgensen, K. A.; *Chem. Rev.*, **1998**, *98*, 863-910. Hashimoto, T.; Maruoka, K.; *Chem. Rev.*, **2015**, *115*, 5366-5412.
18. Bandini, M.; Cozzi, P. G.; Melchiorre, P.; Umani-Ronchi, A.; *Angew. Chem. Int. Ed.*, **2004**, *43*, 84-87.

## Chapter Three

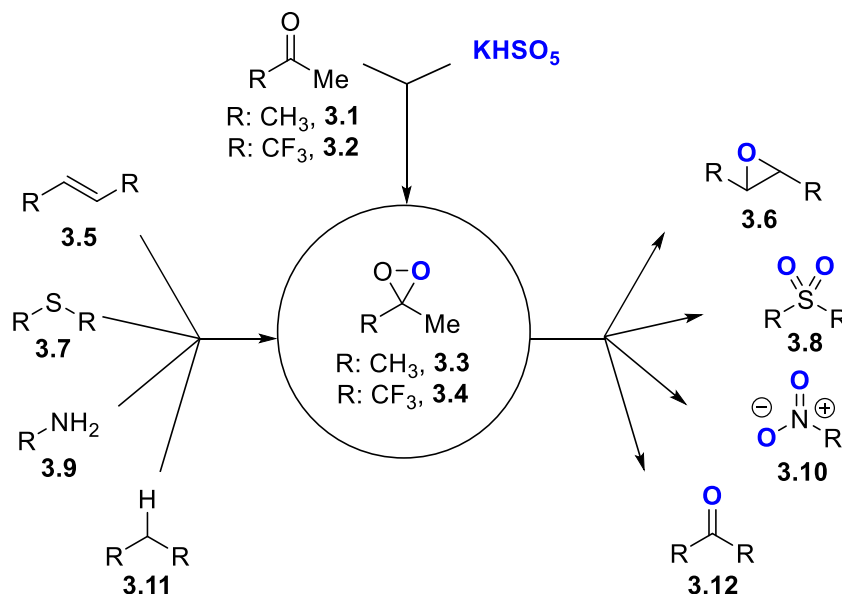
### Catalytic Dioxirane-Mediated Aliphatic C–H Bond Hydroxylation

#### 3.1 Introduction

##### 3.1.1 *Discovery of dioxiranes*

Soon after Curci's original discovery that mixtures of ketones and potassium persulfate formed a new species capable of oxidizing alkynes and alkenes, rather than undergoing a Bayer-Villager rearrangement, Murray and others discovered these adducts are also capable of oxidizing heteroatoms, arenes, and unactivated aliphatic C–H bonds (**Figure 3.1**).<sup>1,2</sup> Studies conducted by Murray and coworkers suggested that the responsible intermediate is not a Criegee-type carbonyl oxide, but rather a three membered cyclic organic peroxide (dimethyldioxirane, DMDO, **3.3**).<sup>3</sup>



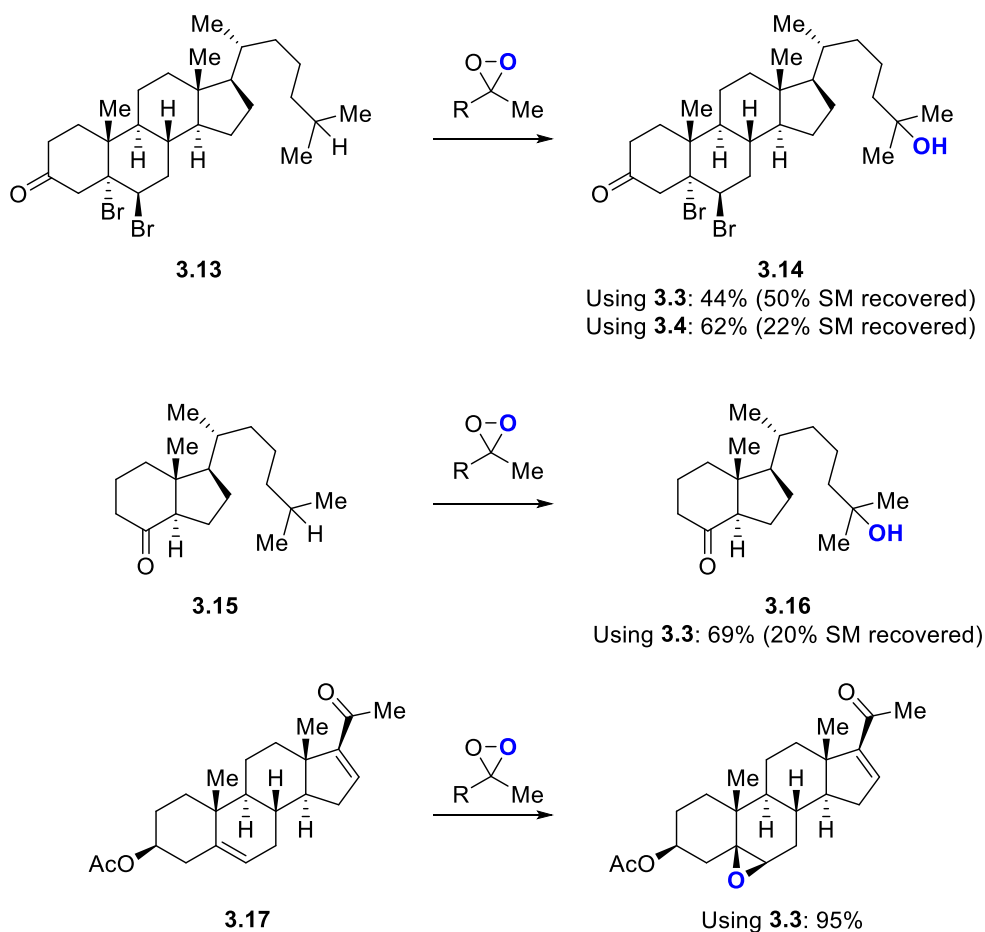
**Figure 3.1:** Reactivity of dimethyldioxirane and trifluoromethyl(methyl)dioxirane

Curci and coworkers introduced a fluorinated derivative of dimethyldioxirane (trifluoromethyl(methyl)dioxirane, TFDO, **3.4**) with greatly improved reactivity.<sup>4</sup> Reactivity was enhanced by the electron withdrawing trifluoromethyl group, giving a dioxirane with reaction rates several thousand times faster than dimethyldioxirane. This increased reactivity was met with increased instability: TFDO solutions quickly decompose through radical mechanisms on prolonged storage or in the presence of trace metal ions. Utility of TFDO was further complicated by the high volatility of the ketone precursor, 1,1,1-trifluoroacetone (b.p.: 23 °C).<sup>4</sup> Despite these drawbacks, the power observed of TFDO led to rapid exploration of new reactivity

The electrophilic nature of these reagents renders them highly selective for oxidation of the most electron rich site present on the molecule. Curci and others

leveraged this selectivity in the oxidation of natural products (**Figure 3.2**).<sup>5</sup> Despite the presence of multiple similarly reactive C-H bonds, oxidations proceeded cleanly affording products in moderate to high yields.

**Figure 3.2:** Dioxirane oxidations of natural products



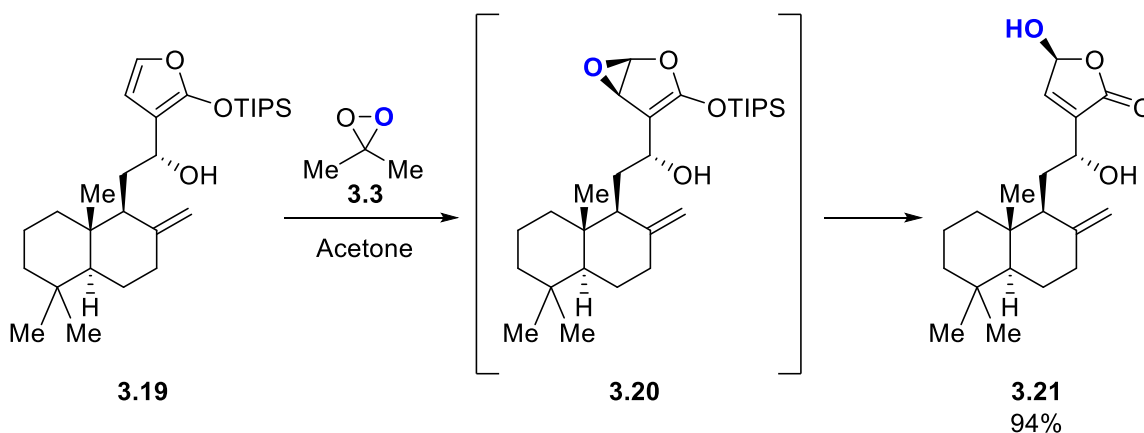
Over the following years a broad range of natural product reaction partners were discovered, with these transformations all sharing the hallmark selectivity observed in dioxirane oxidations. This breadth of reactivity revealed that dioxirane oxidations are predictable, selective, and high yielding transformations that can

operate on complex molecules. These desirable qualities ultimately led to adoption of dioxiranes as synthetic tools, especially for use in late stage transformations.

### 3.1.2 Use of dioxirane oxidations in total synthesis

In Boukouvalas' total synthesis of (+)-Zerumin B (**3.21**), DMDO is used to install the final oxygenation pattern in the natural product (**Scheme 3.1**).<sup>6</sup> Oxygen incorporation occurs at the most sterically accessible nucleophilic reaction site. Even though the molecule contains nine reactive aliphatic C–H bonds, three allylic C–H bonds, three double bonds, and an unprotected alcohol, the oxidation proceeds smoothly providing **3.21** in 94% yield.

**Scheme 3.1:** (+)-Zerumin B end game

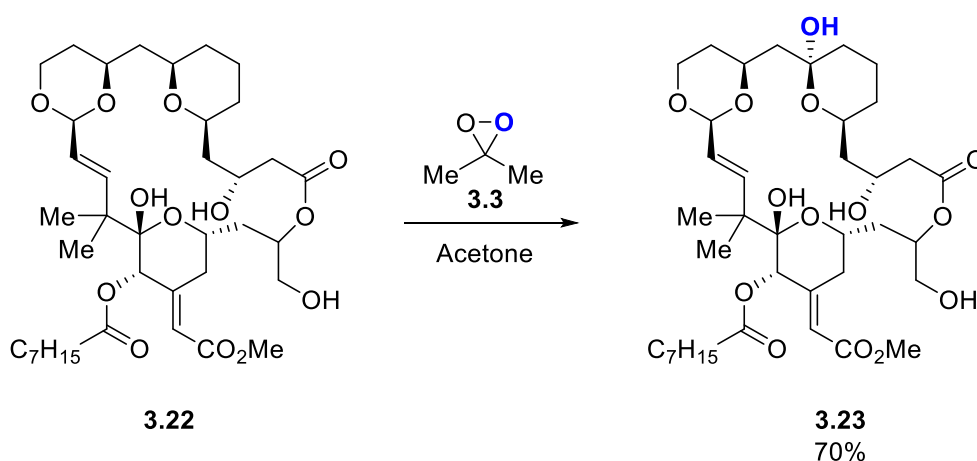


### 3.1.3 Use of dioxirane oxidations in natural product diversification

The ability to functionalize complex molecules has also led to use of dioxiranes in derivitization of natural products. In Wender and coworkers'

exploration of simplified Bryostatin 1 analogues, DMDO was able to selectively oxygenate heavily functionalized Bryostatin analog **3.22** that contains multiple unprotected reaction centers including ethers, acetals, alcohols, and double bonds (**Scheme 3.2**).<sup>7</sup>

**Scheme 3.2:** Protecting group free Bryostatin diversification



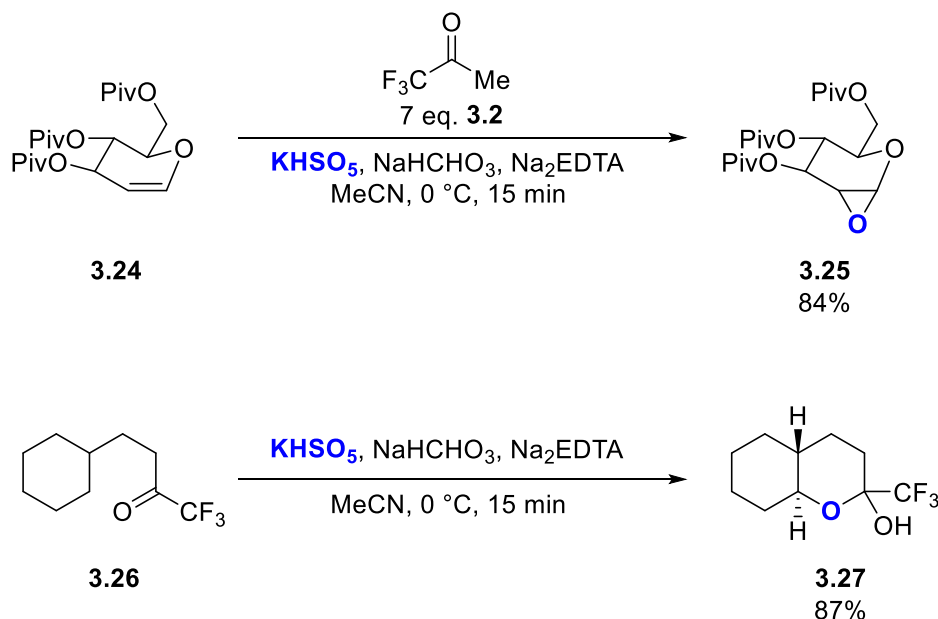
### 3.1.4 Development of *in situ* protocols for dioxirane oxidations

Typical dioxirane oxidations employ pre-prepared dilute (ca. 0.02 M) solutions of dioxirane in its parent ketone, demanding a labor and material intensive procedure. Although early examples exist of methods which allow *in situ* formation of dioxiranes for epoxidation reactions, Yang and coworkers developed general conditions which allow for the *in situ* generation of dioxiranes for use in hydroxylation reactions.<sup>8</sup> By using super-stoichiometric amounts of ketone in MeCN, TFDO mediated epoxidation reactions can be conducted quickly in a single

flask (**Scheme 3.3**). Further studies by Yang showed these conditions can be extended to include intramolecular C–H bond hydroxylation.<sup>9</sup>

---

**Scheme 3.3:** *In situ* dioxirane formation



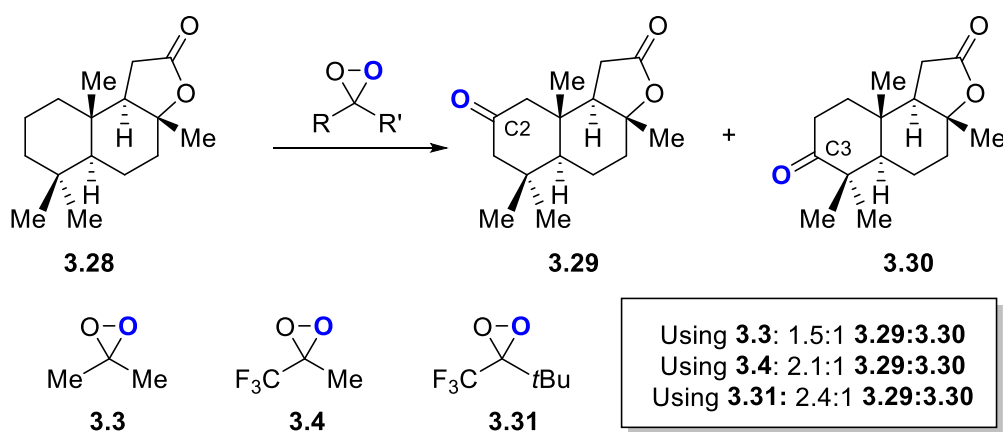
### 3.1.5 Catalytic dioxirane epoxidation

Use of catalytic amounts of ketones to conduct epoxidations have been known for some time, with the first highly enantioselective catalysts developed by Yang and coworkers in 1996.<sup>10</sup> This led to an explosion in research into dioxirane catalysis, with a wide range of structurally and electronically diverse catalysts being discovered.<sup>11</sup> This range of catalysts ultimately allowed for the asymmetric epoxidation of all possible alkene substitution patterns.

Despite these developments, catalytic dioxirane mediated C–H hydroxylation remained undiscovered. Although it is known that site selectivity can

be influenced by dioxirane structure (**Scheme 3.4**), the catalyst-controlled site- and stereo-selectivity unlocked with catalytic epoxidation reactions remained elusive for hydroxylation.<sup>12</sup> Having access to a toolbox of catalysts that offer complimentary site selectivity would be a powerful new paradigm for C–H hydroxylation chemistry.

**Scheme 3.4:** Structure-dependent selectivity

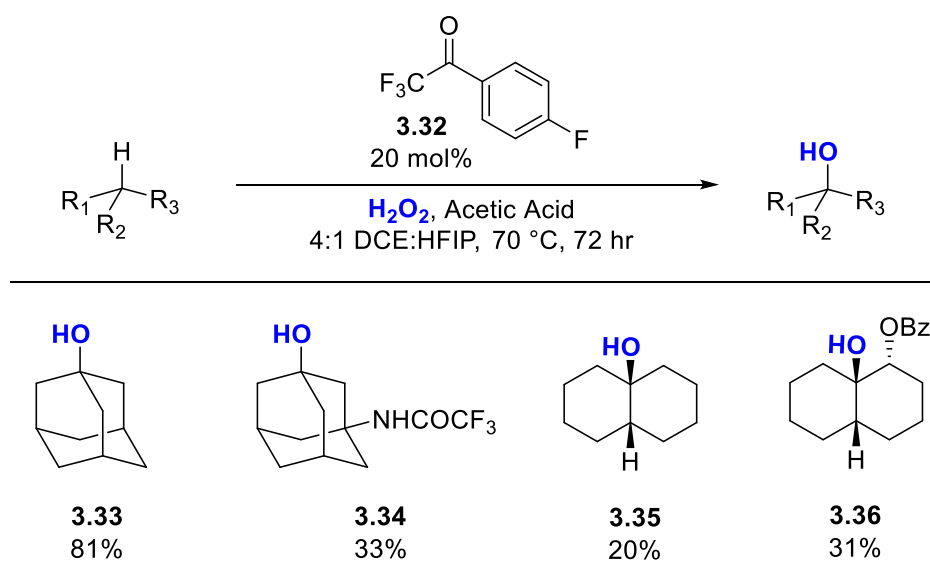


### 3.1.6 Catalytic dioxirane C–H hydroxylation

The first discovery of a catalytic dioxirane mediated aliphatic C–H bond hydroxylation was reported by Hilinski and Pierce in 2014.<sup>13</sup> Trifluoroacetophenones, previously published as epoxidation catalysts, were used under newly developed conditions to perform C–H hydroxylation with up to 81% yield (**Table 3.1**). Substrate scope was limited to highly reactive substrates with other cyclic or acyclic substrates showing only trace conversion. During these

investigations, ketone fluorination and use of the strong hydrogen bonding solvent 1,1,1,3,3,3-hexafluoroisopropanol (HFIP) were determined to be critical for reactivity.<sup>14</sup> Although scope of reaction partners failed to replicate isolated or *in situ* dioxirane protocols, this report provided a framework for future exploration of conditions.

**Table 3.1:** First reported catalytic dioxirane mediated C–H hydroxylation reaction



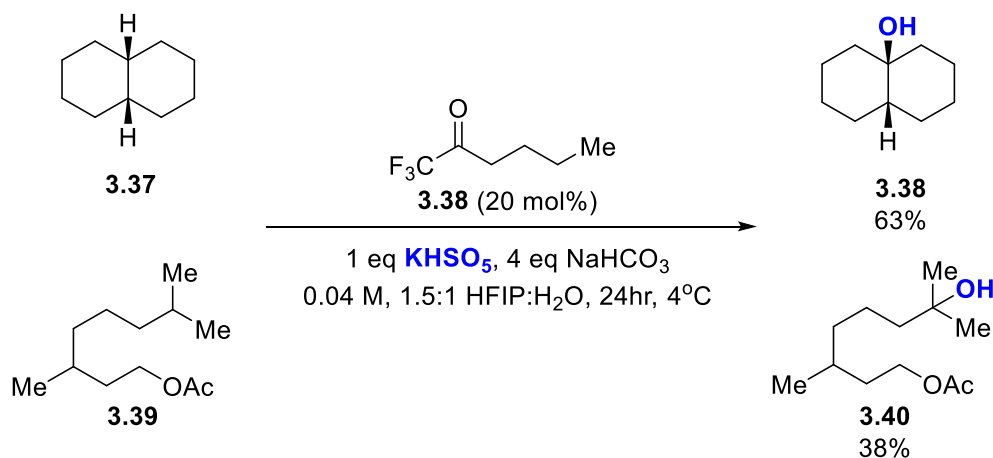
## 3.2 Reaction Optimization

### 3.2.1 Selection of initial reaction conditions

We used a combination of previously reported conditions to reexamine a set of initial conditions for catalytic dioxirane-mediated C–H hydroxylation reaction. A water-HFIP mixture was chosen as the solvent based on

conditions used for *in situ* formation of dioxiranes and related electrophilic oxygen transfer reagents.<sup>12</sup> The terminal oxidant chosen was a potassium persulfate-bicarbonate buffer that has been used extensively as a stoichiometric terminal oxidant in catalytic dioxirane-mediated epoxidation reactions. Although many C–H bond hydroxylation reactions employ 1,1,1-trifluoroacetone as the dioxirane precursor, its volatility (b.p. 23 °C) led us to consider more easily handled ketones. We instead chose to use commercially available, easily handled 1,1,1-trifluorohexan-2-one (**3.38**) at 20 mol% loading. We were delighted to find that *cis*-decalin was hydroxylated in 63% yield after 24 hours at 4 °C (**Scheme 3.5**). We also tested substrates known to be unreactive under our previously reported catalytic conditions, as the hydroxylation of *cis*-decalin represented a two-fold increase in yield. Gratifyingly, the hydroxylation of 3,7-dimethyloctanol acetate (**3.39**) proceeded in 38% conversion.

**Scheme 3.5:** Catalytic C-H hydroxylation under unoptimized conditions



Reactions performed on 0.1 mmol scale. Corrected GC yields reported.



### 3.2.2 Further development of reaction parameters

During these first attempts we noticed that despite the miscibility of HFIP and water, addition of persulfate buffer created two distinct phases. As it is unclear how **3.38** and its corresponding dioxirane partition between the organic and aqueous phases in our reaction conditions, several phase-transfer catalysts were screened for yield improvements (**Table 3.2**). Inclusion of either 18-crown-6 and tetrabutylammonium hydrogensulfate showed similar increases in conversion. Ammonium hydrogensulfate is capable of “salting in” organic compounds into the aqueous layer but is also capable of delivering persulfate into the organic layer.<sup>15</sup> The similar activity of 18-crown-6, which acts solely as an organic-phase solubilizer of potassium salts, suggests that dioxirane formation and reactivity occur within the HFIP layer of the reaction. Interestingly, higher loadings of 18-crown-6 led to a decrease in substrate conversion, likely due to hydroxylation of 18-crown-6. This nonproductive pathway may become more significant in the hydroxylation of less reactive substrates. Tetrabutylammonium hydrogensulfate was chosen as the phase-transfer catalyst due to its superior performance.

**Table 3.2:** Investigation of phase transfer catalysts

Phase-transfer Catalyst	Mol% Loading	GC Yield
None	-	63%
18-Crown-6	2.5	60%
18-Crown-6	5	76%
18-Crown-6	10	68%
<i>n</i> Bu <sub>4</sub> NHSO <sub>4</sub>	2.5	77%
<b><i>n</i>Bu<sub>4</sub>NHSO<sub>4</sub></b>	<b>5</b>	<b>80%</b>

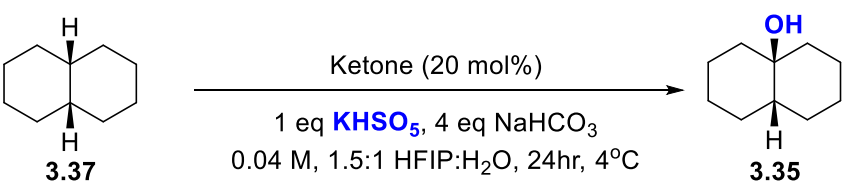
Reactions performed on 0.1 mmol scale. Corrected GC yields reported.

We further tuned the initial reaction parameters to increase the yields of less reactive substrates. Optimal catalyst loading proved to be 20 mol% with less conversion observed with lower catalyst loading. With catalyst loading higher than 20 mol% lower conversion was observed likely due to collision between dioxiranes or dioxiranes and oxidants, leading to the formation of molecular oxygen. This tentative explanation was supported by an increase in gas evolution as catalyst loading was increased.

Several other ketones known to engage in stoichiometric and catalytic oxidation reactions were tested for catalytic activity (**Table 3.3**). Although DMDO is a competent hydroxylation reagent, acetone displayed poor catalytic activity

under our conditions. 1,1,1-Trifluoroacetone afforded similar conversion to catalyst **3.38** under our reaction conditions, validating the use of **3.38** as a conveniently handled 1,1,1-trifluoroacetone surrogate. The slight differences in yield observed may be due to the difficulty in measuring microliter quantities of 1,1,1-trifluoroacetone rather than any intrinsic difference in catalyst performance. Interestingly, 4'-trifluoromethyl-2,2,2-trifluoroacetophenone which has been reported as a catalyst for epoxidation and hydroxylation reactions was a poor catalyst under our new conditions. In this case, noticeable catalyst degradation occurred over the course of the reaction due to a persulfate induced Bayer-Villager rearrangement.

**Table 3.3:** Investigation of catalysts

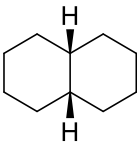
		
Ketone	Mol% Loading	GC Yield
1,1,1-Trifluorohexanone	10	48%
<b>1,1,1-Trifluorohexanone</b>	<b>20</b>	<b>80%</b>
1,1,1-Trifluorohexanone	30	73%
Acetone	20	5%
1,1,1-Trifluoroacetone	20	65%
2,2,2,4'-Tetrafluoroacetophenone	20	17%

Reactions performed on 0.1 mmol scale. Corrected GC yields reported.

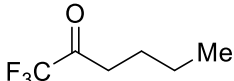
Other solvents commonly employed in dioxirane mediated oxidations, such as 2,2,2-trifluoroethanol (TFE) or acetonitrile, led to lower reactivity (**Table 3.4**).

High dilution was required to fully solubilize the terminal oxidant: an increase in concentration from 0.04 M to 0.1 M left substantial amounts of undissolved material in the aqueous layer and was met with a 75% decrease in product formation. Interestingly, altering the HFIP:water ratio to circumvent using large quantities of HFIP led to drastically lowered yields. Several other changes were explored such as aqueous layer pH, temperature, and addition of metal scavengers, but none showed positive impact on reaction performance.

**Table 3.4:** Investigation of solvents



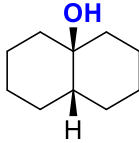
**3.37**



**3.38** (20 mol%)

---

1 eq **KHSO<sub>5</sub>**, 4 eq NaHCO<sub>3</sub>  
 2.5 mol% 18-Crown-6  
 0.04 M, Solvent, 24hr, 4°C



**3.35**

Solvent (Ratio)	GC Yield
MeCN:H <sub>2</sub> O (1.5:1)	25%
TFE:H <sub>2</sub> O (1.5:1)	40%
HFIP:H <sub>2</sub> O (1.5:1)	80%
HFIP:H <sub>2</sub> O (1:5)	16%
HFIP:H <sub>2</sub> O (5:1)	61%

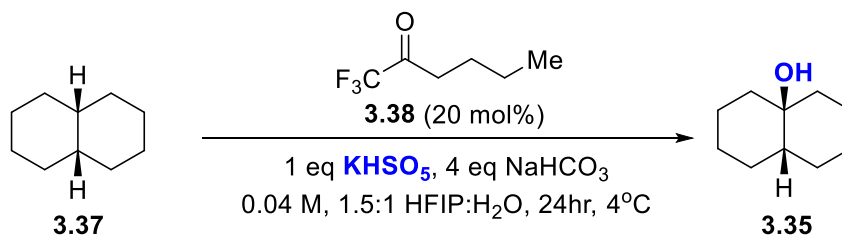
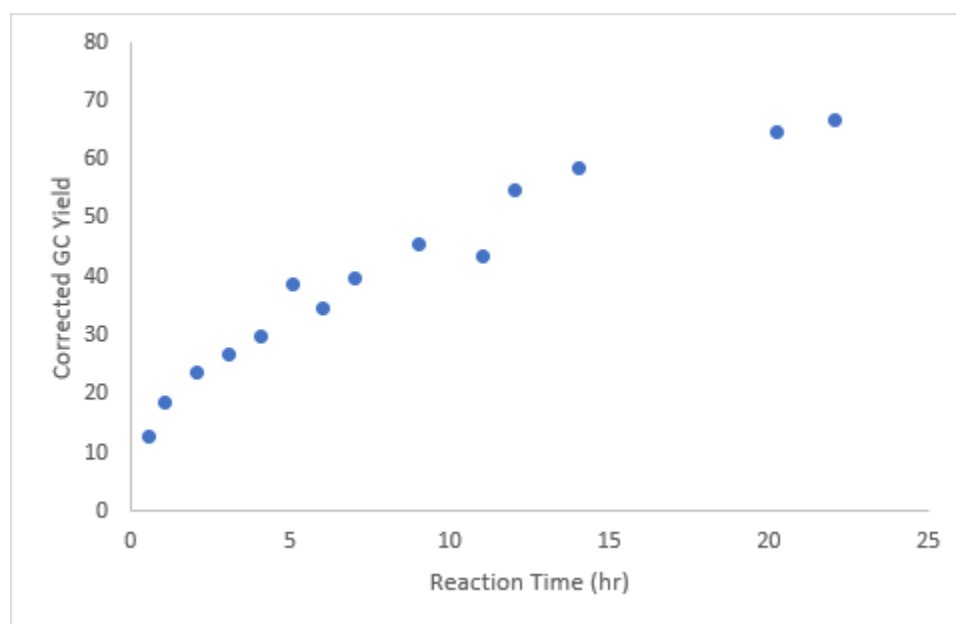
Reactions performed on 0.1 mmol scale. Corrected GC yields reported.

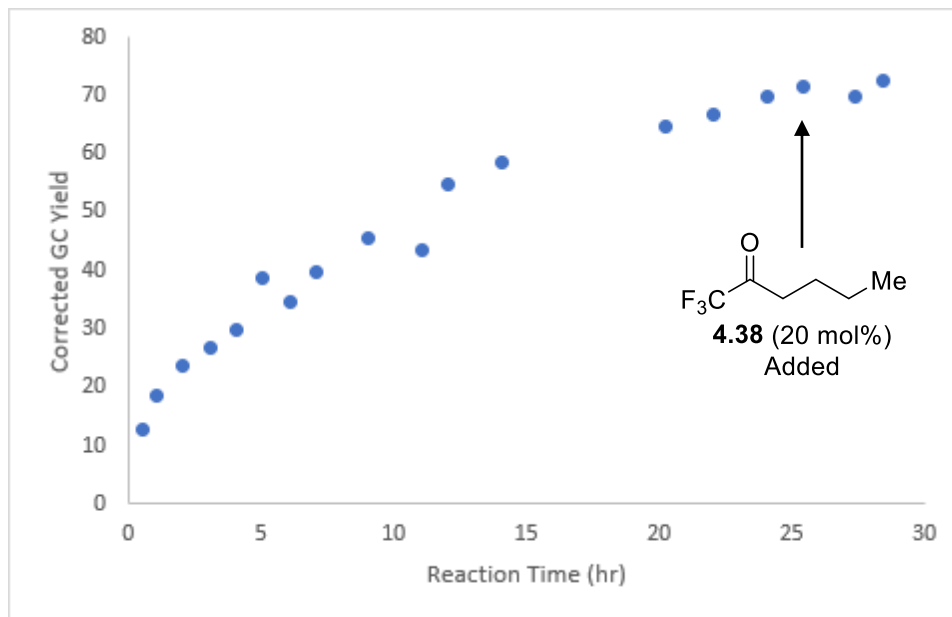
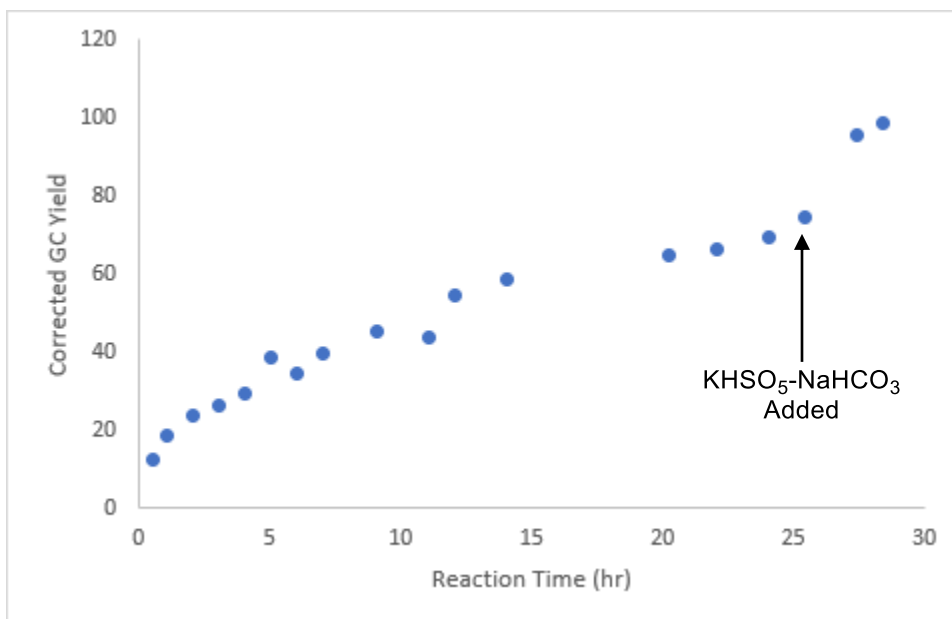
### 3.2.3 Recovery experiments

While highly reactive substrates such as *cis*-decalin could be hydroxylated in high yields after initial reaction optimization, attempts using less

activated substrates resulted in lower yields. Several recovery experiments were conducted to determine the conversion limiting factor in the reaction, as both catalyst or terminal oxidant could be nonproductively consumed over the course of the reaction (**Figure 3.3**). A plot of conversion of *cis*-decalin verses time was first established, which featured a cessation of catalytic activity at *ca.* 25 hours (**Figure 3.3a**). No additional reactivity was observed when the reaction mixture was spiked with an additional 20 mol% of catalyst **3.38** at 25 hours, indicating that catalyst consumption is not the sole contributor to halted reactivity (**Figure 3.3b**). A strong recovery effect is noticed when an additional equivalent of persulfate-bicarbonate mixture is added at this point, with complete hydroxylation of *cis*-decalin occurring over the next few hours (**Figure 3.3c**). From these experiments we concluded that unproductive consumption of our terminal oxidant was largely responsible for limited conversion.

Unfortunately, the use of more than 1 eq persulfate and 4 eq bicarbonate resulted in *decreased* hydroxylation activity. Use of additional equivalents of oxidant were only beneficial when they are added after the first equivalent has been consumed.

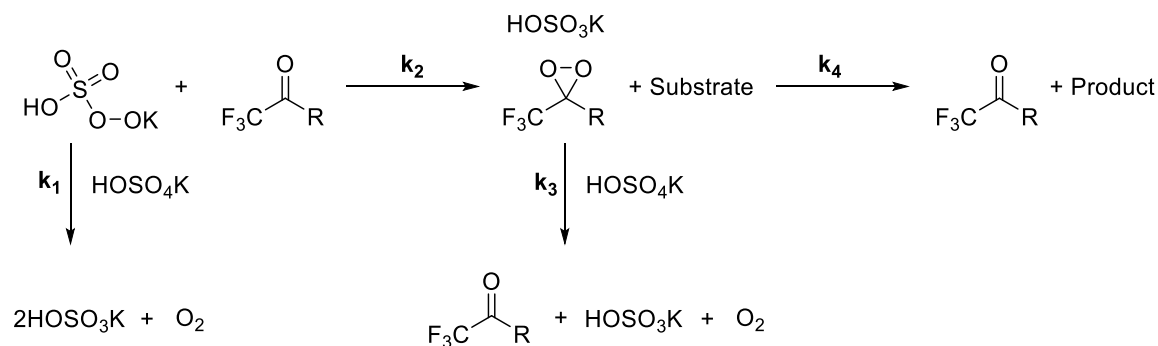
**Figure 3.3:** Recovery experiments; *cis*-decalin hydroxylation**3a:** Standard conditions

**3b:** Ketone added to reaction mixture**3c:** persulfate/bicarbonate added to the reaction mixture

### 3.2.4 Steady state approximation

The fate of the terminal oxidant is ultimately either incorporation of oxygen into the product or the production of singlet oxygen gas through two major routes (**Scheme 3.6**).<sup>16</sup> By assuming the concentration of dioxirane is constant and low throughout the course of the reaction, a steady state approximation can be used to determine rate equations for both product and byproduct formation (**Equation 3.1**). This steady state approximation is greatly simplified by the irreversible nature of these reactions.

**Scheme 3.6:** Routes of potassium persulfate consumption



**Equation 3.1:** Steady state approximation

$$\frac{d[\text{oxygen}]}{dt} = [\text{persulfate}]^2 \left[ \frac{(k_1 + k_2 k_3 [\text{ketone}])}{k_3 [\text{oxone}] + k_4 [\text{substrate}]} \right]$$

$$\frac{d[\text{product}]}{dt} = \frac{k_2 k_4 [\text{persulfate}] [\text{ketone}] [\text{substrate}]}{k_3 [\text{persulfate}] + k_4 [\text{substrate}]}$$



As the denominator in both equations is the same, it is unlikely to impact the proportion between productive and nonproductive consumption of oxidant. As revealed in the recovery experiments, it appears catalyst **3.38** is not appreciably consumed during the reaction, allowing its concentration to be treated as a constant. These assumptions allow further simplification of the rate equations (Equation 3.2).

---

**Equation 3.2:** Simplified rate equations

$$\frac{d[\text{oxygen}]}{dt} = (k_1 + k_2 k_3)[\text{persulfate}]^2$$

$$\frac{d[\text{product}]}{dt} = (k_2 k_4[\text{persulfate}][\text{substrate}])$$

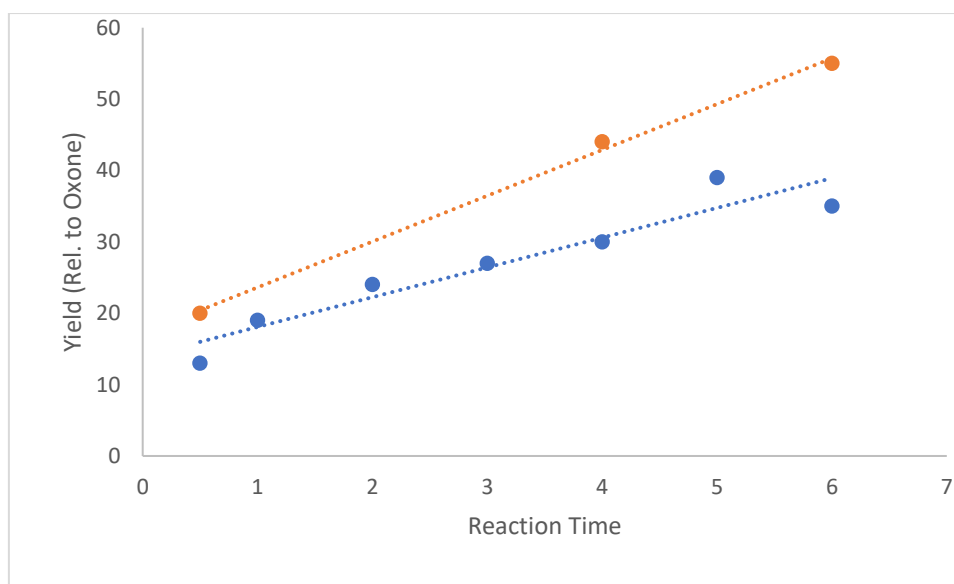

---

In these simplified rate equations, product formation has a first order dependence on persulfate concentration whereas oxygen formation has a second order dependence on persulfate concentration. This suggests that the fate of the terminal oxidant is biased towards product formation at lower concentrations of persulfate, which is well supported by previous experiments and literature reports.

To further explore this prediction, *cis*-decalin was exposed to the reaction using two protocols for oxidant addition. In one trial, persulfate was added as a single portion at the beginning of the reaction; in the other, persulfate was added

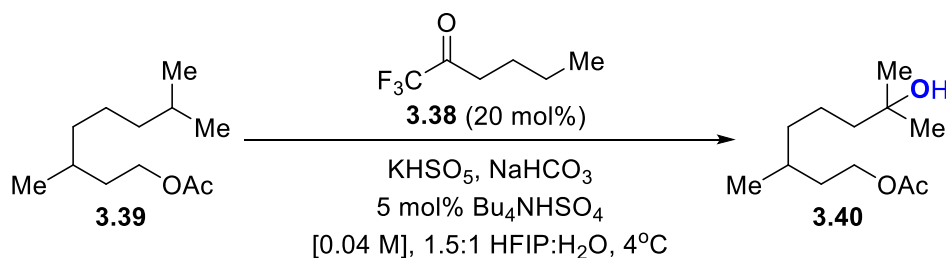
portion-wise (**Figure 3.4**). When hydroxylation yield is calculated based on persulfate as the limiting reagent, a noticeable enhancement in persulfate consumption efficiency emerged.

**Figure 3.4:** Comparison of efficiency of oxidant consumption



Gold: portionwise addition of oxone. Blue: single addition of oxone

Although there is a noticeable decrease in the recovery effect with subsequent additions of persulfate-bicarbonate, likely due to limited solubility of additional oxidant and overall changes to the colligative properties of the solution, this oxidant addition protocol allowed less reactive substrates to be hydroxylated in yields analogous to isolated dioxiranes. This portionwise addition protocol allowed high conversion of oxidation-resistant substrates (**Table 3.5**).

**Table 3.5:** Optimized oxidant addition protocol

Eq. Oxone	Eq. $\text{NaHCO}_3$	Addition Type	Reaction Time	GC Yield
1 eq	4 eq	Single portion	24 hr	46% Yield
2 eq	8 eq	Single portion	24 hr	46% Yield
2 eq	8 eq	Two portions ( $t = 0, 24 \text{ hr}$ )	48 hr	73% Yield

**Final Yield** (3 eq oxone, 12 eq  $\text{NaHCO}_3$ ,  $t = 0, 24, 48 \text{ hr}$ ;  $t_{\text{tot}} = 72 \text{ hr}$ ): 85% Yield

Reactions performed on 0.1 mmol scale. Corrected GC yields reported.

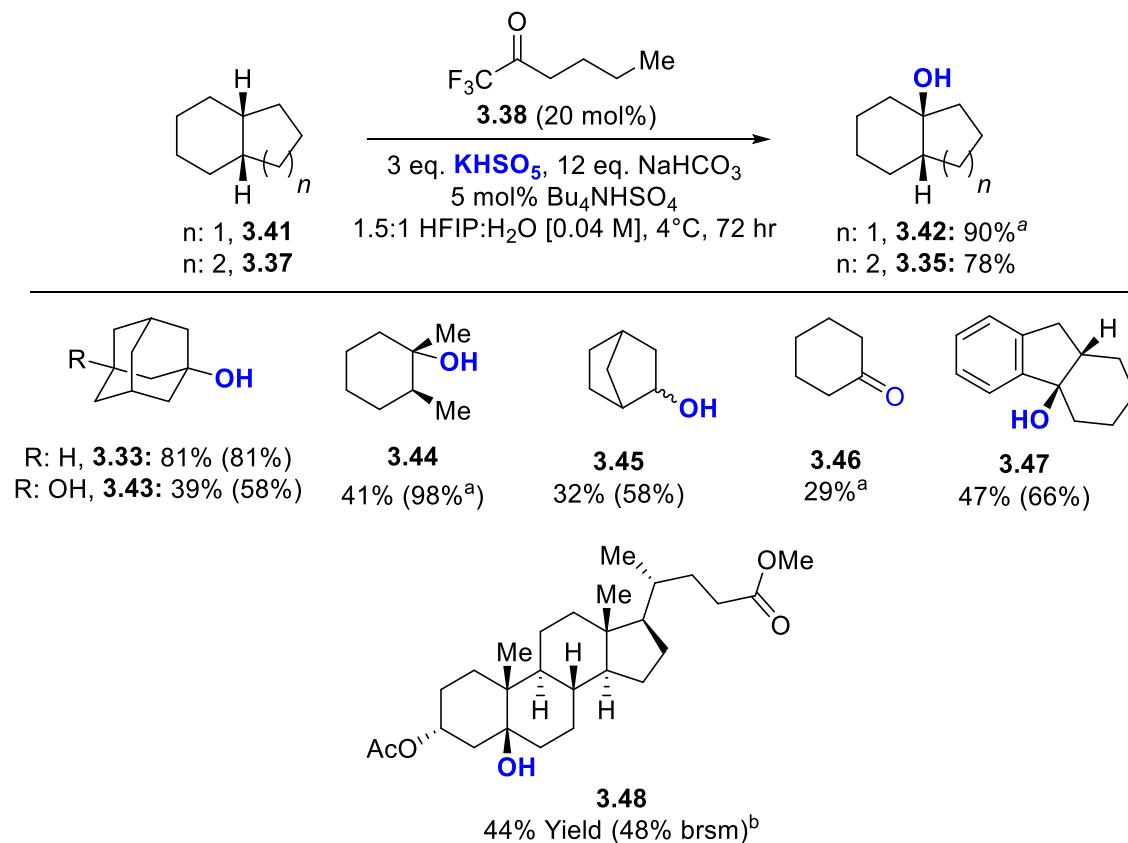
### 3.3 Scope of Reaction Partners

#### 3.3.1 Cyclic substrates

In general, cyclic substrates were singly hydroxylated in good to excellent yields. Several substrates offered higher yields than were obtained from the previously reported dioxirane catalytic system and scope was expanded to previously unreactive partners under catalytic conditions (**Table 3.6**). Although many of these substrates were insoluble in HFIP, reactivity could be attained with vigorous stirring. Adamantane and norbornane were both insoluble solids that required the addition of DCM as a cosolvent to allow hydroxylation to occur (**3.33**,

**3.45).** By optimizing the minimal amount of cosolvent required, conversion remained high.

Although each substrate contains multiple C–H bonds, oxidation is limited to a single carbon due to sensitivity of dioxiranes to inductive effects. Each hydroxylation event reduces the electron density of nearby C–H bonds, slowing the rate of subsequent oxidation events. This effect is demonstrated nicely when comparing oxidation of adamantane and 1-adamantanol: 1-adamantanol is sluggish to react providing hydroxylated product in less than half of the yield as adamantane provided (**3.33**, **3.43**).

**Table 3.6:** Scope of cyclic hydroxylation substrates

Reactions performed on 0.5 mmol scale with three additions of persulfate-bicarbonate at 24 h intervals. Isolated yields. Yields in parenthesis are yields based on recovered starting material.  
<sup>a</sup>Corrected GC yield in parenthesis. <sup>b</sup>Yield after two reaction cycles.

In some cases, the scope of reactive partners extended beyond tertiary C–H bonds to include methylene oxidation. Cyclohexane, for example, was oxidized cleanly to cyclohexanone (**3.46**) with only trace amounts of Bayer-Villager

oxidation products observed. A small amount of cyclohexanol is present early in the reaction indicating the formation of cyclohexanone involves two separate hydroxylations. Norbornane was selectively hydroxylated to a 1:3 mixture of *exo*- and *endo*-norborneol (**3.45**). Overoxidation of norborneol to norcamphor is inhibited by geometric constraints, as first observed with stoichiometric dioxirane reagents.<sup>2</sup>

Hydroxylation of a benzylic substrate (**3.47**) suggests an improvement in substrate scope in comparison to other available catalytic methods. In our hands, both the White-Chen iron catalyst<sup>17</sup> and Du Bois benzoisothiazole catalyst<sup>18</sup> preferentially oxidized the electron neutral arene over the tertiary C–H bond.

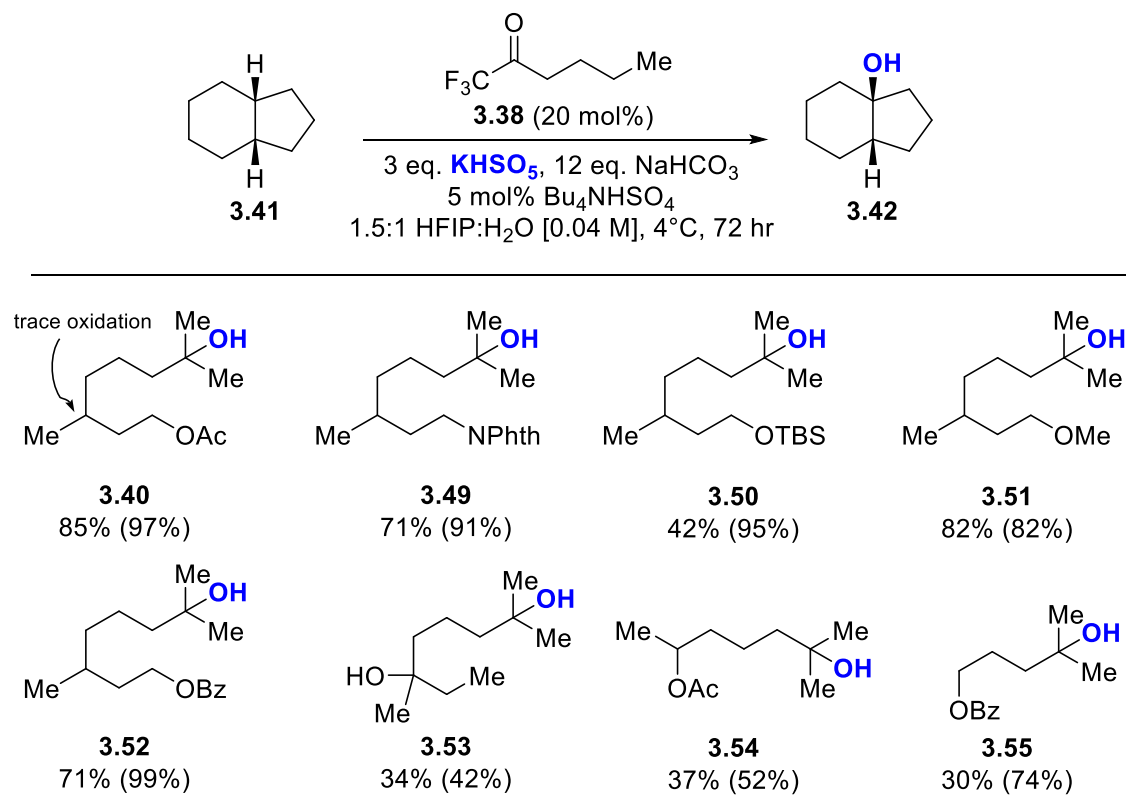
The high selectivity of these oxidations allowed for hydroxylation of complex natural products containing multiple similarly reactive C–H bonds. In the case of protected lithocholic acid derivative, a single major product was formed in greater than 10:1 selectivity over other hydroxylation products (**3.48**). Although this substrate was slow to react, yields were improved by recovering starting material and resubjecting it to the reaction conditions.

### 3.3.2 Acyclic substrates

A range of acyclic substrates featuring less activated C–H bonds can also be hydroxylated in good to excellent yields (**Table 3.7**). The deactivating effect of inductive withdrawing groups (*vide supra*) leads to high selectivity (often >15:1) between distal and proximal tertiary C–H bonds. These inductive effects also

dissuade polyhydroxylation from occurring. The power of this effect is noticeable in progressively shortening linear esters: a six-carbon spacer between the electronic withdrawing group and reaction site provides the hydroxylated product **3.52** 71% yield, whereas a three-carbon spacer provides the product **3.55** in 30% yield. Substrates where the reaction site is separated by only one carbon from an electron withdrawing group are unreactive.

**Table 3.7:** Scope of acyclic hydroxylation substrates



Reactions performed on 0.5 mmol scale with three additions of persulfate-bicarbonate at 24 h intervals. Isolated yields. Yields in parenthesis are yields based on recovered starting material.

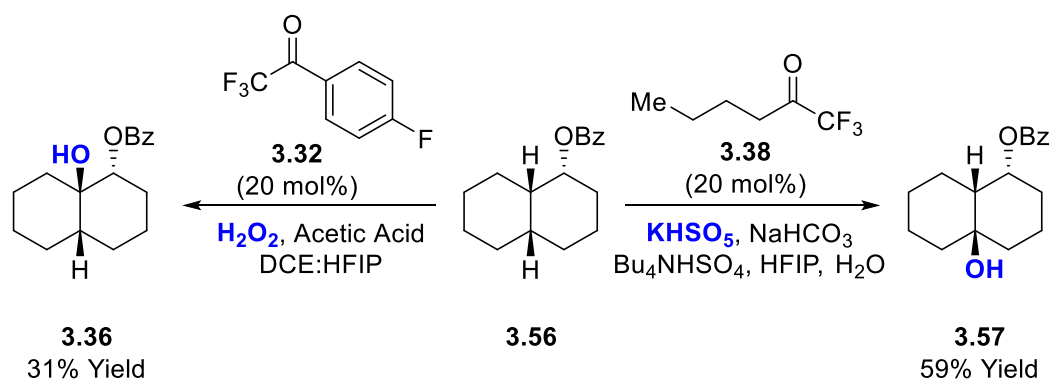
The near-neutral pH of our reaction conditions allows catalytic reactivity with acid sensitive functional groups, such as silyl ethers. Du Bois and White catalysts both require acidic conditions for hydroxylation. As such, hydroxylation under those conditions in our hands resulted in rapid silyl ether cleavage followed by oxidation of the primary alcohol. Interestingly, methyl ethers were also tolerated despite literature precedence that TFDO will easily oxidized ethers and acetals, again highlighting the mildness of our method.<sup>2</sup>

### 3.3.3 Complementary selectivity between dioxirane catalysts

In the hydroxylation of *cis*-decalin benzoate, our new catalytic system gives complementary reactivity to the previously reported catalytic dioxirane hydroxylation. In the first report, using trifluoroacetophenone derived dioxiranes, *cis*-decalinol ester **3.56** was selectively hydroxylated at the tertiary C–H bond proximal to the electron withdrawing group (**Scheme 3.7**).<sup>13</sup> Under the new conditions, oxidation instead takes place exclusively at the distal tertiary C–H bond. In each case, the alternative regioisomer was detected in only trace quantities. These complementary results nicely demonstrate the usefulness of having different methods for catalytic hydroxylation. Further investigation must be conducted to efficiently take advantage of these alternate regioselectivities, with the overall goal of having a toolbox of methods capable of predictably reacting with disparate C–H bonds in a complex molecule.

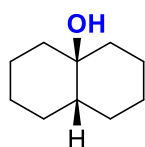


---

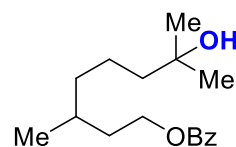
**Scheme 3.7:** Catalyst controlled selectivity


### 3.3.4 Comparison of methods

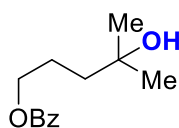
Several substrates that were catalytically hydroxylated by catalyst **3.38** have been reported in prior catalytic or stoichiometric hydroxylation reactions. This information provides a concise comparison across several approaches to aliphatic C–H bond hydroxylation (**Table 3.8**).

**Table 3.8:** Comparison of hydroxylation methods**3.35**

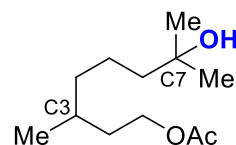
This work: 78%  
 Isolated TFDO: 92%  
 Hilinski, 2014: 22%

**3.52**

This work: 71%  
*in situ* TFDO: 54%  
 Du Bois, 2009: 70%

**3.55**

This work: 30%  
 Du Bois, 2014: 71%

**3.40**

This work: 85%; 17:1 C7:C3  
 White, 2007: 43%; 5:1 C7:C3  
*in situ* TFDO: 54%; 4:1 C7:C3

Hydroxylation of *cis*-decalin with catalyst **3.38** gave similar conversion (albeit lower isolated yields due to workup problems) to isolated TFDO and far outcompetes other hydroxylation methods reported by our lab which suffer from product degradation or additional hydroxylation events.<sup>4,13</sup> In the case of 3,7-dimethyloctanol benzoate, **3.38** catalyzed reactions far outcompeted the standard *in situ* TFDO approach.<sup>19</sup> The mildness of our conditions was reflected in lower

yields for less activated substrates. For example, the harsher Du Bois oxidation system was able to hydroxylate C–H bonds near inductive withdrawing groups, whereas our catalyzed method could not provide hydroxylation products in synthetically useful yields.<sup>18</sup>

The selectivity observed for distal over proximal tertiary C–H bonds in **3.40** reflects the potential synthetic utility of having a milder catalyst system that is incapable of hydroxylating near electron withdrawing groups. Whereas the more reactive White-Chen catalyst provides hydroxylated products with poor discrimination between C–H bonds, these catalyzed reactions generate only trace quantities of proximal hydroxylation.<sup>17</sup> Interestingly, *in situ* TFDO conditions also provided poor discrimination between hydroxylation sites, suggesting that our high degree of selectivity is not entirely catalyst dependent but could be dependent on conditions instead.<sup>19</sup> Further investigation into the impact of reaction conditions on oxidation selectivity is discussed in Chapter 5.

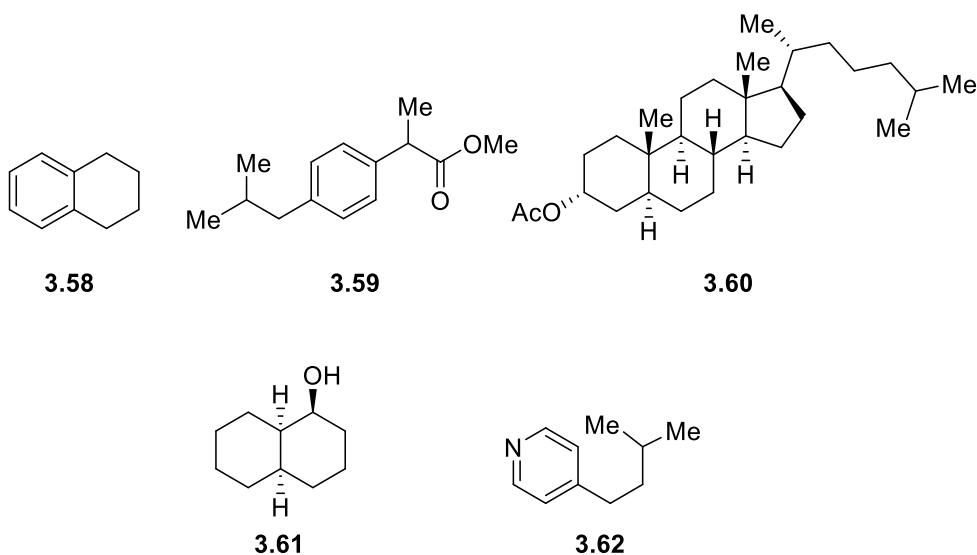
### 3.3.5 Incompatible substrates

Several substrates expected to perform well under our reaction conditions offered little selectivity or no conversion (**Table 3.9**). Despite being able to hydroxylate an electron neutral benzylic substrate, similar arenes did not afford hydroxylated products. In the case of ibuprofen methyl ester **3.59**, no reactivity was observed despite possession of C–H bonds similar to those previously known to react with TFDO<sup>4</sup>. For tetralin (**3.58**), the major products were derived from arene

oxidation, suggesting that a highly reactive aliphatic C-H bond is required to outcompete arene oxidation. Compounds containing unprotected oxidizable groups such as free alcohols (**3.61**) or nucleophilic amines (**3.62**) undergo heteroatom oxidation instead of C-H bond hydroxylation.

---

**Table 3.9:** Unreactive substrates

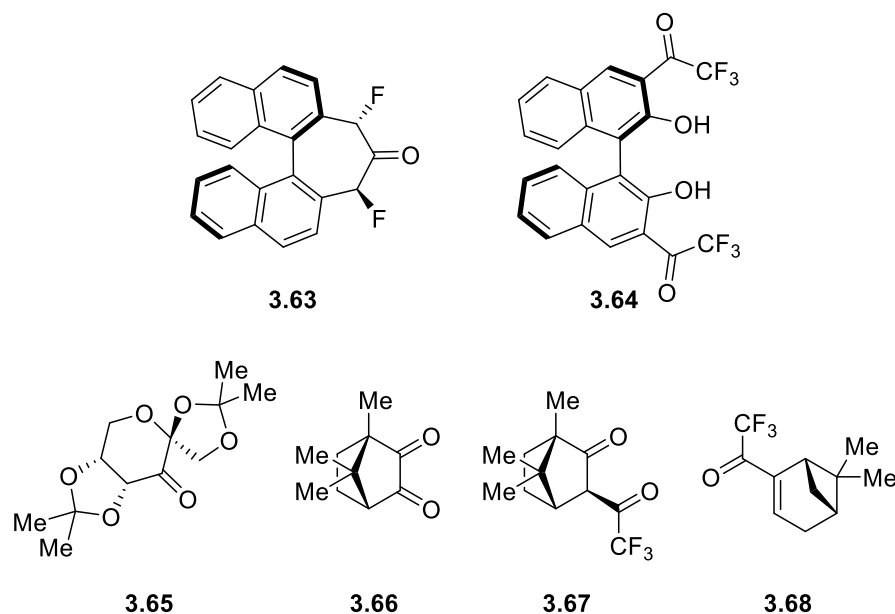


Cholesterol derivative **3.60** provided hydroxylation products in <10 % yield despite known reactivity with isolated TFDO.<sup>4</sup> This is exemplary of one of the major drawbacks to our method: the amount of DCM cosolvent needed to solubilize many complex substrates prevents catalytic activity. To expand the scope of reaction partners, new solvent systems compatible with catalytic activity or other solubilizing strategies must be explored.

### 3.4 Exploration of Chiral Catalysts

With catalytic conditions capable of approximating reactivity observed in stoichiometric TFDO oxidations in hand, we turned our attention to an investigation of the C–H bond hydroxylation abilities of chiral catalysts known to catalyze asymmetric epoxidation reactions (**Figure 3.5**).<sup>11</sup> Despite a broad screening of catalyst structures with varying structural features, none were capable of hydroxylating *cis*-decalin or 1,2-dimethylcyclohexane in greater than trace amounts.

**Figure 3.5:** Chiral catalysts that fail to promote hydroxylation

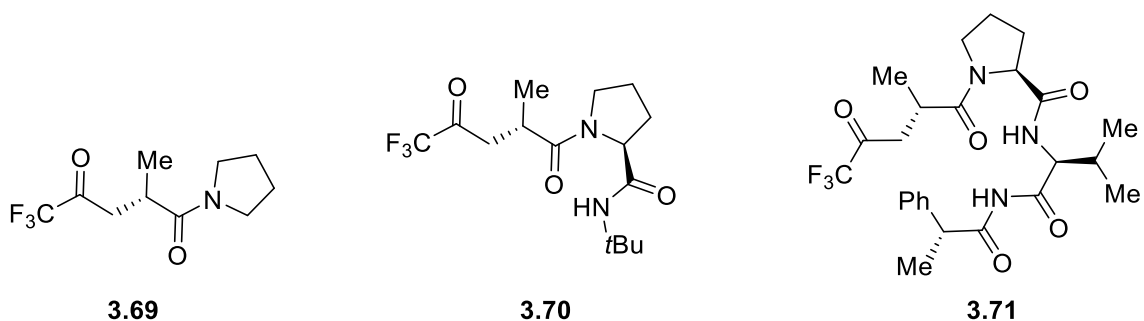


Overall, the catalyst structures explored differ drastically from catalyst **3.38** in steric bulk, lipophilicity, and electron deficiency. Miller and coworkers, however, have discovered a series of peptidic epoxidation catalysts that replicate many of

the structural features of our catalyst (**Figure 3.6**).<sup>20</sup> Additional work should be undertaken to explore the capabilities of these catalysts in C–H hydroxylation reactions.

---

**Figure 3.6:** Miller type epoxidation catalysts



### 3.5 Conclusions

We have discovered the first catalytic dioxirane mediated C–H hydroxylation reaction that approximates the reactivity of widely used stoichiometric dioxiranes. The method utilizes mild, near neutral conditions affording tolerance for a range of sensitive functional groups. Continuing exploration of alternative solvent systems capable of solubilizing complex molecules and investigation of additional catalyst scaffolds must be undertaken to increase the utility of this method.

### 3.6 Experimental Details

#### 3.6.1 General Methods

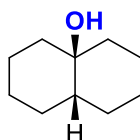
All commercially obtained reagents were obtained in the highest grade and used as received. Dichloromethane was purified by degassing with argon and drying through alumina columns. Flash column chromatography was conducted with 230-400 mesh silica gel purchased from Fisher Scientific.  $^1\text{H}$ ,  $^{13}\text{C}$ , and  $^{19}\text{F}$  NMR spectra were acquired at 300 K on Bruker or Varian spectrometers at 600 Mhz. Chemical shifts are reported in parts per million (ppm  $\delta$ ) referenced to the residual  $^1\text{H}$  peak of the solvent. The following abbreviations are used to indicate signal multiplicity: s - singlet, d - doublet, t - triplet, q - quartet, m - multiplet and br - broad. Gas chromatography was performed using an Agilent 7820A GC with FID detector, using *n*-dodecane as an internal standard for GC yield calculations. Normal phase chiral HPLC was performed using an Agilent 1260 HPLC equipped with a diode-array detector. IR spectra were recorded on a Thermo Scientific Nicolet iS5 with iD5 ATR attachment. High resolution mass spectrometry was performed by the University of Illinois at Urbana-Champaign Mass Spectrometry Lab using Waters Q-TOF ESI or Waters oa-TOF EI spectrometers.

#### 3.6.2 General method for hydroxylation

Oxone triple salt (308.0 mg, 0.5 mmol, 1 eq.), sodium bicarbonate (168.0 mg, 2 mmol, 4 eq.), tetra-*n*-butylammonium hydrogensulfate (8.5 mg, 0.025 mmol, 0.05 eq.), and substrate (0.5 mmol, 1 eq.) were weighed out into a five dram screw

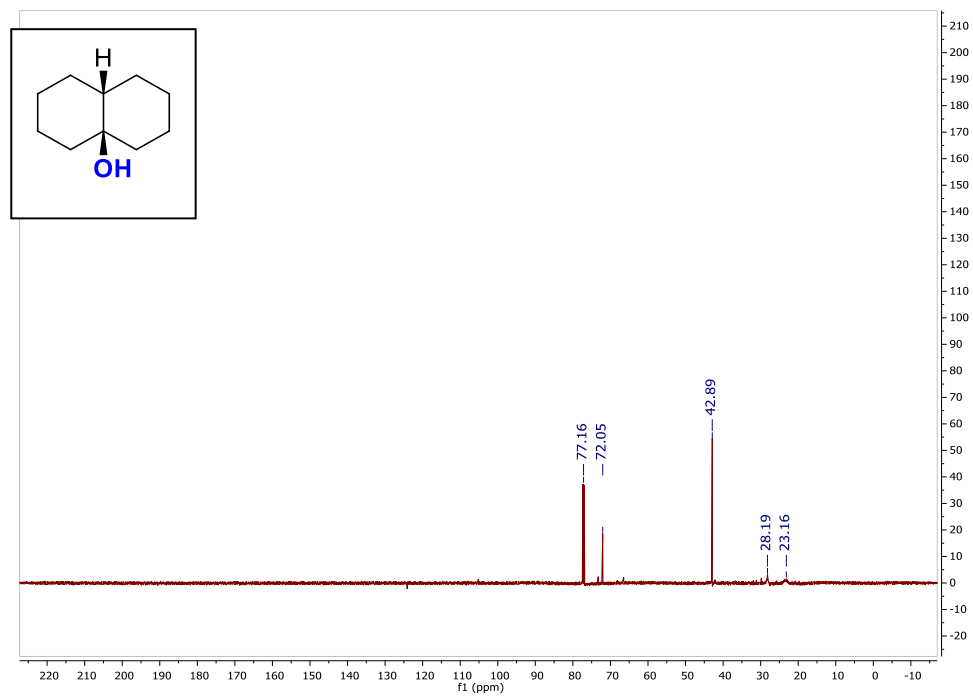
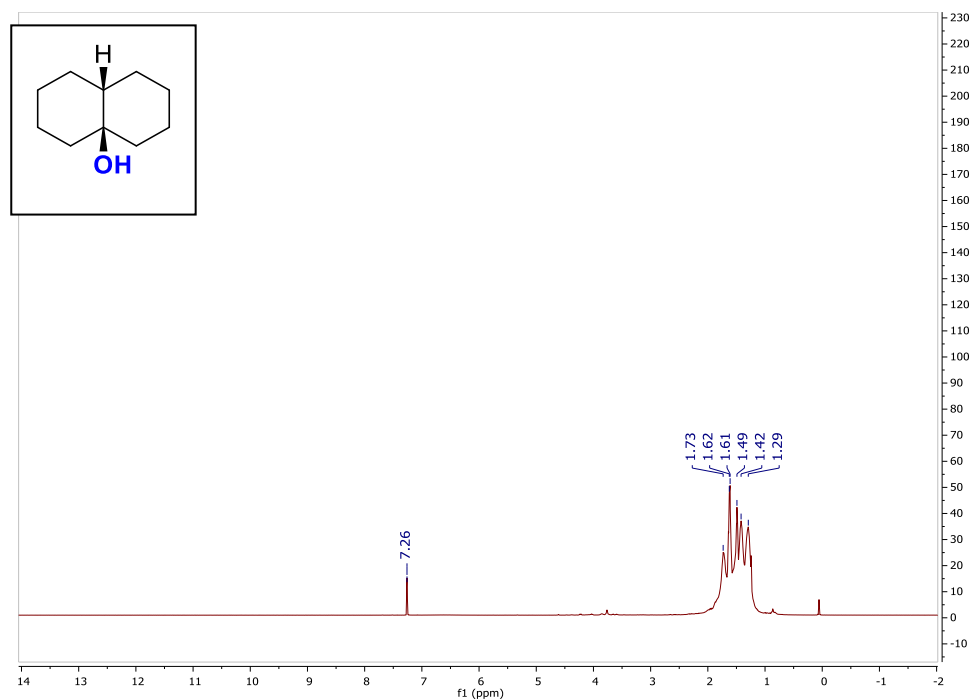
top vial equipped with a stir bar. DI water (5 mL) was added and the suspension was mixed gently until foaming subsided. To this was added HFIP (7 ml) followed by trifluorohexanone (15 mg, 0.02 mmol, 0.2 eq.). The vial was tightly capped and stirred vigorously at 4 °C for 24 hrs. Two additional portions of Oxone (308.0 mg, 0.5 mmol, 1 eq.) and sodium bicarbonate (168.0 mg, 2 mmol, 4 eq.) were added at 24 and 48 h, respectively, giving a total reaction time of 72 hours. Upon reaction completion, the resulting suspension was diluted with 10 mL brine and 10 mL EtOAc. The layers were separated, and extracted with 5x10 mL EtOAc. The resulting organic layers were combined, concentrated on a rotary evaporator, and purified by flash chromatography.

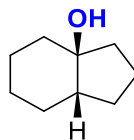
### 3.6.3 Characterization of reaction products



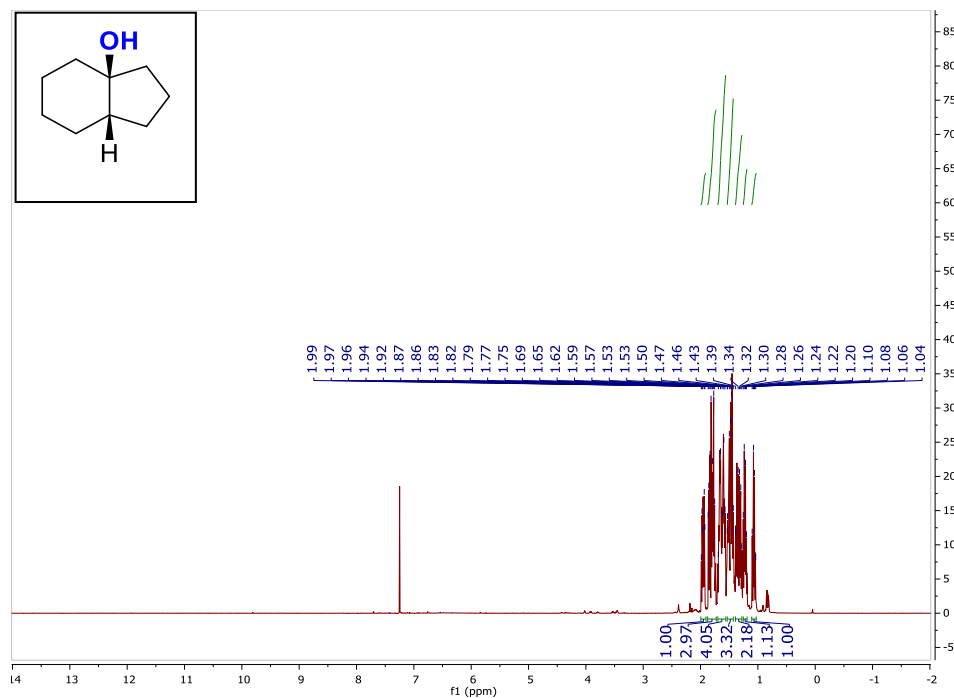
**cis-9-Decalinol 3.35** *cis*-Decalin was hydroxylated using a modification of the general procedure in which 7g of NaCl was added to the crude reaction mixture. The reaction mixture was purified after workup using silica gel flash chromatography (EtOAc) to give product as 60 mg of colorless needles (0.390 mmol, 78% yield). **<sup>1</sup>H NMR** (600 MHz, CDCl<sub>3</sub>) δ 1.73 – 1.29 (m, 18H) ppm; **<sup>13</sup>C NMR** (150 MHz, CDCl<sub>3</sub>) δ 77.16, 72.05, 42.89, 28.19 (br), 23.16 (br) ppm. NMR spectra are consistent with literature reports.<sup>2</sup>

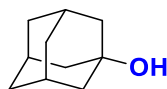
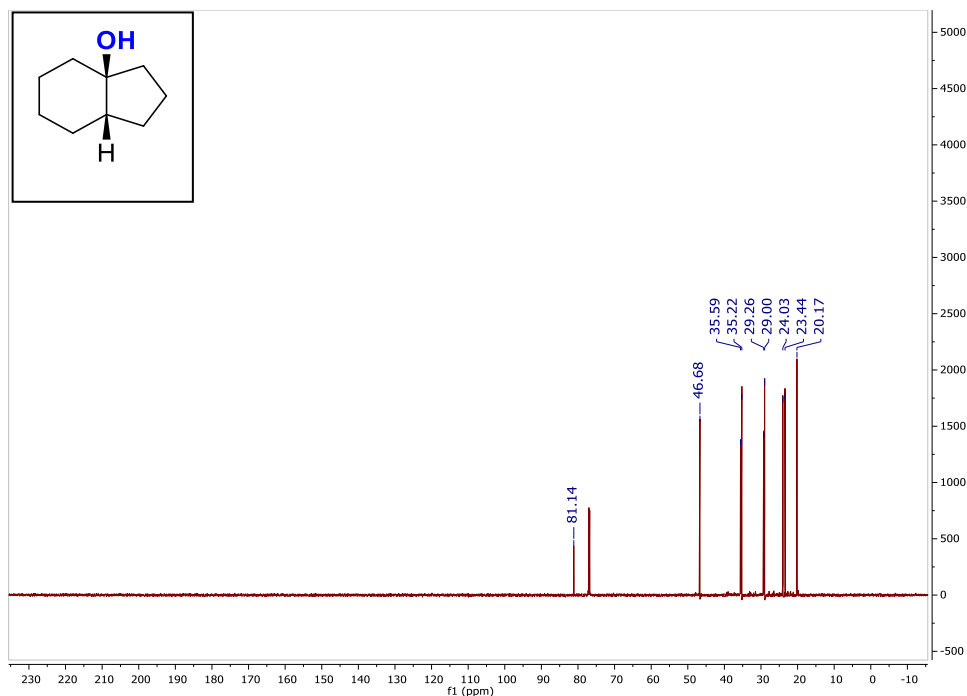




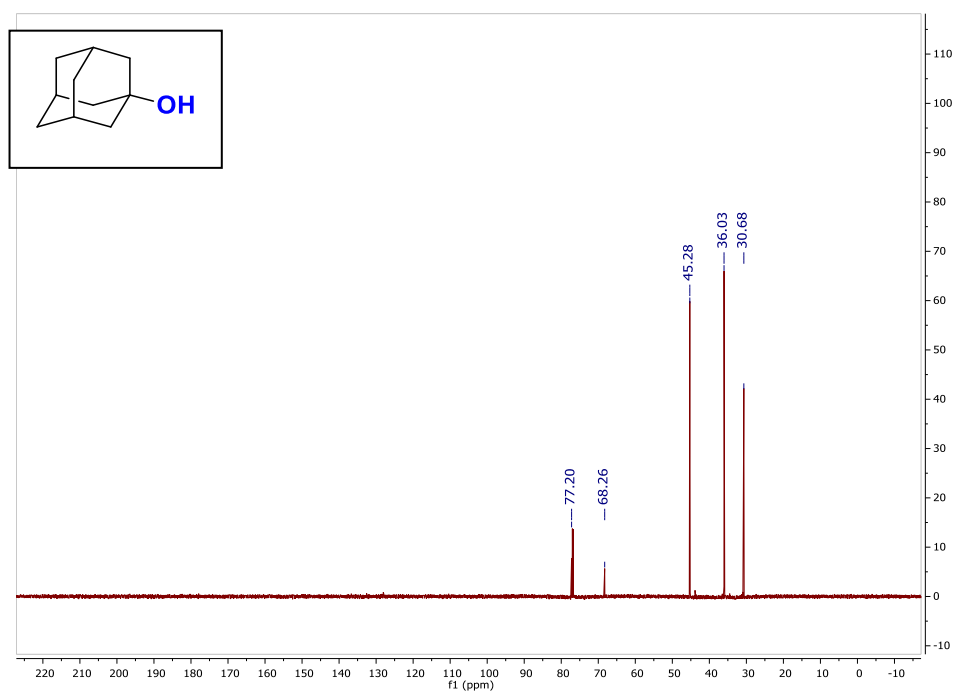
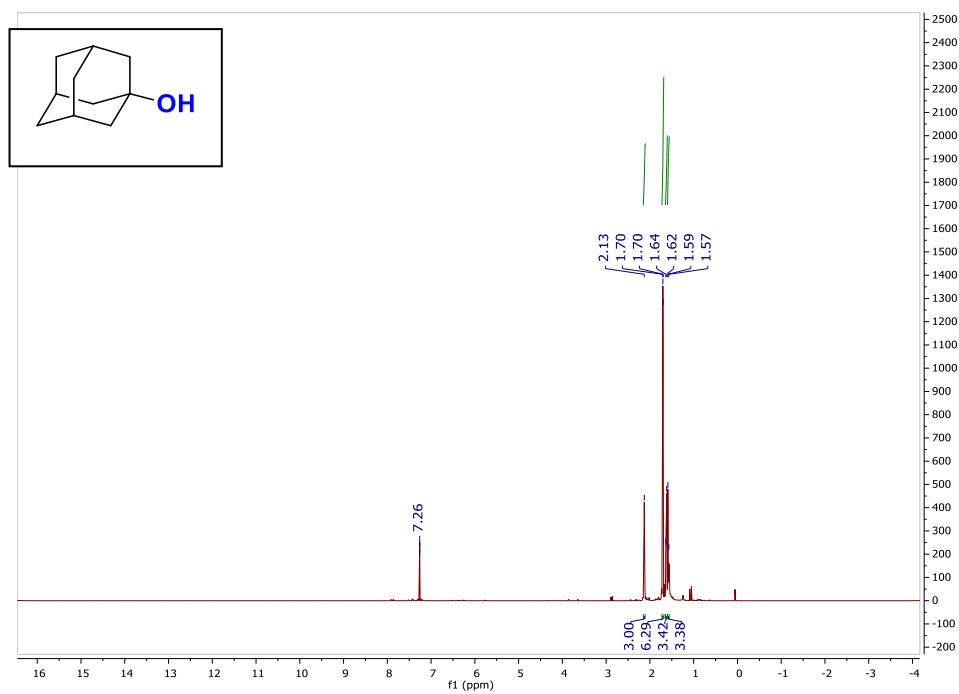


**(3a*S*,7a*S*)-Octahydro-3aH-inden-3a-ol 3.42** *cis*-Perhydroindan was hydroxylated using the general procedure. The reaction mixture was purified after workup using silica gel flash chromatography (solvent gradient: 10% to 50% Et<sub>2</sub>O/pentane) to give product as 63 mg of a white solid (0.450 mmol, 90% yield). <sup>1</sup>H NMR (600 MHz, CDCl<sub>3</sub>) δ 1.99 – 1.90 (m, 1H), 1.88 – 1.73 (m, 3H), 1.70 – 1.56 (m, 4H), 1.53 – 1.43 (m, 3H), 1.39 – 1.28 (m, 2H), 1.25 – 1.19 (m, 1H), 1.11 – 1.03 (m, 1H) ppm; <sup>13</sup>C NMR (151 MHz, CDCl<sub>3</sub>) δ 81.14, 46.68, 35.59, 35.22, 29.26, 29.00, 24.03, 23.44, 20.17 ppm. NMR spectra are consistent with literature reports. <sup>2</sup>



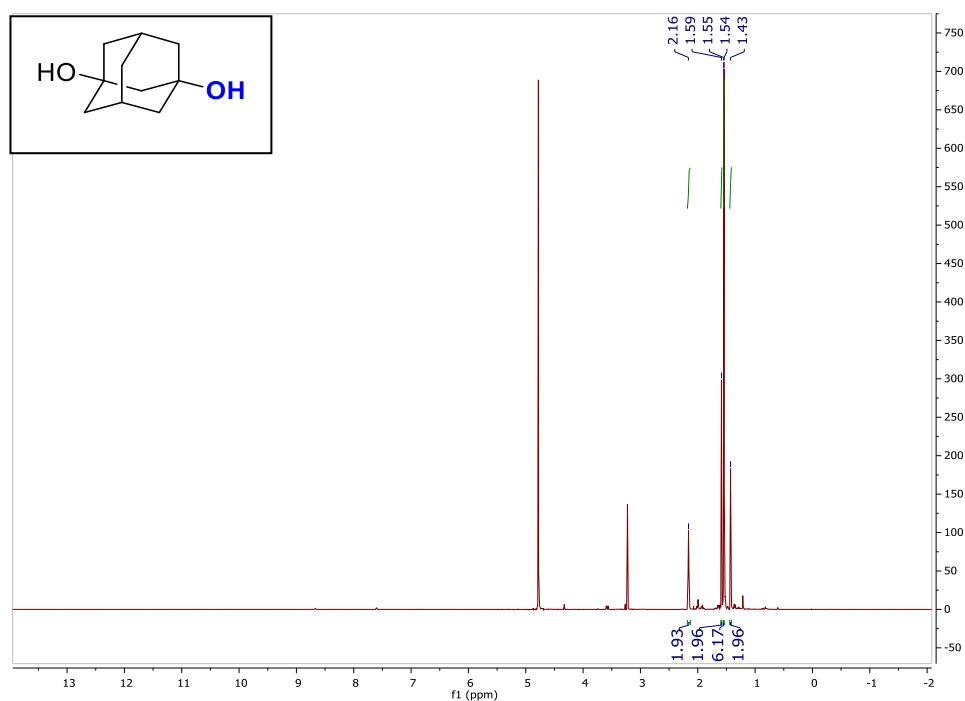


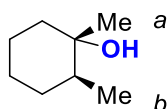
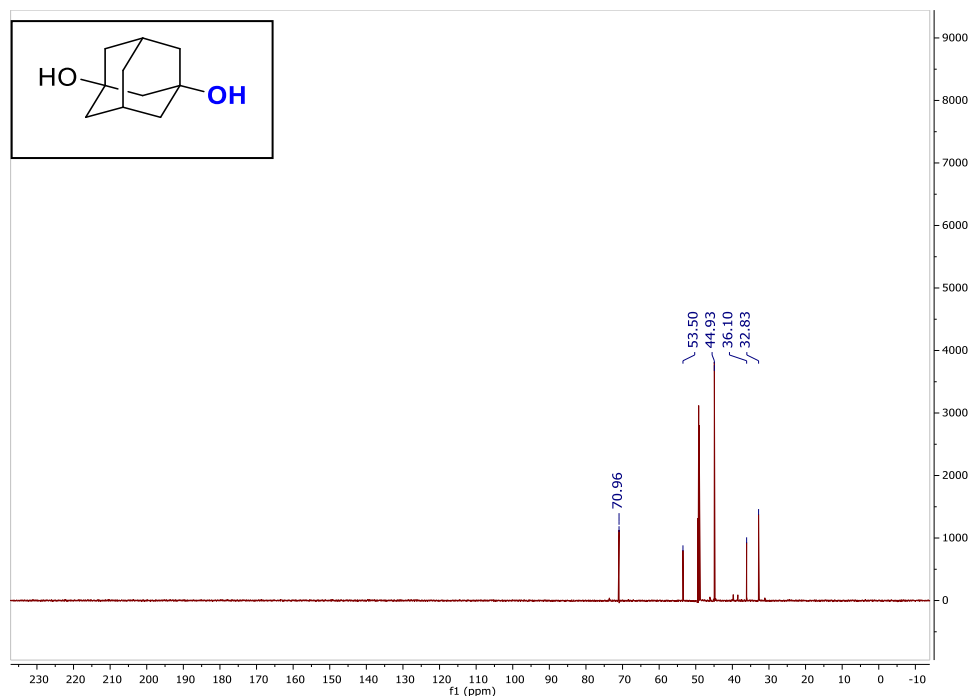
**1-Adamantanol 3.33** Adamantane was hydroxylated using Modification A of the general procedure. The reaction mixture was diluted with 15mL of brine and extracted with EtOAc (3x40mL). The combined organic layers were dried over Na<sub>2</sub>SO<sub>4</sub> and solvent was removed under reduced pressure to give product as 62 mg of white solid (0.407 mmol, 81% yield). **<sup>1</sup>H NMR** (600 MHz, CDCl<sub>3</sub>) δ 2.13 (m, 3H) 1.70 (d, *J* = 3.1 Hz, 6H), 1.63 (d, *J* = 12.6 Hz, 3H), 1.58 (d, *J* = 12.4 Hz, 3H) ppm; **<sup>13</sup>C NMR** (150 MHz, CDCl<sub>3</sub>) δ 68.44, 45.45, 36.20, 30.85 ppm. NMR spectra are consistent with literature reports.<sup>2</sup>





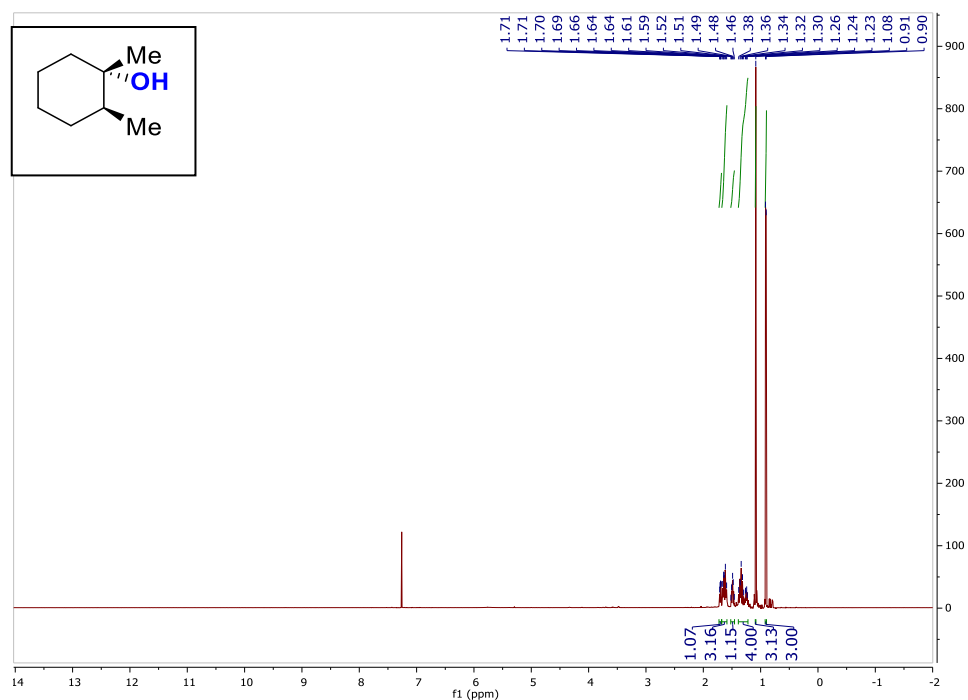
**Adamantane-1,3-diol 3.43** 1-Adamantanol was hydroxylated using the general procedure. The reaction mixture was purified after workup using silica gel flash chromatography (solvent gradient: 20% to 100% EtOAc/hexanes) to give the recovered starting material (26 mg, 0.168 mmol) and product as 32 mg of white solid (0.193 mmol, 39% yield, 58% brsm).. **<sup>1</sup>H NMR** (600 MHz, MeOD-*d*<sub>4</sub>) δ 2.16 (s, 2H), 1.59 (s, 2H), 1.54 (d, *J* = 3.1 Hz, 6H), 1.43 (s, 2H) ppm; **<sup>13</sup>C NMR** (151 MHz, MeOD-*d*<sub>4</sub>) δ 70.96, 53.50, 44.93, 36.10, 32.83 ppm. NMR spectra are consistent with literature reports.<sup>2</sup>

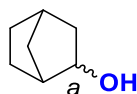
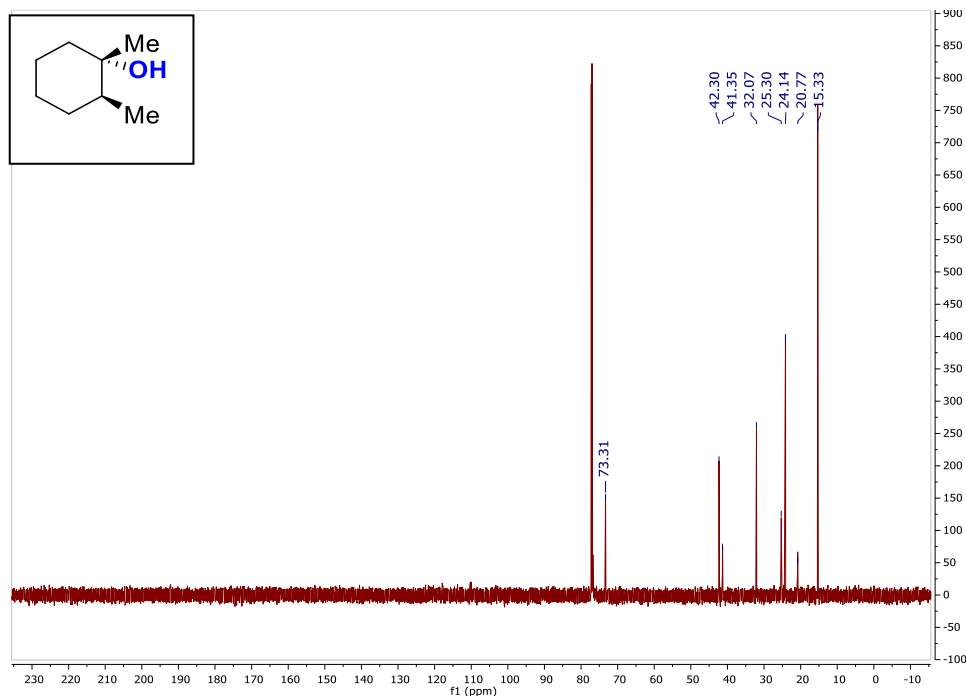




**1,2-Dimethylcyclohexan-1-ol** **3.44** *cis*-1,2-Dimethylcyclohexane was hydroxylated using the general procedure. The reaction mixture was purified after workup using silica gel flash chromatography (solvent gradient: 0% to 30% Et<sub>2</sub>O/pentane) to give product as 27 mg of volatile oil (0.210 mmol, 41% yield). **<sup>1</sup>H NMR** (600 MHz, CDCl<sub>3</sub>) δ 1.70 (dd, *J* = 9.6, 5.1 Hz, 1H), 1.68 – 1.59 (m, 3H), 1.52 – 1.46 (m, 1H), 1.39 – 1.22 (m, 4H), 1.08 (H<sub>a</sub>, s, 3H), 0.91 (H<sub>b</sub>, d, *J* = 6.8 Hz, 3H) ppm; **<sup>13</sup>C NMR** (151 MHz, CDCl<sub>3</sub>) δ 73.31, 42.30, 41.35, 32.07, 25.30, 24.14,

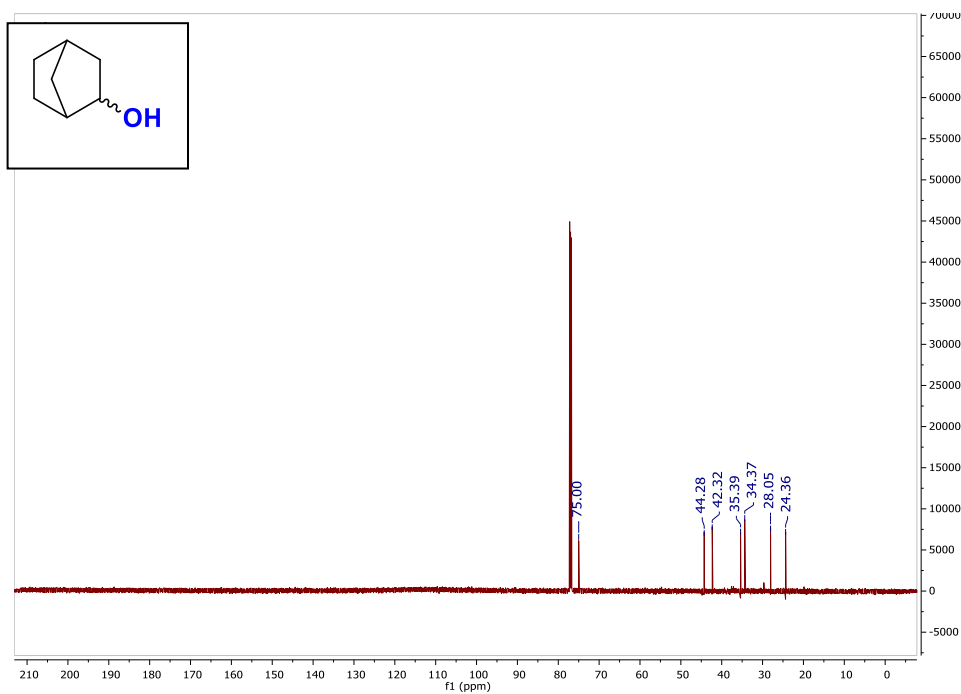
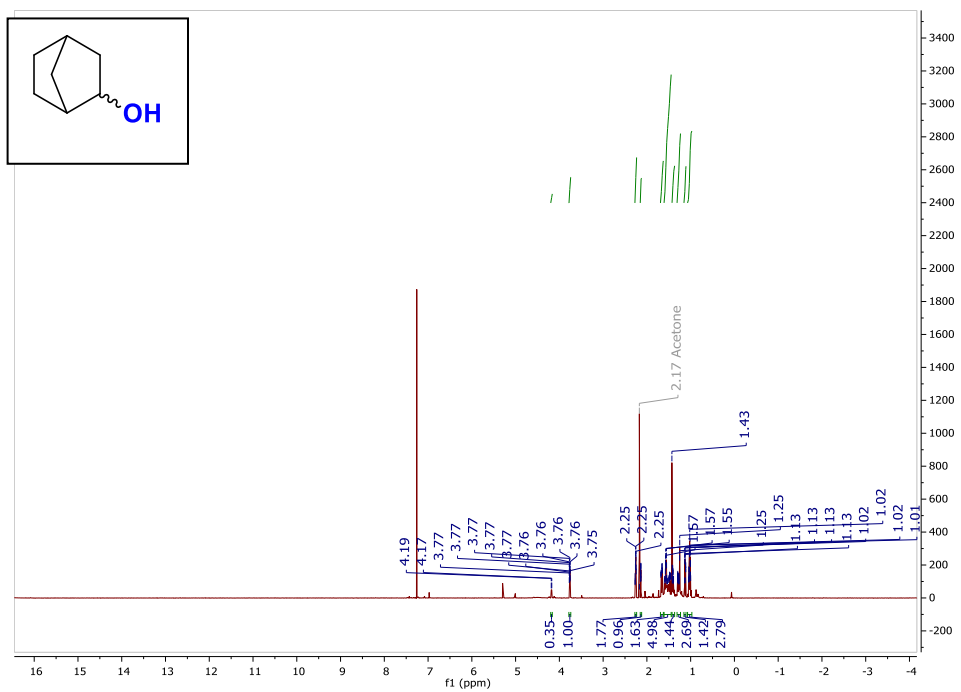
20.77, 15.33. NMR spectra are consistent with literature reports.<sup>2</sup> In a separate reaction, *cis*-1,2-dimethylcyclohexane was hydroxylated using the general procedure. Mixtures of authentic samples of **3.44** and *n*-dodecane were analyzed by GC to determine a burn ratio of 2.02. 25  $\mu$ L of *n*-dodecane (0.11 mmol) was added to the crude reaction mixture which was sampled and analyzed by GC-FID to give a corrected yield of 98%.

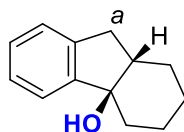




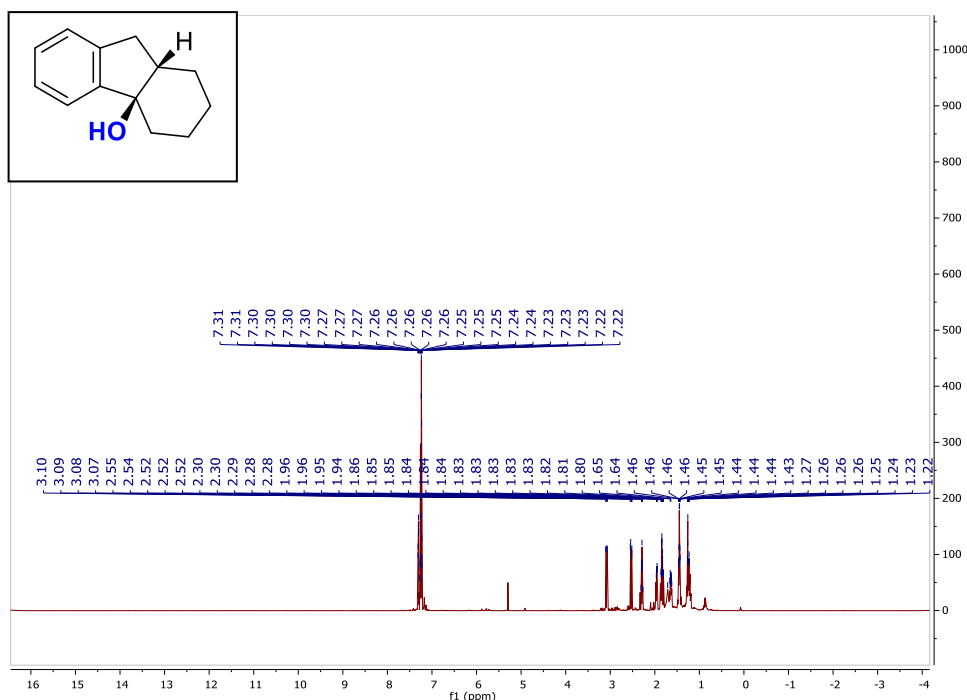
**Norborneol 3.45** Norbornane was hydroxylated using Modification A of the general procedure. The reaction mixture was purified after workup using silica gel flash chromatography (solvent gradient 10%-50% Et<sub>2</sub>O/pentane) to give the recovered starting material (22 mg, 0.229 mmol) and product as a colorless waxy solid (17.7 mg, 32% yield, 58% brsm, 3:1 *exo:endo*). **<sup>1</sup>H NMR** (600 MHz, CDCl<sub>3</sub>) δ 4.18 (H<sub>a</sub>-endo, m, 1H), 3.76 (H<sub>a</sub>-exo, ddt, *J* = 6.9, 2.3, 1.1 Hz, 1H), 2.27 – 2.23 (m, 2H), 2.14 (dq, *J* = 5.2, 1.3 Hz, 1H), 1.66 (ddd, *J* = 13.2, 6.8, 2.6 Hz, 2H), 1.61 – 1.45 (m, 5H), 1.43 – 1.37 (m, 1H), 1.31 – 1.23 (m, 3H), 1.15 – 1.11 (m, 1H), 1.07 – 0.97 (m, 3H) ppm; **<sup>13</sup>C NMR** (151 MHz, CDCl<sub>3</sub>) δ 75.00, 44.28, 42.32, 35.39, 34.37, 28.05, 24.36 ppm. NMR spectra are consistent with commercial sources.

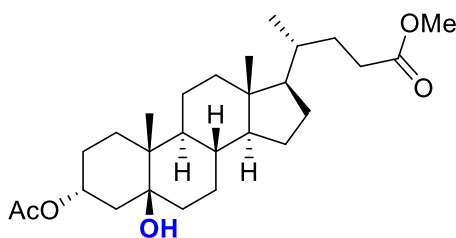
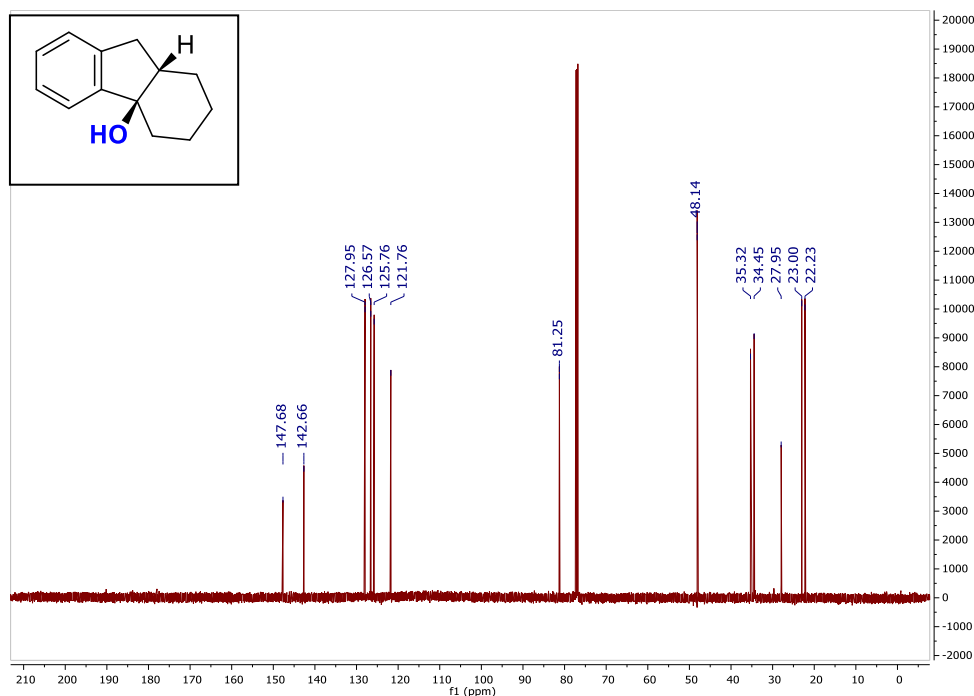






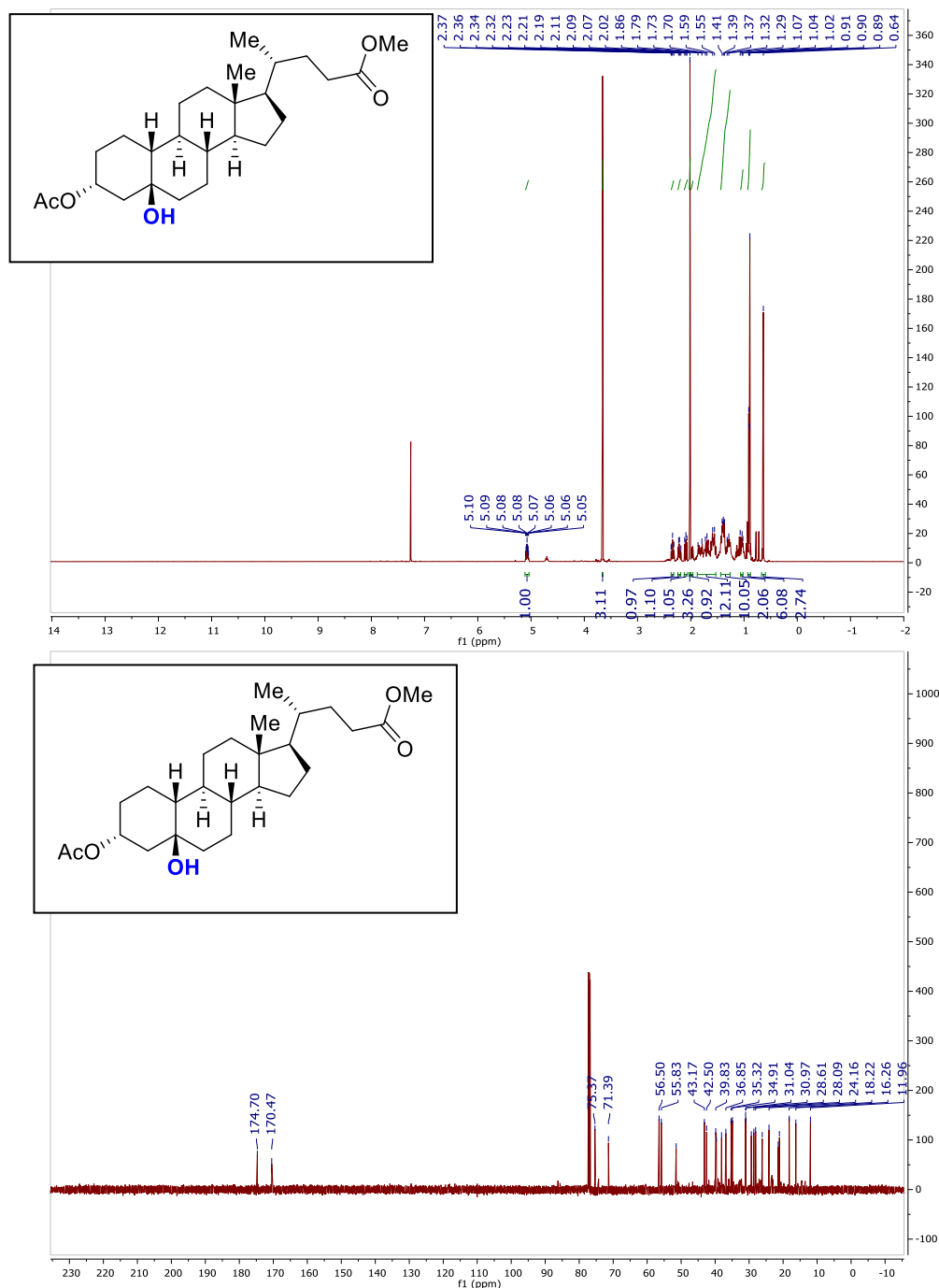
**cis-1,2,3,4,9a-Pentahydro-4a-hydroxy-fluorene 3.47** *cis*-1,2,3,4,4a,9a-Hexahydrofluorene was hydroxylated using the general procedure. The reaction mixture was purified after workup using silica gel flash chromatography (solvent gradient 0% to 40% EtOAc/hexanes) to give the recovered starting material (24 mg, 0.125 mmol) and product as a brown, waxy solid (44 mg, 47% yield, 66% brsm). **<sup>1</sup>H NMR** (600 MHz, CDCl<sub>3</sub>) δ 7.34 – 7.27 (ArH, m, 1H), 7.29 – 7.19 (ArH, m, 3H), 3.08 (H<sub>a</sub>, dd, *J* = 15.6, 6.6 Hz, 1H), 2.57 – 2.49 (H<sub>a</sub>, m, 1H), 2.29 (ddd, *J* = 12.7, 7.1, 5.9 Hz, 1H), 1.98 – 1.92 (m, 1H), 1.89 – 1.79 (m, 2H), 1.71 (s (br), 1H), 1.65 – 1.60 (m, 1H), 1.48 – 1.40 (m, 2H), 1.28 – 1.20 (m, 2H) ppm; **<sup>13</sup>C NMR** (151 MHz, CDCl<sub>3</sub>) δ 147.68, 142.66, 127.95, 126.57, 125.76, 121.76, 81.25, 48.14, 35.32, 34.45, 27.95, 23.00, 22.23 ppm. **IR** (film, cm<sup>-1</sup>): 2924, 2854, 1456, 1386, 1220, 752 (s), 715 (s); **HRMS** *m/z* (ESI<sup>+</sup>): Calculated for C<sub>13</sub>H<sub>16</sub>O [M]<sup>+</sup>: 188.12012, found 188.11982.

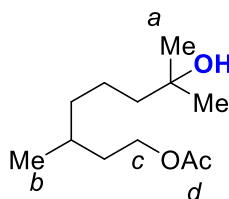




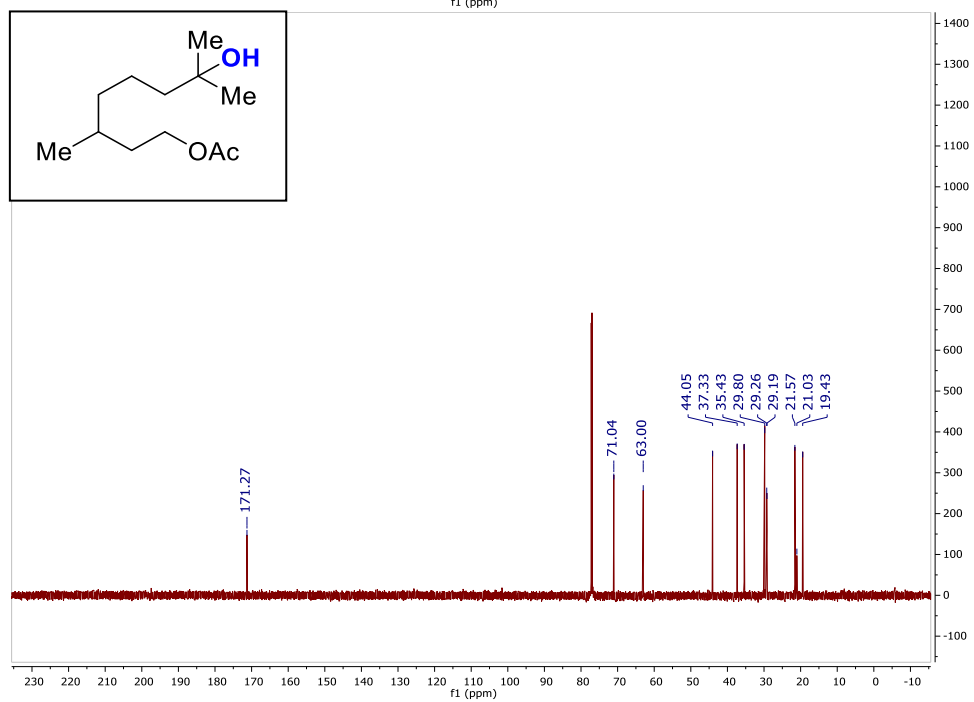
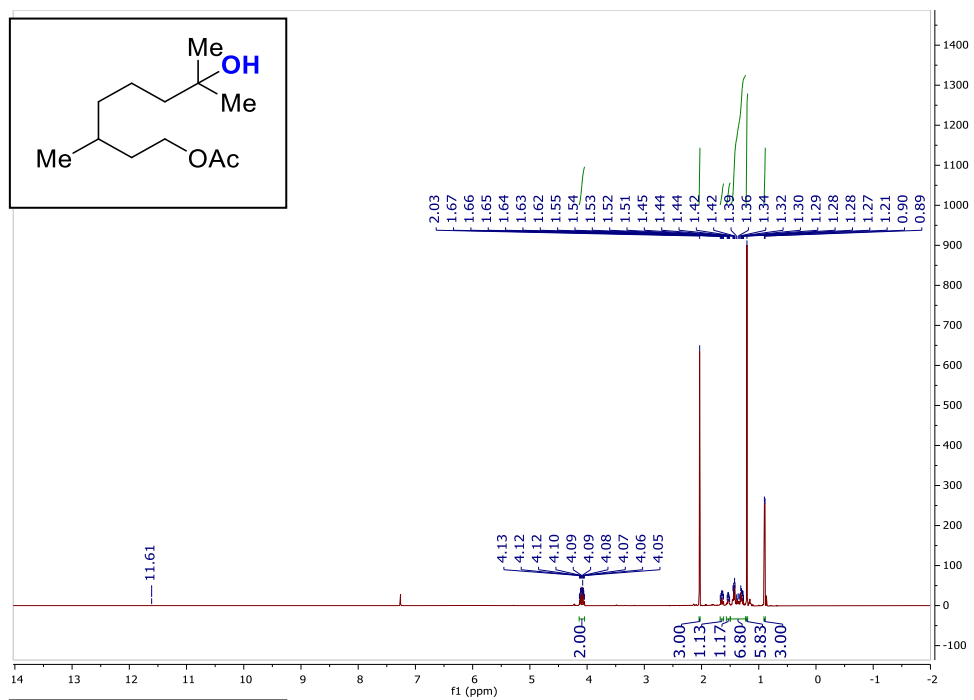
**Lithicholic Acid Derivative 3.48** Acetyl lithocholic acid methyl ester was hydroxylated using the general procedure. The reaction mixture was purified after workup using silica gel flash chromatography (solvent gradient: 20% to 60% EtOAc/hexanes) to give the recovered starting material (82 mg, 0.190 mmol) and product as 74 mg of white solid (0.164 mmol, 33% yield, 53% brsm). The recovered starting material was resubjected to the reaction conditions to give after a second cycle, recovered starting material (35 mg, 0.080 mmol) and product as 25 mg of white solid (0.056 mmol, 30% yield, 51% brsm). Overall, 99 mg of product (0.220 mmol, 44% yield, 53% brsm) was recovered. <sup>1</sup>H NMR (600 MHz, CDCl<sub>3</sub>) δ 5.07 (tq, *J* = 10.4, 5.0 Hz, 1H), 3.66 (d, *J* = 3.1 Hz, 3H), 2.37 – 2.32 (m, 1H), 2.22 (d, *J* = 9.7 Hz, 1H), 2.12 – 2.06 (m, 1H), 2.02 (s, 3H), 2.00 – 1.96 (m, 1H), 1.88 – 1.53 (m, 12H), 1.44 – 1.26 (m, 10H), 1.03 (m, 2H), 0.93 – 0.88 (m,

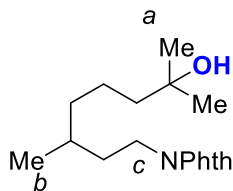
6H), 0.64 (s, 3H);  $^{13}\text{C}$  NMR (151 MHz,  $\text{CDCl}_3$ )  $\delta$  174.70, 170.47, 75.37, 71.39, 56.50, 55.83, 51.47, 43.17, 42.50, 39.83, 39.64, 38.11, 36.85, 35.32, 34.91, 31.04, 30.97, 29.36, 28.61, 28.09, 26.15, 24.16, 21.43, 21.09, 18.22, 16.26, 11.96 ppm. NMR spectra are consistent with literature reports.<sup>21</sup>





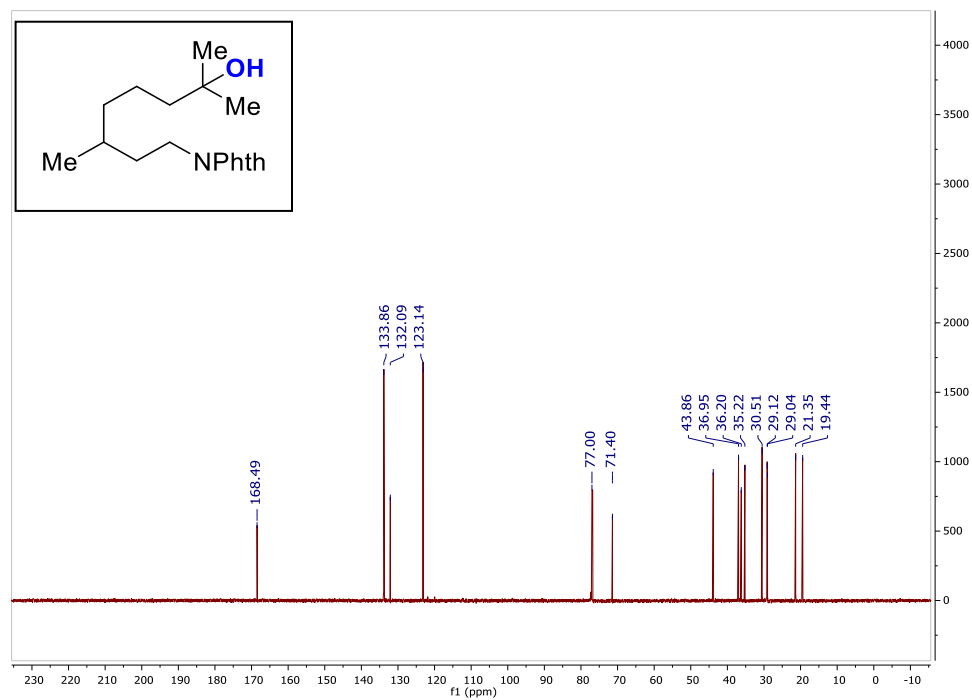
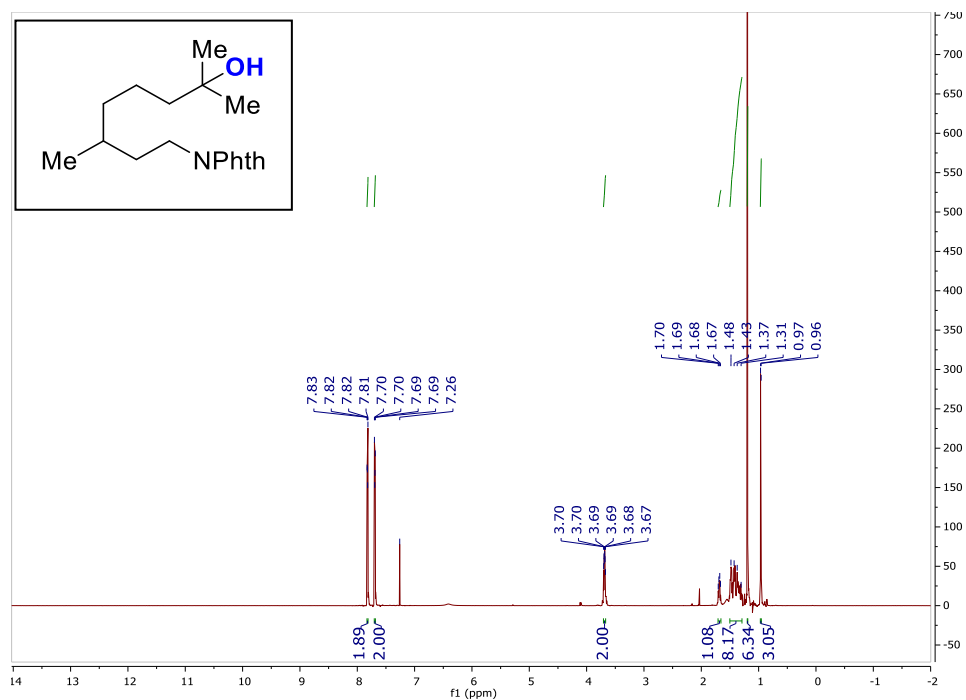
**7-Hydroxy-3,7-dimethyloctyl acetate 3.40** 3,7-Dimethyloctyl acetate was hydroxylated using the general procedure. The reaction mixture was purified after workup using silica gel flash chromatography (solvent gradient: 5% to 30% EtOAc/hexanes) to give the recovered starting material (13.2 mg, 0.065 mmol) and product as 92 mg of clear oil (0.420 mmol, 85% yield, 97% brsm). **<sup>1</sup>H NMR** (600 MHz, CDCl<sub>3</sub>): δ 4.14 – 4.04 (H<sub>c</sub>, m, 2H), 2.03 (H<sub>d</sub>, s, 3H), 1.67 – 1.61 (m, 1H), 1.57 – 1.50 (m, 1H), 1.50 – 1.23 (m, 7H), 1.21 (H<sub>a</sub>, s, 6H), 0.90 (H<sub>b</sub>, d, *J* = 6.6 Hz, 3H) ppm; **<sup>13</sup>C NMR** (151 MHz, CDCl<sub>3</sub>): δ 172.00, 71.93, 63.24, 43.76, 37.13, 35.26, 29.68, 28.95, 28.90, 21.42, 20.95, 19.47 ppm. NMR spectra are consistent with literature reports.<sup>21</sup>



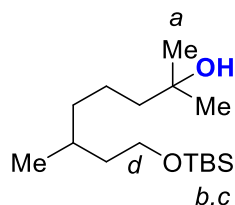


**2-(7-Hydroxy-3,7-dimethyloctyl)isoindoline-1,3-dione      3.49      2-(3,7-**

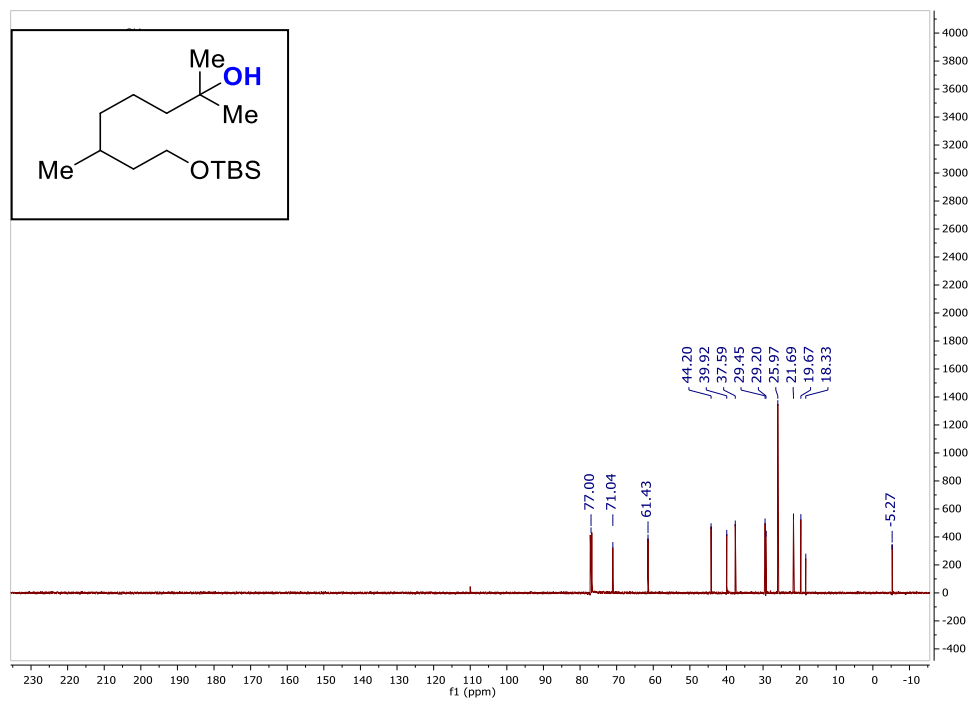
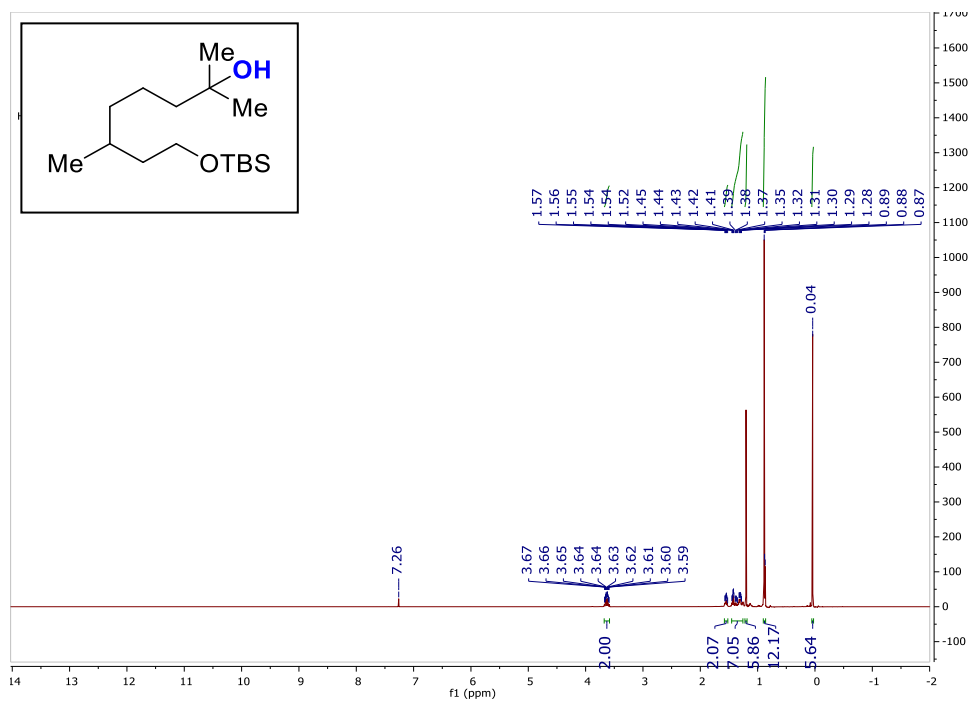
Dimethyloctyl)isoindoline-1,3-dione was hydroxylated using the general procedure. The reaction mixture was purified after workup using silica gel flash chromatography (solvent gradient: 20% to 40% EtOAc/hexanes) to give the recovered starting material (29.7 mg, 0.105 mmol) and product as 109 mg of clear oil (0.360 mmol, 71% yield, 91% brsm). **<sup>1</sup>H NMR** (600 MHz, CDCl<sub>3</sub>): δ 7.81 (H<sub>Ar</sub>, dd, *J* = 5.4, 3.1 Hz, 2H), 7.68 (H<sub>Ar</sub>, dd, *J* = 5.5, 3.0 Hz, 2H), 3.73 – 3.62 (H<sub>c</sub>, m, 2H), 1.72 – 1.62 (m, 1H), 1.52 – 1.20 (m, 8H), 1.18 (H<sub>a</sub>, s, 6H), 0.95 (H<sub>b</sub>, d, *J* = 6.3 Hz, 3H) ppm; **<sup>13</sup>C NMR** (150 MHz, CDCl<sub>3</sub>): δ 168.49, 133.86, 132.09, 123.14, 121.87, 71.40, 43.86, 36.95, 36.20, 35.22, 30.51, 29.15, 29.12, 29.04, 21.35, 19.44 ppm. NMR spectra are consistent with literature reports.<sup>21</sup>

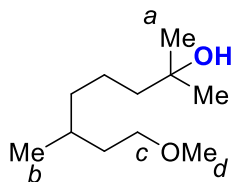




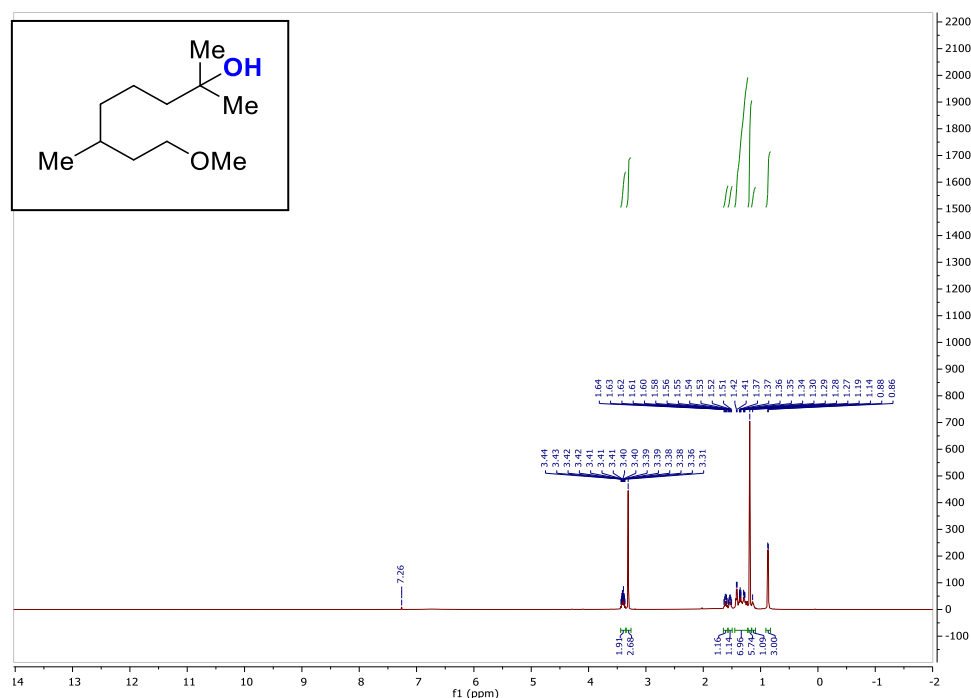


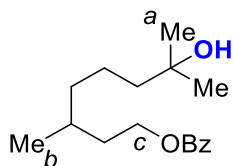
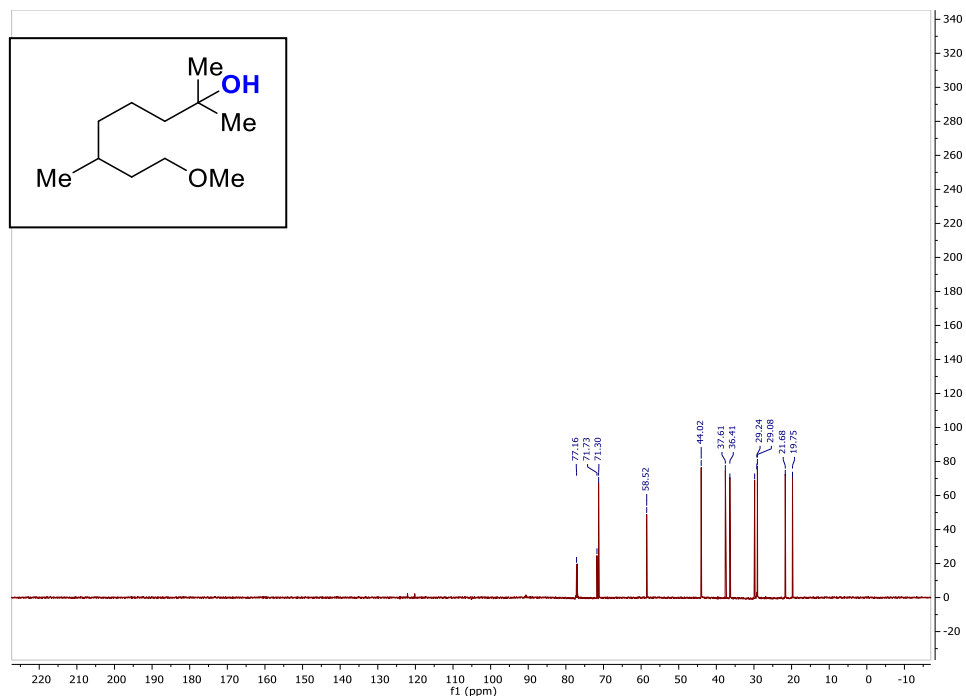
**((*tert*-Butyldimethylsilyl)oxy)-2,6-dimethyloctan-2-ol 3.50** *tert*-Butyl((3,7-dimethyloctyl)oxy)dimethylsilane was hydroxylated using the general procedure. The reaction mixture was purified after workup using silica gel flash chromatography (solvent gradient: 10% to 40% Et<sub>2</sub>O/pentane) to give the recovered starting material (80.6 mg, 0.280 mmol) and product as 57 mg of clear oil (0.210 mmol, 42% yield, 95% brsm). **<sup>1</sup>H NMR** (600 MHz, CDCl<sub>3</sub>): δ 3.68 – 3.58 (H<sub>d</sub>, m, 2H), 1.55 (td, *J* = 12.2, 11.2, 6.0 Hz, 2H), 1.45 – 1.26 (m, 7H), 1.20 (H<sub>a</sub>, s, 6H), 0.89 (H<sub>b</sub>, m, 12H), 0.04 (H<sub>c</sub>, s, 6H) ppm; **<sup>13</sup>C NMR** (150 MHz, CDCl<sub>3</sub>): δ 71.04, 61.43, 44.20, 39.92, 37.59, 29.45, 29.20, 25.97, 21.69, 19.67, 18.33, -5.27 ppm. **IR** 2955 (m), 2930 (m), 1094 (s), 840 (s), 775 (s) cm<sup>-1</sup>. **HRMS** (TOF-ES<sup>+</sup>): *m/z* calc'd for [C<sub>16</sub>H<sub>36</sub>OSiNa]<sup>+</sup>: 311.2382; found: 311.2391.





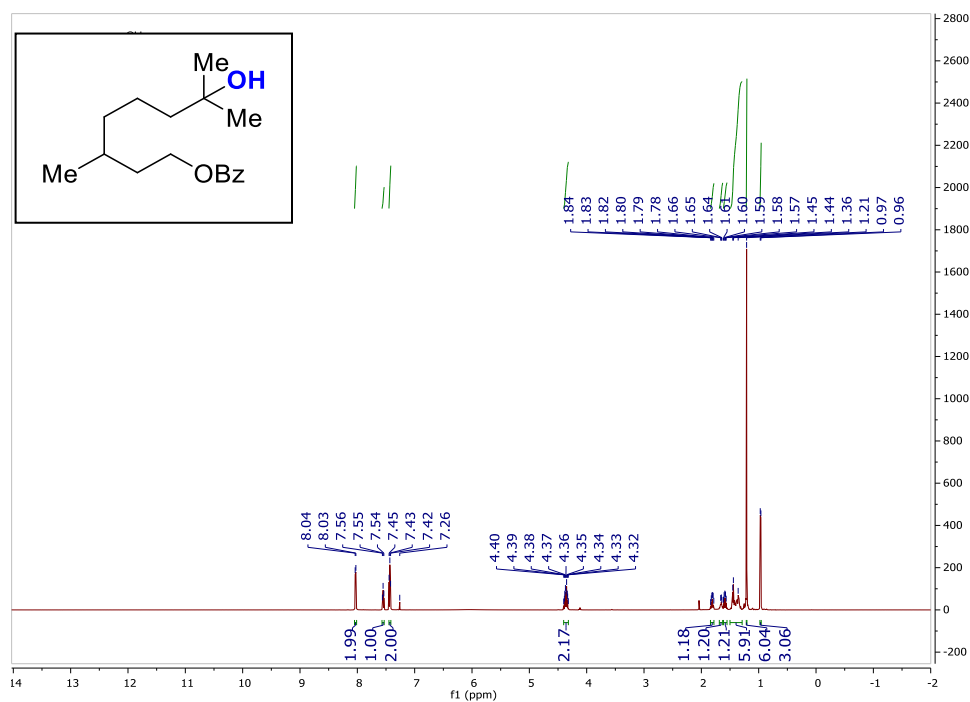
**8-Methoxy-2,6-dimethyloctan-2-ol 3.51** 1-Methoxy-3,7-dimethyloctane was hydroxylated using the general procedure. The reaction mixture was purified after workup using silica gel flash chromatography (solvent gradient 0% to 40% Et<sub>2</sub>O/pentane) to give product as 77 mg of colourless oil (0.409 mmol, 82% yield). **<sup>1</sup>H NMR** (600 MHz, CDCl<sub>3</sub>) δ 3.44 – 3.35 (H<sub>c</sub>, m, 2H), 3.31 (H<sub>d</sub>, s, 3H), 1.61 (dq, *J* = 13.3, 7.1 Hz, 1H), 1.53 (dq, *J* = 13.0, 6.5 Hz, 1H), 1.45 – 1.22 (m, 7H), 1.19 (H<sub>a</sub>, s, 6H), 1.14 (m, 1H), 0.87 (H<sub>b</sub>, d, *J* = 6.7 Hz, 3H) ppm; **<sup>13</sup>C NMR** (150 MHz, CDCl<sub>3</sub>) δ 71.73, 71.30, 58.52, 44.02, 37.61, 36.41, 29.82, 29.24, 29.08, 21.68, 19.75 ppm. NMR spectra are consistent with literature reports.<sup>21</sup>

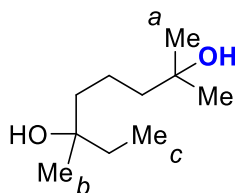
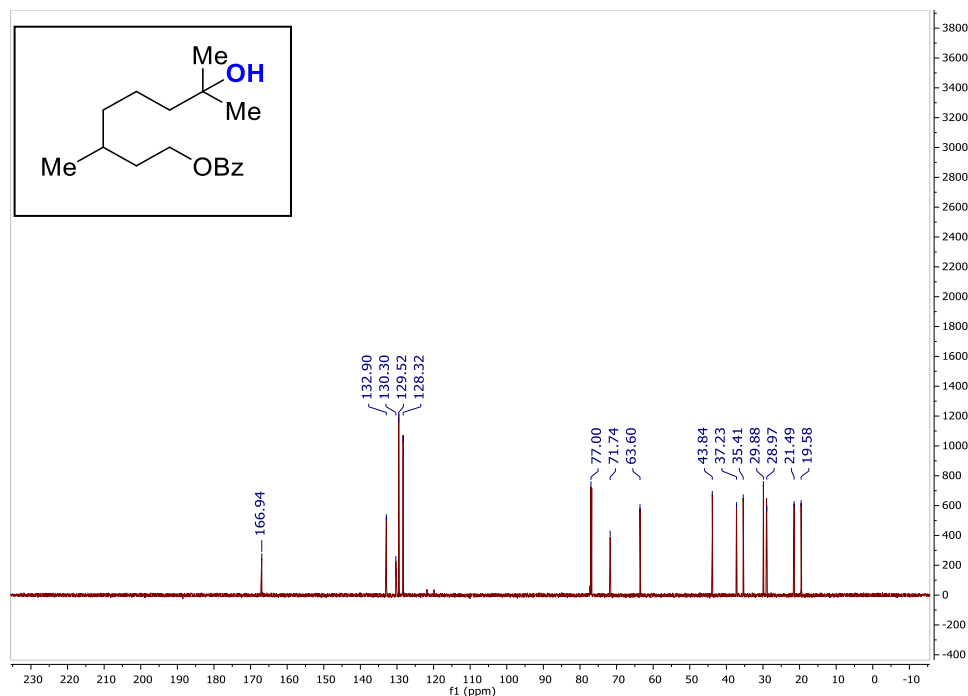




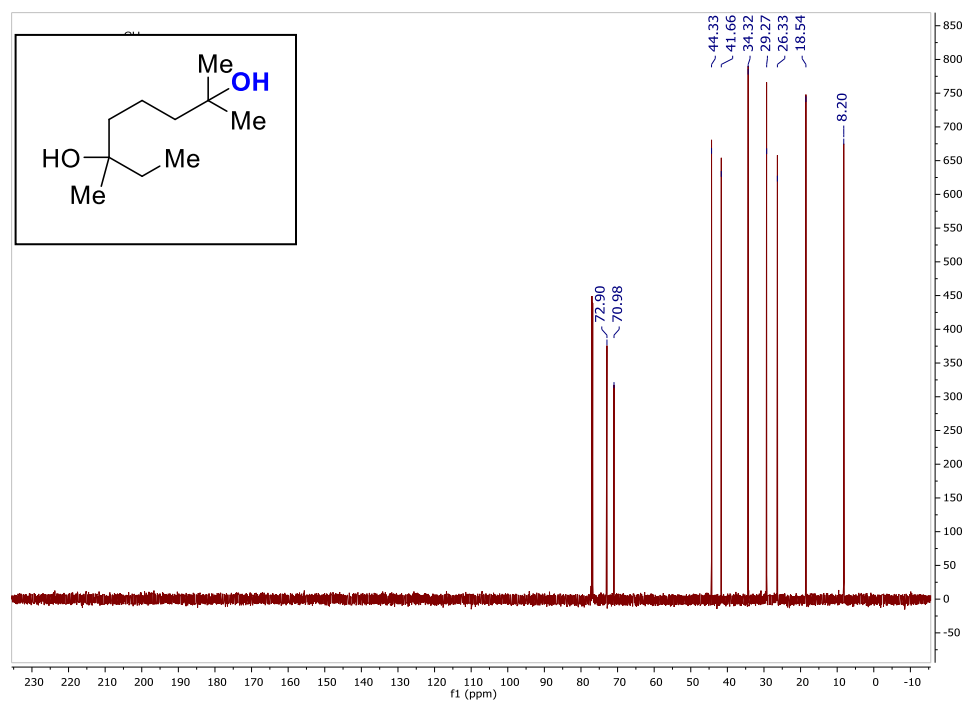
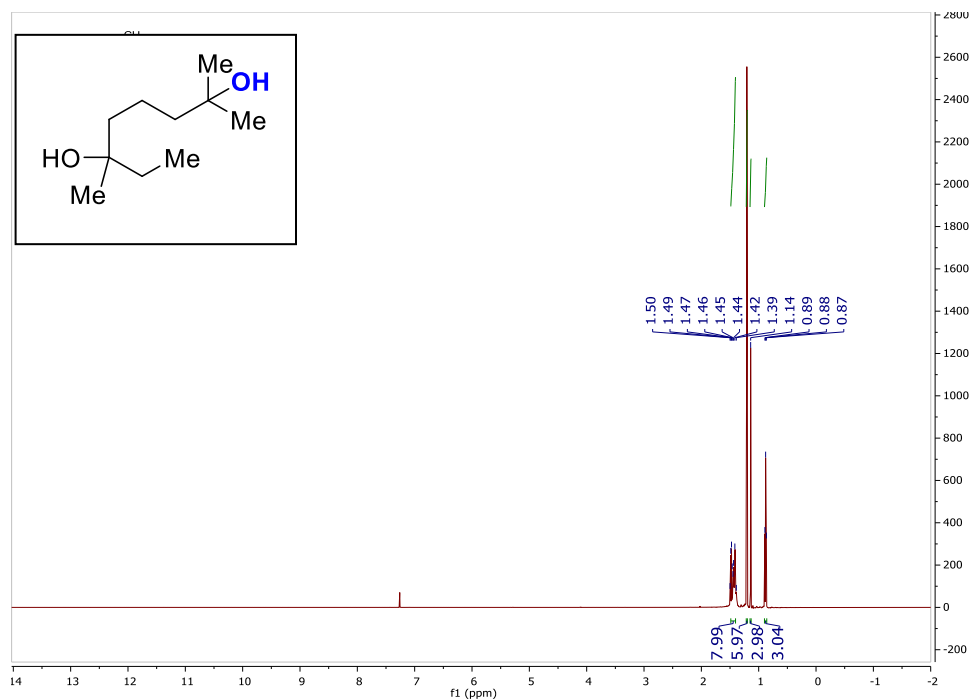
**7-Hydroxy-3,7-dimethyloctyl benzoate 3.52** 3,7-Dimethyloctyl benzoate was hydroxylated using the general procedure. The reaction mixture was purified after workup using silica gel flash chromatography (solvent gradient: 5% to 30% EtOAc/hexanes) to give the recovered starting material (40.7 mg, 0.156 mmol) and product as 99 mg of clear oil (0.356 mmol, 71% yield, 100% brsm).  $^1\text{H}$  NMR (600 MHz,  $\text{CDCl}_3$ ):  $\delta$  8.02 ( $\text{H}_{\text{Ar}}$ , d,  $J = 7.7$  Hz, 2H), 7.54 ( $\text{H}_{\text{Ar}}$ , t,  $J = 7.4$  Hz, 1H), 7.42 ( $\text{H}_{\text{Ar}}$ , t,  $J = 7.7$  Hz, 2H), 4.40 – 4.29 ( $\text{H}_{\text{c}}$ , m, 2H), 1.80 (dq,  $J = 13.3, 7.0$  Hz, 1H), 1.60 (ddq,  $J = 34.4, 13.9, 7.0, 6.6$  Hz, 2H), 1.46 – 1.41 (m, 2H), 1.41 – 1.29 (m, 3H),

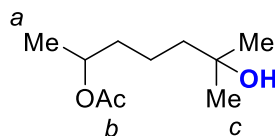
1.20 (H<sub>a</sub>, s, 6H), 0.95 (H<sub>b</sub>, d,  $J$  = 6.6 Hz, 3H) ppm; <sup>13</sup>C NMR (150 MHz, CDCl<sub>3</sub>):  $\delta$  166.94, 132.90, 130.30, 129.52, 129.49, 128.32, 121.80, 119.88, 71.74, 63.60, 43.84, 37.24, 35.41, 29.88, 29.76, 29.03, 28.97, 21.49, 19.58 ppm. NMR spectra are consistent with literature reports.<sup>21</sup>



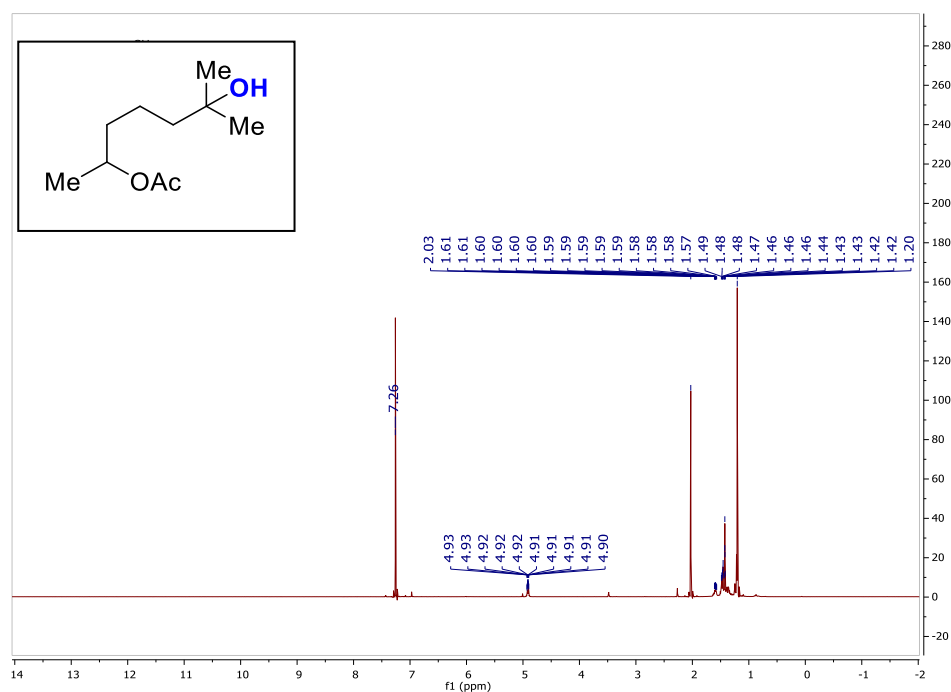


**2,6-Dimethyloctane-2,6-diol 3.53** 3,7-Dimethyloctan-3-ol was hydroxylated using the general procedure. The reaction mixture was purified after workup using silica gel flash chromatography (solvent gradient: 20% to 50% EtOAc/hexanes) to give the recovered starting material (16.0 mg, 0.100 mmol) and product as 29 mg of a white solid (0.168 mmol, 34% yield, 42% brsm). <sup>1</sup>H NMR (600 MHz, CDCl<sub>3</sub>) δ 1.49 – 1.40 (m, 8H), 1.21 (H<sub>a</sub>, s, 6H), 1.14 (H<sub>b</sub>, s, 3H), 0.88 (H<sub>c</sub>, t, *J* = 7.5 Hz, 3H) ppm; <sup>13</sup>C NMR (151 MHz, CDCl<sub>3</sub>) δ 72.90, 70.98, 44.33, 41.66, 34.32, 29.27, 26.33, 18.54, 8.20 ppm. NMR spectra are consistent with literature reports.<sup>21</sup>

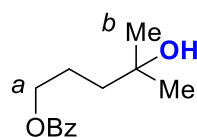
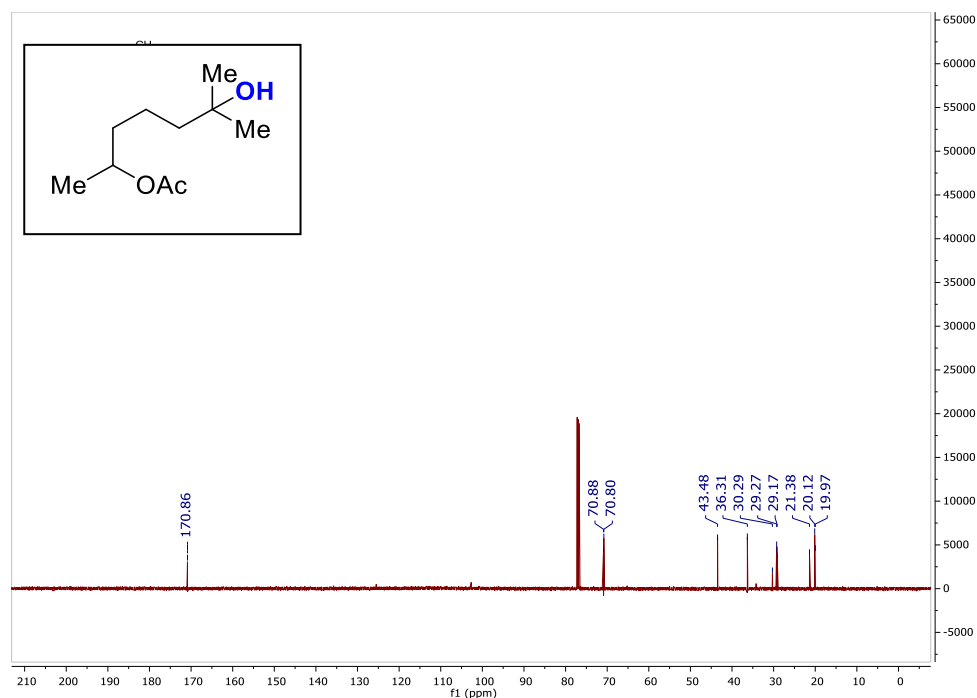




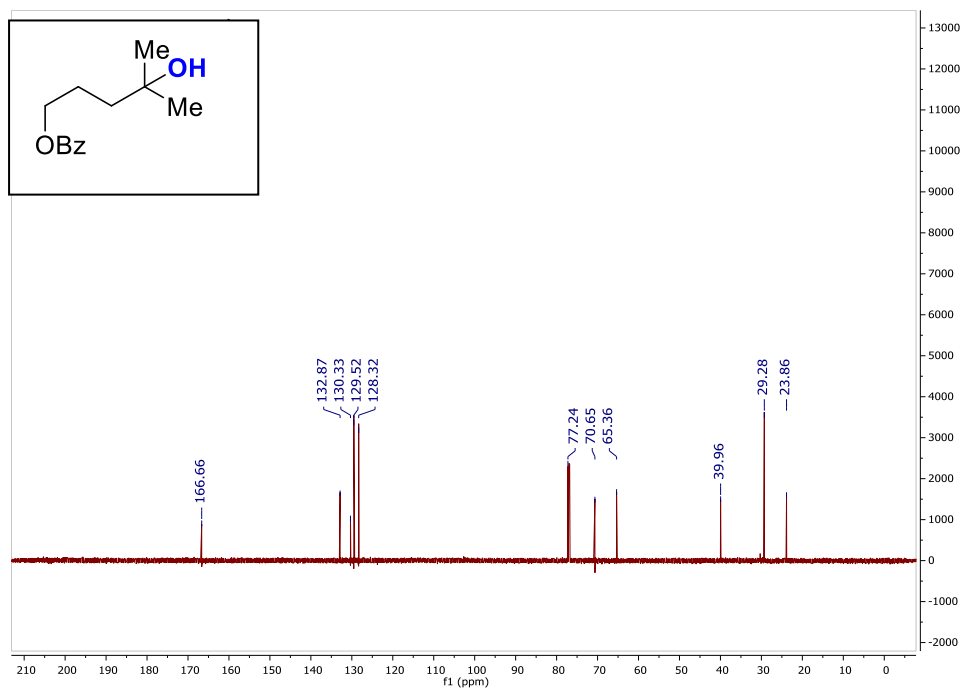
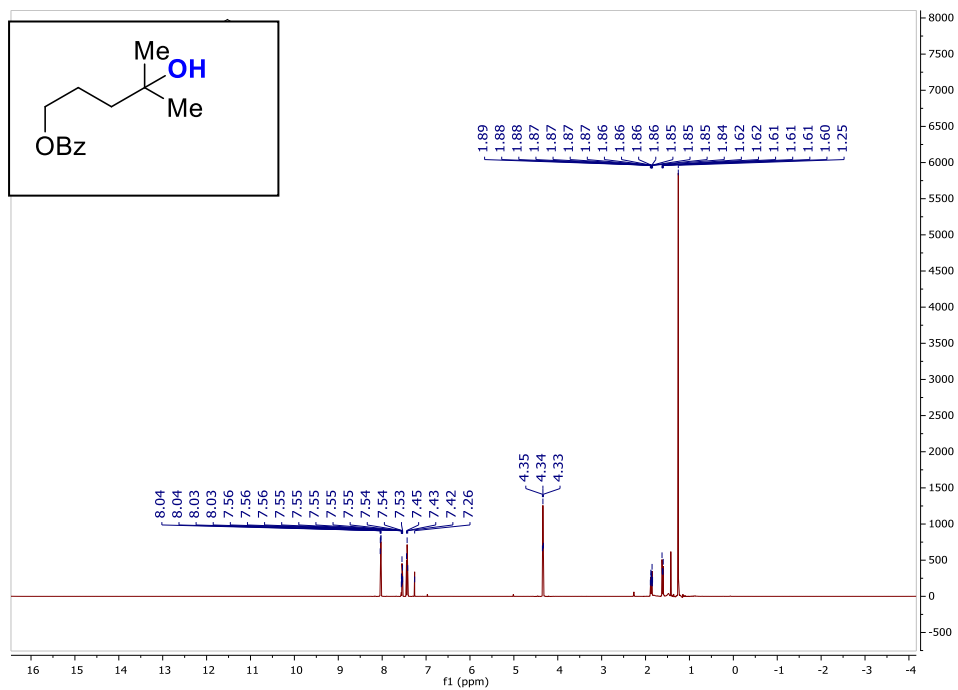
**6-Hydroxy-6-methylheptan-2-yl acetate 3.54** Methylheptan-2-yl acetate was hydroxylated using the general procedure. The reaction mixture was purified after workup using silica gel flash chromatography (solvent gradient 10%-50% Et<sub>2</sub>O/pentane) to give the recovered starting material (31 mg, 0.164 mmol) and product as a colorless oil (38. mg, 37% yield, 52% brsm). **<sup>1</sup>H NMR** (600 MHz, CDCl<sub>3</sub>) δ 4.96 – 4.87 (m, 1H), 2.03 (H<sub>b</sub>, s, 3H), 1.63 – 1.56 (m, 1H), 1.49 – 1.36 (m, 6H), 1.21 (H<sub>a</sub>, H<sub>c</sub>, br, 9H) ppm; **<sup>13</sup>C NMR** (151 MHz, CDCl<sub>3</sub>) δ 170.86, 70.88, 70.80, 43.48, 36.31, 30.29, 29.27, 29.17, 21.38, 20.12, 19.97 ppm. NMR spectra are consistent with literature reports.<sup>21</sup>

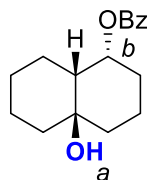






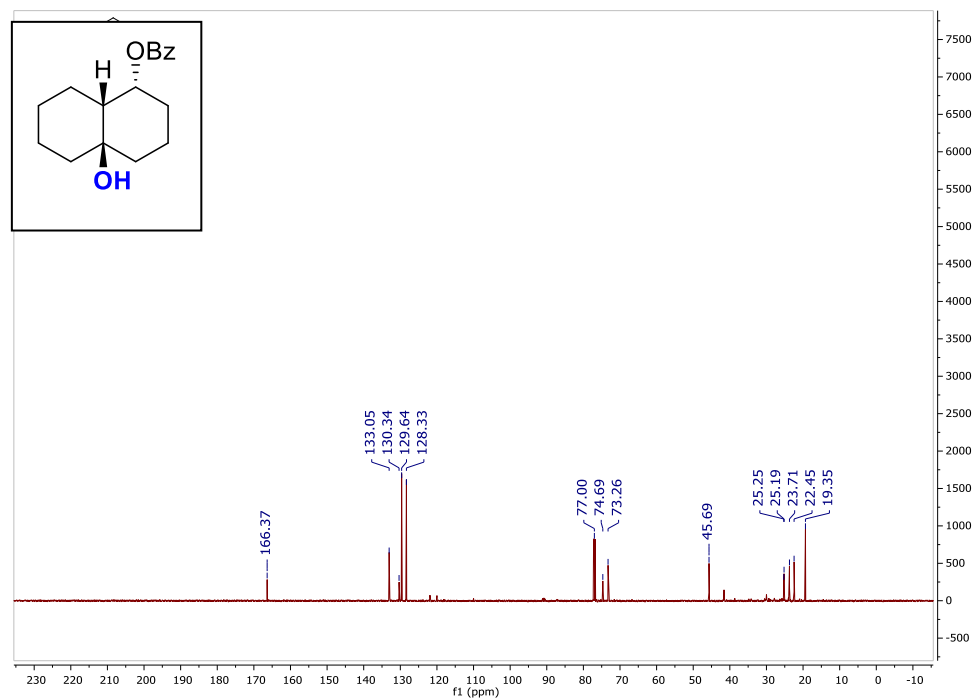
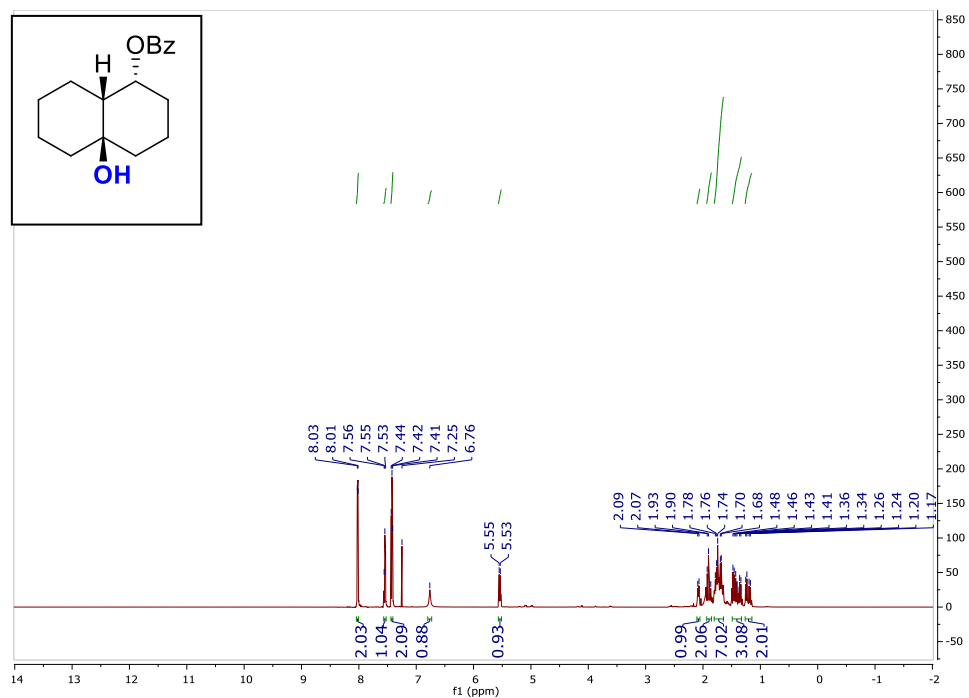
**4-Hydroxy-4-methylpentyl benzoate 3.55** 4-Methylpentyl benzoate was hydroxylated using the general procedure. The reaction mixture was purified after workup using silica gel flash chromatography (solvent gradient 10% to 50% Et<sub>2</sub>O/pentane) to give the recovered starting material (61 mg, 0.39 mmol) and product as a colorless oil (33 mg, 30% yield, 74% brsm).  **$^1\text{H}$  NMR** (600 MHz, CDCl<sub>3</sub>)  $\delta$  8.04 (H<sub>Ar</sub>, dd,  $J$  = 8.4, 1.3 Hz, 2H), 7.57 – 7.52 (H<sub>Ar</sub>, m, 1H), 7.43 (H<sub>Ar</sub>, t,  $J$  = 7.9 Hz, 2H), 4.34 (H<sub>a</sub>, t,  $J$  = 6.7 Hz, 2H), 1.90 – 1.82 (m, 2H), 1.66 – 1.58 (m, 2H), 1.25 (H<sub>b</sub>, s, 6H) ppm;  **$^{13}\text{C}$  NMR** (151 MHz, CDCl<sub>3</sub>)  $\delta$  166.66, 132.87, 130.33, 129.52, 128.32, 77.24, 70.65, 65.36, 39.96, 29.28, 23.86 ppm. NMR spectra are consistent with literature reports.<sup>21</sup>





**(4a*R*,8a*R*)-4a-Hydroxydecahydronaphthalen-1-yl benzoate 3.57** (4a*S*,8a*S*)-

decahydronaphthalen-1-yl benzoate was hydroxylated using the general procedure. The reaction mixture was purified after workup using silica gel flash chromatography (solvent gradient: 20% to 40% EtOAc/hexanes) to give the recovered starting material (59 mg, 0.230 mmol) and product as 81 mg of clear oil (0.296 mmol, 59% yield, 100% brsm). **<sup>1</sup>H NMR** (600 MHz, CDCl<sub>3</sub>): δ 8.02 (H<sub>Ar</sub>, d, *J* = 8.4 Hz, 2H), 7.55 (H<sub>Ar</sub>, t, *J* = 7.4 Hz, 1H), 7.42 (H<sub>Ar</sub>, t, *J* = 7.8 Hz, 2H), 6.76 (H<sub>a</sub>, br, 1H), 5.54 (H<sub>b</sub>, d, *J* = 11.9 Hz, 1H), 2.08 (d, *J* = 12.9 Hz, 1H), 1.94 – 1.85 (m, 2H), 1.80 – 1.64 (m, 7H), 1.49 – 1.33 (m, 3H), 1.22 (dd, *J* = 35.7, 12.7 Hz, 2H) ppm; **<sup>13</sup>C NMR** (150 MHz, CDCl<sub>3</sub>): δ 166.37, 133.05, 130.34, 129.64, 128.33, 74.69, 73.26, 45.69, 25.25, 25.19, 23.71, 22.45, 19.35 ppm. NMR spectra are consistent with literature reports.<sup>13</sup>



### 3.7 References

1. Murray, R. W.; Ramachandran, V.; *Photochem. And Photobiol.*, **1979**, 30, 187-189.
2. Curci, R.; Fiorentino, M.; Troisi, L.; Edwards, J. O.; *J. Org. Chem.*, **1980**, 45, 4758-4760. Murray, R. W.; Jeyaraman, R.; Mohan, L.; *Tet. Lett.*, **1986**, 27, 2335-2336. Murray, R. W.; Jeyaraman, R.; Mohan, L. *J. Am. Chem. Soc.*, **1985**, 108, 2470-2473. Crandall, J. K.; Zucco, M.; Kirsch, R. S.; Coppert, D. M.; *Tet. Lett.*, **1991**, 32, 5441-5444. Curci, R.; D'Accolti, L.; Fiorentino, M.; Fusco, C.; *Tet. Lett.*, **1992**, 33, 4225-4228.
3. Murray, R. W.; Jeyaraman, R.; *J. Org. Chem.*, **1985**, 50, 2847-2853.
4. Mello, R.; Fiorentino, M.; Sciacovelli, O.; Curci, R.; *J. Org. Chem.*, **1988**, 53, 3890-3891.
5. Bovicelli, P.; Lupattelli, P.; Mincione, E.; Prencipe, T.; Curci, R.; *J. Org. Chem.*, **1992**, 57, 2182-2184. Bovicelli, P.; Lupattelli, P.; Mincione, E.; *J. Org. Chem.*, **1992**, 57, 5052-5054.
6. Boukouvalas, J.; Wang, J.; Marion, O.; Ndzi, B.; *J. Org. Chem.*, **2006**, 71, 6670-6673.
7. Wender, P. A.; Hilinski, M. K.; Mayweg, A. V. M.; *Org. Lett.*, **2005**, 7, 79-82.

8. Murray, R. W.; *Chem. Rev.*, **1989**, 89, 1187-1201. Adam, W.; Curci, R.; Edwards, J. O.; *Acc. Chem. Res.*, **1989**, 22, 205-211. Yang, D.; Wong, M.; Yip, Y.; *J. Org. Chem.*, **1995**, 60, 3887-3889.
9. Yang, D.; Wong, M.; Wang, X.; Tang, Y.; *J. Am. Chem. Soc.*, **1998**, 120, 6611-6612.
10. Yang, D.; Yip, Y.; Tang, M.; Wong, M.; Zheng, J.; Cheung, K.; *J. Am. Chem. Soc.*, **1996**, 118, 491-492.
11. For leading review see: Wong, O. A.; Shi, Y.; *Chem. Rev.*, **2008**, 108, 3958-3987.
12. Zou, L.; Paton, R. S.; Eschenmoser, A.; Newhouse, T. R.; Baran, P. S.; Houk, K. N.; *J. Org. Chem.*, **2013**, 78, 4037-4048.
13. Pierce, C. J.; Hilinski, M. K.; *Org. Lett.*, **2014**, 16, 6504-6507.
14. For influence of hydrogen bonding on dioxirane reactivity, see: Murray, R. W.; Gu, H.; *J. Phys. Org. Chem.*, **1996**, 9, 751-758.
15. Hyde, A. M.; SULTanksi, S. L.; Waldman, J. H.; Zhong, Y.; Shevlin, M.; Peng, F.; *Org. Process Res. Dev.*, **2017**, 21, 1355-1370.
16. Denmark, S. E.; Forbes, D. C.; Hays, D. S.; DePue, J. S.; Wilde, R. G.; *J. Org. Chem.*, **1995**, 60, 1391-1407.
17. Chen, M. S.; White, C.; *Science*, **2007**, 318, 783-787.

18. Brodsky, B. H.; Du Bois, J.; *J. Am. Chem. Soc.*, **2005**, *127*, 15391-15393.
19. Fung, Y.; Yan, S.; Wong, M.; *Org. Biomol. Chem.*, **2012**, *10*, 3122-3130.
20. Romney, D. K.; Miller, S. J.; *Org. Lett.*, **2012**, *14*, 1138-1141.
21. Wang, D.; Shuler, W. G.; Pierce, C. J.; Hilinski, M. K.; *Org. Lett.*, **2015**, *18*, 3826-3829.

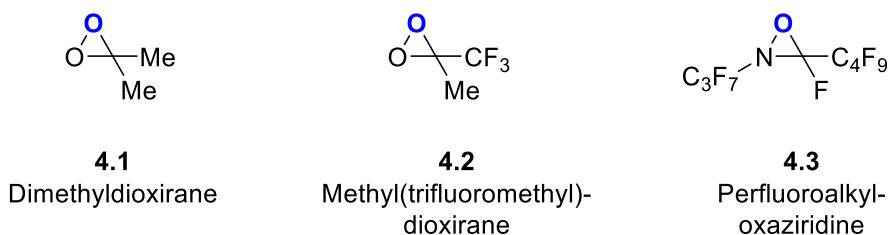
## Chapter Four

### Iminium Salt Catalyzed C–H Functionalization

#### 4.1 Introduction

Resnati and coworkers introduced *aza*-analogs of dioxiranes that can perform electrophilic hydroxylation of unactivated C–H bonds (**Figure 4.1**).<sup>1</sup> These oxaziridines display similar trends to dioxiranes: their reactivity is enhanced by inclusion of electron withdrawing groups, and they react with the most electron rich bonds present in a molecule.

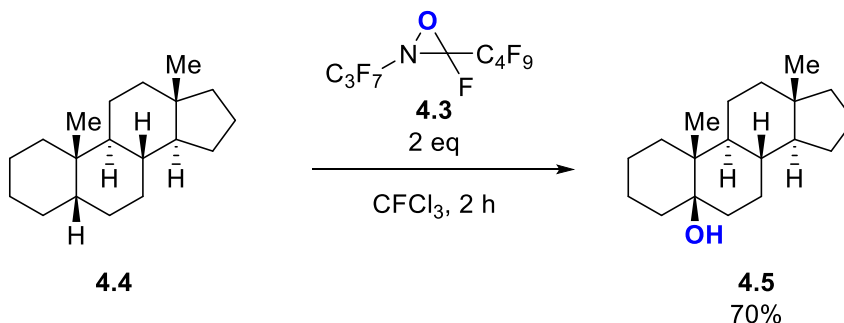
**Figure 4.1:** Stoichiometric organic reagents for C–H bond hydroxylation



These oxaziridines are stable indefinitely and can be prepared from commercially available perfluoroalkylamines.<sup>1</sup> Soon after the initial discovery of their reactivity, it was discovered that oxaziridines can selectively and stereospecifically functionalize C–H bonds in complex molecules (**Scheme 4.1**).<sup>2</sup> This work solidified their place as a viable alternative to dioxirane-mediated oxidations.

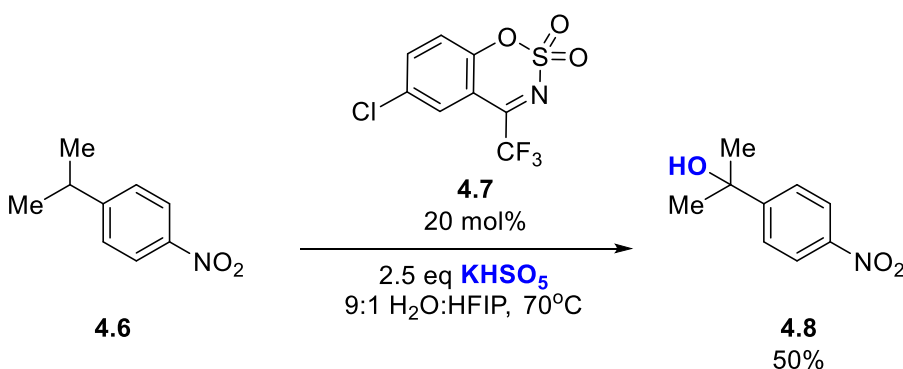


---

**Scheme 4.1:** Oxaziridine mediated hydroxylation of complex molecules


Several years after these initial reports, Du Bois and coworkers developed conditions that allow catalytic oxaziridine mediated C–H bond hydroxylation, establishing the earliest examples of organocatalytic hydroxylation (**Scheme 4.2**).<sup>3</sup> Hydroxylated products were obtained in 50 – 80% yield with a variety of small molecule organics. Catalysts required the incorporation of electron withdrawing groups to be effective C–H bond hydroxylation reagents.

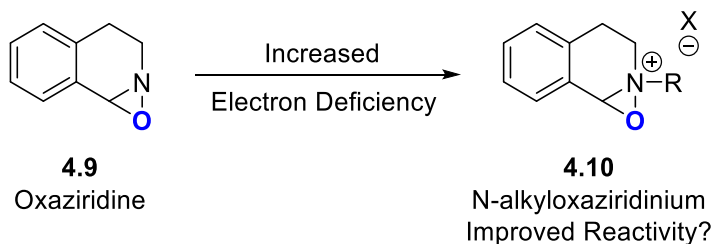
---

**Scheme 4.2:** Organocatalytic oxaziridine mediated hydroxylation of C–H bonds


A related class of cationic oxidants was being researched concurrently with the development of oxaziridine chemistry. These oxaziridiniums are

rendered more electron deficient- and more reactive- due to the formal positive charge centered on the nitrogen atom (**Figure 4.2**).<sup>4</sup>

**Figure 4.2:** Hypothesis for catalyst design



Although extensively researched for catalytic epoxidation, surprisingly, no examples existed of oxaziridinium mediated C–H bond hydroxylation.<sup>4</sup> We undertook the development of an organocatalytic oxaziridinium mediated hydroxylation reaction to investigate potential improved reactivity in comparison to existing oxaziridine catalyzed methods.

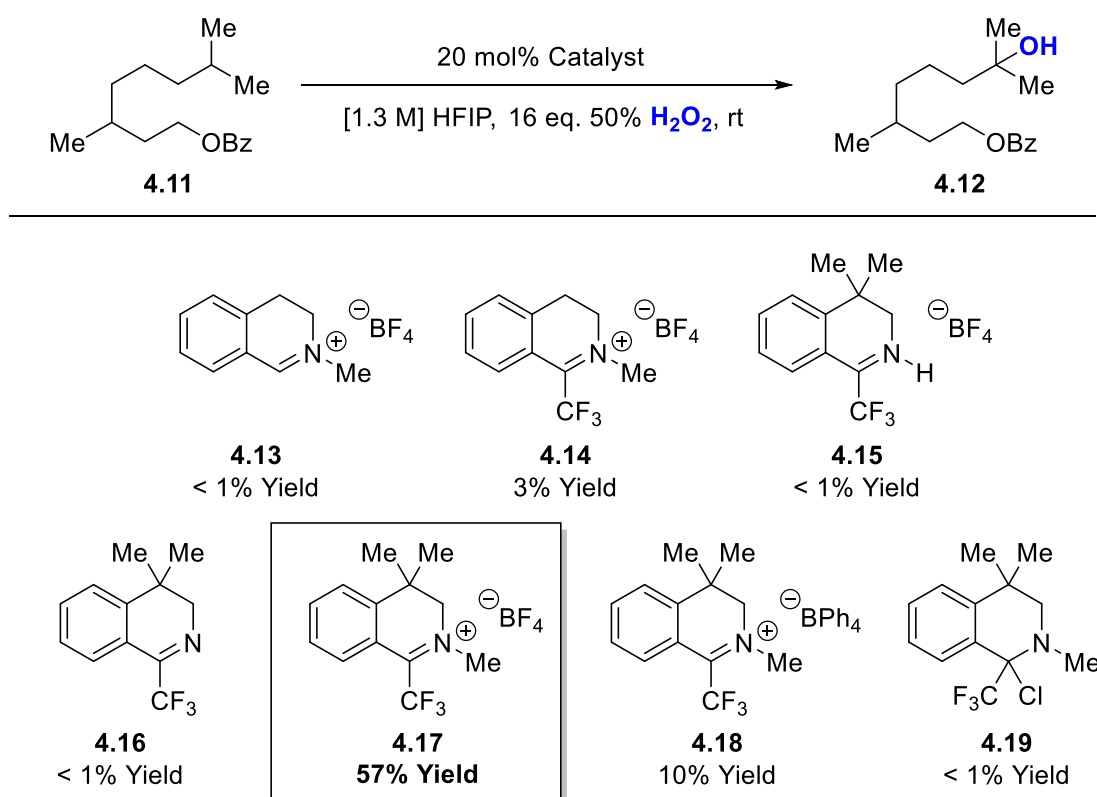
## 4.2 Reaction Discovery and Optimization

### 4.2.1 Selection of reaction conditions

Optimization of a catalytic oxaziridinium mediated C–H bond hydroxylation reaction began with an investigation of catalyst structure (**Table 4.1**). Attempts to use Lusinchi-type dihydroisoquinolinium **4.13** for the hydroxylation of 3,7-dimethyloctanol benzoate using fluoroalcohol-peroxide conditions provided only trace quantities of hydroxylated products.<sup>5</sup> We developed a new dihydroisoquinolinium salt **4.14** bearing a trifluoromethyl group based on the rate enhancement it provides in related dioxirane and oxaziridine mediated

hydroxylations.<sup>3</sup> This new catalyst provided hydroxylated products in trace yield. In his initial report, Lusinchi noted that these salts aromatize under oxidative conditions to form catalytically inactive isoquinoliniums.<sup>5</sup> The inclusion of a benzylic *gem*-dimethyl group blocked this decomposition pathway, leading to highly active C–H bond hydroxylation catalyst **4.17**.

**Table 4.1:** Impact of catalyst structure on reactivity



Reactions performed on 0.2 mmol scale. Corrected GC yields and conversions reported.

The use of a tetrafluoroborate counterion provided important for reactivity. Nucleophilic counterions (e.g.:  $\text{Cl}^-$ ,  $\text{AcO}^-$ ) form  $\alpha$ -functionalized amines **4.19** that

are unreactive under our conditions. Inclusion of more lipophilic counterions (**4.18**,  $\text{BPh}_4^-$ ) also led to poor reactivity under the biphasic conditions employed.

Optimization of reaction conditions revealed that room temperature mixtures of HFIP and 50% hydrogen peroxide were ideal for reactivity (**Table 4.2**). Reduction in the amount of HFIP present through the inclusion of cosolvents used in other C–H bond hydroxylation procedures led to significant reduction in yield. This lessened activity could be due to the stabilization effect of HFIP on related trifluoromethyloxaziridines observed by Du Bois and coworkers.<sup>3</sup> The use of acidic conditions ( $\text{pH} < 4$ ) are also highly important for reactivity: reactions buffered at pH 4 provided hydroxylation products in much lower yields. These requirements for reactivity are all consistent with an acid catalyzed oxaziridinium formation and oxaziridinium mediated C–H bond hydroxylation.

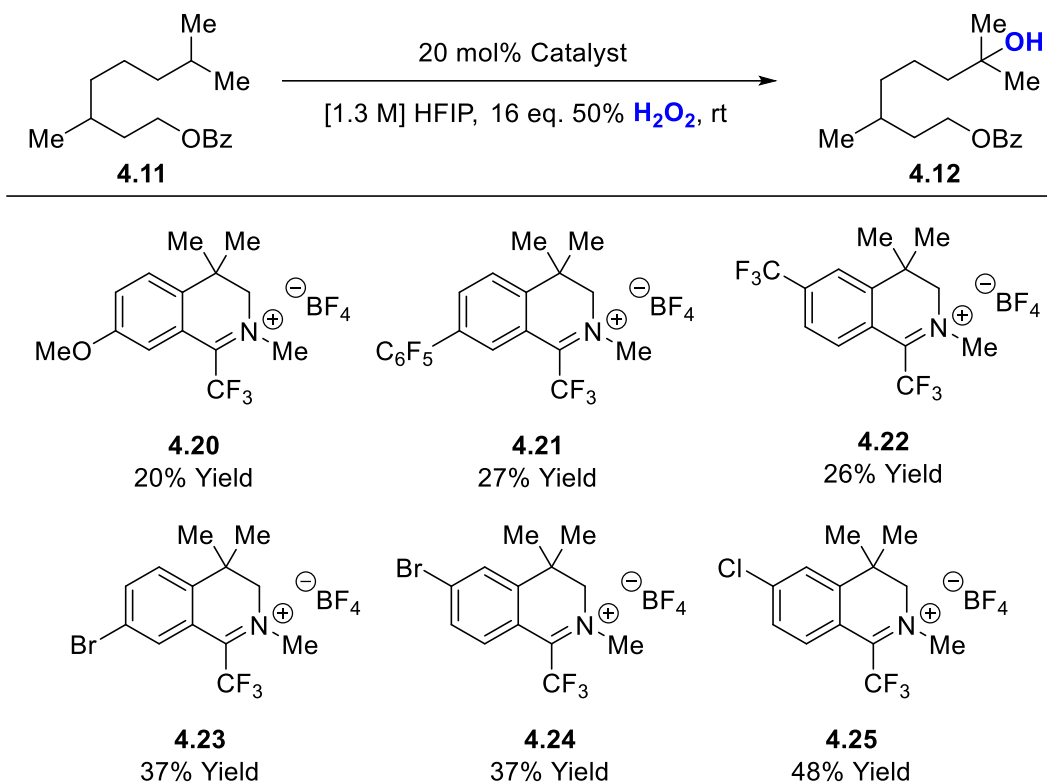
**Table 4.2:** Impact of reaction conditions on conversion and yield

Entry	Deviation from Conditions	Conversion %	Yield %
1	None	70	57
2	MeCN:HFIP (1.3:1)	2	< 1
3	EtOAc:HFIP (1.3:1)	< 1	< 1
4	DCE:HFIP (1.3:1)	< 1	< 1
5	4 °C	46	43
6	50 °C	49	25
7	pH 4 buffer	15	7

Reactions performed on 0.2 mmol scale. Corrected GC yields and conversions reported.

#### 4.2.2 Exploration of electronic effects on catalyst activity

Increasing the electron deficiency through aryl substitution has been demonstrated to enhance the reactivity of catalytic oxaziridines.<sup>3</sup> As such, a variety of catalyst analogs bearing electron withdrawing and donating groups were tested for activity (**Table 4.3**). Electron neutral catalysts operated best under our reaction conditions despite advantages attained by the inclusion of electron withdrawing groups in related oxaziridine chemistry.

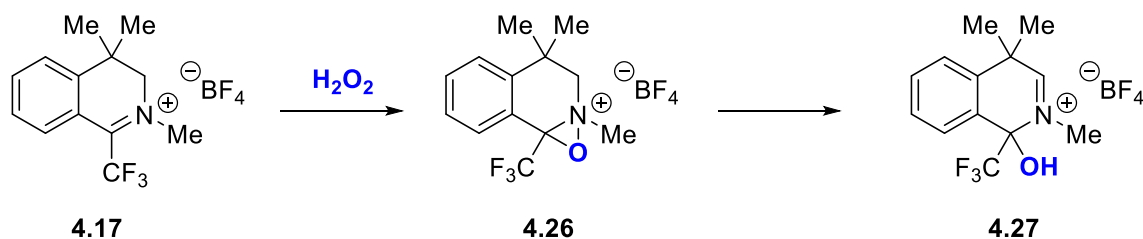
**Table 4.3:** Electronic effects on catalyst activity

Reactions performed on 0.2 mmol scale. Corrected GC yields and conversions reported.

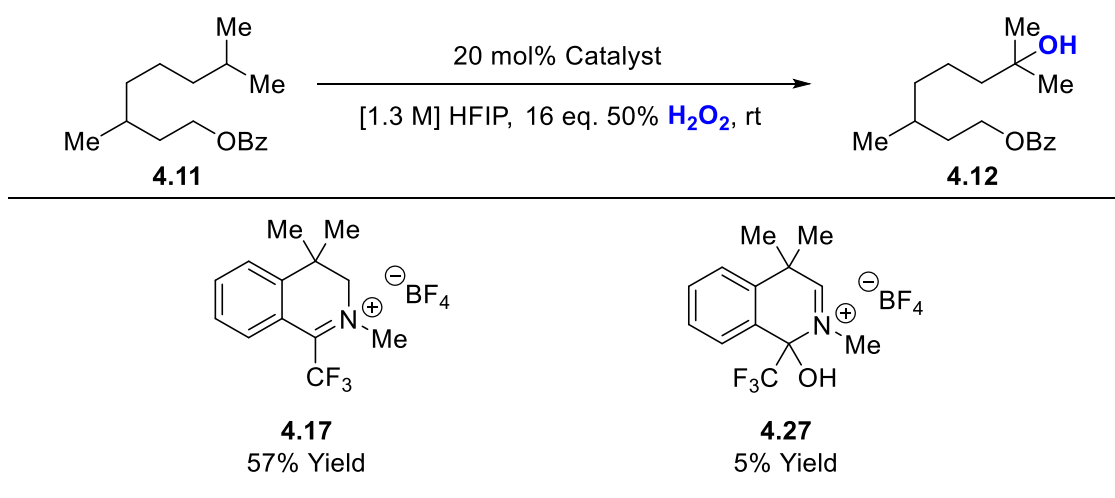
We posited that we may be increasing the reactivity of our oxaziridinium by inclusion of electron withdrawing groups, but that we were simultaneously increasing the rate of oxaziridinium decomposition. Although the previously reported decomposition pathway was blocked by the incorporation of the *gem*-dimethyl group, degradation product **4.27** was observed in the reaction mixture presumably arising from elimination of the oxaziridinium (**Scheme 4.3**). This rearranged iminium formed from catalyst degradation lacks the benefit of the

trifluoromethyl group: in control reactions using this product as the catalyst, hydroxylation products were isolated in low yields (**Table 4.4**).

**Scheme 4.3:** Oxaziridinium degradation



**Table 4.4:** Activity comparison of catalyst and degraded catalyst

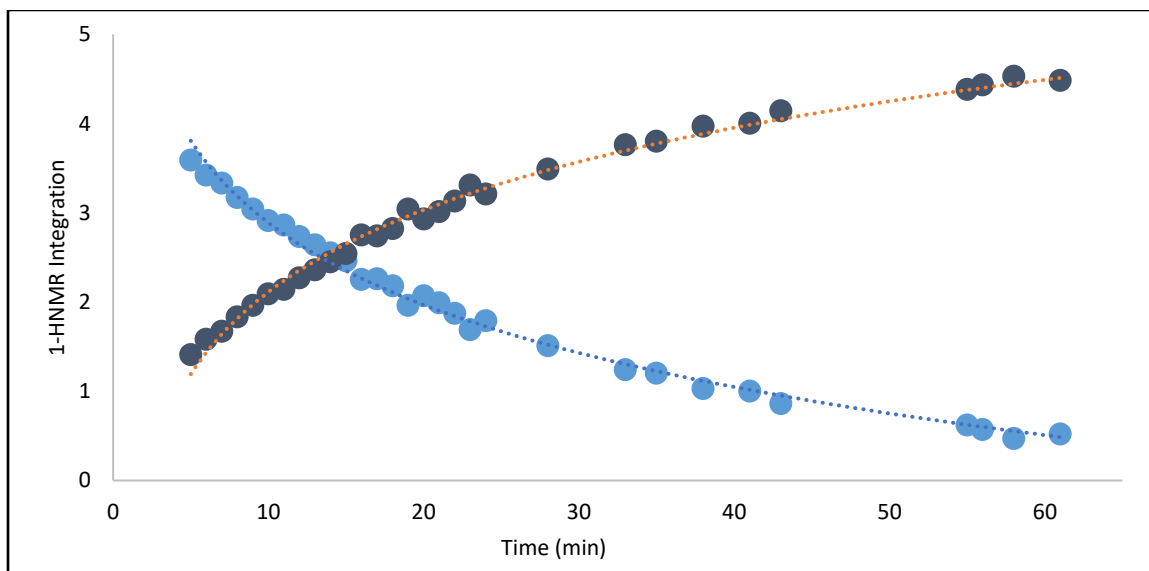
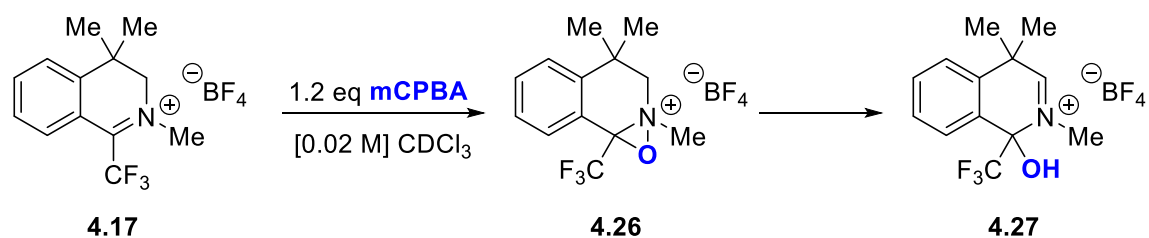


The instability of the oxaziridinium prevented its isolation or observation under the hydroxylation reaction conditions. However, oxaziridinium formation and degradation could be monitored by use of a CDCl<sub>3</sub> solution of iminium salt and *m*-CPBA. Although these conditions are incompatible with catalytic C–H hydroxylation of most substrates and lack the stabilizing effects of HFIP, we used

them as a rough approximation for understanding the kinetics of oxaziridinium formation and degradation under our conditions.

Under these conditions, oxaziridinium formation occurs spontaneously upon addition of *m*-CPBA to the iminium salt. Monitoring of proton integration revealed that subsequent degradation of the oxaziridinium follows first order kinetics (**Figure 4.3**).

**Figure 4.3:** NMR monitoring of oxaziridinium degradation





Both strongly electron withdrawing groups (e.g.: CF<sub>3</sub>) and strongly electron donating groups (e.g.: OMe) decrease the half-life of the oxaziridinium, offering a possible explanation for their poor reactivity under our conditions (**Table 4.5**). Surprisingly, halogenation increased the stability of the oxaziridinium which does not correlate to their hydroxylation capability. This may suggest a combination of oxaziridinium stability, reactivity and solubility play an important role in catalyst activity.

**Table 4.5:** Half-life of substituted oxaziridiniums

4.28  $\xrightarrow{[0.02 \text{ M}] \text{CDCl}_3}$  4.29

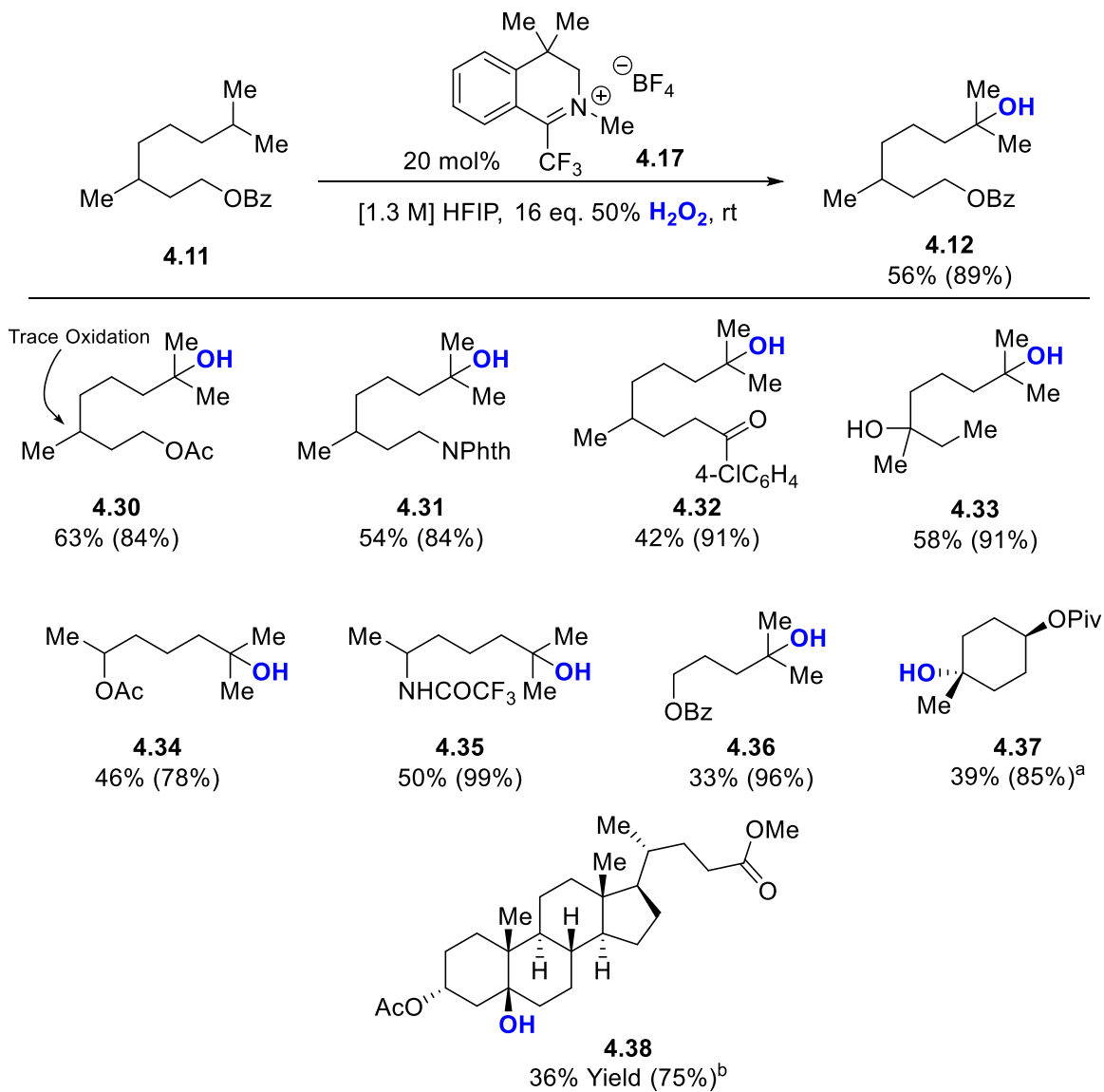
Entry	Substitution	Half-life (min)	Hydroxylation Yield %
1	R=H, R <sub>1</sub> =H	17.5	57
2	R=Cl, R <sub>1</sub> =H	34.4	48
3	R=Br, R <sub>1</sub> =H	34.5	37
4	R=H, R <sub>1</sub> =Br	35.0	37
5	R=CF <sub>3</sub> , R <sub>1</sub> =H	21.8	26
6	R=H, R <sub>1</sub> =OMe	13.6	20

### 4.3 Catalytic C–H Bond Hydroxylation

#### 4.3.1 Hydroxylation of tertiary C–H bonds

The substrates commonly used to test C–H bond hydroxylation reactions match well with previous reports in terms of scope and yields (**Table 4.6**).<sup>1-3</sup>

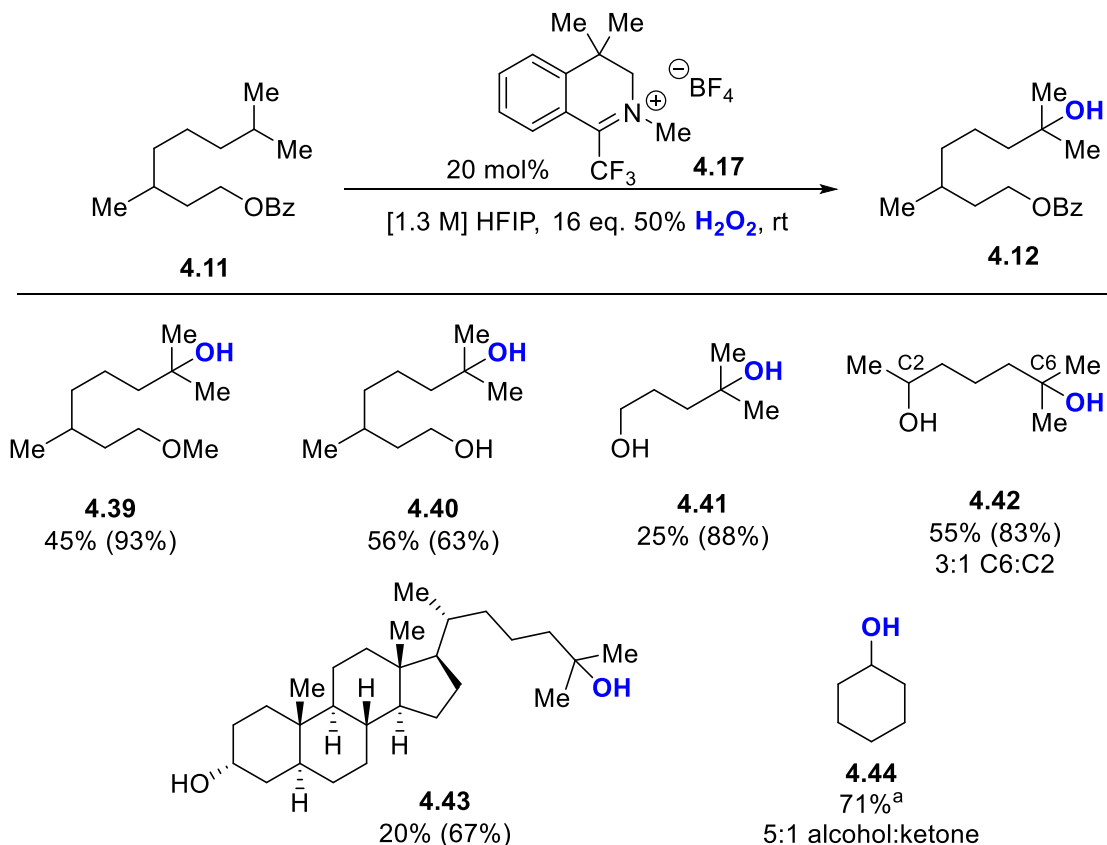
Sensitivity towards deactivating groups, typical of electrophilic oxidants, was observed. The high degree of remote vs. proximal hydroxylation selectivity observed for 3,7-dimethyloctanol acetate with dioxirane oxidations (>28:1) was also observed with iminium salt catalysts (19:1). The disparity in selectivity between these catalysts, that share common conditions, against those previously reported (ca. 5:1)<sup>6</sup> suggest that a combination of catalyst and conditions are responsible for this selectivity.

**Table 4.6:** Hydroxylation of tertiary aliphatic C–H bonds

Reactions performed on 0.4 mmol scale. Isolated yields. Yields in parenthesis: yields based on recovered starting material. <sup>a</sup>40 mol % iminium salt was used. <sup>b</sup>Reaction time = 48 hr. 20 mol% Iminium salt and 16 eq.  $\text{H}_2\text{O}_2$  were added at 0 and 24 h.

#### 4.3.2 Chemoselective aliphatic C–H hydroxylation

Commonly employed C–H bond hydroxylation reagents will preferentially oxidize heteronuclear functionality over aliphatic C–H bonds. For example, dioxiranes are known to oxidize unhindered primary alcohols to carboxylic acids.<sup>7</sup> As such, use of these methods require protecting groups to limit reactivity to unactivated C–H bonds. The iminium salt catalyst, however, preferentially reacts with unactivated C–H bonds in the presence of unprotected, easily oxidized functionality.

**Table 4.7:** Selective aliphatic C–H bond oxidation

Reactions performed on 0.4 mmol scale. Isolated yields. Yields in parenthesis: yields based on recovered starting material. <sup>a</sup>Corrected GC yield. DCM required to solubilize cyclohexane.

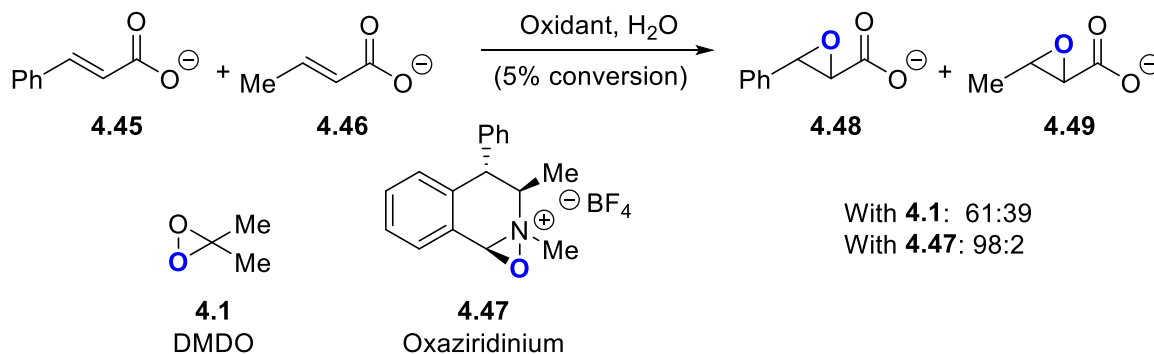
In each case, products arising from alcohol oxidation are minor constituents of the crude reaction mixture. The degree of unwanted oxidation is substrate dependent: primary alcohols and ethers are largely unreactive, but secondary alcohols exhibit significant oxidation. Interestingly, no products arising from alcohol oxidation were observed in the hydroxylation of cyclic secondary alcohol containing dehydrocholesterol (**4.43**).

The selectivity against alcohol oxidation under these conditions allowed for the selective hydroxylation of cyclohexane, providing cyclohexanol in 59% GC yield with only 12% formation of cyclohexanone. This is contrary to other commonly used electrophilic oxidation reagents, which provide cyclohexanone as the exclusive product,<sup>3,6</sup> suggesting that iminium salt catalysts may be able to install stereochemically enriched alcohols at prochiral reaction sites. Investigation was undertaken to determine what gives rise to this unusual selectivity.

#### **4.4 Investigation of Chemoselectivity in C–H Hydroxylations**

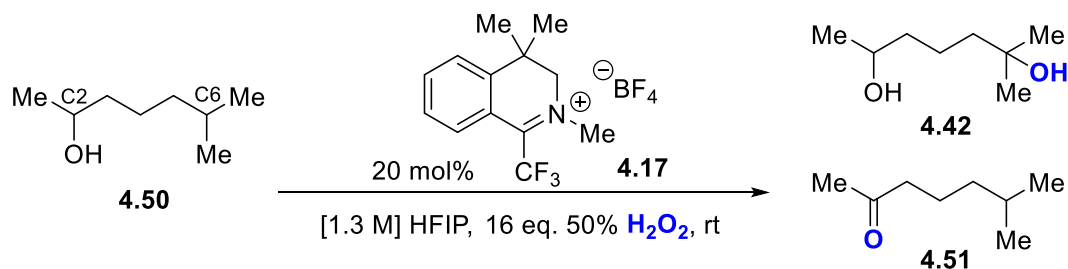
##### *4.4.1 Hydrophobic rate enhancement*

Breslow and Biscoe identified that dihydroisoquinolinium derived oxaziridiniums engage in hydrophobic clustering during epoxidation reactions, which allows for an increase in reaction rate of oxidations.<sup>8</sup> In a competition experiment between cinnamic and crotonic acids, oxaziridiniums are uniquely selective amongst other oxidants for reactivity with the more lipophilic cinnamic acid (**Scheme 4.4**).

**Scheme 4.4:** Hydrophobic interactions driving oxidative selectivity

We explored whether hydrophobic clustering was responsible for the selectivity observed in our dihydroisoquinolinium salt catalyzed hydroxylation reactions through the inclusion of additives that are known to either enhance or disrupt hydrophobic interactions. 6-Methyl-2-heptanol was chosen as a model substrate for exploring these additives.

The introduction of salts is known to increase the ionic strength of reaction media, increasing the strength of hydrophobic clusters.<sup>9</sup> Ideally, inclusion of salts should increase the selectivity for aliphatic C–H bond hydroxylation over alcohol oxidation. Considerations had to be made to ensure that the salts added would not affect the reactivity of the iminium salt or alter the pH of the reaction medium. Overall, no significant effects were imparted to selectivity by addition of salts, providing preliminary evidence that selectivity was not derived from hydrophobic effects (**Table 4.8**).

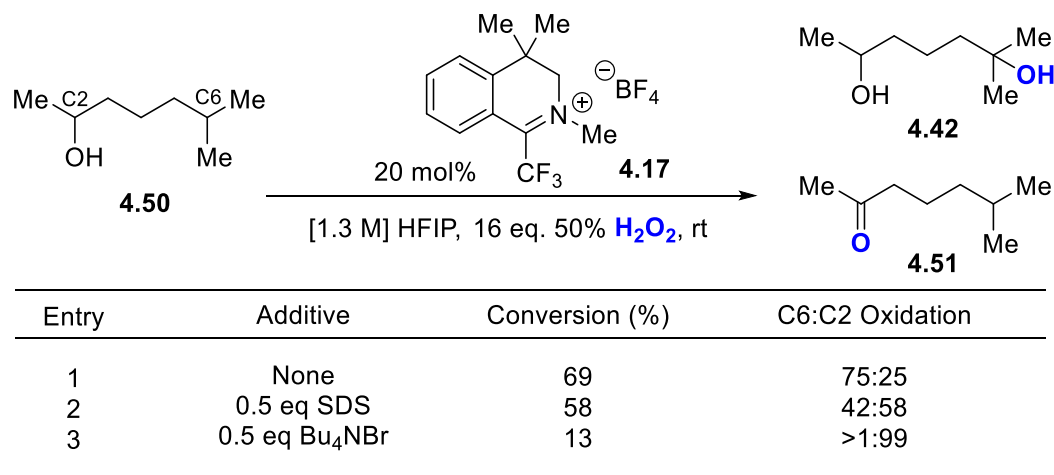
**Table 4.8:** Salt effects on chemoselectivity

Entry	Additive	Conversion (%)	C6:C2 Oxidation
1	None	69	75:25
2	[0.01 M] LiCl	70	72:28
3	[0.1 M] LiCl	2	n.d.
4	[0.1 M] NaCl	1	n.d.
5	[0.5 M] $\text{NaBF}_4$	72	75:25
6	[8 M] $\text{NaBF}_4$	46	69:31
7	[1 M] $(\text{NH}_4)_2\text{SO}_4$	56	72:28
8	[5 M] $(\text{NH}_4)_2\text{SO}_4$	42	72:28
9	[0.1 M] $\text{Na}_2\text{EDTA}$	41	69:31

Reactions performed on 0.2 mmol scale. Corrected GC yields reported.

The addition of dispersing agents provided the first evidence that hydrophobic interactions played a key role: addition of sodium dodecylsulfate (SDS) or  $n\text{Bu}_4\text{NBr}$  both led to considerable erosion of chemoselectivity (**Table 4.9**). SDS is particularly notable as reaction efficiency was maintained, suggesting that the reactivity observed is a result of an oxaziridinium mediated process. As bromide is known to form bromine radicals on exposure to peroxide, the lack of chemoselectivity in  $n\text{Bu}_4\text{NBr}$  containing reactions may be a consequence of radical based oxidations.



**Table 4.9:** Effect of dispersing agents on chemoselectivity

Reactions performed on 0.2 mmol scale. Corrected GC yields reported.

Cyclodextrins are known to support hydrophobic interactions in their central pore and have been used to direct hydroxylation to hydrophobic sites in TFDO mediated oxidations.<sup>10</sup> If hydrophobic clustering was predominantly responsible for chemoselectivity, the addition of cyclodextrins should substantially enhance the effect, however; no such enhancement was observed (**Table 4.10**).

**Table 4.10:** Effect of cyclodextrins on chemoselectivity

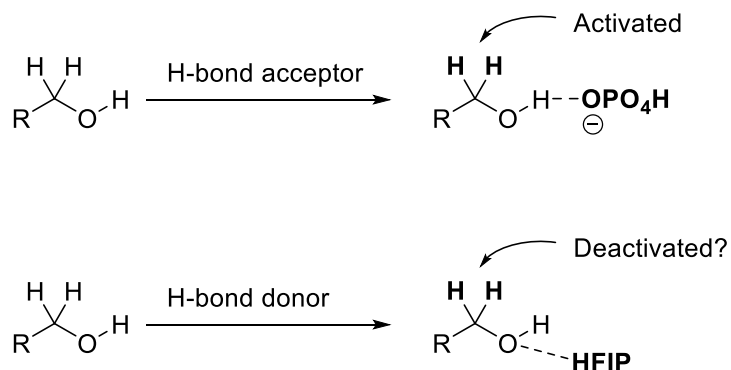
Entry	Additive	Conversion (%)	C6:C2 Oxidation
1	None	69	75:25
2	0.1 eq $\gamma$ cyclodextrin	73	74:26
3	0.1 eq $\beta$ cyclodextrin	75	75:25
4	0.5 eq $\beta$ cyclodextrin	41	78:22
5	1.0 eq $\beta$ cyclodextrin	44	76:24

Reactions performed on 0.2 mmol scale. Corrected GC yields reported.

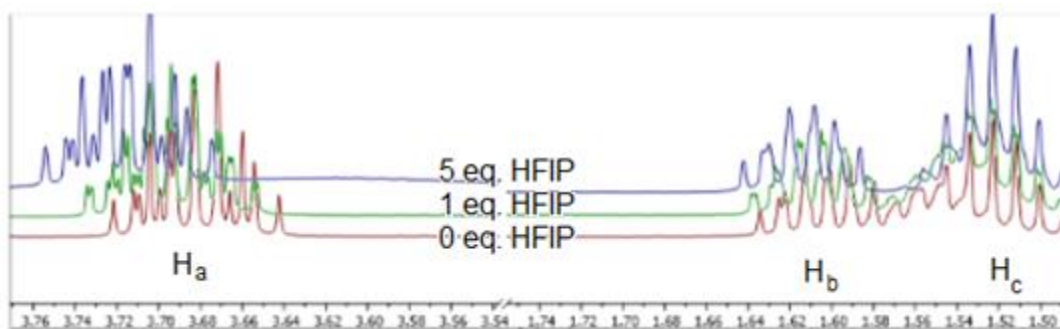
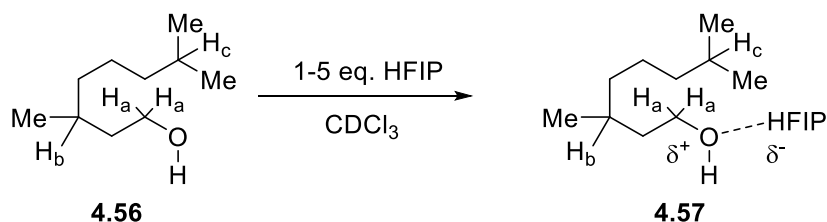
#### 4.4.2 Solvent effects

Macmillan and coworkers reported that inclusion of the hydrogen bond acceptor  $n\text{Bu}_4\text{NPO}_3\text{H}$  can weaken  $\alpha\text{-C-H}$  bonds of alcohols and increase their reactivity.<sup>11</sup>

We hypothesized that HFIP may act as a hydrogen bond donor, deactivating and protecting  $\alpha\text{-C-H}$  bonds from oxidation (**Figure 4.4**).

**Figure 4.4:** Modulation of bond strength through hydrogen bonding

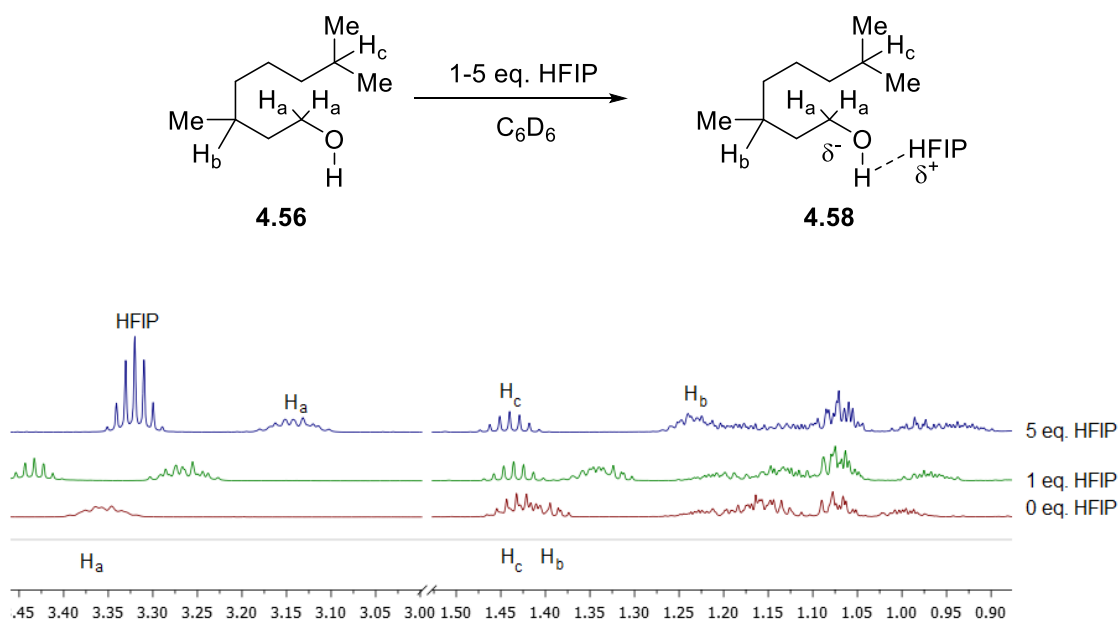
The hypothesis that HFIP hydrogen bonding led to increased distal versus proximal selectivity was tested by titrating HFIP into a  $\text{CDCl}_3$  solution of 3,7-dimethyloctanol. Noticeable downfield shifting of protons occurs as HFIP is titrated in, which corresponds to decreased reactivity with electrophilic oxidants (**Figure 4.5**).

**Figure 4.5:** Impact of HFIP on  $^1\text{H}$  chemical shift in  $\text{CDCl}_3$ 

The degree by which protons signals shift correspond to distance from the hydrogen bonding site. Protons rendered unreactive under our conditions shift substantially downfield, while protons attached to the predominant reaction site are largely unchanged. Independent investigation conducted by Costas further supported this claim and demonstrated this effect is general and can be employed in transition metal catalyzed reactions.<sup>12</sup> The inability to use this strategy for in situ deactivation of amines is currently unknown.

When this experiment is run in deuterobenzene, the opposite trend is seen in which protons of 3,7-dimethyloctanol are shifted upfield, suggesting HFIP may alternate between hydrogen bonding modes based on solvent polarity (**Figure 4.6**).

**Figure 4.6:** Impact of HFIP on  $^1\text{H}$  chemical shift in  $\text{C}_6\text{D}_6$

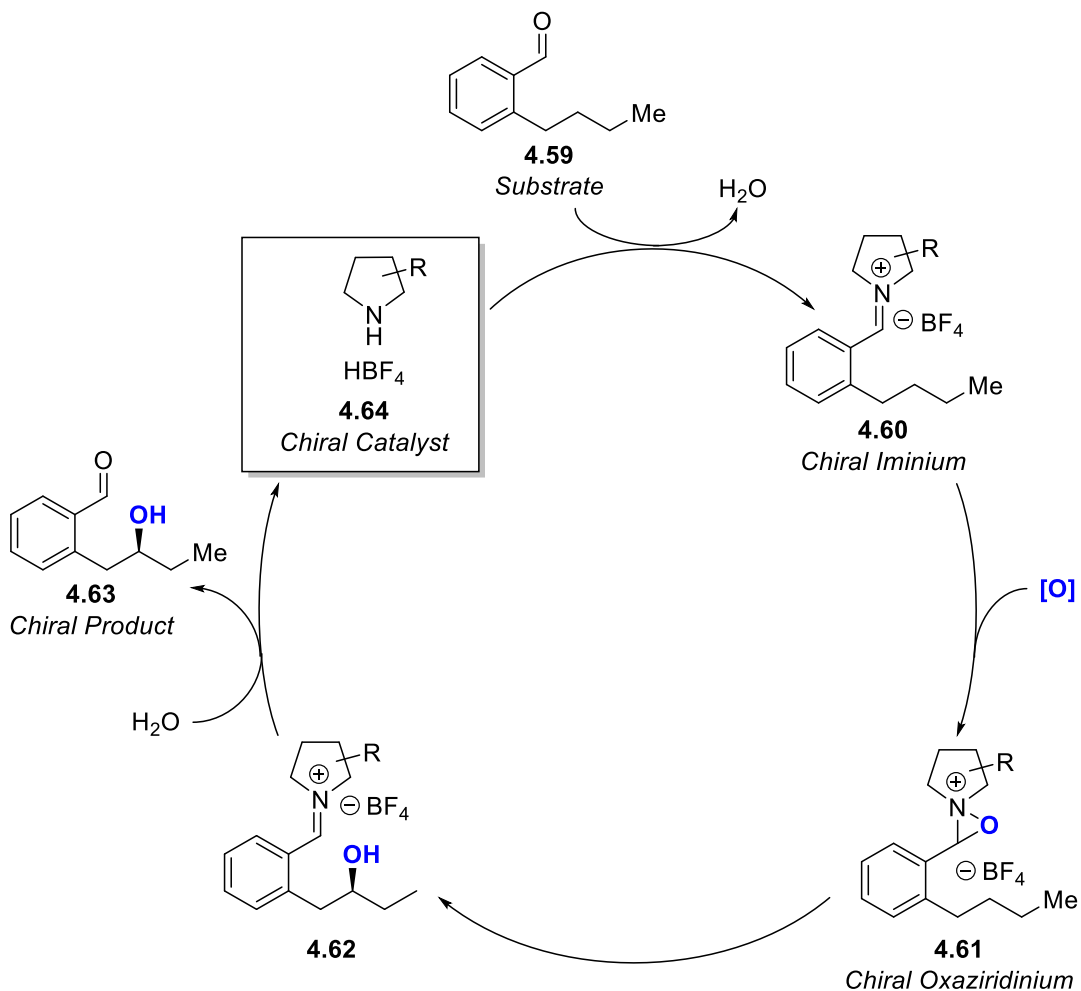


Interestingly, catalytic dioxirane mediated hydroxylations do not display this chemoselectivity despite being conducted in HFIP. There is some preference for aliphatic C–H bond hydroxylation early in the reaction that erodes as more potassium persulfate-sodium bicarbonate is added over the course of the reaction. These salts along with SDS and *n*Bu<sub>4</sub>NBr tested for hydrophobic cluster disruption may alter HFIP hydrogen bonding, rendering the reaction nonselective.

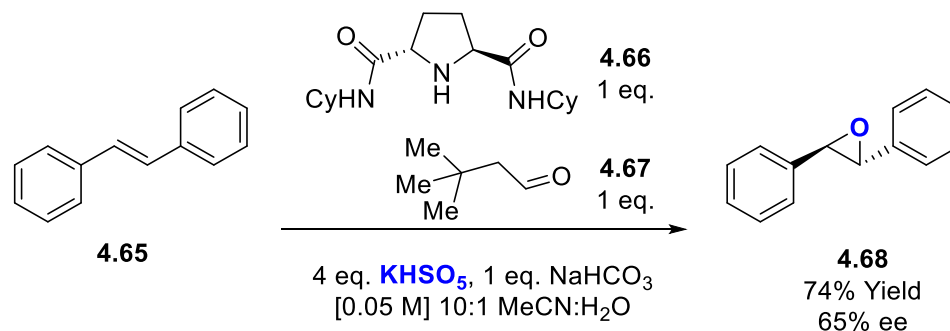
## 4.5 In situ formation of iminiums

### 4.5.1 General approach and methods

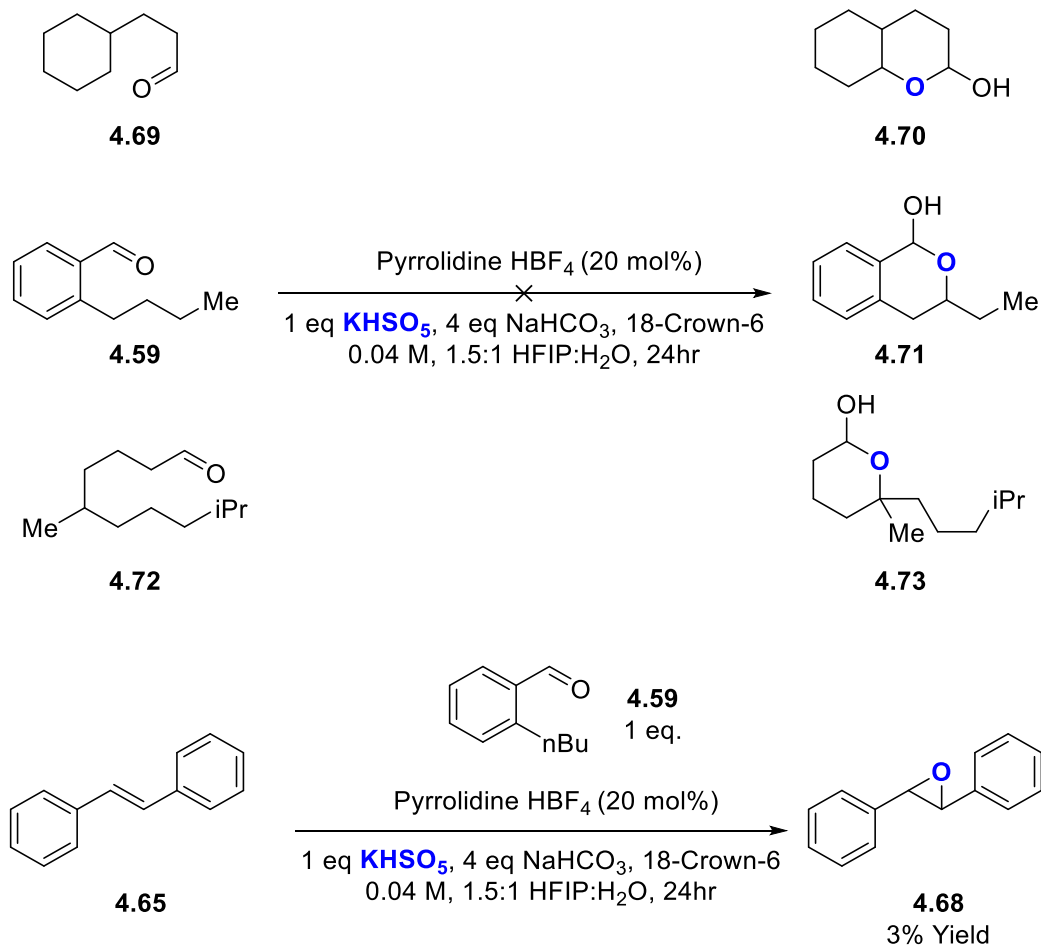
We envisioned that we could leverage our selective methylene hydroxylation to perform directed asymmetric intramolecular oxidations. Ideally, we desired to use a chiral catalytic amine to form an iminium then oxaziridinium in situ (**Scheme 4.5**).

**Scheme 4.5:** Proposed catalytic cycle for intramolecular hydroxylation

Investigation conducted by Yang and coworkers demonstrated the feasibility of this method by generating oxaziridiniums in situ from stoichiometric amounts of carbonyl and amine compounds.<sup>13</sup> When using a chiral amine, asymmetric epoxidations of alkenes was possible (**Scheme 4.6**).

**Scheme 4.6:** Yang in situ oxaziridinium formation

In a first attempt, conditions for oxidation (H<sub>2</sub>O<sub>2</sub>-HFIP) led to rapid oxidation of pyrrolidine HBF<sub>4</sub>. It was ultimately determined that the conditions used in dioxirane catalysis (HFIP/H<sub>2</sub>O with persulfate-bicarbonate) led to slower catalyst degradation. The phase transfer catalyst 18-crown-6 was added to aid in the transfer of oxidant between organic and aqueous layers. Epoxidation of *trans*-stilbene was possible under these conditions but no intramolecular C–H bond hydroxylation was observed (**Scheme 4.7**).

**Scheme 4.7:** Attempted intramolecular C–H bond hydroxylation


Reactions performed on 0.1 mmol scale. Corrected GC yields reported.

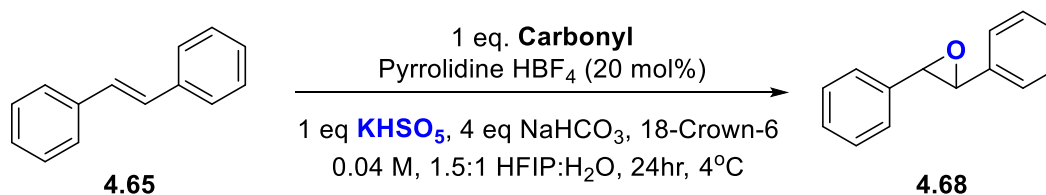
Amine salts are known to activate persulfate in non-oxaziridinium mediated epoxidation of alkenes, but control experiments indicated that both the carbonyl and the amine were essential for reactivity.<sup>14</sup> We tentatively concluded that an oxaziridinium was forming and was responsible for oxidative activity.



#### 4.5.2 Identification of suitable carbonyl components

The steric environment of the carbonyl compound had a substantial impact on the yield of *trans*-stilbene epoxidation (**Table 4.11**). Sterically encumbered carbonyls failed to provide *trans*-stilbene oxide in appreciable quantities. This may be a consequence of iminium longevity: carbonyls that form unstable iminiums may have unfavorable equilibria that reduce the amount of oxaziridinium formed. This sensitivity was also observed under Yang in situ formation conditions.<sup>13</sup> Trifluoromethylketones performed oxidations in the absence of amine, suggesting dioxirane formation may be responsible for epoxidation.

**Table 4.11:** Impact of carbonyl component on oxaziridinium formation

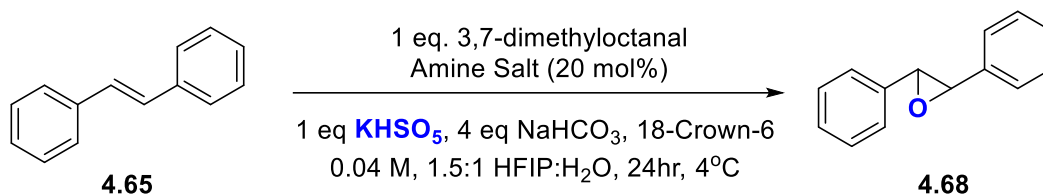


Entry	Carbonyl	Epoxidation Yield (%)
1	—	0
2	2-Butylbenzaldehyde	3
3	3,7-Dimethyloctanal	90
4	3-Cyclohexylpropanal	90
5	Pivaldehyde	0
6	Cyclopentanone	10
7	Cyclohexanone	24
8	1,1,1-Trifluorohexanone	100
9	2,2,2-Trifluoroacetophenone	0

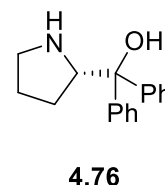
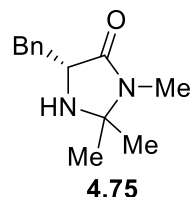
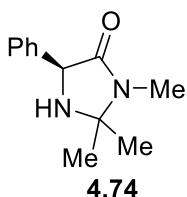
Reactions performed on 0.1 mmol scale. Corrected GC yields reported.

#### 4.5.3 Identification of suitable amine catalysts

Several pyrrolidine-based amines were competent catalysts in *trans*-stilbene oxidation (**4.12**). Interestingly, amines known to participate in *in situ* iminium catalysis failed to perform epoxidations. It is unclear if this is due to the longevity of the iminium in solution or difficulties in oxaziridinium formation. Amines in conjugation with aromatic rings also failed to induce epoxidation. Further investigation is required to understand the remarkable sensitivity to steric and electronic environments of the amine catalysts.

**Table 4.12:** Impact of amine catalyst on oxaziridinium formation

Entry	Amine Salt	Epoxidation Yield (%)
1	Pyrrolidine HBF <sub>4</sub>	90
2	Pyrrolidine HOTf	100
3	Diisopropylamine HBF <sub>4</sub>	0
4	Proline	9
5	Pyrrolidine (R)-BINOL-PO <sub>2</sub> H	90
6	N-Methylaniline HBF <sub>4</sub>	trace
7	Indoline HBF <sub>4</sub>	0
8	2-Methylindoline HBF <sub>4</sub>	trace
9	<b>4.74</b> HBF <sub>4</sub>	trace
10	<b>4.75</b> HBF <sub>4</sub>	0
11	<b>4.76</b> HBF <sub>4</sub>	trace



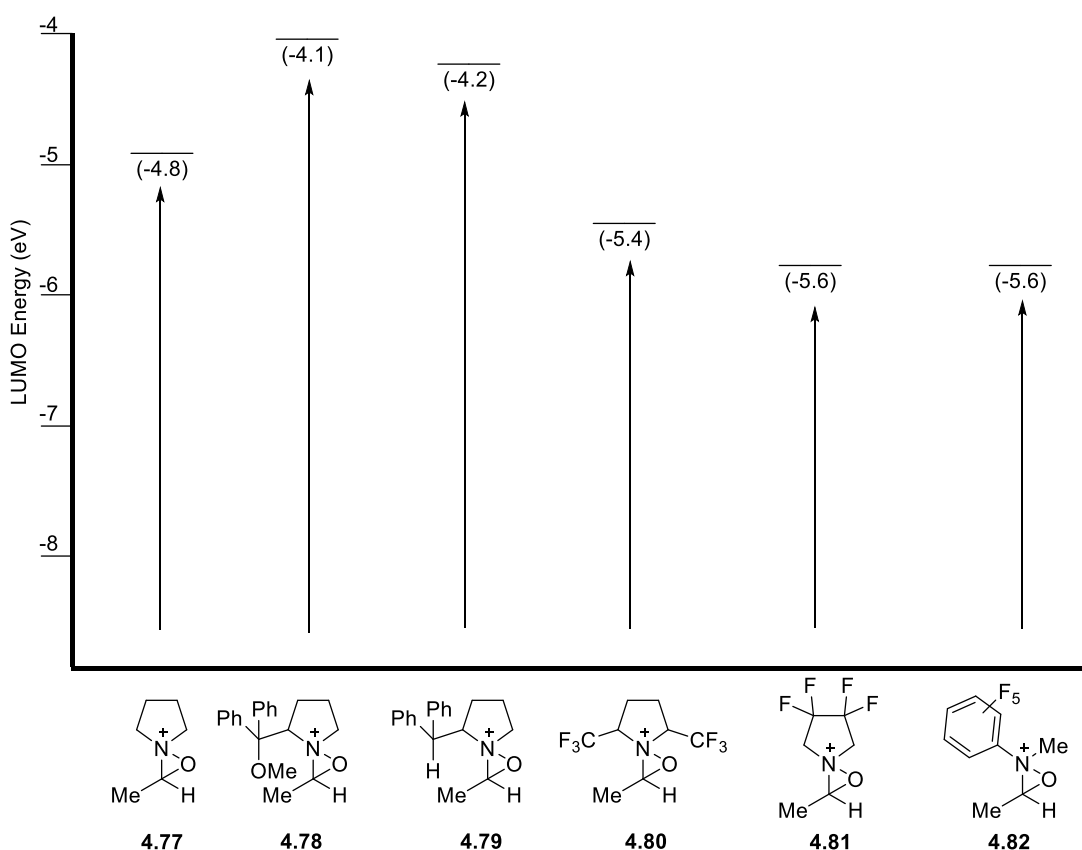
Reactions performed on 0.1 mmol scale. Corrected GC yields reported.

#### 4.5.4 Future directions for development of a C–H bond hydroxylation reaction

The electron deficiency of the oxaziridinium is critical for hydroxylation reactivity, as shown by the catalyst screenings during the development of isolated iminium salt catalysts for C–H bond hydroxylation. As electron deficient carbonyl compounds are susceptible to dioxirane formation, electron deficiency would likely

need to be incorporated within the amine catalyst. The LUMO energy of a series of oxaziridiniums generated from various pyrrolidines were calculated using DFT calculations (**Figure 4.7**). Those possessing lower energy LUMO's correspond to more reactive catalysts.

**Figure 4.7:** Calculated LUMO energies of various oxaziridiniums



Calculations performed with Spartan using B3LYP/6-31G.

Although N-methylpentafluoroanilinium tetrafluoroborate is predicted to be an excellent catalyst by DFT calculations, it failed to epoxidate *trans*-stilbene under our conditions, possibly due to iminium or oxaziridinium instability. A middle ground

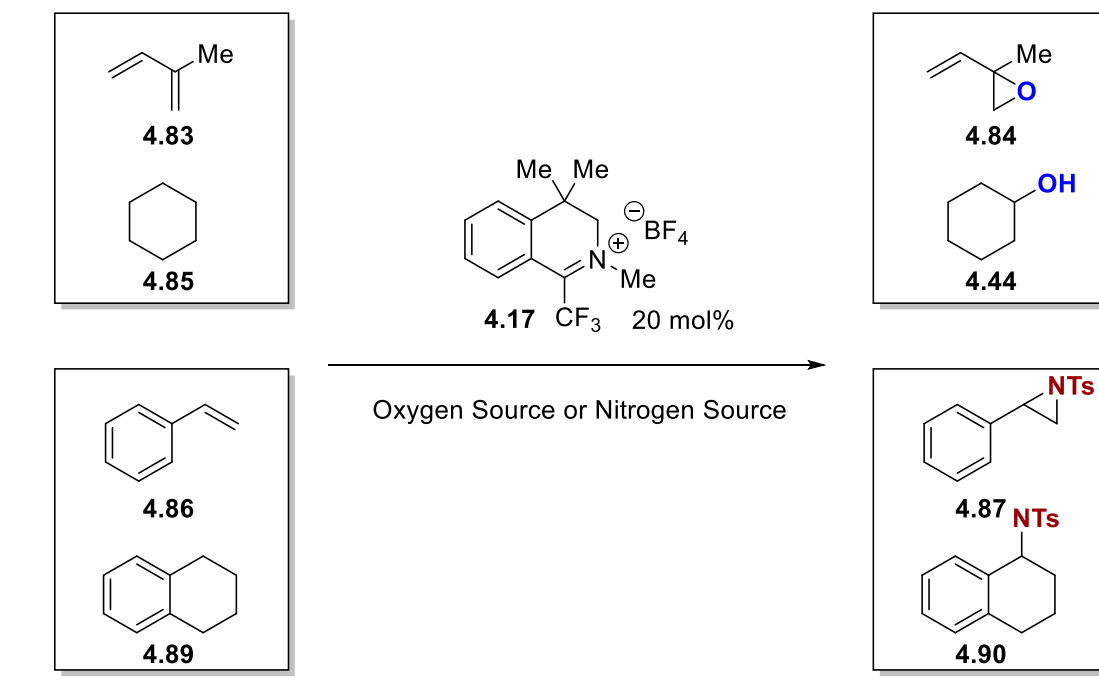
of electron deficiency may need to be discovered that allows both oxaziridinium formation and C–H bond hydroxylation.

## 4.6 Chiral Iminium Salt Catalysts

### 4.6.1 Introduction to asymmetric iminium salt atom transfer catalysis

The iminium salt **4.17**, developed in our lab and detailed in chapter 5, catalyzes the epoxidation and aziridination of olefins as well as the hydroxylation and amination of aliphatic C–H bonds.<sup>40</sup> In all these modes of reactivity, iminium salt **4.17** is capable of transforming prochiral centers into racemic functionalized products (**Scheme 4.8**).

**Scheme 4.8:** Iminium salt catalyzed functionalization of prochiral substrates

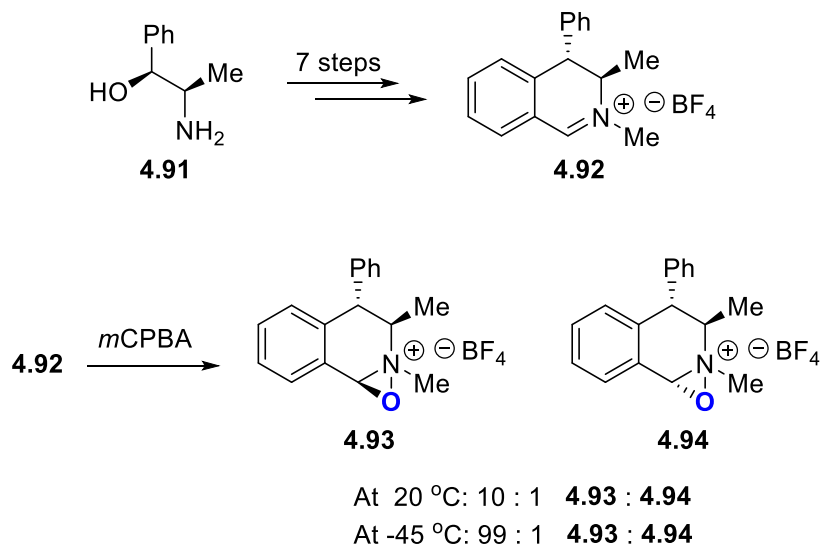


Asymmetric iminium salt mediated epoxidation was first reported by Bohé in 1993.<sup>15</sup> Since then, considerable efforts have been devoted to the development of improved catalysts and conditions that have allowed asymmetric epoxidations to proceed in high yields with high enantioselectivity.<sup>16</sup> As epoxidation is believed to share a similar transition state geometry to C–H bond functionalization, the knowledge generated in the development of these catalysts could provide insight and direction into the development of new organocatalysts derived from iminium salt **4.17** that perform asymmetric aziridination, C–H bond hydroxylation, and C–H bond amination.

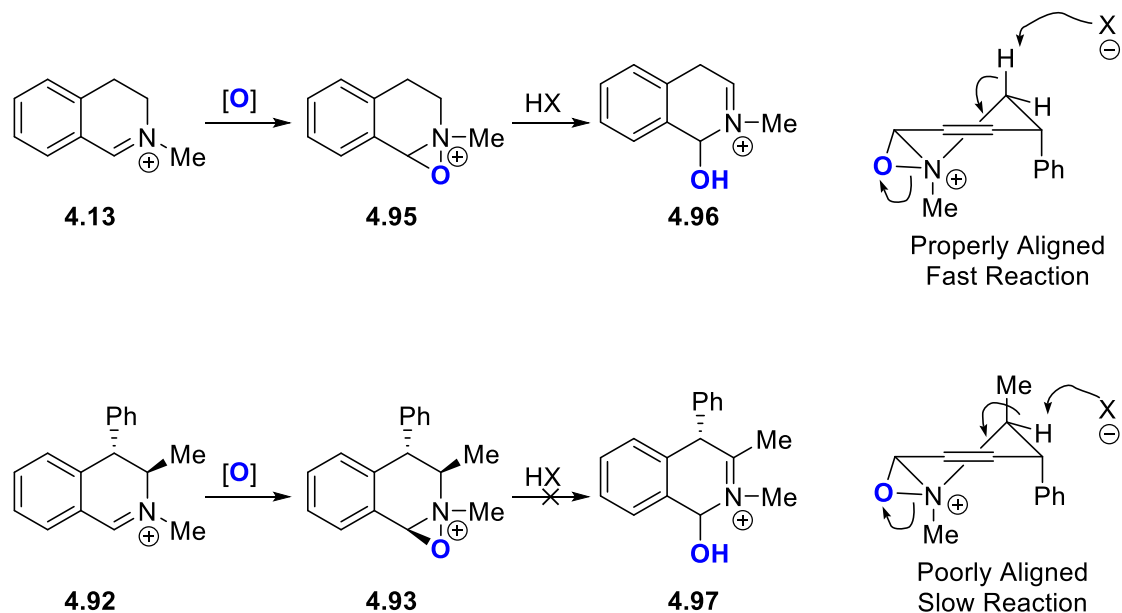
#### *4.6.2 Norepinephrine derived iminium catalysts*

In Bohé's initial reports, the chiral dihydroisoquinolinium salt **4.92** was synthesized in seven steps from naturally occurring (-)-norepinephrine (**Scheme 4.9**).<sup>15</sup> It was found that the oxaziridinium **4.93** formed from these salts could be used in asymmetric epoxidation of styrenes as stoichiometric oxidants or as organocatalysts, providing products of modest enantiopurity (< 60% ee).<sup>15,17</sup> A significant impact of solvent on oxidation rate and enantioselectivity was observed (e.g.: 42% ee in CH<sub>2</sub>Cl<sub>2</sub> vs 1% ee in benzene), sparking an interest in the development of a wide range of catalyst structures that operate under varying reaction conditions.

---

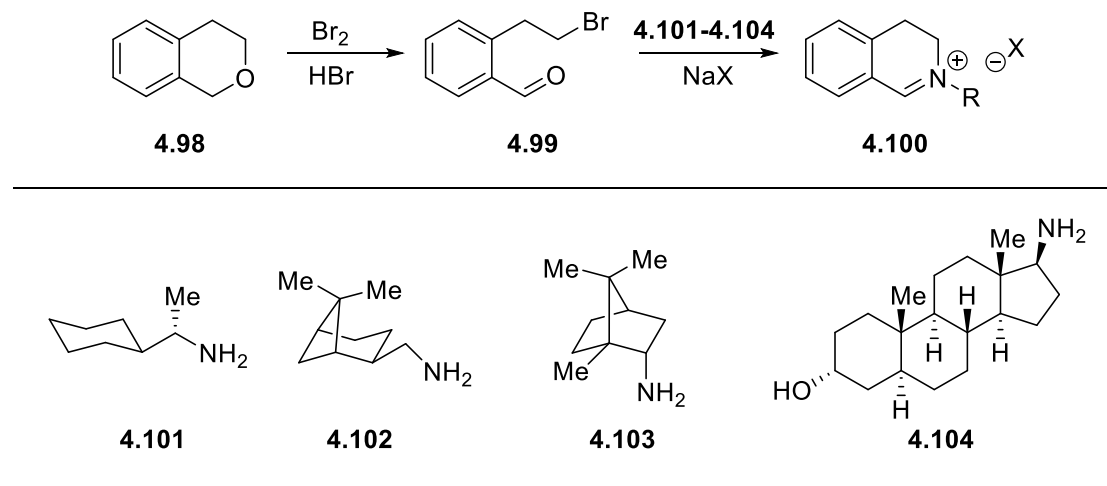
**Scheme 4.9:** The first chiral epoxidation organocatalyst


The chiral substituents present on iminium salt **4.92** also improved catalyst stability compared to iminium salt **4.13** first reported by Luschini.<sup>18</sup> The antiperiplanar arrangement of adjacent protons required for degradation of **4.95** to inactive **4.96** are blocked when chiral substituents are introduced (**Scheme 4.10**). As such, the reaction rate of **4.93** degradation to **4.97** is slowed, allowing broader substrate scope and higher conversion.

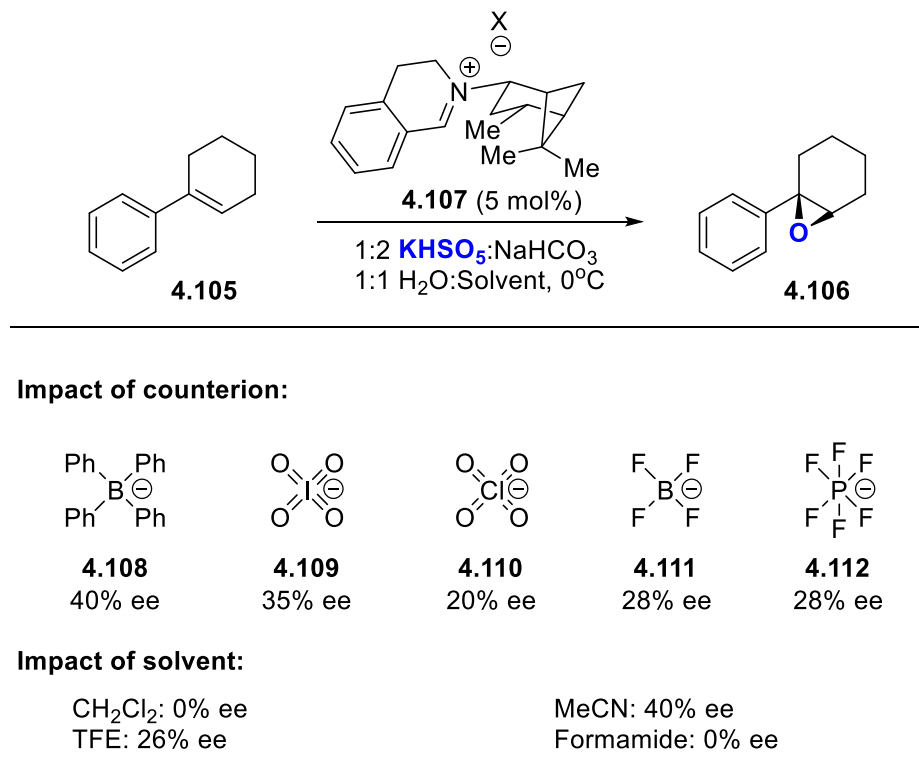
**Scheme 4.10:** Routes for catalyst degradation

**4.6.3 Iminium salts from chiral amines**

Page and coworkers developed a new route to iminium salts that allowed rapid screening of catalysts generated from a late-stage intermediate and naturally occurring chiral amines.<sup>19</sup> In this route, bromo-aldehyde **4.98** generated in one step by oxidative ring opening of isochroman was condensed with a variety of amines (**4.101-4.104**) to form iminium salt catalysts (**Figure 4.8**). This synthesis required no purification, establishing a library of chiral catalysts of type **4.100** in two synthetic steps. These catalysts offered little stereocontrol for epoxidation of styrenes, except for *trans*-stilbene which could be epoxidized in 73% ee.



**Figure 4.8:** Library synthesis of chiral iminium salts

Follow up investigation revealed that both counterion solvent strongly impacted enantioselectivity of reactions catalyzed by iminium salts of type **4.100**. In the epoxidation of **4.105** catalyzed by iminium salt **4.107**, higher enantioselectivity was observed for more strongly coordinating counterions (**Figure 4.9**).<sup>20</sup> The exception enantiocontrol provided by **4.107**-tetraphenylborate was rationalized as an additional contribution by  $\pi$ -stacking. In total, they speculated that counterion coordination increased the effective steric bulk of **4.107**, providing increased discrimination between diastereomeric transition states.

**Figure 4.9:** Impact of ion coordination and solvent on enantioselectivity

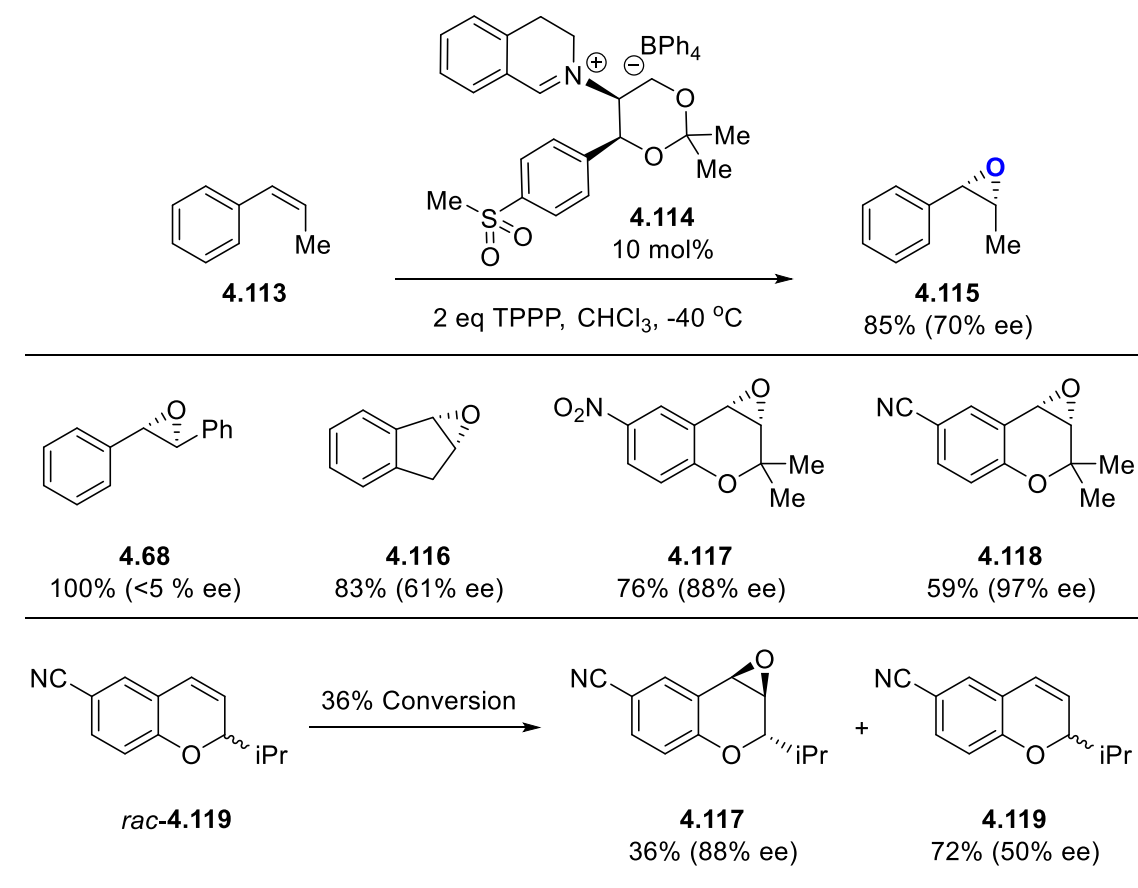
Although the discovery of iminium salts of type **4.100** provided insight into structural features and reaction conditions important for enantiocontrol, they provided enantioenriched products in only a limited number of examples. Additional substitution patterns, including carbohydrates, did not improve upon these initial results.<sup>21</sup>

#### 4.6.4 Acetonide substituted dihydroisoquinoliniums

*N*-alkyl dihydroisoquinolinium salts bearing chiral acetonides provided the first examples of catalytic epoxidations proceeding with high enantiocontrol. These salts have been shown to operate under both aqueous and nonaqueous

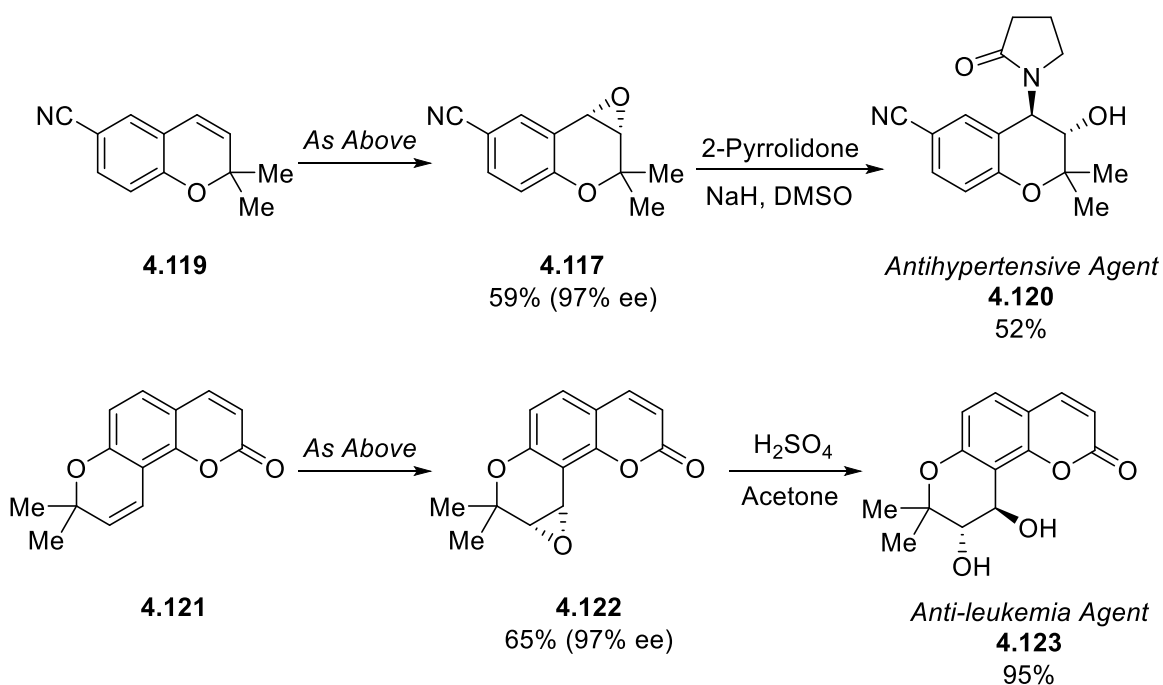
conditions, allowing a range of oxidants, solvents, and temperatures to be utilized.<sup>22,23</sup> Low temperature, organic phase epoxidation ( $\text{CHCl}_3$ ,  $-40^\circ\text{C}$ ) ultimately proved to be most successful, furnishing cis-alkene-derived epoxides **4.115**-**4.118** with excellent (60-97% ee) enantiomeric purity (**Figure 4.10**) when using catalyst **4.114**. When racemic alkenes of type **4.119** were subjected to the reaction conditions, kinetic resolution was possible.<sup>24</sup>

**Figure 4.10:** High enantioselectivity in dihydroisoquinolinium catalyzed epoxidation



The enantiocontrol demonstrated by this catalyst led to some of the earliest reports of iminium salt catalyzed epoxidation in total synthesis (**Scheme 4.11**).<sup>22,25</sup> In both cases, the absolute stereochemistry of the desired products is set using catalyst **4.114**.

**Scheme 4.11:** Dihydroisoquinolinium catalysis in total synthesis



#### 4.6.5 Binaphthyl or biphenyl azepinium catalysts: structure and reactivity

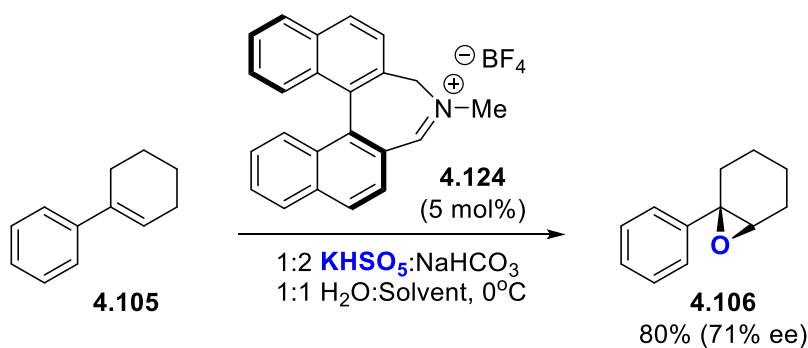
Inspired by the use and success of binaphthalene ligands in asymmetric transition metal catalyzed reactions, Aggarwal introduced the first binaphthyl-substituted iminium epoxidation catalyst **4.124** in 1996.<sup>26</sup> These initial results established a new scaffold for future catalyst development, but failed to improve upon yields, scope, and enantioselectivity obtained with dihydroisoquinolinium

catalysts (**Scheme 4.12a**). Replacement of the *N*-methyl group with substituents containing additional chiral elements by Page and coworkers gave substantial improvement to enantioselectivity, yet still limited to the small subset of olefins previously examined.<sup>27</sup>

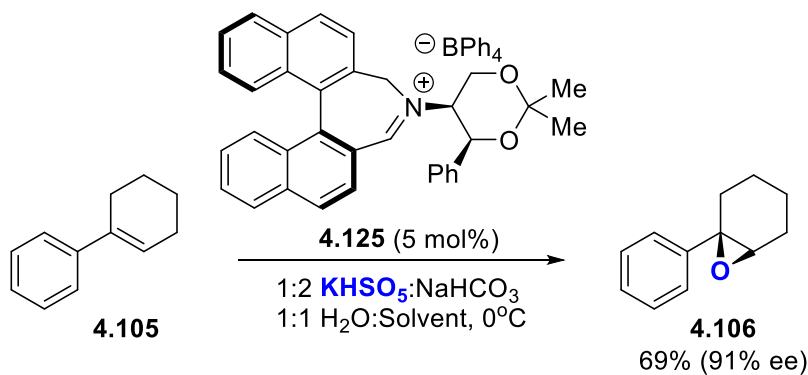
---

**Scheme 4.12:** Binaphthalene azepinium catalyst

**a) Aggarwall azepiniums**



**b) Page azepiniums**



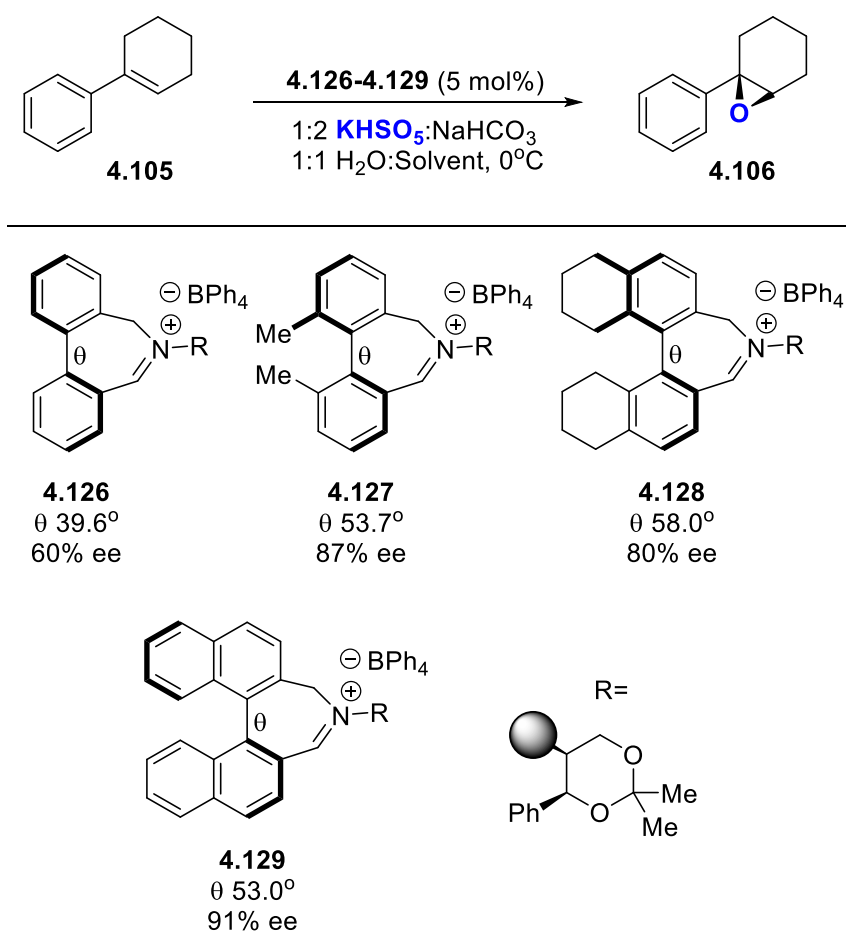

---

A significant correlation between dihedral angle along the axis of chirality and enantioselectivity of epoxidation was observed by Lacour and coworkers.<sup>28</sup>

This methodology was adopted by Page, together providing correlations of

dihedral angles and stereoselectivity for an expansive library of biaryl catalysts (**Figure 4.11**).<sup>29</sup> Across these two data sets, a weak correlation between dihedral angle and enantioselectivity was observed. Enantioselectivity was also determined by a complex interplay of dihedral angle, catalyst substitution, and transition state geometry.

**Figure 4.11:** General trend for dihedral angle impact on enantioselectivity



#### 4.6.6 Impact of oxidant on enantioselectivity

In addition to solvent and counterion effects previously explored, Page and coworkers discovered that choice of oxidant used in iminium catalyzed epoxidations can affect enantioselectivity, presumably through alteration of diastereoselectivity during oxaziridinium formation (**Table 4.13**).<sup>30,31</sup>

**Table 4.13:** Impact of oxidant on enantioselectivity

**4.105**      **4.126** (10 mol%)      **4.106**

Oxidant  
MeCN, 0°C

Entry	Oxidant System	Active Oxidant	ee (%)
1	KHSO <sub>5</sub> , NaHCO <sub>3</sub>	HSO <sub>5</sub> <sup>-</sup>	60
2	NaOCl, K <sub>2</sub> CO <sub>3</sub>	ClO <sup>-</sup>	56
3	H <sub>2</sub> O <sub>2</sub> , LiOH	HOO <sup>-</sup>	28
4	H <sub>2</sub> O <sub>2</sub> , Na <sub>2</sub> CO <sub>3</sub>	CO <sub>4</sub> <sup>2-</sup>	36

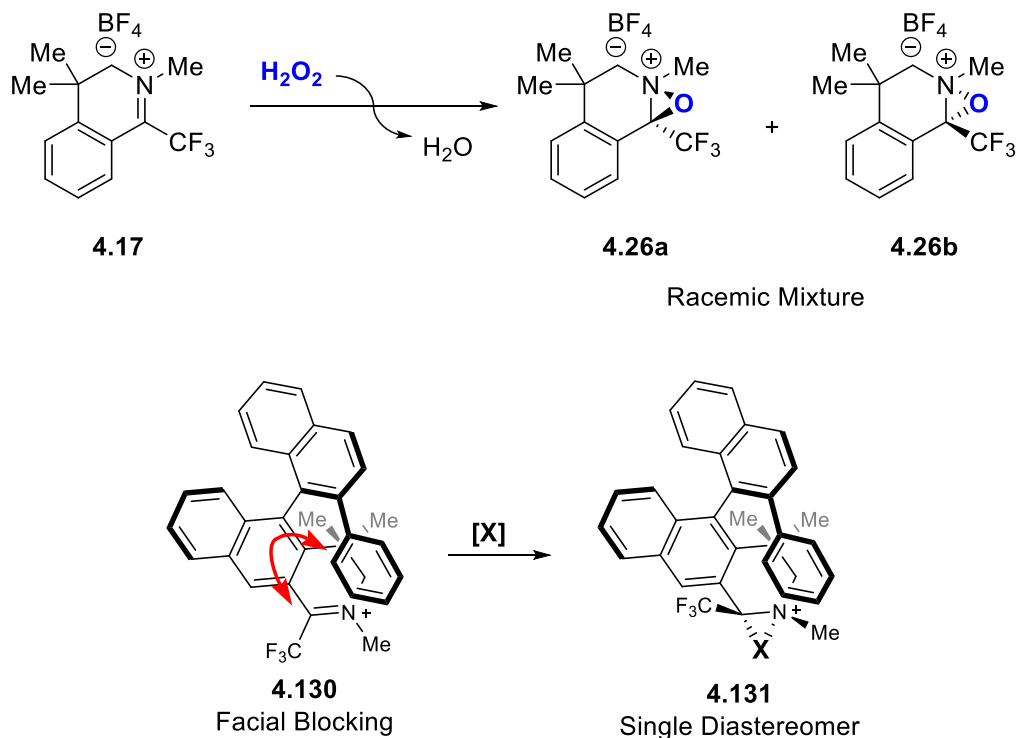
The combined effects of catalyst structure, counterion coordination ability, solvation effects, and oxidant choice on enantioselectivity highlight the challenges associated with iminium salt catalysis.

#### 4.6.7 Design of a chiral atom transfer catalyst

Based on the sensitivity to substitution revealed in our initial iminium salt screening, we chose the aromatic ring for the basis of structural elaboration.

Binaphthelene based catalysts were chosen as they are neither strongly electron donating or withdrawing (**Scheme 4.13**).

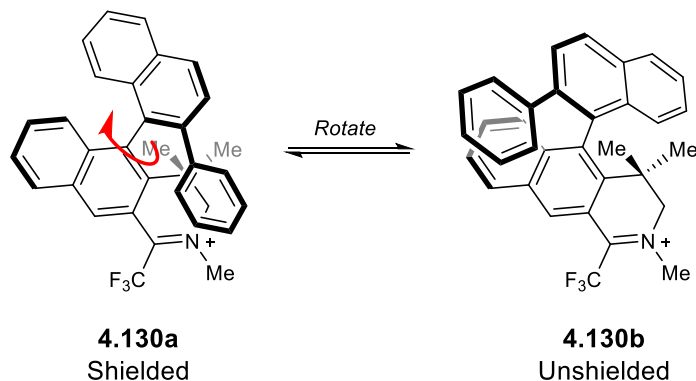
**Scheme 4.13:** Proposed catalyst structures for asymmetric transformations



For this approach to be a successful strategy, the blocking group must adequately shield one face of the iminium from nucleophilic attack (**Figure 4.12**). Additionally, the dihedral angle between the naphthalene rings must be such that the blocking group extends over the iminium bond in its energetically favorable conformations. If the naphthalene rings are perpendicular to each other, the blocking group would likely offer poor facial discrimination.

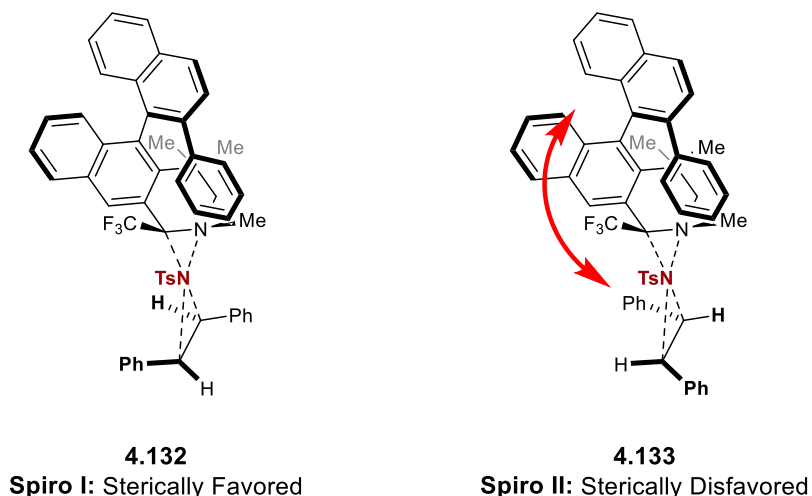


**Figure 4.12:** Effect of dihedral angle on blocking ability



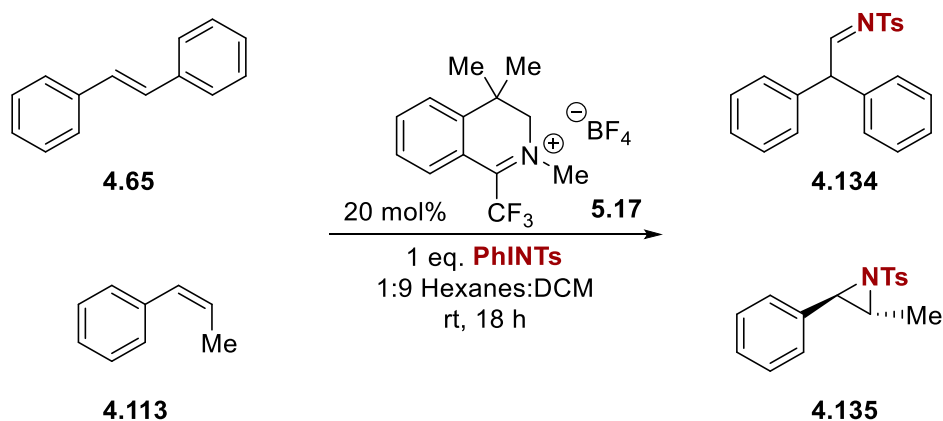
#### 4.6.8 Transition states and mechanistic concerns

Based on initial analysis of possible transition states, these binaphthalene iminium salt catalysts would perform best in the epoxidation or aziridination of *trans*-1,2-disubstituted alkenes (**Figure 4.13**). The facial selectivity preference is most easily shown in the case of symmetrically substituted alkenes. In the disfavored transition state, substitution on the alkene is forced into the binaphthalene ring system. The energy difference in transition states between prochiral faces should rely on the size of alkene substituents.

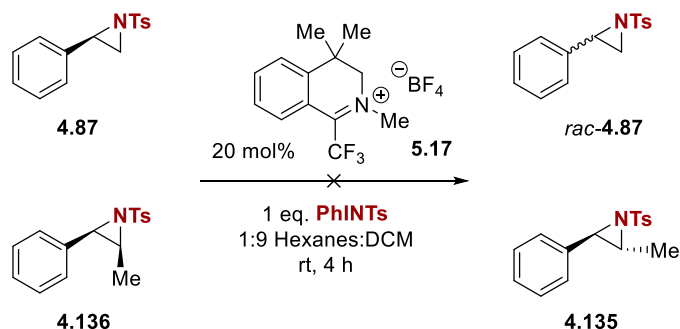
**Figure 4.13:** Transition states for asymmetric aziridination

Several assumptions must be made for this predictive model to be valid. First, it assumes a diaziridinium intermediate that aziridates through a concentrated, spiro transition state. Evidence of a diaziridinium salt existing in the reaction mixture was provided in the report detailing the discovery of iminium salt catalyzed aminations.<sup>32</sup> Calculations by Houk and coworkers suggest that diaziridinium mediated aziridinations proceed through a distorted, but concerted, spiro transition state, analogous to those calculated for oxaziridines and oxaziridiniums.<sup>33</sup>

Despite these calculations, both *cis*- $\beta$ -methylstyrene and *trans*-stilbene provide aminated products that would arise from carbocationic intermediates (**Scheme 4.14**), suggesting that aziridinations proceed through a stepwise, cationic mechanism. It is currently unclear how this may impact transition states and enantioselectivity.

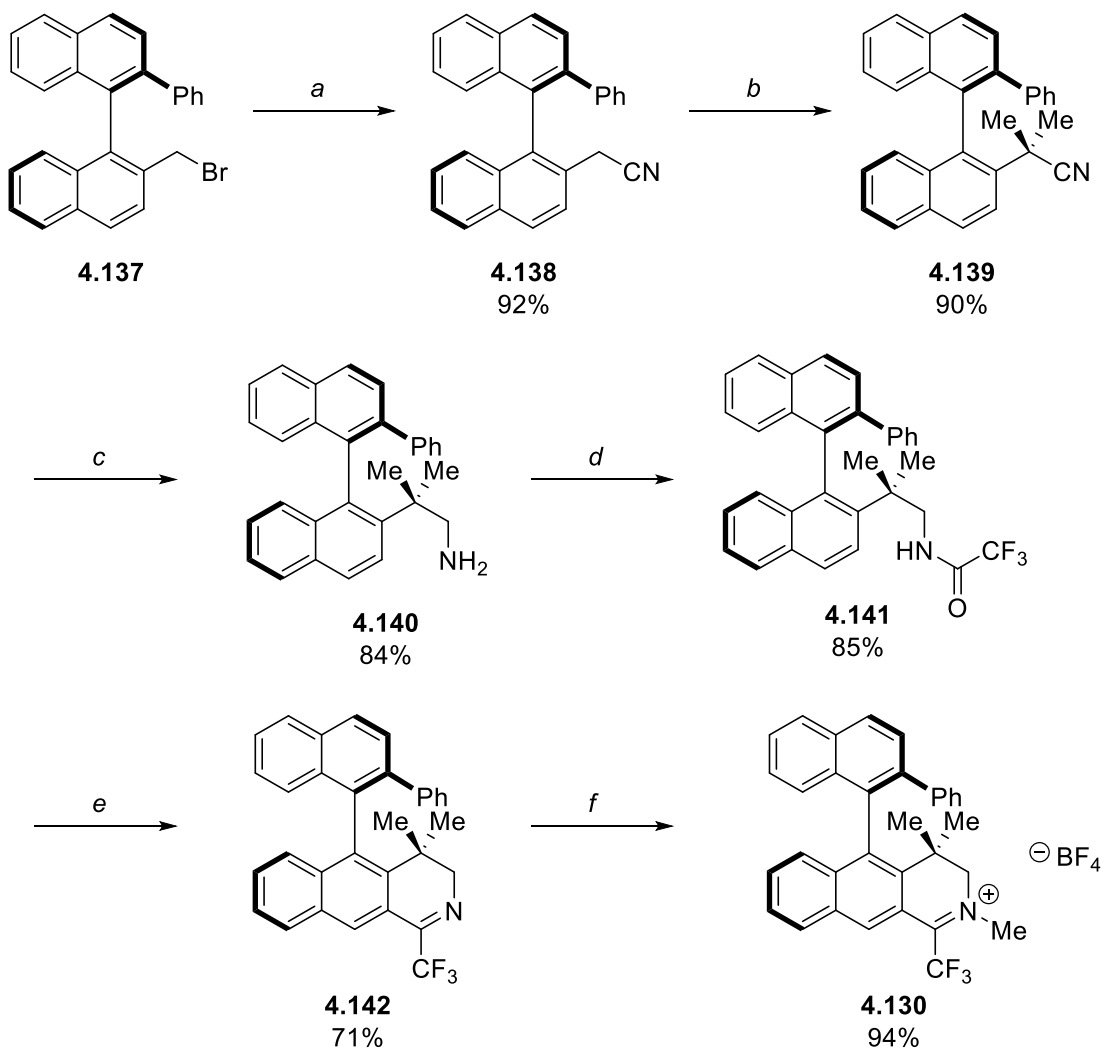
**Scheme 4.14:** Carbocation rearrangement products from aziridinations

For the aziridinations to proceed with enantiocontrol, there must also must only limited racemization of products over the course of the reaction. Two experiments were conducted to probe this possibility (**Scheme 4.15**). In one, enantioenriched (>95% ee) styrene aziridine was exposed to the reaction conditions for several hours, after which no erosion of enantiopurity was observed. Additionally, *cis*-2-methyl-3-phenyl-1-tosylaziridine was exposed to the reaction mixture. No formation of *trans*-aziridine **4.135** was observed over the course of the reaction. These results suggest significant racemization does not occur under our reaction conditions.

**Scheme 4.15:** Testing for racemization under reaction conditions

#### 4.6.9 Synthetic route to catalysts

Synthesis of chiral iminium salt catalysts began with the generation of chiral benzylic nitriles with preinstalled blocking groups (**Scheme 4.16**). These benzylic nitriles were obtained in five steps from (R)-BINOL using reported procedures.<sup>17</sup> S<sub>N</sub>2 methylation with methyl iodide and LAH reduction provided chiral dimethylphenethylamines, which were converted to dihydroisoquinolines using triflic anhydride mediated Bischler-Napieralski cyclizations. Methylation with trimethyloxonium tetrafluoroborate provided iminium salt catalysts in ten steps (ca. 8% overall yield) from (R)-BINOL.

**Scheme 4.16:** Synthesis of chiral catalysts

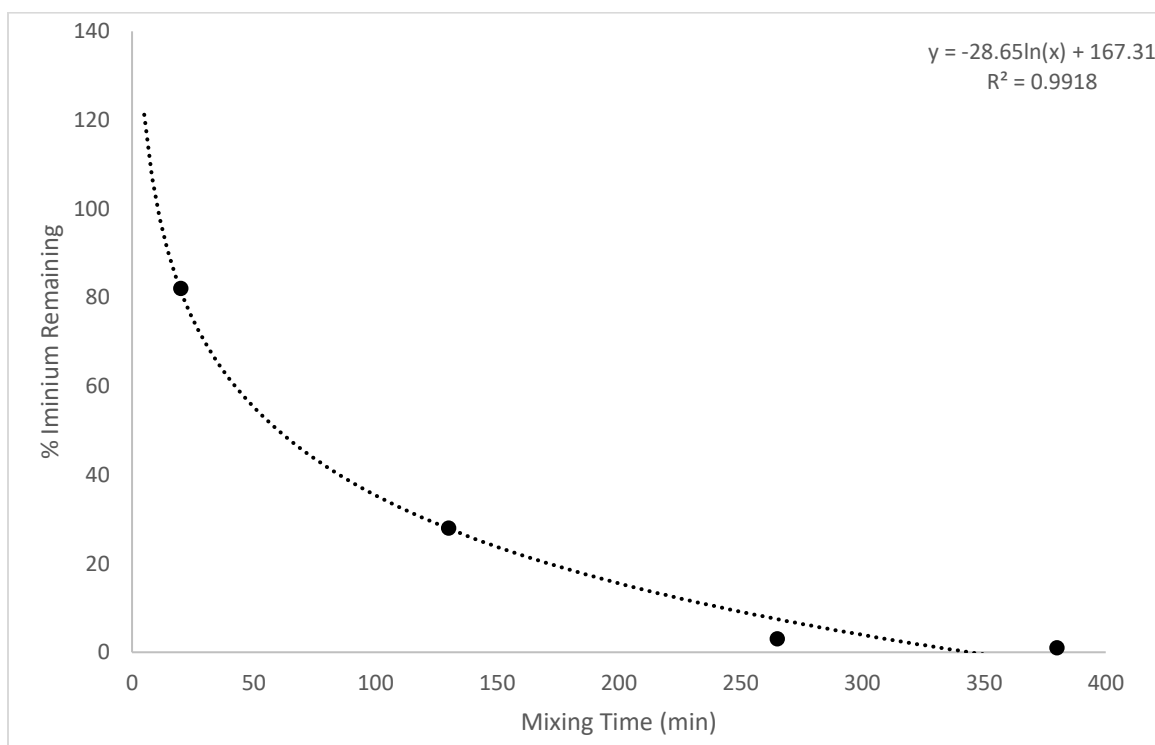
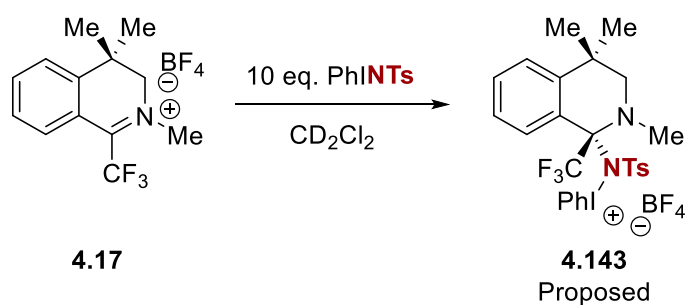
a) 3 eq KCN, EtOH b) 2.6 eq NaH, 3 eq MeI, THF c) LAH, THF d) 2 eq pyridine, 1.2 eq TFAA e) 1.2 eq 2-chloropyridine, 1.1 eq triflic anhydride, 1,2-DCE f) Me<sub>3</sub>OBF<sub>4</sub>, DCM

**4.6.10 NMR experiments to probe diastereoselective diaziridinium formation**

The interaction of PhINTs with the iminium salt catalyst can be monitored by <sup>19</sup>F-NMR. While it is uncertain what species is being formed in this reaction, demethylated iminium and diaziridine have been ruled out by comparison with

authentic samples. It is unlikely that the species present is diaziridinium, due to the difficulty in isolating or characterizing this species. As such, we have tentatively identified the species which forms as an PhINTs-iminium adduct. This reaction appears to be irreversible and can be monitored by  $^{19}\text{F}$  integration (**Figure 4.14**).

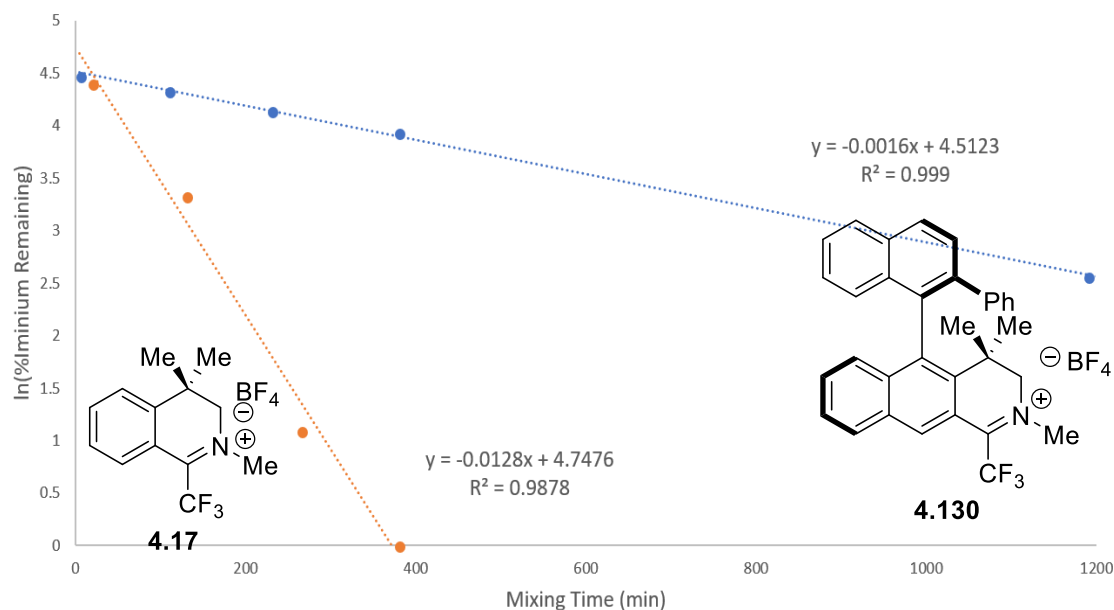
**Figure 4.14:** Reaction of iminium salts and PhINTs



A single diastereomer of the PhINTs-iminium adduct forms when the chiral iminium salt is subjected to the NMR experiment, suggesting that a phenyl group is sufficient for blocking one face of the iminium. Alternatively, rapid equilibrium may be taking place leading to a coalescence between the two diastereomers.

The rate of PhINTs incorporation is an order of magnitude slower with the chiral iminium than that of the achiral iminium (**Figure 4.15**). Use of the Eyring equation predicts a 1.3 kcal/mol energy difference in activation energy of adduct formation between the two catalysts.

**Figure 4.15:** PhINTs incorporation in **4.17** and **4.130**

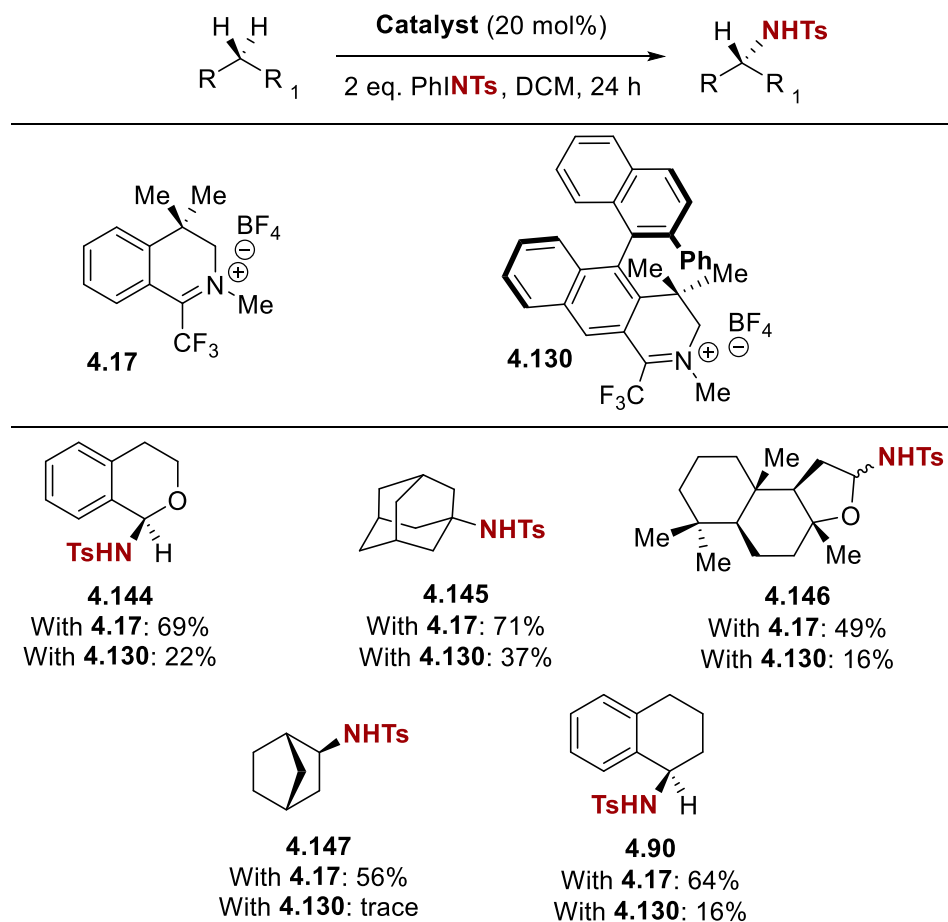


#### 4.6.11 Initial reactivity in C–H functionalization

Chiral iminium salt **4.130** failed to react under our hydroxylation conditions. Fortunately, it was able to catalyze C–H amination of ethereal, tertiary, and

secondary C–H bonds (**Table 4.14**). In the case of isochroman, a racemic product was obtained.

**Table 4.14:** C–H bond amination



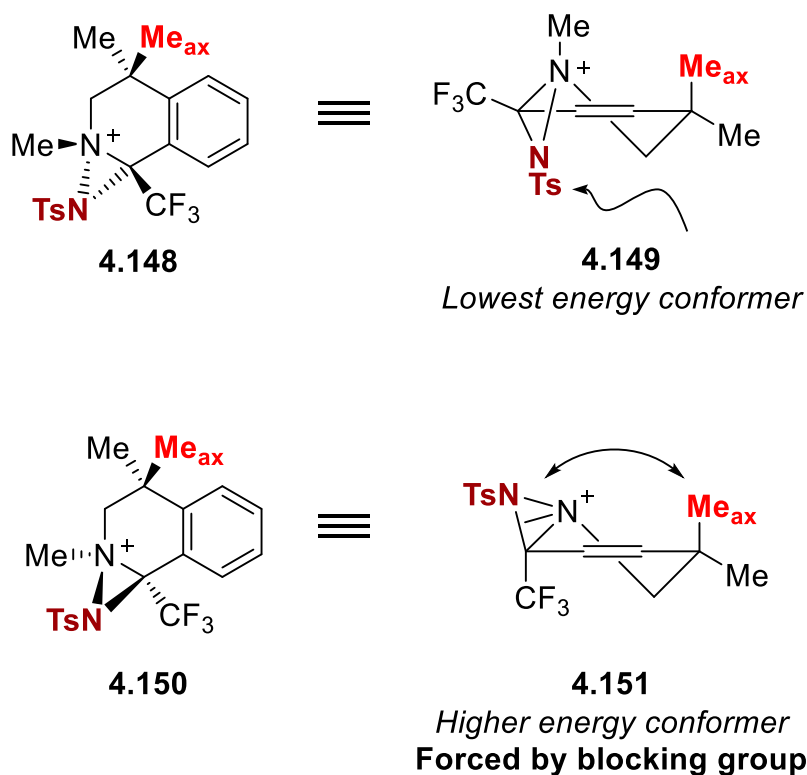
Reactions performed on 0.5 mmol scale. Isolated yields reported.

The lower reactivity in amination reactions could be explained by the diaziridinium conformation forced by the blocking group. In the achiral iminium, diaziridinium formation can take place such that it is opposite the axial methyl group of the *gem*-dimethyl substituent (**Figure 4.16**). However, when there is a



blocking group shielding one face of the iminium, both the axial methyl group and diaziridinium should reside on the same plane of the ring, likely increasing the steric penalty for diaziridinium formation. This hypothesis is supported by rates of PhINTs/iminium adduct formation: the 1.3 kcal/mol  $\Delta\Delta G^\ddagger$  difference in activation energy could be due to this unfavorable interaction. As such, catalysts lacking the *gem*-dimethyl group may show improved reactivity.

**Figure 4.16:** Steric interactions of facially blocked diaziridiniums

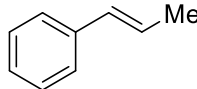
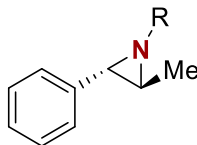
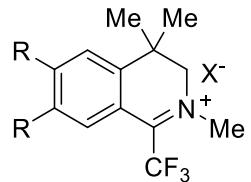


#### 4.6.12 Low temperature aziridinations

Aziridination of styrene using the chiral iminium salt led to racemic products, as predicted by the transition state model. Unfortunately, aziridination of *trans*-

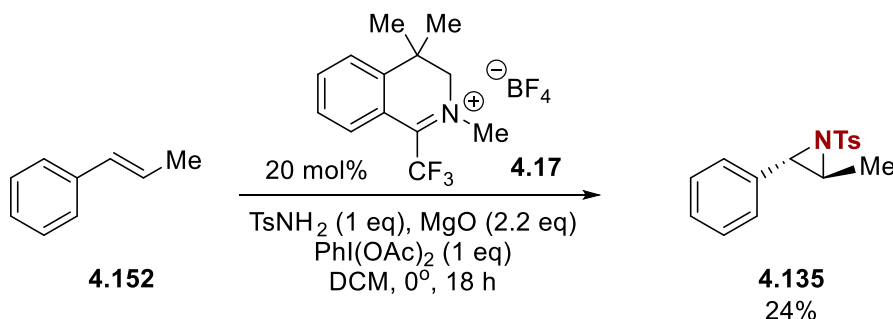
stilbene led to carbocation rearrangement products instead of the desired aziridine. As enantiocontrol and product distribution can be enhanced or altered at lower temperatures, a screening of conditions for low temperature aziridinations was conducted. All combinations of catalysts, iodinanes, solvents, and temperatures screened in led to no greater than trace quantities of aziridine (**Table 4.15**).

**Table 4.15:** Unsuccessful low temperature aziridinations

 <p><b>4.152</b></p>	<p>Catalyst (Loading)</p> <p>Iodinane (Equiv)</p> <p>Solvent [Conc]</p> <p>Temp, 24 h</p>			 <p><b>4.135</b></p>
 <p>R = Cl, Br, OMe, CF<sub>3</sub></p> <p>X = BF<sub>4</sub>, BArF<sub>4</sub></p> <p>(10-30 mol%)</p>	<p>PhINR</p> <p>R = Ts</p> <p>R = SO<sub>2</sub>C<sub>6</sub>H<sub>5</sub>CF<sub>3</sub></p> <p>R = SO<sub>2</sub>C<sub>6</sub>H<sub>5</sub>NO<sub>2</sub></p> <p>R = SO<sub>3</sub>CH<sub>2</sub>CCl<sub>3</sub></p> <p>(1-2 eq)</p>	<p>Solvent</p> <p>DCM</p> <p>ACN</p> <p>MeNO<sub>2</sub></p> <p>(0.01-1.0 M)</p>	<p>Temp</p> <p>-40</p> <p>-20</p> <p>-10</p> <p>0</p>	

In each reaction, no noticeable solubilization of iodine occurred. As such, we adopted an in situ iodine formation developed by Du Bois to address this insolubility.<sup>34</sup> Use of diacetoxyiodobenzene and tosylamide at 0 °C provided yields of the aziridine on par with those obtained using the optimized room temperature aziridination protocol (**Scheme 4.17**).

---

**Scheme 4.17:** Partially optimized low temperature aziridination



---

**4.7 Conclusions**

We have developed an iminium salt catalyst capable of C–H bond hydroxylation and amination, as well as epoxidation and aziridination. These reactions are capable of selective reactivity with methylene carbons, allowing the installment of chiral centers on prochiral molecules. Additional investigation needs to be conducted to identify catalysts or strategies that will allow asymmetric functionalization of C–H bonds.

**4.8 Experimental Details**
*4.8.1 General Methods*

All commercially obtained reagents were obtained in the highest grade and used as received. Dichloromethane was purified by degassing with argon and drying through alumina columns. Flash column chromatography was conducted with 230–400 mesh silica gel purchased from Fisher Scientific.  $^1\text{H}$ ,  $^{13}\text{C}$ , and  $^{19}\text{F}$  NMR spectra were acquired at 300 K on Bruker or Varian spectrometers at 600 Mhz. Chemical shifts are reported in parts per million (ppm  $\delta$ ) referenced to the residual  $^1\text{H}$  peak

of the solvent. The following abbreviations are used to indicate signal multiplicity: s - singlet, d - doublet, t - triplet, q - quartet, m - multiplet and br - broad. Gas chromatography was performed using an Agilent 7820A GC with FID detector, using *n*-dodecane as an internal standard for GC yield calculations. Normal phase chiral HPLC was performed using an Agilent 1260 HPLC equipped with a diode-array detector. IR spectra were recorded on a Thermo Scientific Nicolet iS5 with iD5 ATR attachment. High resolution mass spectrometry was performed by the University of Illinois at Urbana-Champaign Mass Spectrometry Lab using Waters Q-TOF ESI or Waters oa-TOF EI spectrometers.

#### *4.8.2 General procedure for iminium catalyzed hydroxylations*

H<sub>2</sub>O<sub>2</sub> (360  $\mu$ L, 50%, 6.4 mmol) was added to substrate (0.4 mmol), iminium salt catalyst (26.4 mg, 0.08 mmol), and HFIP (400  $\mu$ L) and stirred at room temperature for 18 h. The mixture was quenched with 2M aqueous Na<sub>2</sub>S<sub>2</sub>O<sub>3</sub> (3 mL) and extracted with EtOAc (4 x 3 mL). The combined organic extracts were dried over MgSO<sub>4</sub>, filtered, concentrated under vacuum, and purified by flash chromatography.

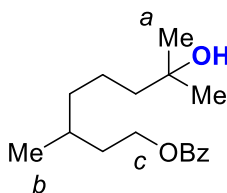
#### *4.8.3 General procedure for iminium catalyzed aminations*

PhINTs (373 mg, 1 mmol) was added to substrate (0.5 mmol) and iminium salt catalyst (33 mg, 0.1 mmol) in DCM (1 mL) in an N<sub>2</sub> glovebox. After 24 h, the crude reaction was loaded directly onto a silica column for purification.

#### *4.8.4 General procedure for iminium catalyzed aziridinations*

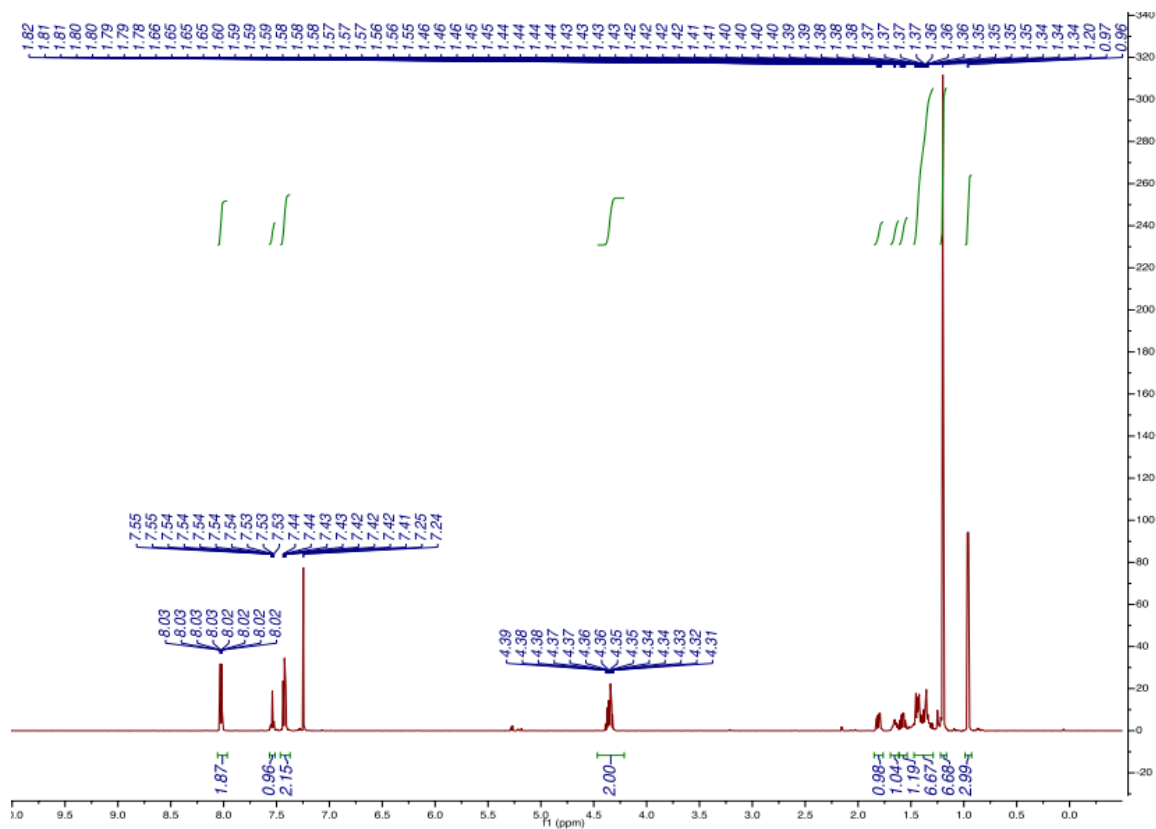
PhINTs (37 mg, 0.1 mmol) was added to substrate (0.1 mmol) and iminium salt catalyst (6.7 mg, 0.02 mmol) in 9:1 DCM:hexanes (0.5 mL) in an N<sub>2</sub> glovebox. After 12 h, the crude reaction was loaded directly onto a silica column for purification.

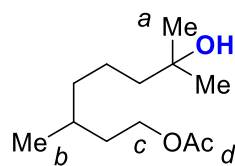
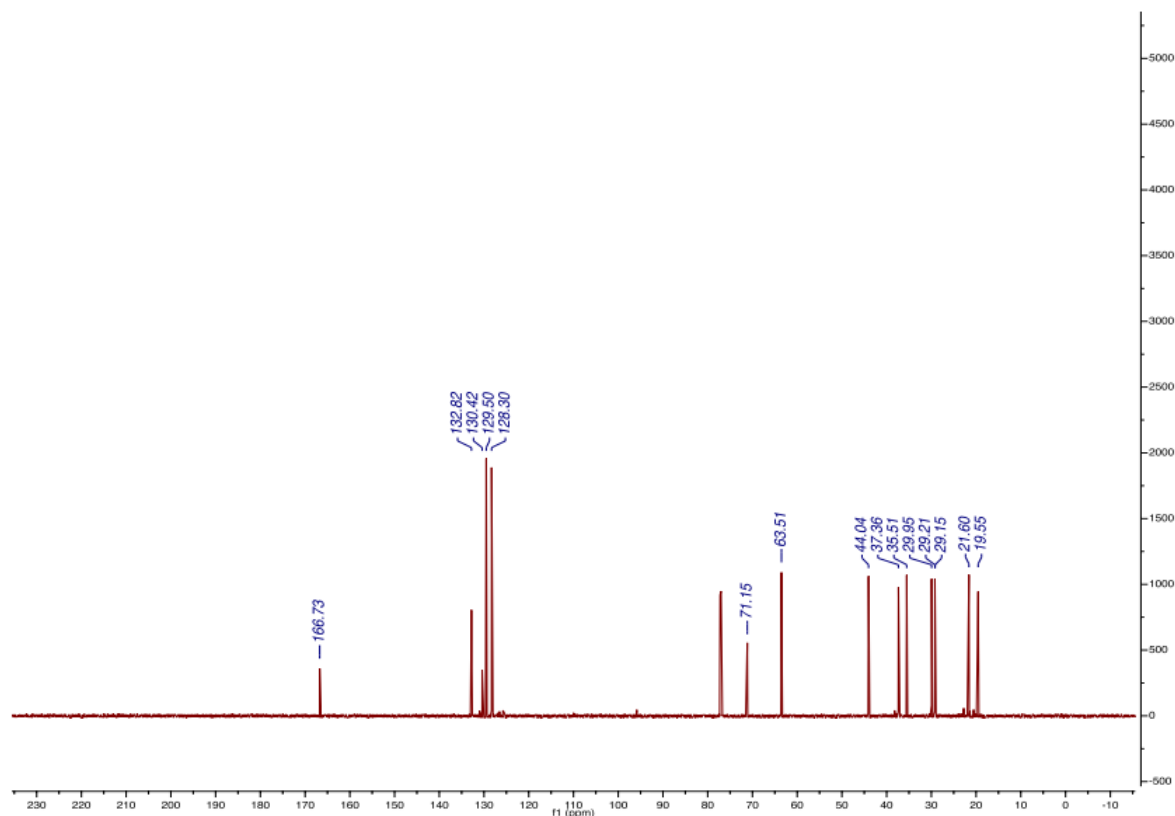
#### 4.8.5 Characterization of reaction products



#### **7-hydroxy-3,7-dimethyloctyl benzoate (4.12)** 3,7-dimethyloctyl benzoate

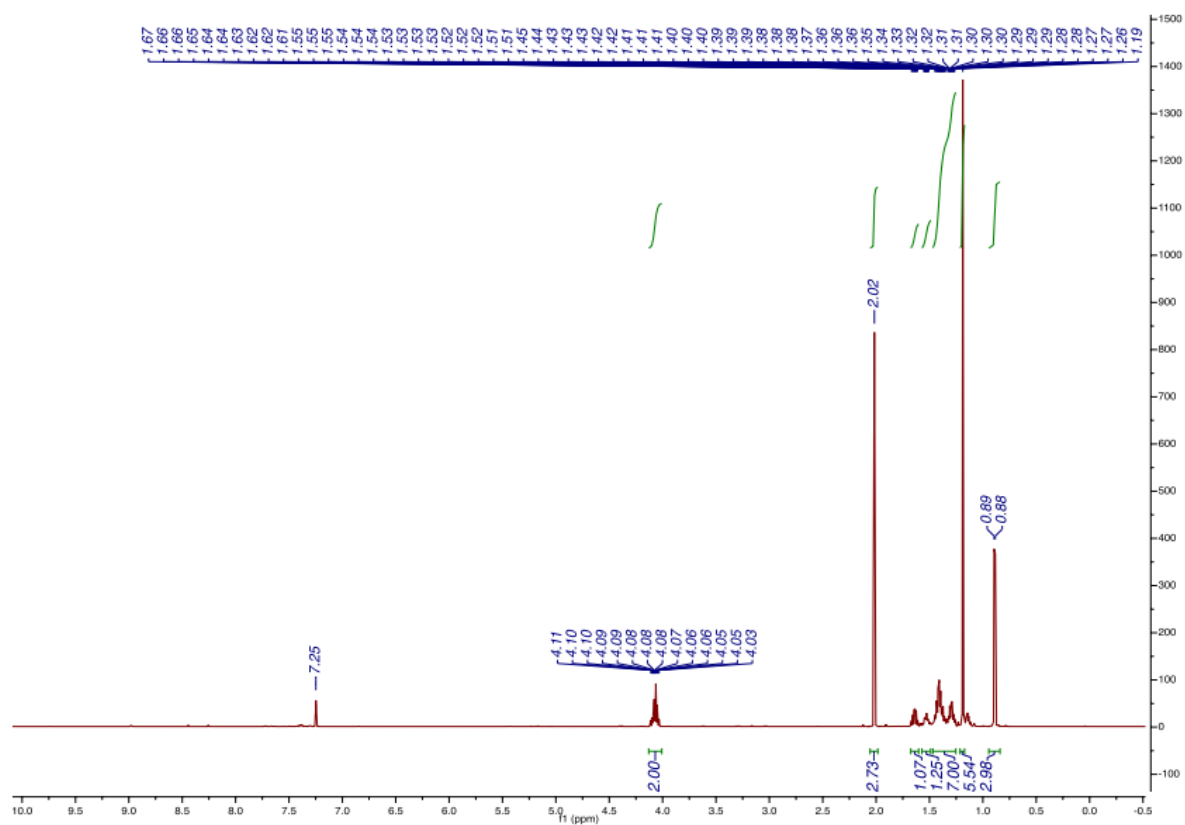
(104.8 mg, 0.4 mmol) was hydroxylated according to the general procedure and purified by chromatography (silica gel, hexanes/EtOAc 25/1 to 5/1) to give product (62.2 mg, 0.22 mmol, 56%) and recovered starting material (34.7 mg, 0.13 mmol, 33%). <sup>1</sup>H NMR (600 MHz, CDCl<sub>3</sub>): δ 8.03 (H<sub>Ar</sub>, dd, J = 8.3, 1.3 Hz, 2H), 7.54 (H<sub>Ar</sub>, tt, J = 7.5, 1.3 Hz, 1H), 7.42 (H<sub>Ar</sub>, t, J = 7.8 Hz, 2H), 4.39 - 4.31 (H<sub>c</sub>, m, 2H), 1.81 (m, 1H), 1.69 - 1.62 (m, 1H), 1.57 (m, 1H), 1.46 - 1.29 (m, 6H), 1.20 (H<sub>a</sub>, s, 6H), 0.96 (H<sub>b</sub>, d, J = 6.6 Hz, 3H) ppm; <sup>13</sup>C NMR (150 MHz CDCl<sub>3</sub>): δ 166.7, 132.8, 130.4, 129.5, 128.3, 71.2, 63.5, 44.0, 37.4, 35.5, 30.0, 29.2, 29.2, 21.6, 19.6 ppm. NMR spectra are consistent with literature reports.<sup>3</sup>



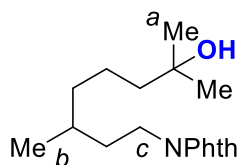
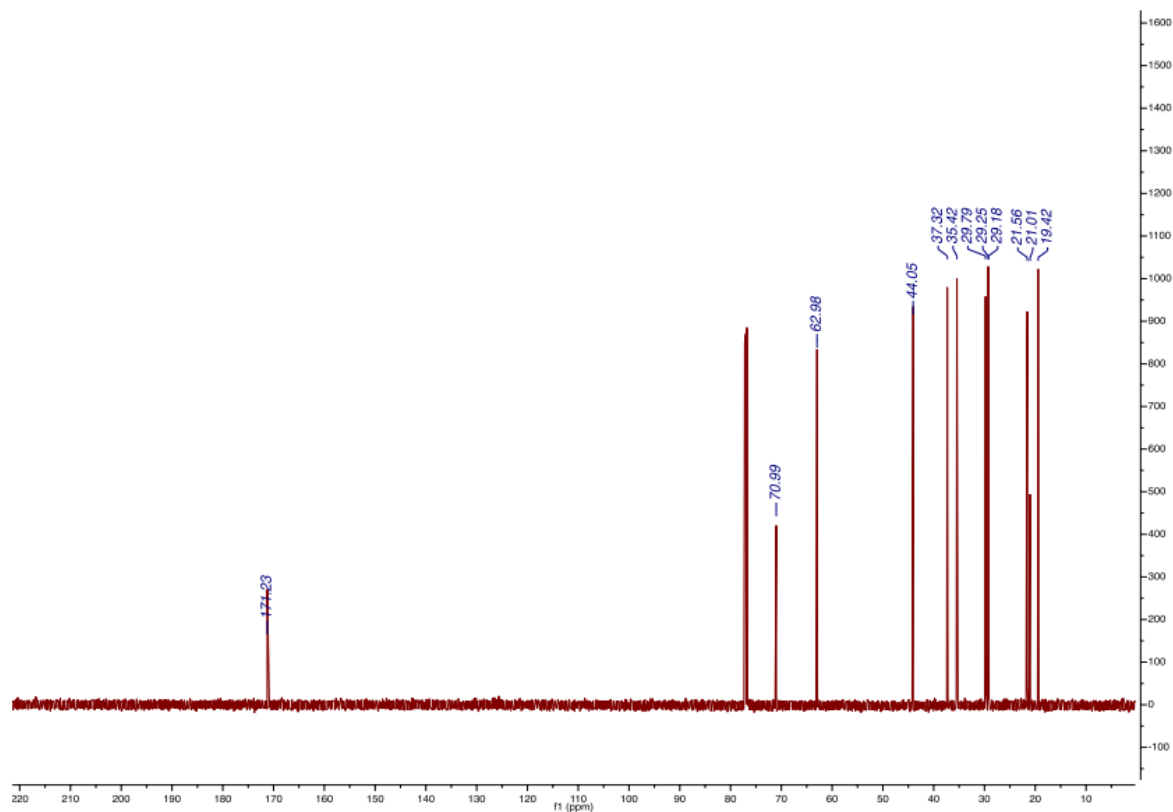


**7-hydroxy-3,7-dimethyloctyl acetate (4.30)** 3,7-dimethyloctyl acetate (68.9 mg, 0.4 mmol) was hydroxylated according to the general procedure and purified by chromatography (silica gel, hexanes/EtOAc 25/1 to 4/1) to give product (34.5 mg, 0.18 mmol, 46%) and recovered starting material (22.3 mg, 0.13 mmol, 32%).  $^1\text{H}$  NMR (600 MHz,  $\text{CDCl}_3$ ):  $\delta$  4.89 ( $\text{H}_c$ , m, 1H), 2.00 ( $\text{H}_d$ , s, 3H), 1.61 - 1.55 (m, 1H), 1.48 - 1.30 (m, 5H), 1.19 ( $\text{H}_b$ , d,  $J = 6.3$  Hz, 3H), 1.18 ( $\text{H}_a$ , s, 6H) ppm;  $^{13}\text{C}$  NMR

(150 MHz CDCl<sub>3</sub>):  $\delta$  170.8, 70.82, 70.80, 43.5, 36.3, 29.2, 29.1, 21.4, 20.1, 20.0 ppm. NMR spectra are consistent with literature reports.<sup>6</sup>



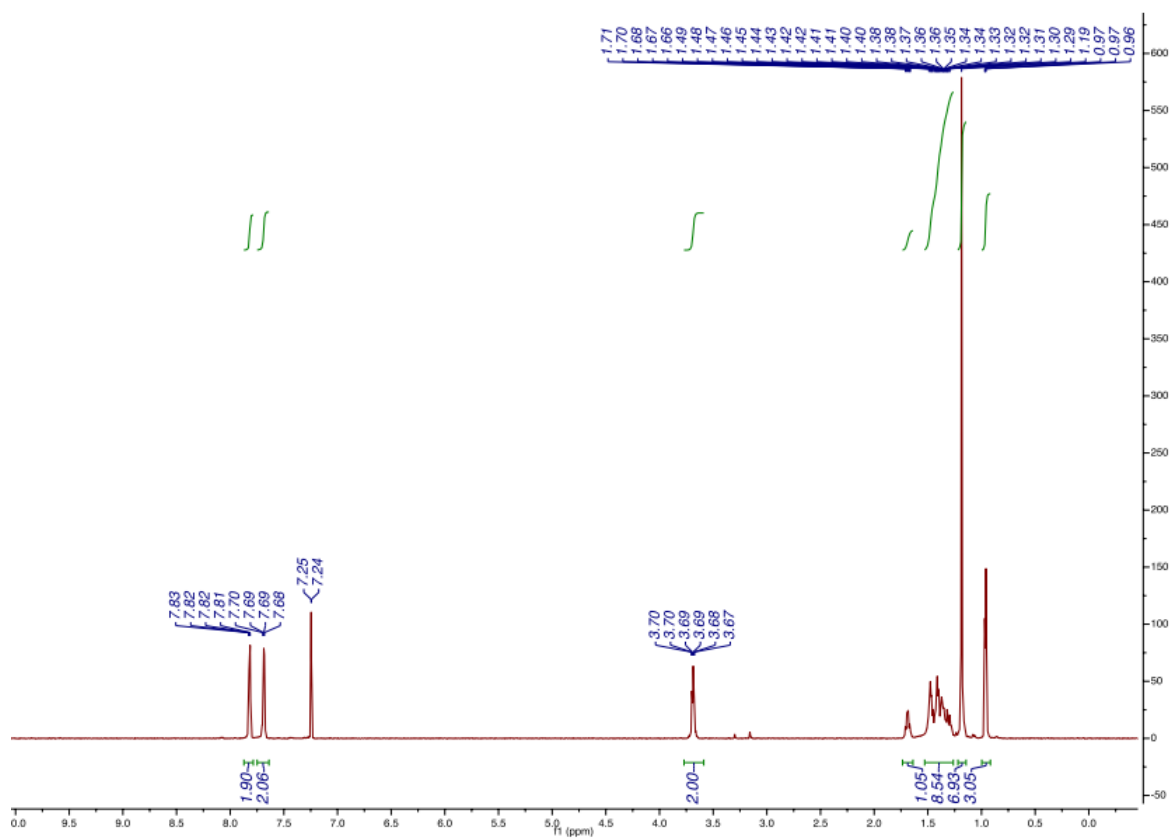


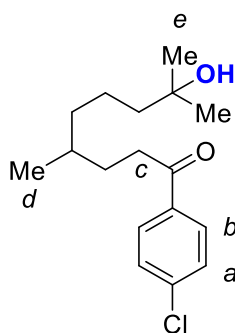
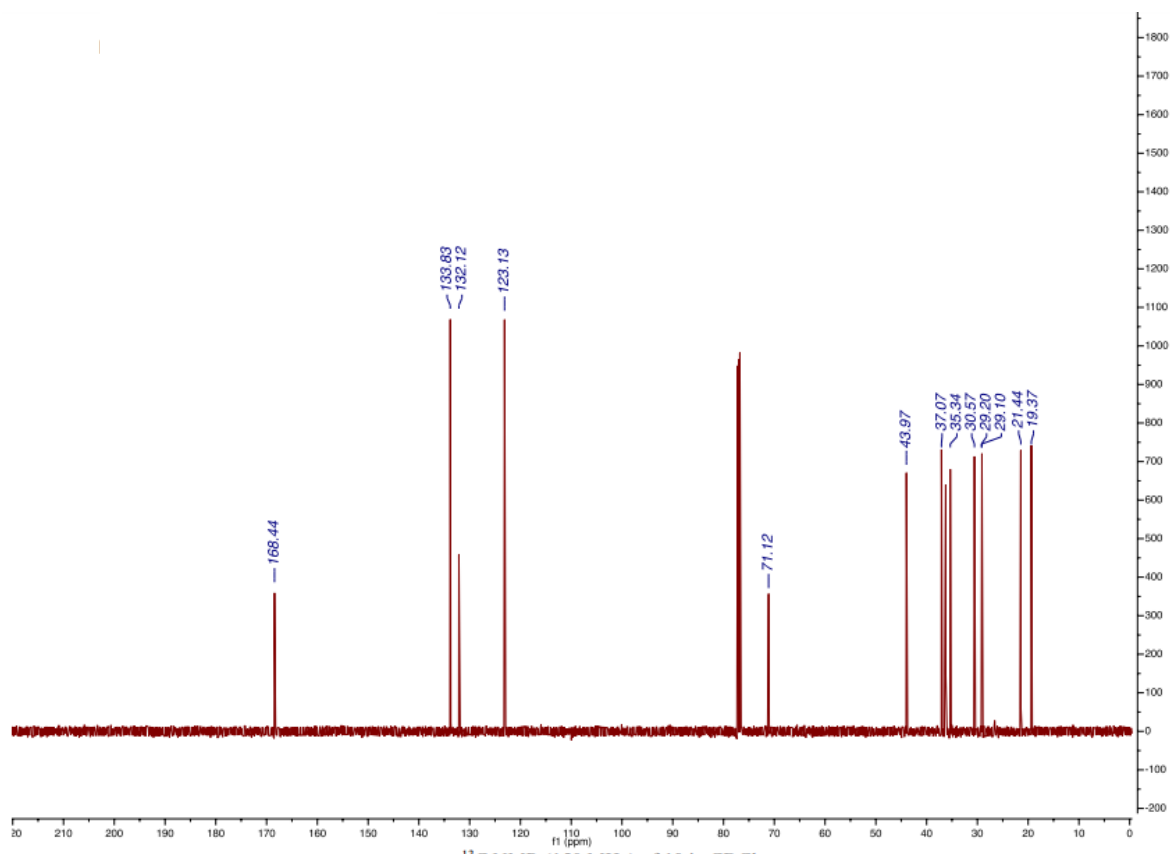


**2-(7-hydroxy-3,7-dimethyloctyl)isoindoline-1,3-dione (4.31)** 2-(3,7-

dimethyloctyl) isoindoline-1,3- dione (115.0 mg, 0.4 mmol) was hydroxylated according to the general procedure and purified by chromatography (silica gel, hexanes/EtOAc 4/1) to give product (65.0 mg, 0.21 mmol, 54%) and recovered starting material (34.2 mg, 0.12 mmol, 30%).  $^1\text{H}$  NMR (600 MHz,  $\text{CDCl}_3$ ):  $\delta$  7.82 ( $\text{H}_{\text{Ar}}$ , dd,  $J = 5.5, 3.0$  Hz, 2H), 7.69 ( $\text{H}_{\text{Ar}}$ , dd,  $J = 5.5, 3.0$  Hz, 2H), 3.69 ( $\text{H}_{\text{c}}$ , m, 2H), 1.69 (q,  $J = 8.0$  Hz, 1H), 1.49 - 1.29 (m, 8H), 1.19 ( $\text{H}_{\text{a}}$ , s, 6H), 0.96 ( $\text{H}_{\text{b}}$ , d,  $J = 6.5$

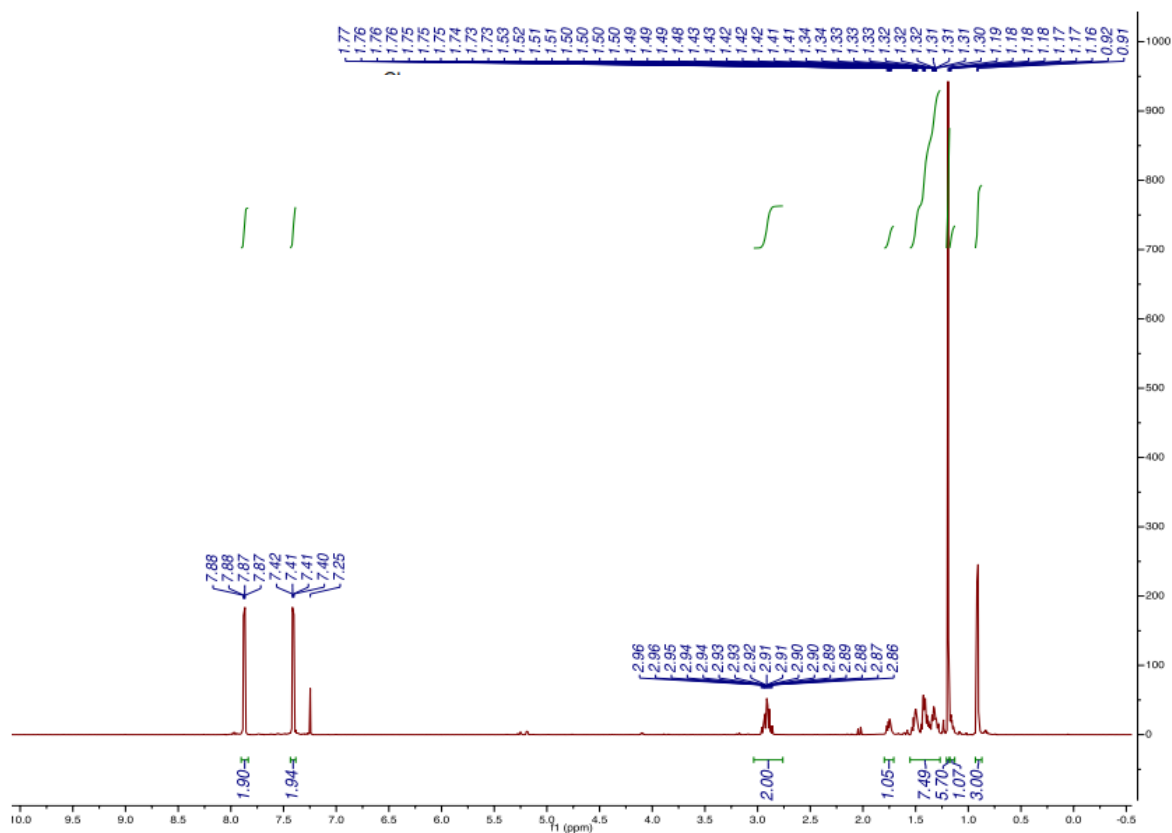
Hz, 3H) ppm;  $^{13}\text{C}$  NMR (150 MHz  $\text{CDCl}_3$ ):  $\delta$  168.4, 133.8, 132.1, 123.1, 71.1, 44.0, 37.1, 36.2, 35.3, 30.6, 29.2, 29.1, 21.4, 19.4 ppm. NMR spectra are consistent with literature reports.<sup>19</sup>

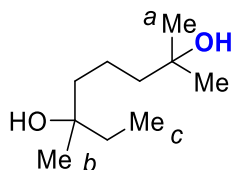
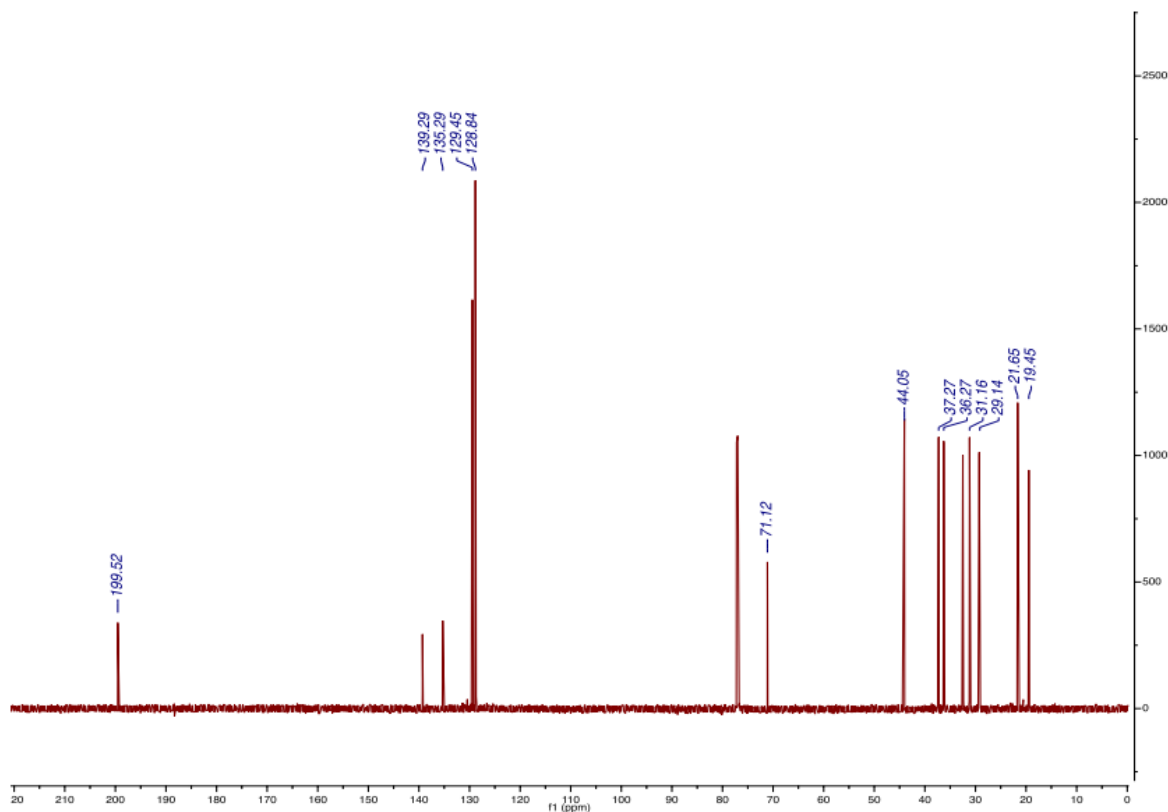




**1-(4-chlorophenyl)-8-hydroxy-4,8-dimethylnonan-1-one (4.32)** 4,8-dimethyl-1-(4-chlorophenyl)-nonanone (112.0 mg, 0.4 mmol) was hydroxylated according to the general procedure and purified by chromatography (silica gel, hexanes/EtOAc 25/1 to 5/1) to give product (50.3 mg, 0.17 mmol, 42%) and recovered starting material (55.2 mg, 0.2 mmol, 49%). <sup>1</sup>H NMR (600 MHz,

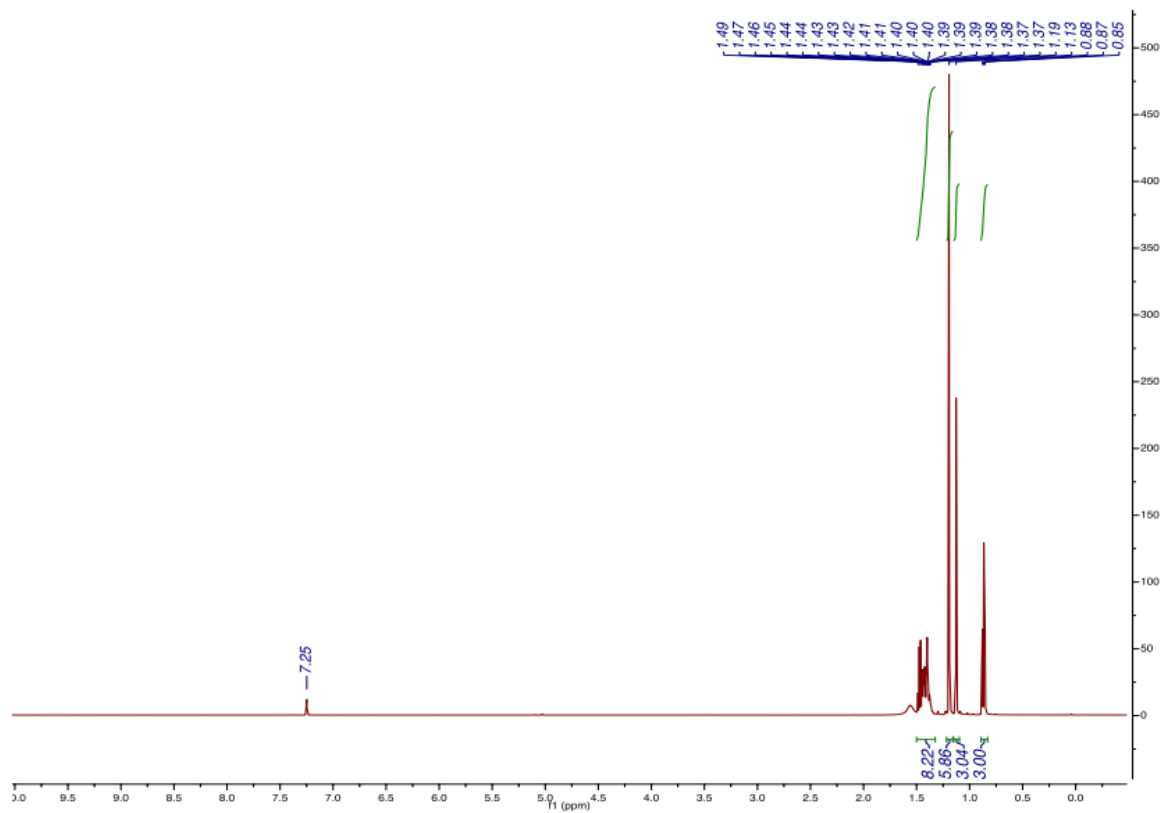
CDCl<sub>3</sub>):  $\delta$  7.87 (H<sub>b</sub>, d, J = 8.6 Hz, 2H), 7.41 (H<sub>a</sub>, d, J = 8.6 Hz, 2H), 2.97 - 2.86 (H<sub>c</sub>, m, 2H), 1.78 - 1.73 (m, 1H), 1.54 - 1.28 (m, 7H), 1.19 (H<sub>e</sub>, s, 9H), 1.17 - 1.14 (m, 1H), 0.91 (H<sub>d</sub>, d, J = 6.4 Hz, 3H) ppm; <sup>13</sup>C NMR (150 MHz CDCl<sub>3</sub>):  $\delta$  199.5, 139.3, 135.3, 129.5, 128.8, 71.1, 44.1, 37.3, 36.3, 32.5, 31.2, 29.3, 29.1, 21.7, 19.5 ppm; IR (film, cm<sup>-1</sup>): 3421 (br), 2935, 1682, 1589, 1378, 1271, 1205, 1092, 1013, 908, 835, 731; HRMS m/z (ESI<sup>+</sup>): Calculated for C<sub>17</sub>H<sub>25</sub>ClNaO<sub>2</sub> [M+Na]<sup>+</sup>: 319.1441, found 319.1429.

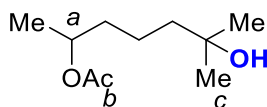
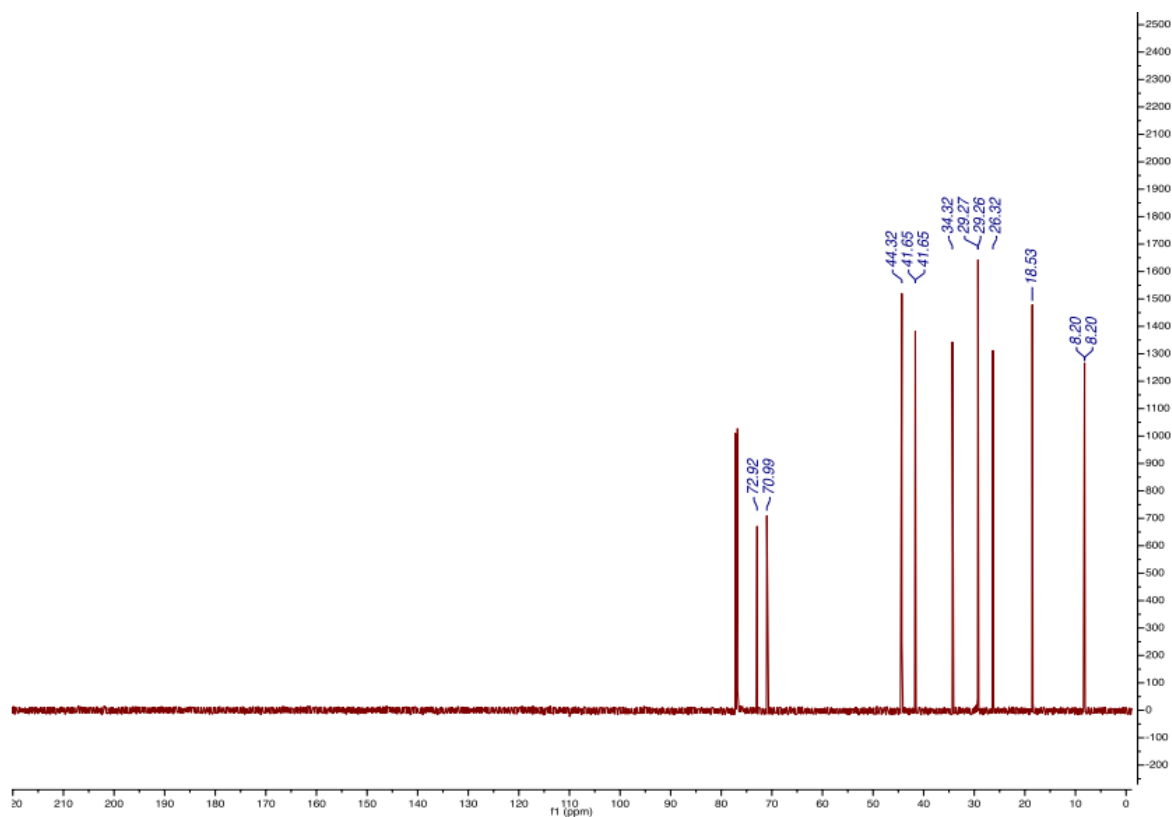




**2,6-dimethyloctane-2,6-diol (4.33)** 3,7-dimethyl-3-octanol (63.3 mg, 0.4 mmol) was hydroxylated according to the general procedure and purified by chromatography (silica gel, hexanes/EtOAc 5/1 to 1/2) to give product (40.5 mg, 0.23 mmol, 58%) and recovered starting material (20.8 mg, 0.13 mmol, 33%).  $^1\text{H}$  NMR (600 MHz,  $\text{CDCl}_3$ ):  $\delta$  1.50 - 1.37 (m, 8H), 1.19 ( $\text{H}_a$ , s, 6H), 1.13 ( $\text{H}_b$ , s, 3H), 0.87 ( $\text{H}_c$ , t,  $J = 7.5$  Hz, 3H) ppm;  $^{13}\text{C}$  NMR (151 MHz,  $\text{CDCl}_3$ ):  $\delta$  72.9, 71.0, 44.3,

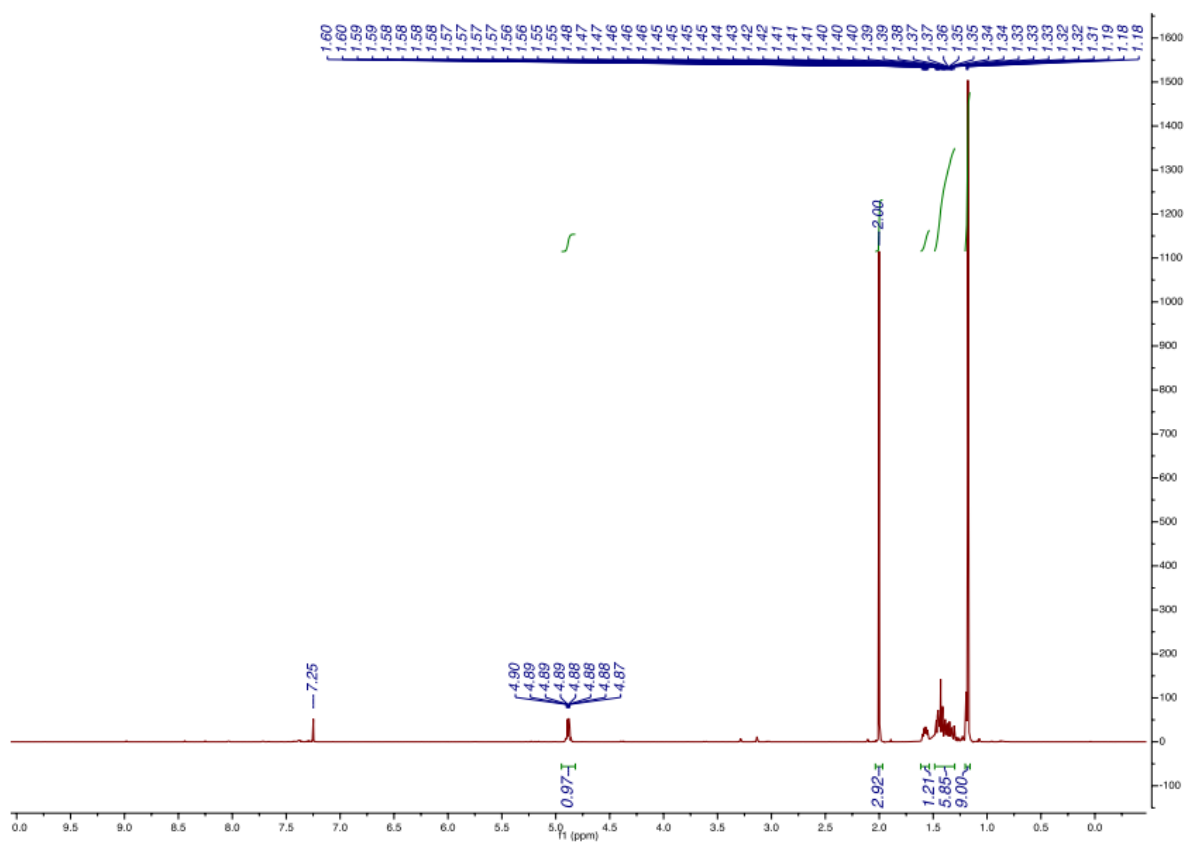
41.7, 34.3, 29.27, 29.26, 26.3, 18.5, 8.20 ppm. NMR spectra are consistent with literature reports.<sup>6</sup>



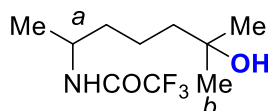
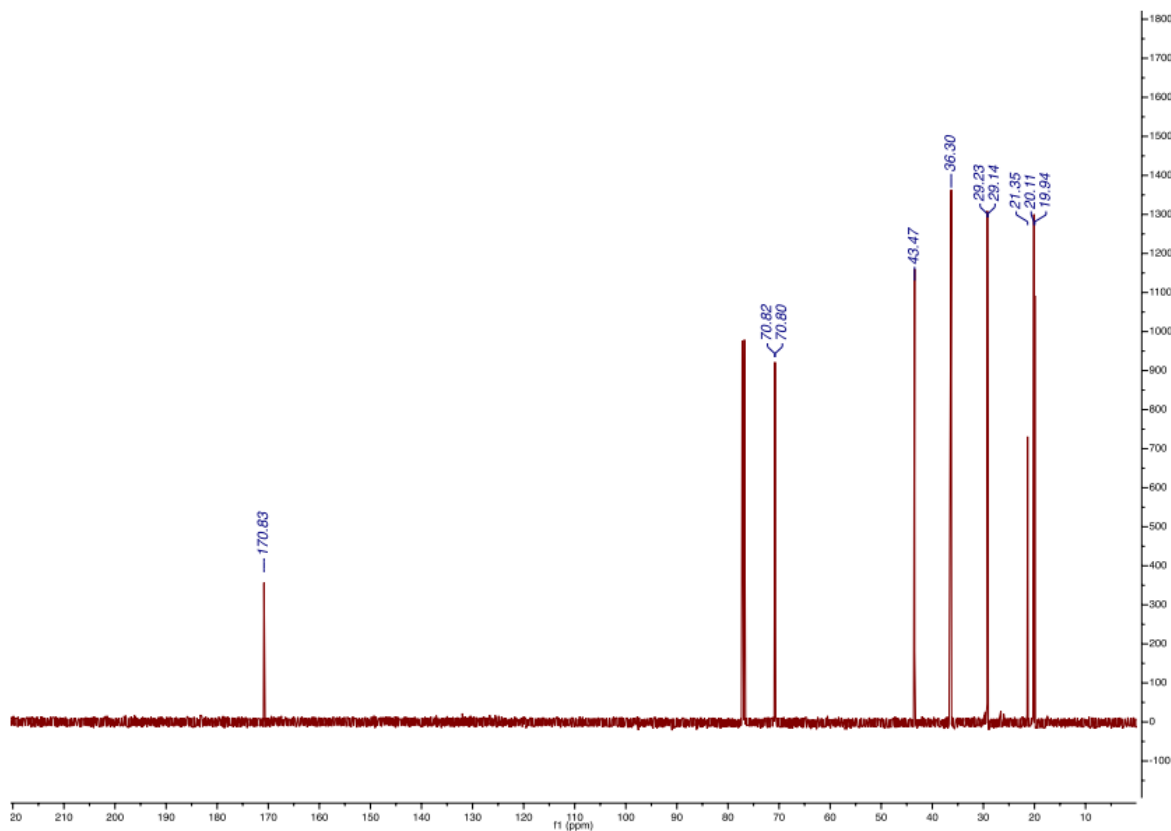


**6-hydroxy-6-methylheptan-2-yl acetate (4.34)** 6-methylheptan-2-yl acetate

(68.9 mg, 0.4 mmol) was hydroxylated according to the general procedure and purified by chromatography (silica gel, hexanes/EtOAc 25/1 to 4/1) to give product (34.5 mg, 0.18 mmol, 46%) and recovered starting material (22.3 mg, 0.13 mmol, 32%).  $^1\text{H}$  NMR (600 MHz,  $\text{CDCl}_3$ ):  $\delta$  4.89 ( $\text{H}_a$ , m, 1H), 2.00 ( $\text{H}_b$ , s, 3H), 1.61 - 1.55 (m, 1H), 1.48 - 1.30 (m, 5H), 1.19 (d,  $J = 6.3$  Hz, 3H), 1.18 ( $\text{H}_c$ , s, 6H) ppm;  $^{13}\text{C}$  NMR (150 MHz  $\text{CDCl}_3$ ):  $\delta$  170.8, 70.82, 70.80, 43.5, 36.3, 29.2, 29.1, 21.4, 20.1, 20.0 ppm. NMR spectra are consistent with literature reports.<sup>6</sup>







**2,2,2-trifluoro-N-(6-hydroxy-6-methylheptan-2-yl)acetamide (4.35)** 2,2,2-

trifluoro-N-(6-methylheptan-2-yl)acetamide (90.1 mg, 0.4 mmol) was

hydroxylated according to the general procedure and purified by chromatography

(silica gel, hexanes/EtOAc 4/1) to give product (48.6 mg, 0.2 mmol, 50%) and

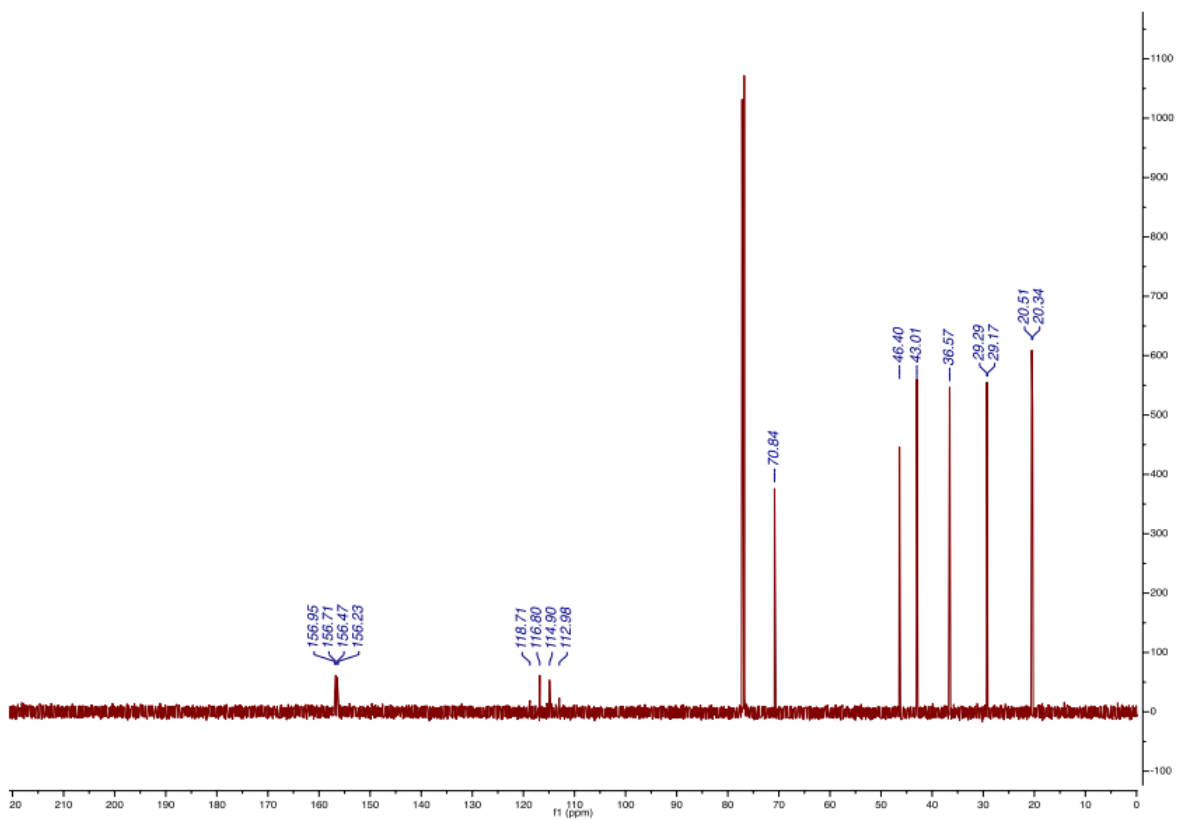
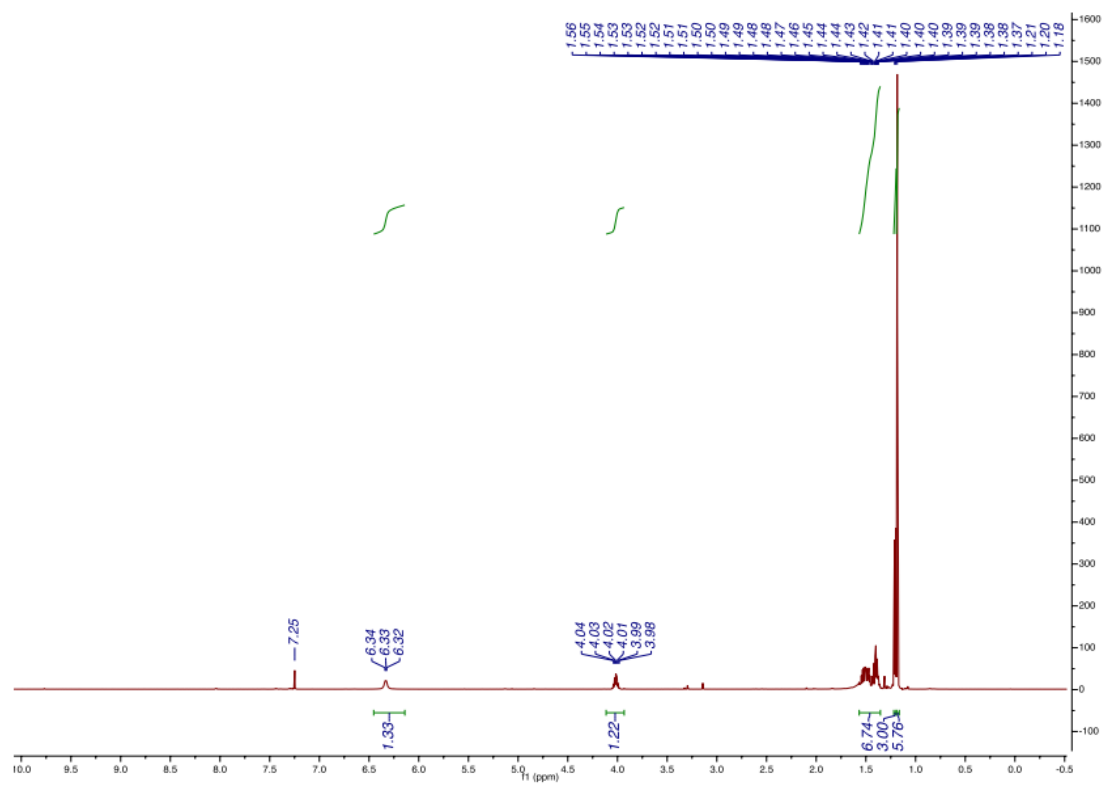
recovered starting material (44.3 mg, 0.196 mmol, 49%).  $^1\text{H}$  NMR (600 MHz,

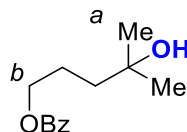
$\text{CDCl}_3$ ):  $\delta$  6.34 (br s, 1H), 4.02 ( $\text{H}_a$ , m, 1H), 1.56 - 1.36 (m, 6H), 1.21 (d,  $J$  = 6.6

Hz, 3H), 1.18 ( $\text{H}_b$ , s, 6H) ppm;  $^{13}\text{C}$  NMR (150 MHz  $\text{CDCl}_3$ ):  $\delta$  156.59 (q,  $J$  = 36

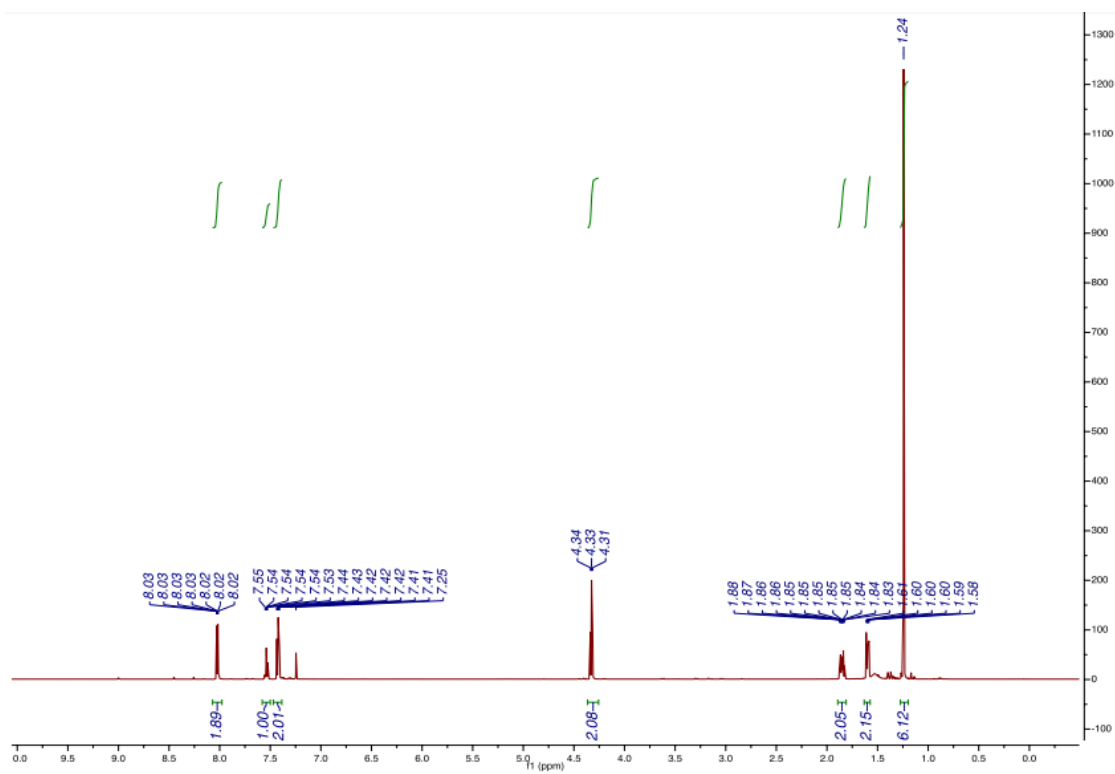
Hz), 115.9 (q,  $J$  = 288 Hz), 70.8, 46.4, 43.0, 36.6, 29.3, 29.2, 20.5, 20.3 ppm;  $^{19}\text{F}$

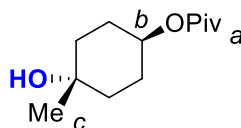
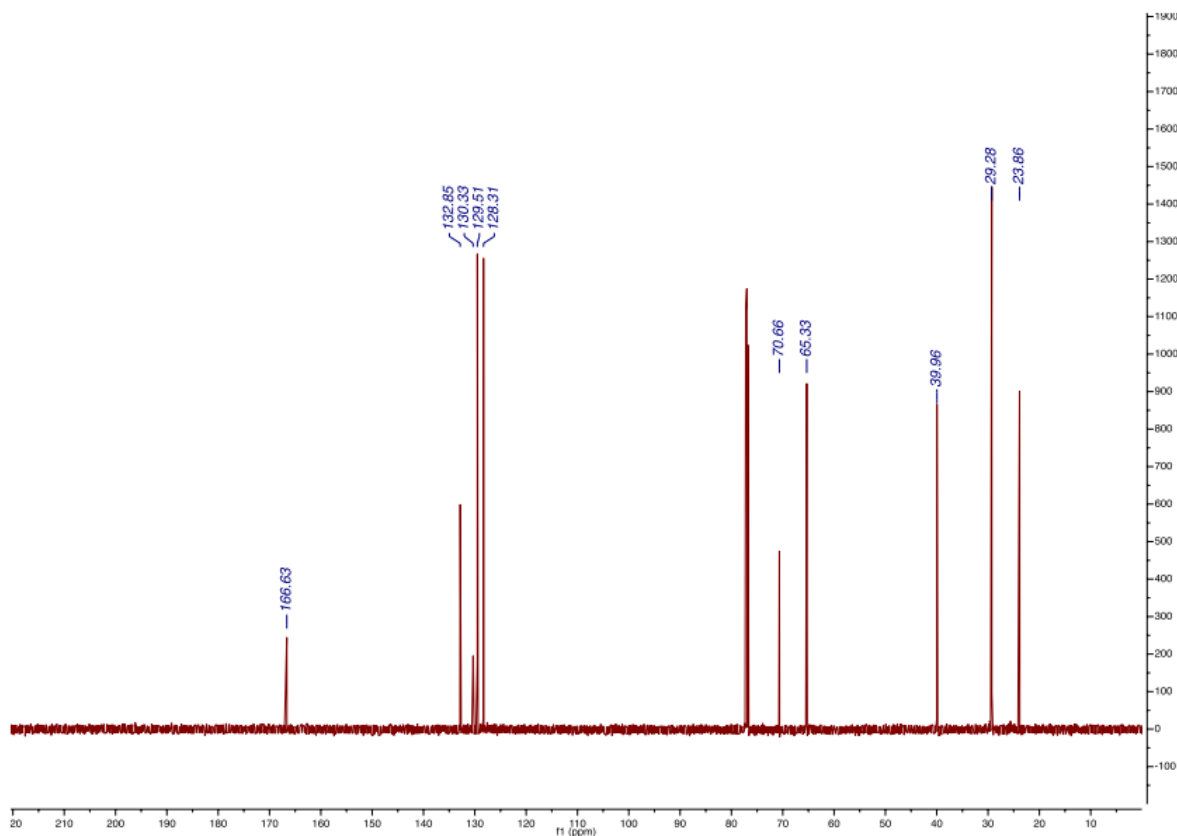
NMR (564 MHz CDCl<sub>3</sub>):  $\delta$  -76.87 ppm. NMR spectra are consistent with literature reports.<sup>6</sup>





**4-hydroxy-4-methylpentyl benzoate (4.36)** 4-methylpentyl benzoate (82.5 mg, 0.4 mmol) was hydroxylated according to the general procedure and purified by chromatography (silica gel, hexanes/EtOAc 25/1 to 4/1) to give product (24.9 mg, 0.11 mmol, 28%) and recovered starting material (53.0 mg, 0.26 mmol, 64%).  $^1\text{H}$  NMR (600 MHz,  $\text{CDCl}_3$ ):  $\delta$  8.02 ( $\text{H}_{\text{Ar}}$ , dd,  $J = 8.4, 1.3$  Hz, 2H), 7.54 ( $\text{H}_{\text{Ar}}$ , tt,  $J = 7.4, 1.3$  Hz, 1H), 7.42 ( $\text{H}_{\text{Ar}}$ , dd,  $J = 8.4, 7.4$  Hz, 2H), 4.33 ( $\text{H}_b$ , t,  $J = 6.6$  Hz, 2H), 1.88-1.83 (m, 2H), 1.61-1.58 (m, 2H), 1.24 ( $\text{H}_a$ , s, 6H) ppm;  $^{13}\text{C}$  NMR (150 MHz  $\text{CDCl}_3$ ):  $\delta$  166.6, 132.9, 130.3, 129.5, 128.3, 70.7, 65.3, 40.0, 29.3, 23.9 ppm. NMR spectra are consistent with literature reports.<sup>3</sup>

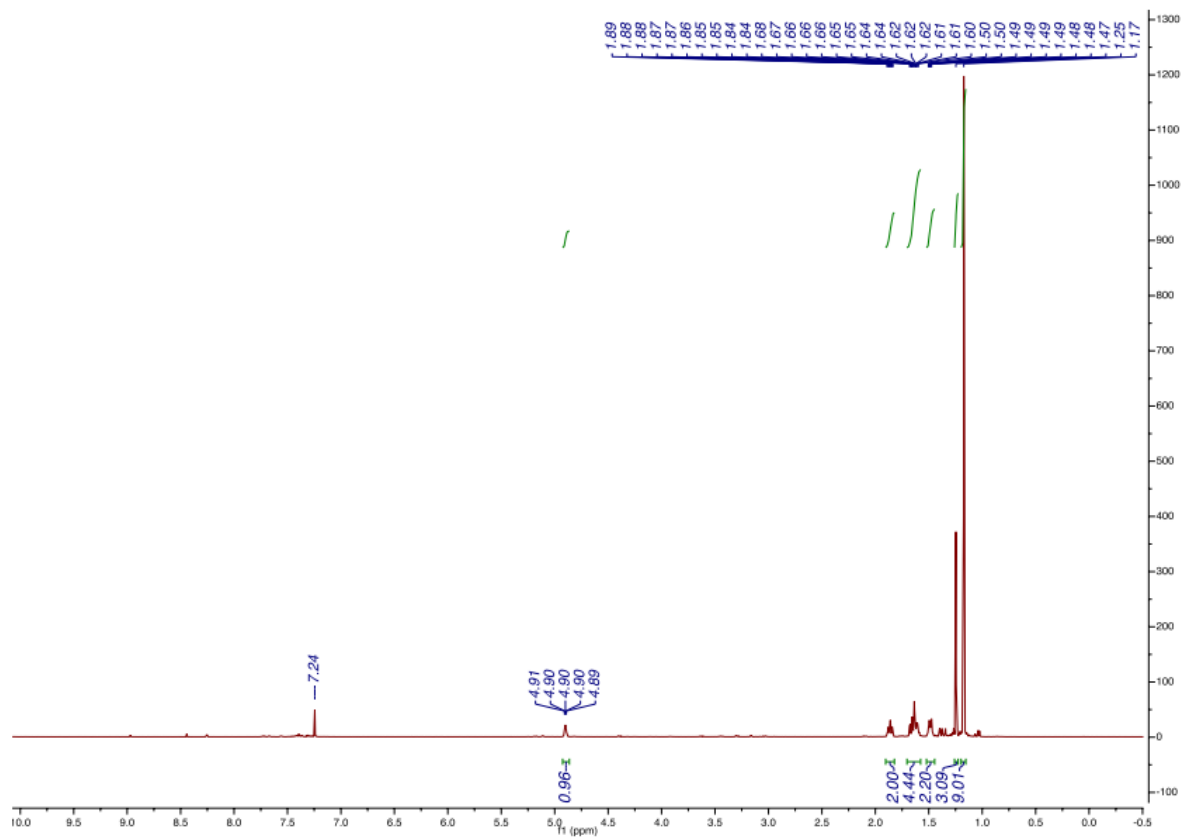


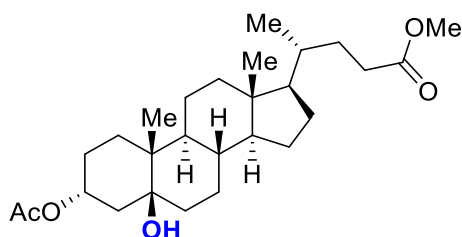
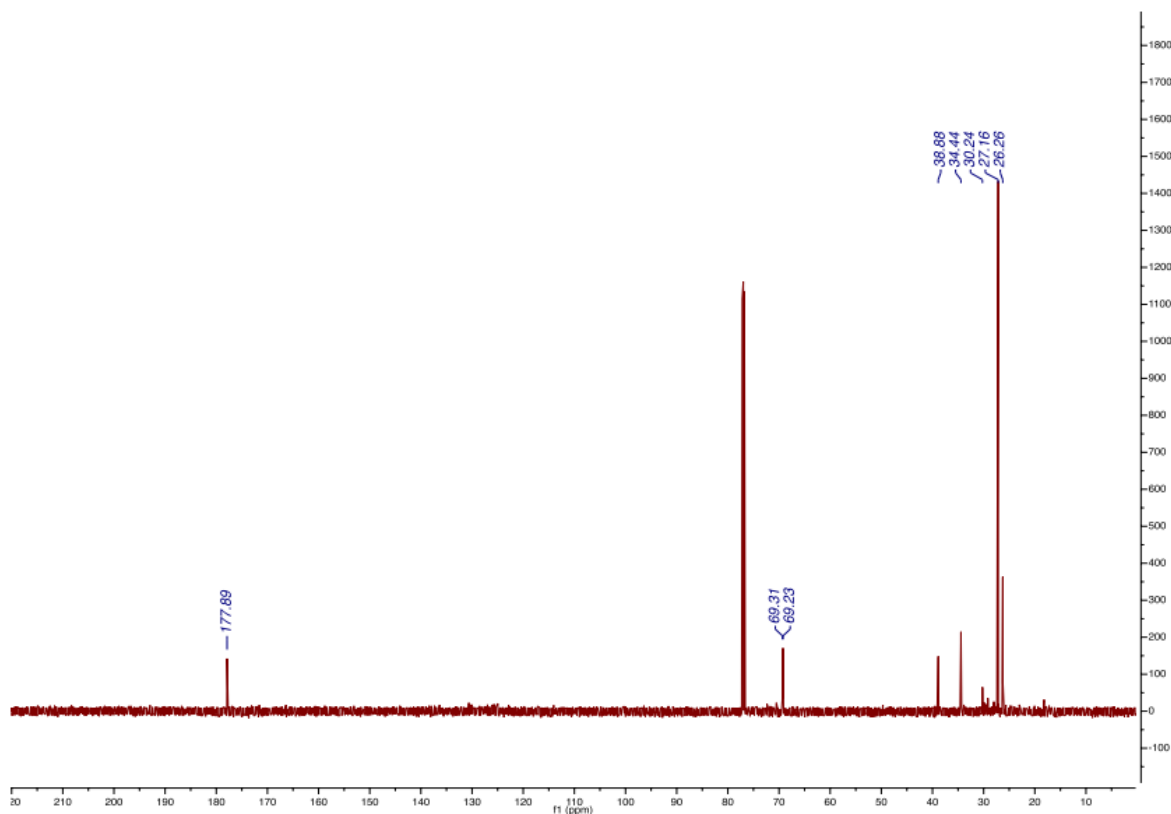


**(*cis*)-4-hydroxy-4-methylcyclohexyl pivalate (4.37)** *cis*-4-methylcyclohexyl

pivalate (39.6 mg, 0.2 mmol) was hydroxylated according to a modification of the general procedure in which 40 mol% catalyst was used and purified by chromatography (silica gel, hexanes/EtOAc 4/1) to give product (16.6 mg, 0.077 mmol, 39%) and recovered starting material (18.4 mg, 0.093 mmol, 46%).  $^1\text{H}$  NMR (600 MHz,  $\text{CDCl}_3$ ):  $\delta$  4.90 ( $\text{H}_b$ , m, 1H), 1.89 - 1.83 (m, 2H), 1.69 - 1.60 (m, 4H), 1.51 - 1.47 (m, 2H), 1.25 ( $\text{H}_c$ , s, 3H), 1.17 ( $\text{H}_a$ , s, 9H) ppm;  $^{13}\text{C}$  NMR (150

MHz CDCl<sub>3</sub>):  $\delta$  177.9, 69.3, 69.2, 38.9, 34.4, 30.2, 27.2, 26.3 ppm. NMR spectra are consistent with literature reports.<sup>3</sup>

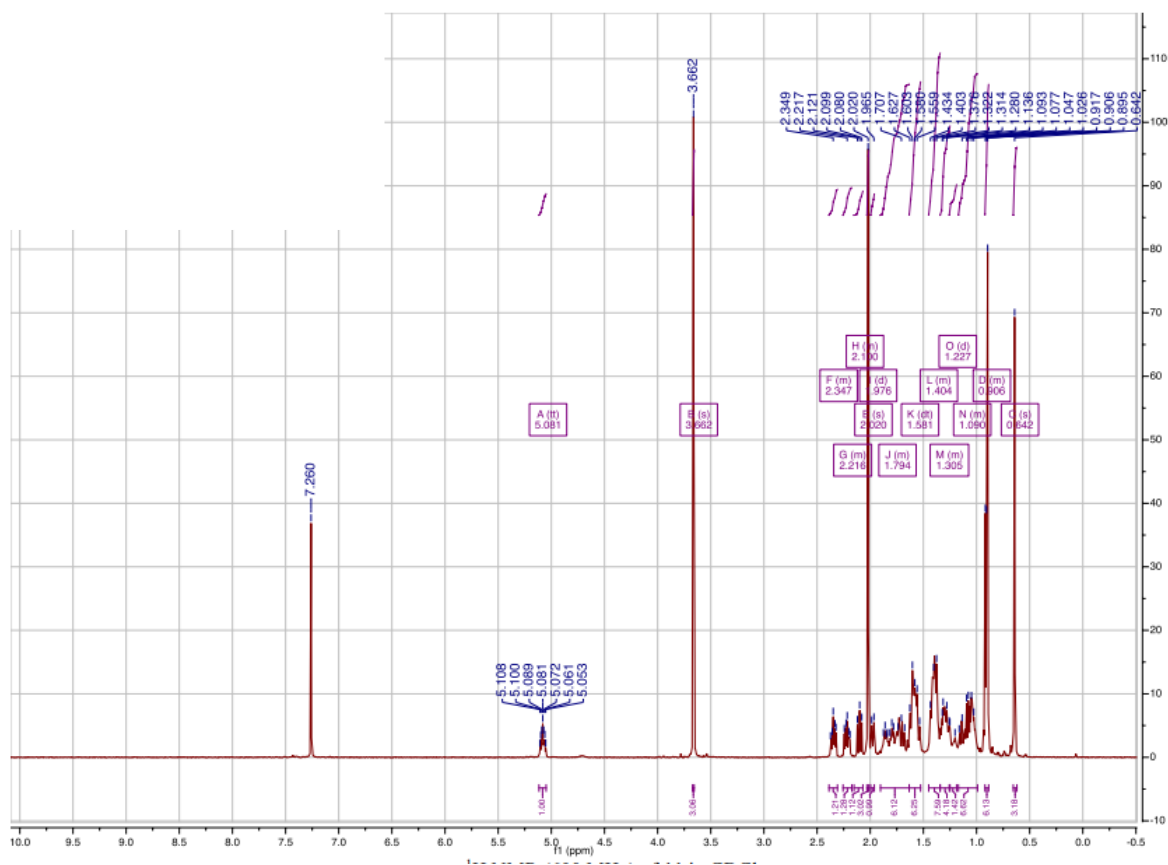


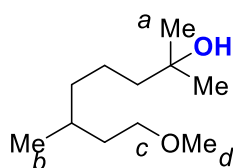
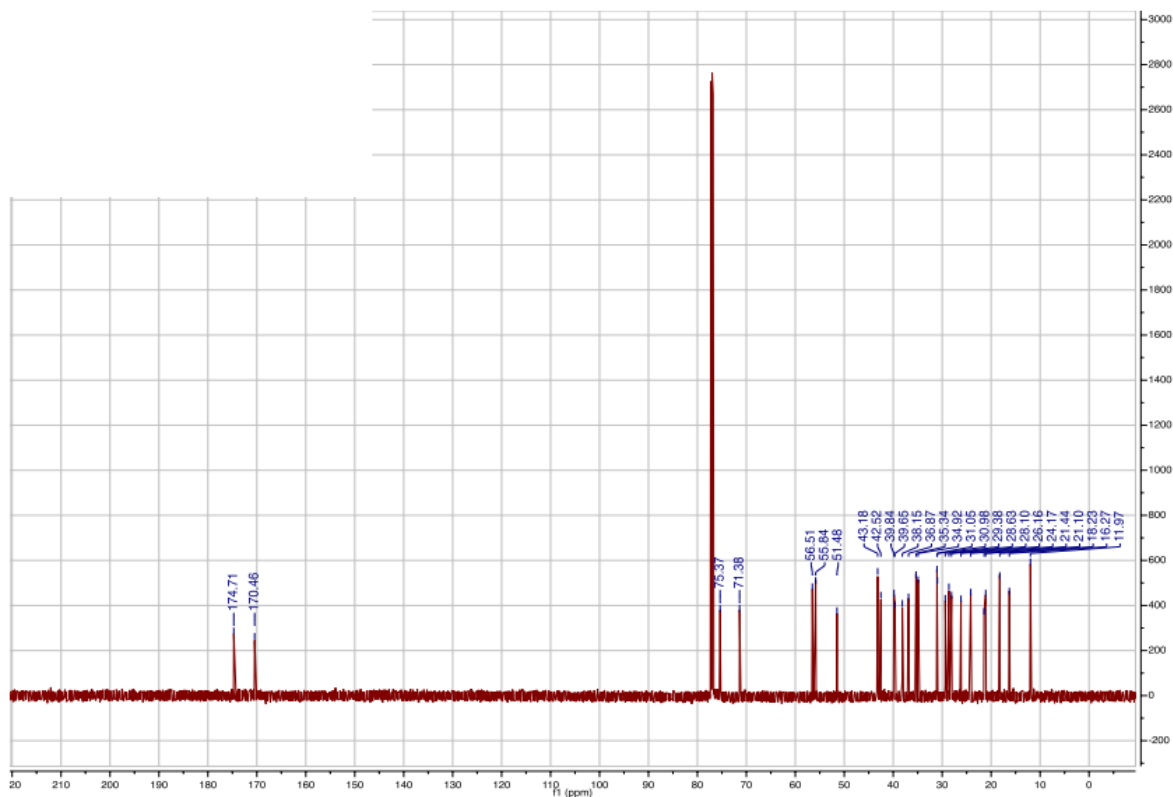


**Hydroxylithocholic acid derivative (4.38)** Methyl 3α-acetoxy-5β-cholan-24-oate (86.1 mg, 0.2 mmol) was hydroxylated using a modified procedure in which 20 mol% catalyst and 16 eq. H<sub>2</sub>O<sub>2</sub> were added in two portions at t=0 h and t=24 h. Purification by chromatography (silica gel, hexanes/EtOAc 10/1 to 3/1) gave product (32.7 mg, 0.073 mmol, 36%) and recovered starting material (33.7 mg, 0.078 mmol, 39%). <sup>1</sup>H NMR (600 MHz, CDCl<sub>3</sub>): δ 5.08 (tt, J = 11.5, 5.0 Hz, 1H),



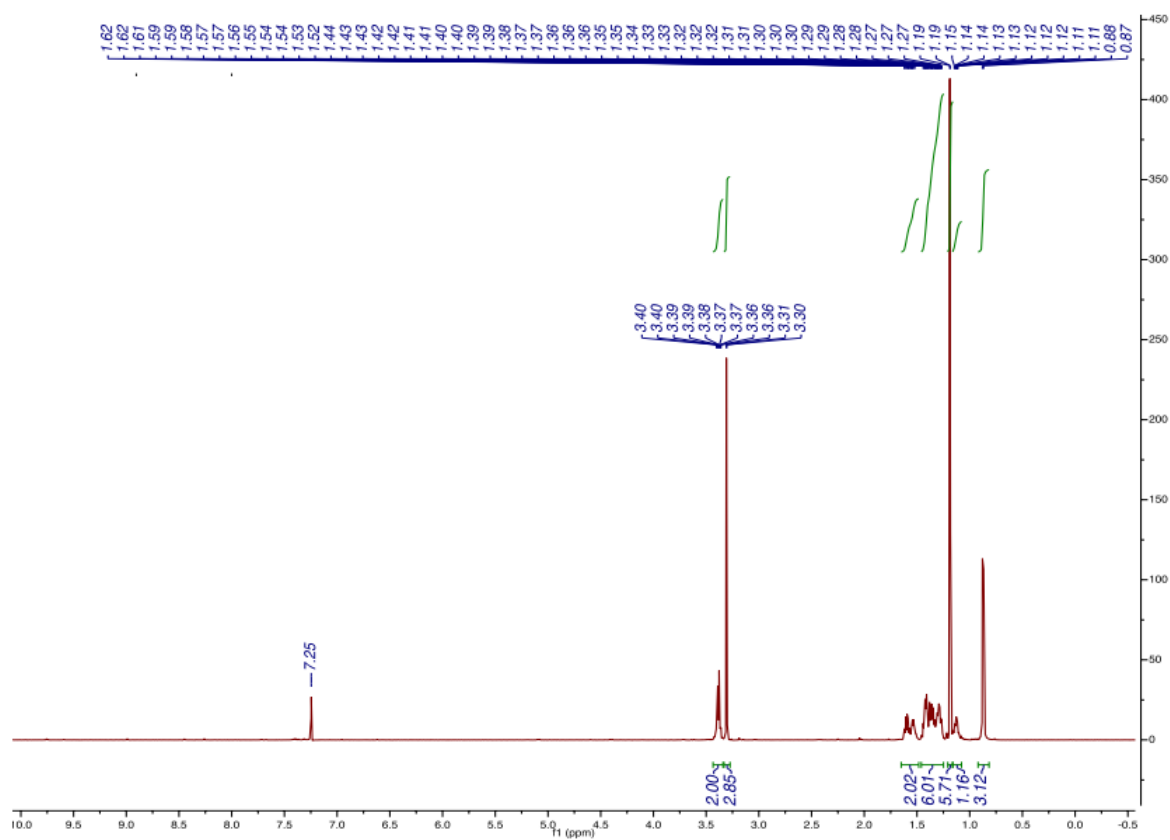
3.66 (s, 3H), 2.39–2.31 (m, 1H), 2.26–2.17 (m, 1H), 2.15–2.07 (m, 1H), 2.02 (s, 3H), 1.98 (d,  $J = 12.6$  Hz, 1H), 1.90–1.63 (m, 6H), 1.58 (dt,  $J = 26.7, 14.4$  Hz, 6H), 1.45–1.34 (m, 8H), 1.34–1.25 (m, 4H), 1.23 (d,  $J = 29.0$  Hz, 1H), 1.17 – 0.99 (m, 7H), 0.92 – 0.89 (m, 6H), 0.64 (s, 3H) ppm;  $^{13}\text{C}$  NMR (151 MHz,  $\text{CDCl}_3$ )  $\delta$  174.7, 170.5, 75.4, 71.4, 56.5, 55.8, 51.5, 43.2, 42.5, 39.8, 39.7, 38.2, 36.9, 35.3, 34.9, 31.1, 31.0, 29.4, 28.6, 28.1, 26.2, 24.2, 21.4, 21.1, 18.2, 16.3, 12.0 ppm. NMR spectra are consistent with literature reports.<sup>2</sup>

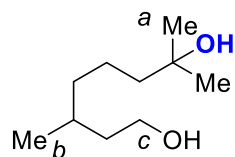
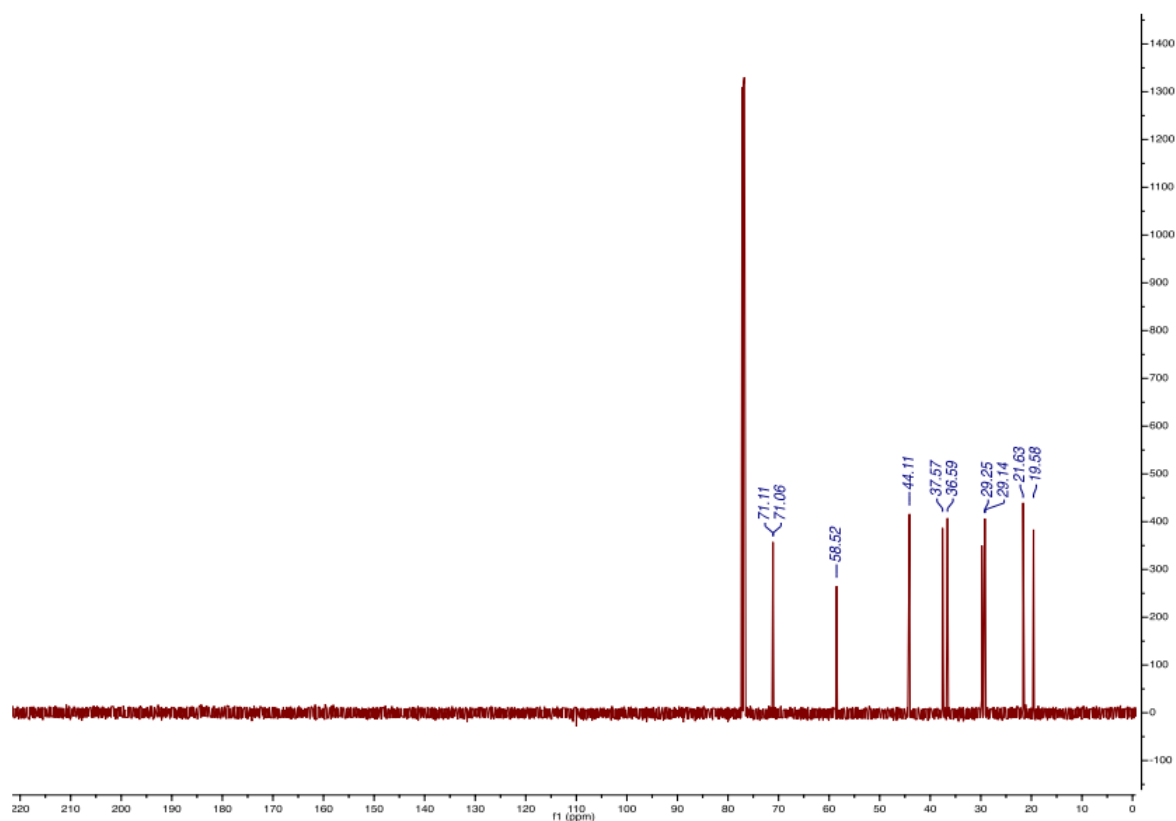




**8-methoxy-2,6-dimethyloctan-2-ol (4.39)** 1-methoxy-3,7-dimethyloctane (69.0 mg, 0.4 mmol) was hydroxylated according to the general procedure and purified by chromatography (silica gel, pentane/Et<sub>2</sub>O 4/1 to 2/1) to give product (34.1 mg, 0.18 mmol, 45%) and recovered starting material (32.8 mg, 0.19 mmol, 48%). <sup>1</sup>H NMR (600 MHz, CDCl<sub>3</sub>): δ 3.38 (H<sub>c</sub>, td, J = 6.9, 5.2 Hz, 2H), 3.31 (H<sub>d</sub>, s, 3H), 1.63 - 1.51 (m, 2H), 1.45 - 1.26 (m, 6H), 1.19 (H<sub>a</sub>, s, 6H), 1.17 - 1.08 (m, 1H), 0.87 (H<sub>b</sub>, d, J = 6.7 Hz, 3H) ppm; <sup>13</sup>C NMR (151 MHz, CDCl<sub>3</sub>): δ 71.11, 71.06,

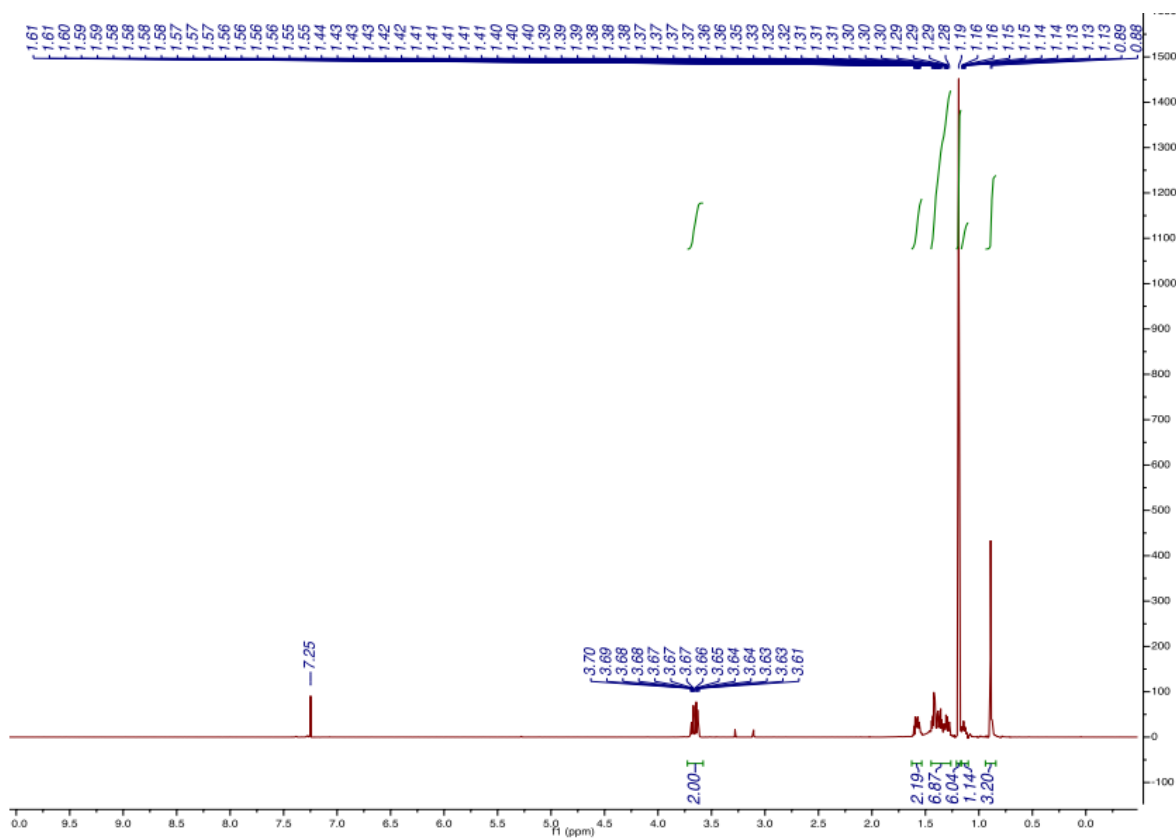
58.5, 44.1, 37.6, 36.6, 29.8, 29.3, 29.1, 21.6, 19.6 ppm. NMR spectra are consistent with literature reports.<sup>20</sup>

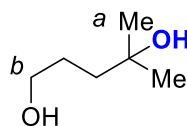
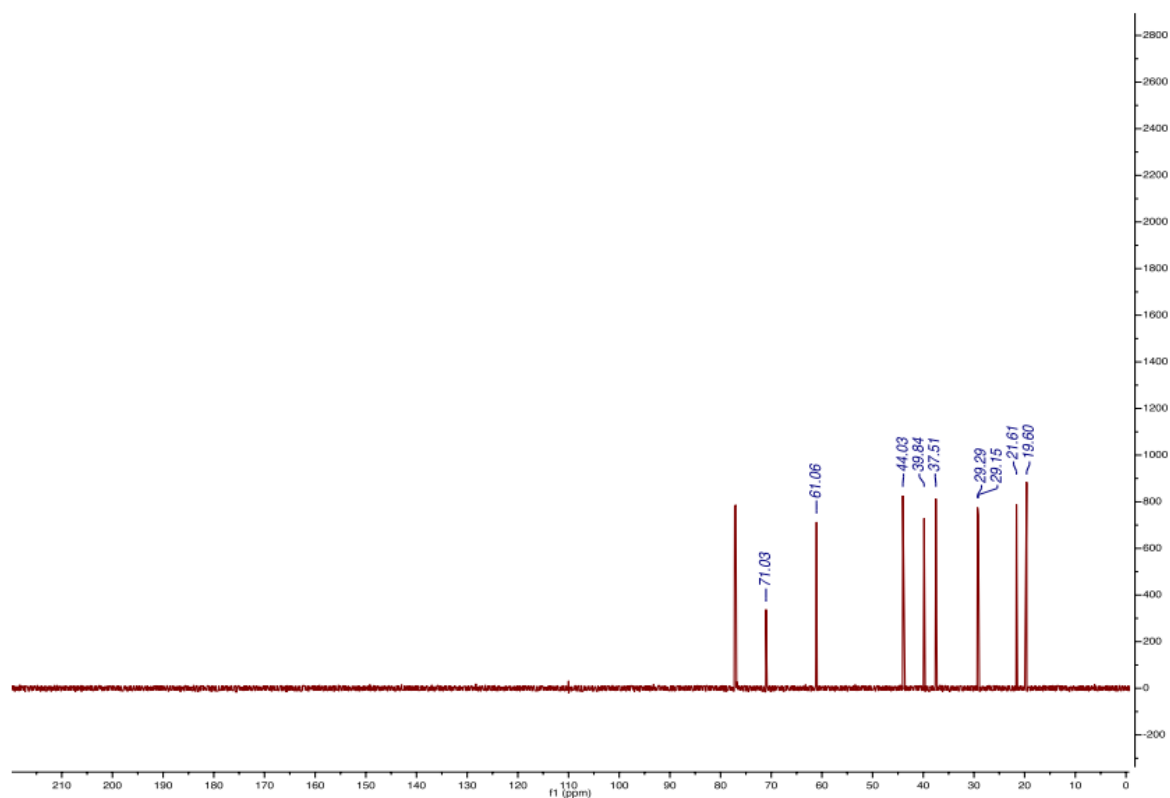




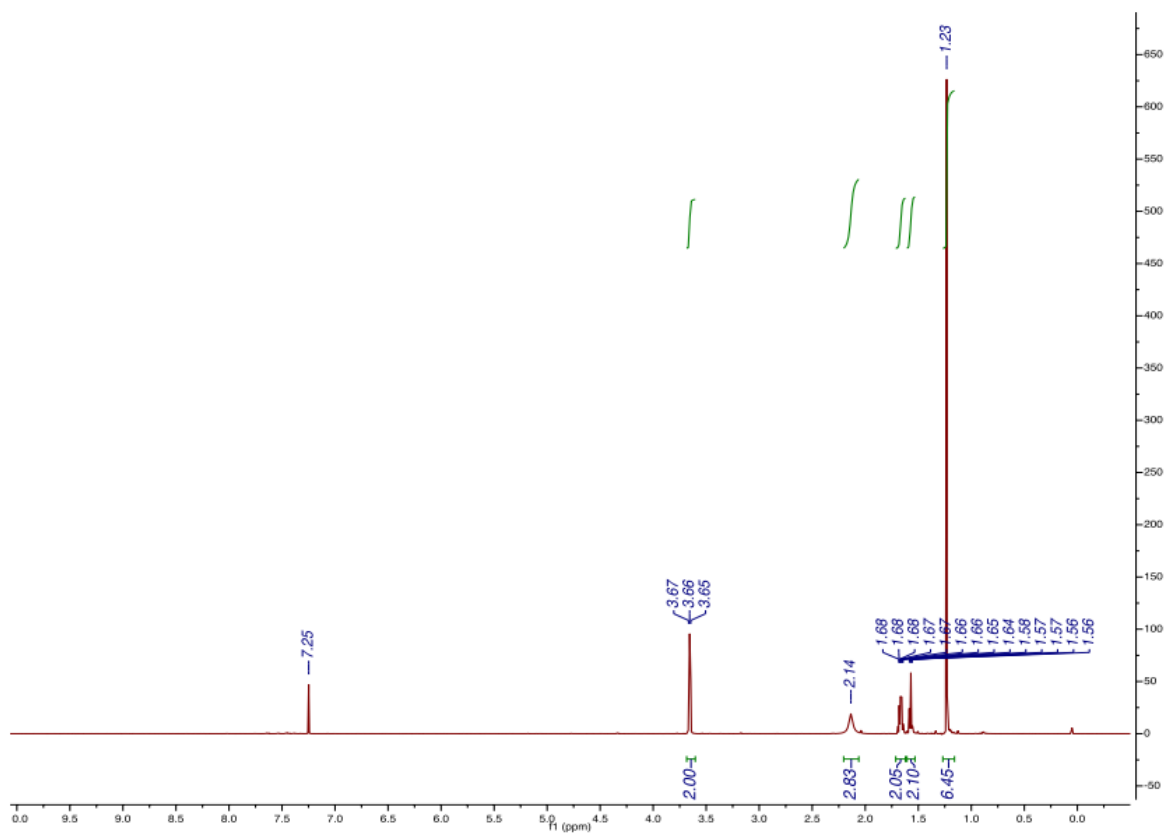
**3,7-dimethyloctane-1,7-diol (4.40)** 3,7-dimethyl-1-octanol (63.3 mg, 0.4 mmol) was hydroxylated according to the general procedure and purified by chromatography (silica gel, hexanes/EtOAc 4/1 to 1/4) give product (38.9 mg, 0.22 mmol, 56%) and recovered starting material (4.4 mg, 0.028 mmol, 7%).  $^1\text{H}$  NMR (600 MHz,  $\text{CDCl}_3$ ):  $\delta$  3.70 - 3.61 ( $\text{H}_c$ , m, 2H), 1.62 - 1.54 (m, 2H), 1.45 - 1.27 (m, 6H), 1.19 ( $\text{H}_a$ , s, 6H), 1.16 - 1.12 (m, 1H), 0.88 ( $\text{H}_b$ , d,  $J = 6.6$  Hz, 3H) ppm;

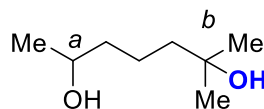
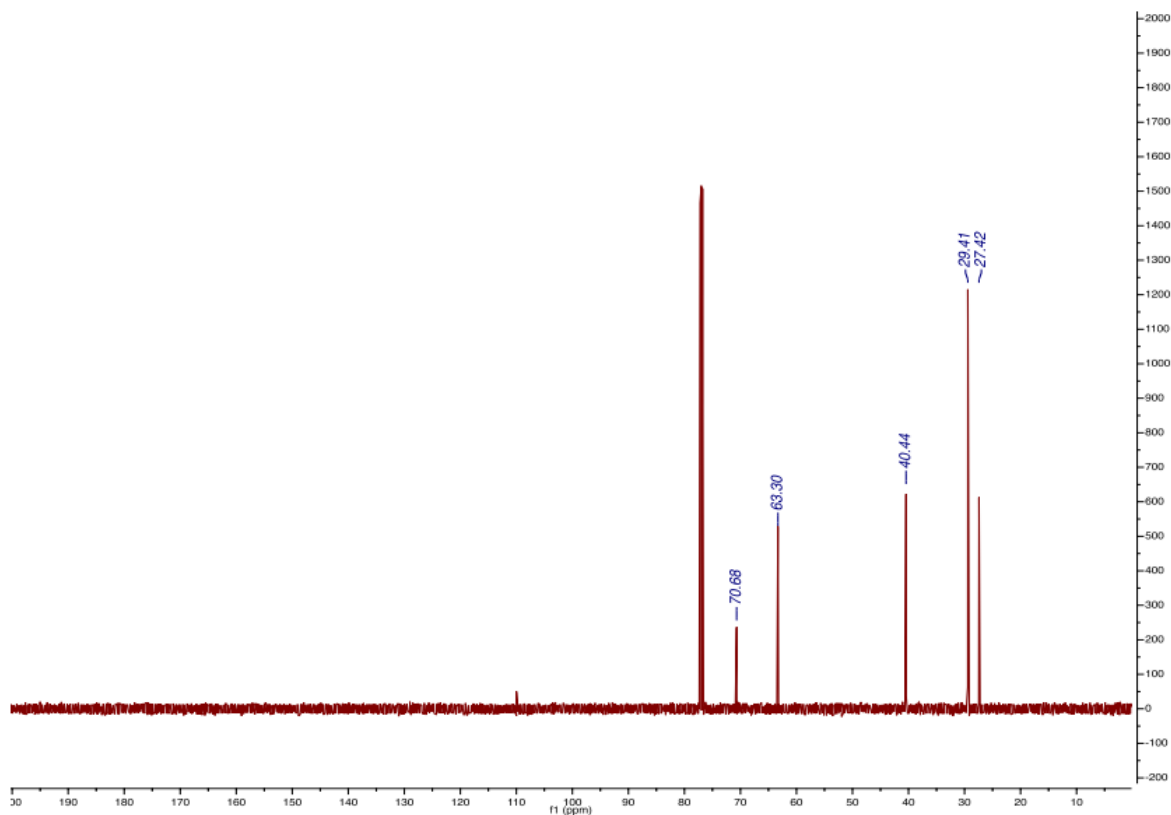
$^{13}\text{C}$  NMR (151 MHz,  $\text{CDCl}_3$ ):  $\delta$  71.0, 61.1, 44.0, 39.8, 37.51, 29.4, 29.3, 29.2, 21.6, 19.6 ppm. NMR spectra are consistent with literature reports.<sup>21</sup>





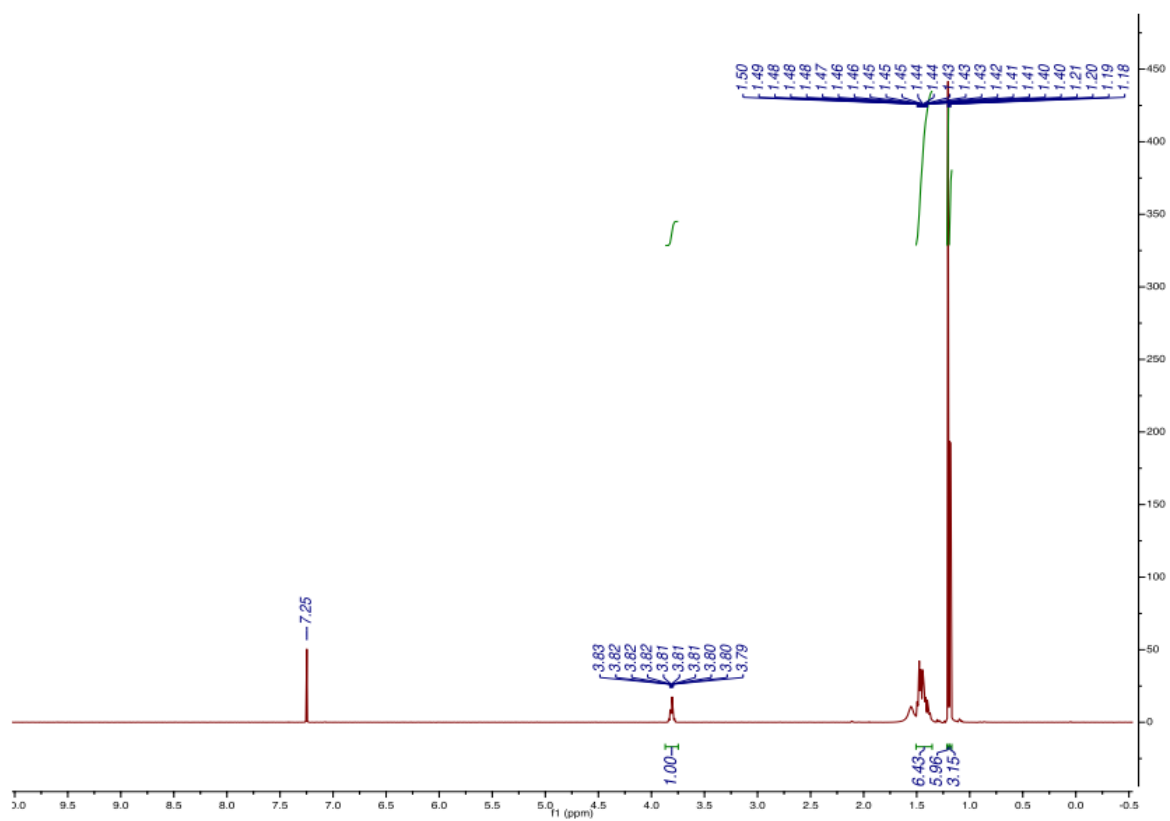
**4-methylpentane-1,4-diol (4.41)** 4-methyl-1-pentanol (40.8 mg, 0.4 mmol) was hydroxylated according to the general procedure and purified by chromatography (silica gel, hexanes/EtOAc 20/1 to 1/5) to give product (11.6 mg, 0.01 mmol, 25%) and recovered starting material (25.7 mg, 0.25 mmol, 63%).  $^1\text{H}$  NMR (600 MHz,  $\text{CDCl}_3$ ):  $\delta$  3.66 ( $\text{H}_b$ , t,  $J = 6.0$  Hz, 2H), 2.14 (br, 2H), 1.67 (m, 2H), 1.60 - 1.55 (m, 2H), 1.23 ( $\text{H}_a$ , s, 6H) ppm;  $^{13}\text{C}$  NMR (151 MHz,  $\text{CDCl}_3$ ):  $\delta$  70.7, 63.3, 40.4, 29.4, 27.4 ppm. NMR spectra are consistent with literature reports.<sup>22</sup>

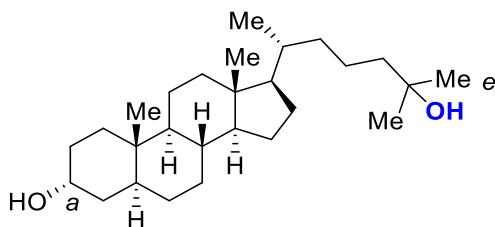
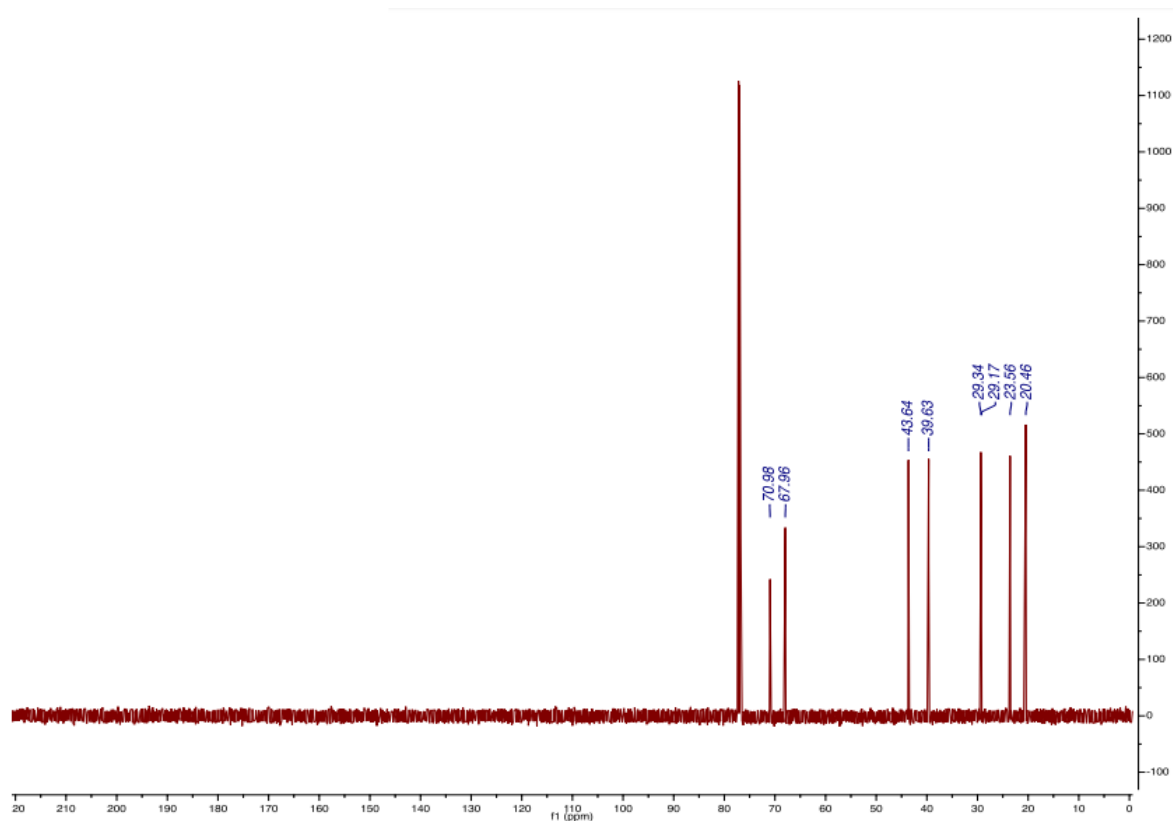




**2-methylheptane-2,6-diol (4.42)** 6-methyl-2-heptanol (52.1 mg, 0.4 mmol) was hydroxylated according to the general procedure and purified by chromatography (silica gel, hexanes/EtOAc 20/1 to 1/5) to give product (24.7 mg, 0.17 mmol, 42%) and recovered starting material (21.4 mg, 0.16 mmol, 41%).  $^1\text{H}$  NMR (600 MHz,  $\text{CDCl}_3$ ):  $\delta$  3.84 - 3.78 ( $\text{H}_a$ , m, 1H), 1.50 - 1.37 (m, 6H), 1.20 ( $\text{H}_b$ , s, 6H), 1.18 (d,  $J = 6.1$  Hz, 3H) ppm;  $^{13}\text{C}$  NMR (151 MHz,  $\text{CDCl}_3$ ):  $\delta$  71.0, 68.0, 43.6, 39.6, 29.3, 29.2, 23.6, 20.5 ppm. NMR spectra are consistent with literature reports.<sup>23</sup>



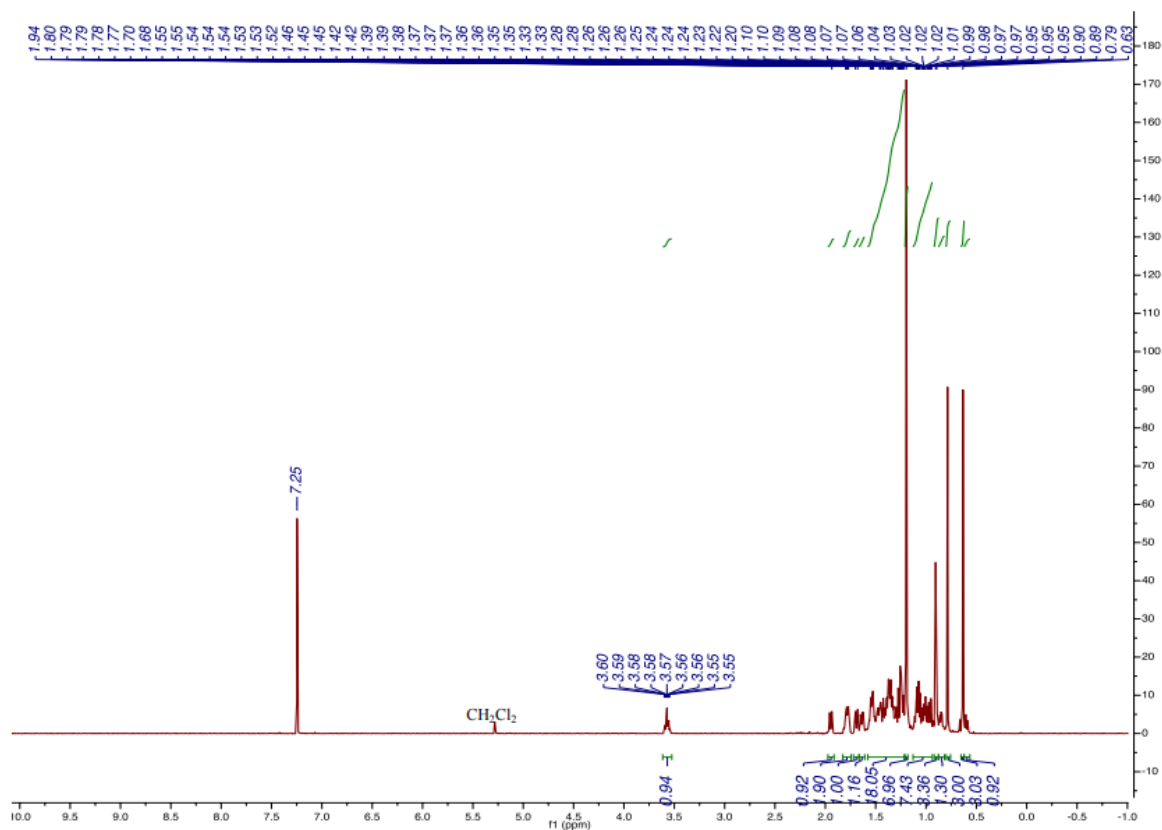


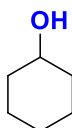
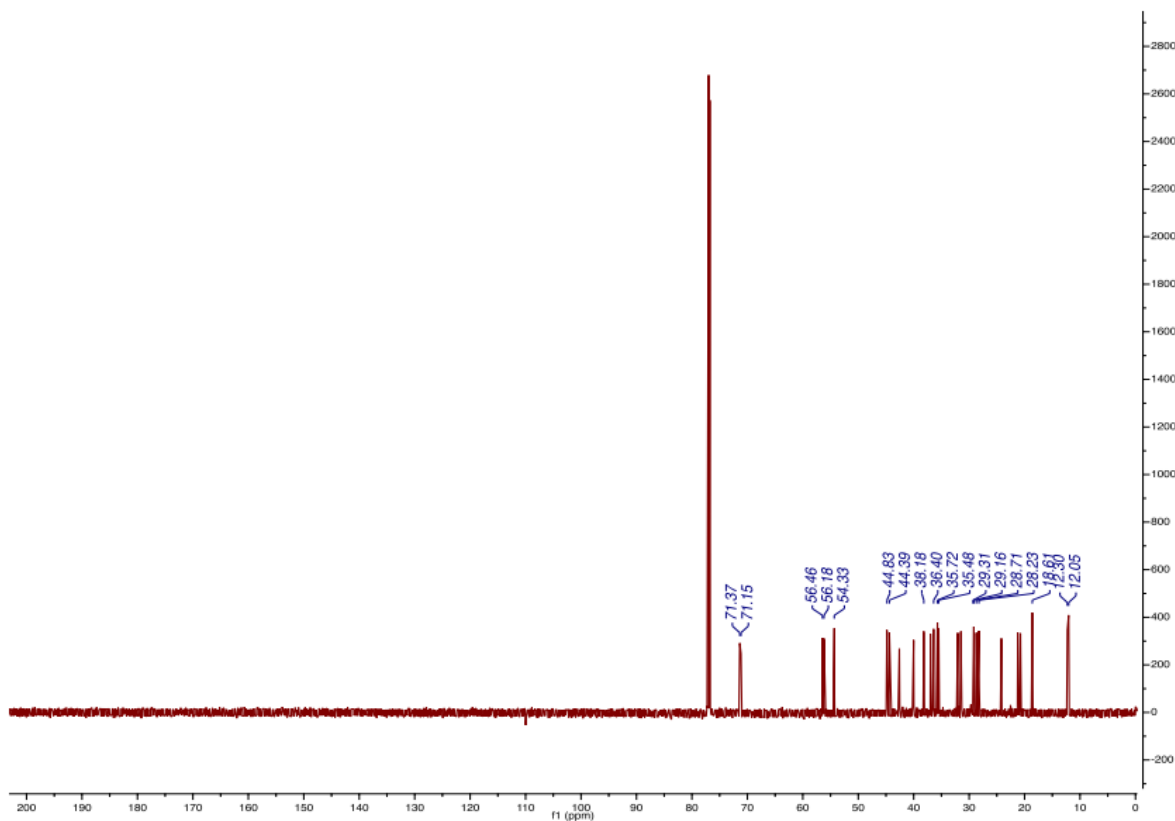


**Hydroxydihydrocholesterol (4.43)** (+)-dihydrocholesterol (77.7 mg, 0.2 mmol)

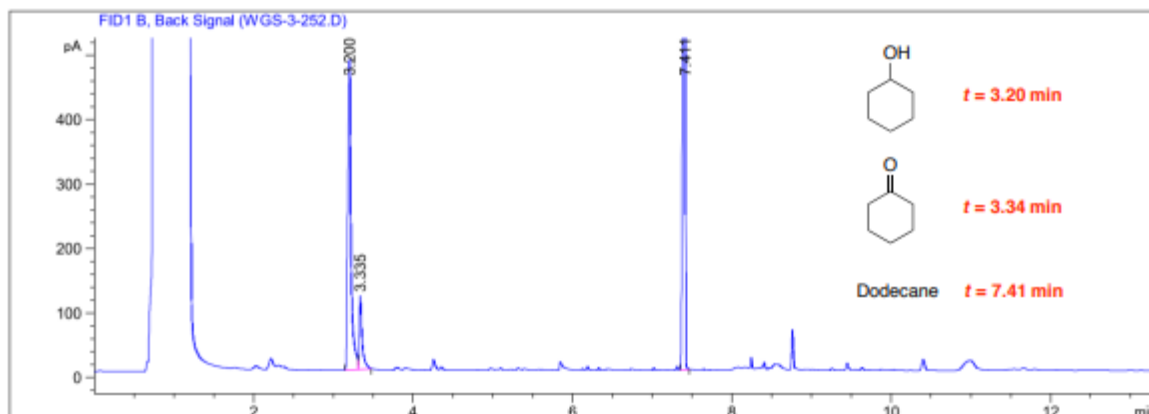
was hydroxylated according to the general procedure and purified by chromatography (silica gel, hexanes/EtOAc/DCM 10/3/3) to give product (16.0 mg, 0.04 mmol, 20%) and recovered starting material (36.8 mg, 0.095 mmol, 47%).  $^1\text{H}$  NMR (600 MHz,  $\text{CDCl}_3$ ):  $\delta$  3.57 ( $\text{H}_a$ , m, 1H), 1.95 (dt,  $J$  = 12.6, 3.5 Hz, 1H), 1.81-1.75 (m, 2H), 1.69 (dt,  $J$  = 13.3, 3.6 Hz, 1H), 1.64 (dq,  $J$  = 12.9, 3.5 Hz, 1H), 1.57 - 1.22 (m, 18H), 1.20 ( $\text{H}_e$ , s, 6H), 1.12 - 0.94 (m, 7H), 0.90 (d,  $J$  = 6.5

Hz, 3H), 0.85 (dt,  $J = 10.7, 6.1$  Hz, 1H), 0.79 (s, 3H), 0.63 (s, 3H), 0.62 - 0.58 (m, 1H) ppm;  $^{13}\text{C}$  NMR (151 MHz,  $\text{CDCl}_3$ ):  $\delta$  71.4, 71.2, 56.5, 56.2, 54.3, 44.8, 44.4, 42.6, 40.0, 38.2, 37.0, 36.4, 35.7, 35.5, 35.4, 32.1, 31.5, 29.3, 29.2, 28.7, 28.2, 24.2, 21.2, 20.8, 18.6, 12.3, 12.1 ppm; IR (film,  $\text{cm}^{-1}$ ): 3294 (br), 2931, 2863, 1468, 1379, 1156, 1041, 911; HRMS  $m/z$  ( $\text{EI}^+$ ): Calculated for  $\text{C}_{27}\text{H}_{48}\text{O}_2$   $[\text{M}]^+$  : 404.3654, found 404.3657;  $[\alpha]_{22}^{\text{D}} = +24.5^\circ$  ( $c = 0.5$ ,  $\text{CH}_3\text{OH}$ ).





**Cyclohexanol (4.44)** Cyclohexane (16.8 mg, 0.2 mmol) was hydroxylated using a modified procedure wherein 100  $\mu$ L DCM was added to the reaction mixture. After 24 h, the organic phase was analyzed by GC after adding dodecane (50  $\mu$ L) as internal standard. GC yield was corrected according to the burn ratios of cyclohexanol and cyclohexanone to dodecane. The reaction produced cyclohexanol in 59% yield and cyclohexanone in 12% yield.



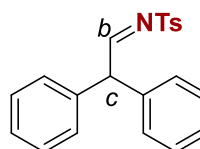
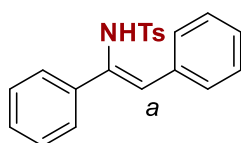
=====  
Area Percent Report  
=====

Burn ratio:  $R_{\text{dodecane/c-hexanol}} = 2.35$   
 $R_{\text{dodecane/c-hexanone}} = 2.42$

Sorted By : Signal  
Multiplier : 1.0000  
Dilution : 1.0000  
Do not use Multiplier & Dilution Factor with ISTDs

Signal 1: FID1 B, Back Signal

Peak #	RetTime [min]	Type	Width [min]	Area [pA*s]	Height [pA]	Area %
1	3.200	BV	0.0442	1409.77820	480.49844	17.89809
2	3.335	VB	0.0360	282.25336	113.64152	3.58340
3	7.411	VB	0.0232	6184.66553	3959.07715	78.51851

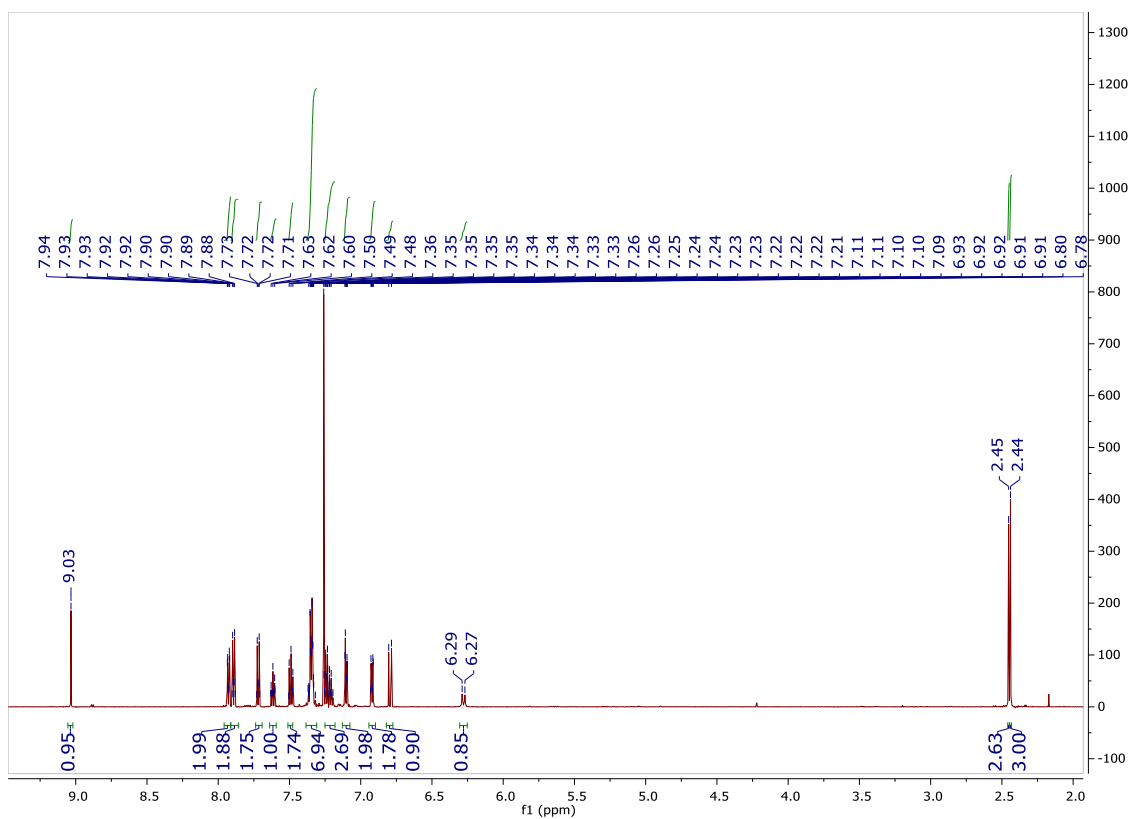


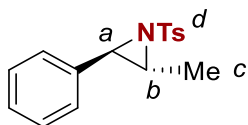
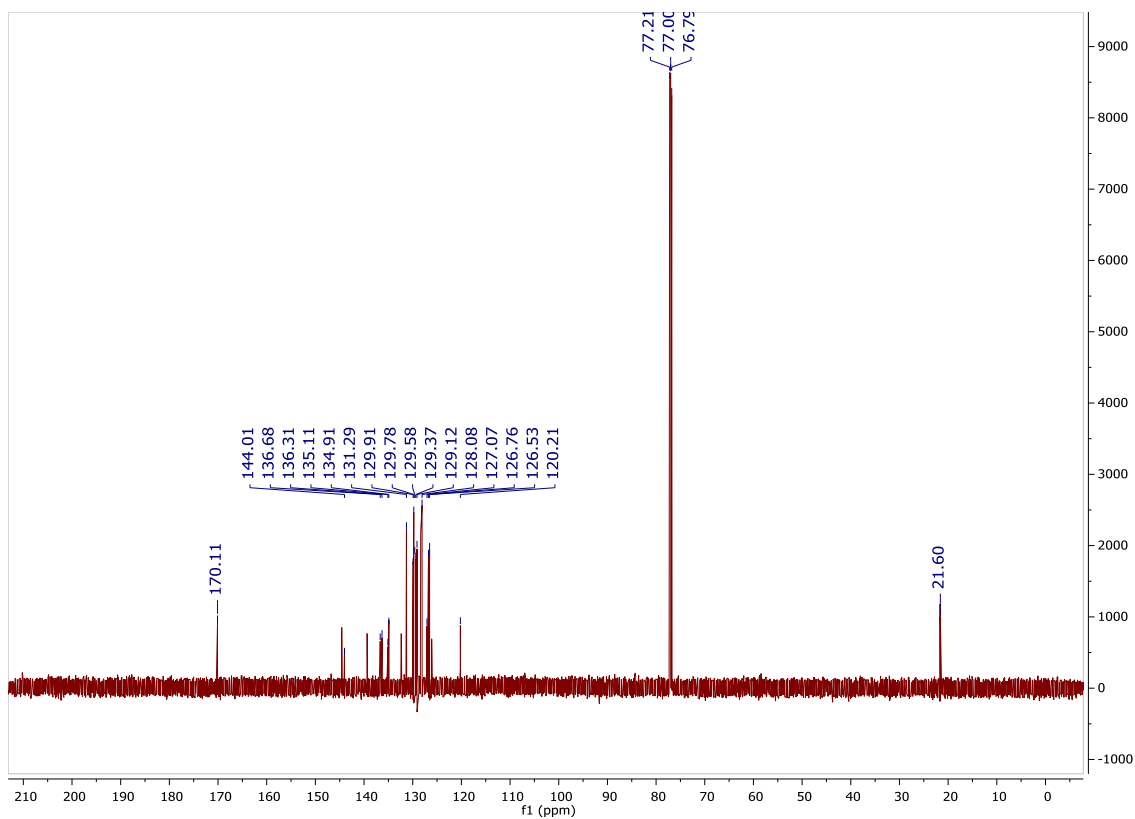
**(Z)-N-(2,2-diphenylethylidene)-4-methylbenzenesulfonamide (4.134)**

*trans*-Stilbene (90 mg, 0.5 mmol) was subjected to the general aziridination procedure.

Purification by column chromatography (silica, 10% to 20% EtOAc/hexanes) gave a mixture of isomeric products (22.7 mg, 0.065 mmol, 13%). <sup>1</sup>H NMR (600 MHz, Chloroform-*d*)  $\delta$  9.03 (H<sub>b</sub>, s, 1H), 7.96 – 7.91 (m, 2H), 7.91 – 7.86 (m, 2H), 7.74 – 7.69 (m, 2H), 7.64 – 7.59 (m, 1H), 7.51 –

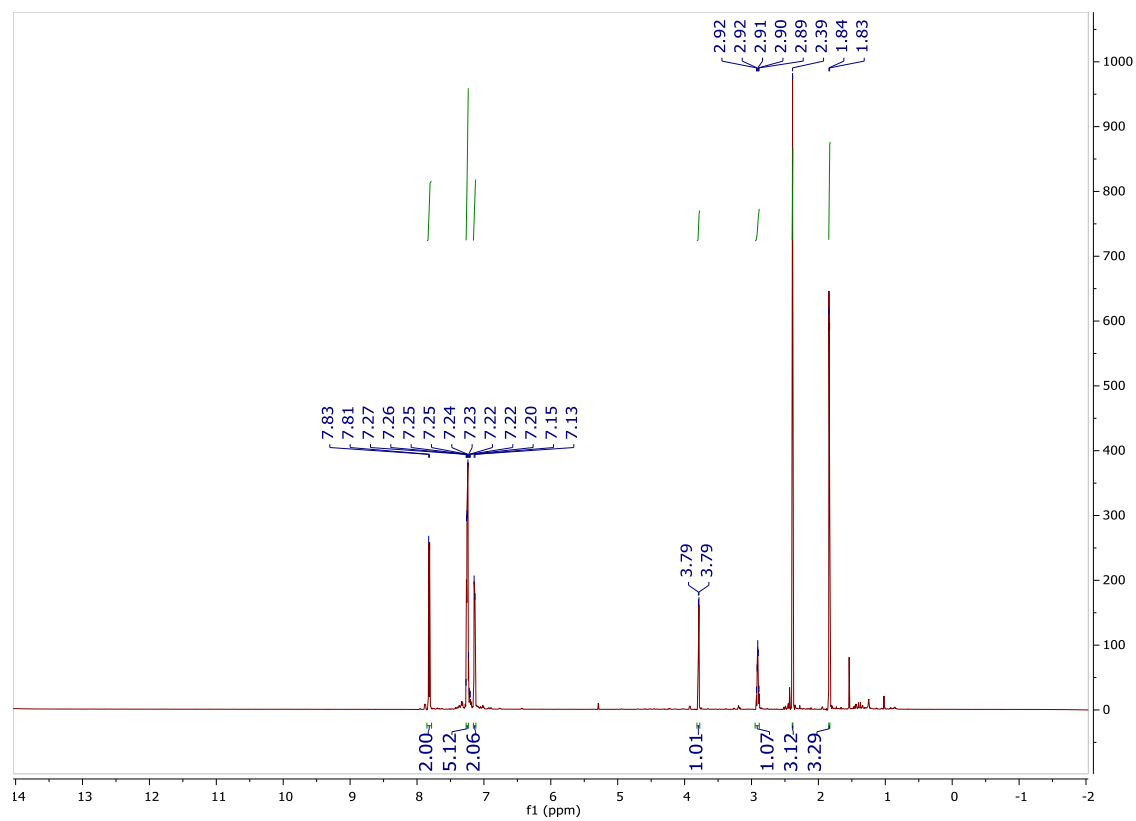
7.48 (m, 2H), 7.38 – 7.31 (m, 7H), 7.25 – 7.18 (m, 3H), 7.13 – 7.08 (m, 2H), 6.94 – 6.90 (m, 2H), 6.79 (d,  $J = 11.6$  Hz, 1H), 6.28 (H<sub>a</sub>, d,  $J = 11.7$  Hz, 1H), 2.45 (s, 3H), 2.44 (s, 3H). <sup>13</sup>C NMR (151 MHz, CDCl<sub>3</sub>)  $\delta$  170.11, 144.01, 136.68, 136.31, 135.11, 134.91, 131.29, 129.91, 129.78, 129.58, 129.37, 129.12, 128.08, 127.07, 126.76, 126.53, 120.21, 77.21, 77.00, 76.79, 21.60. Spectral data match literature reports.



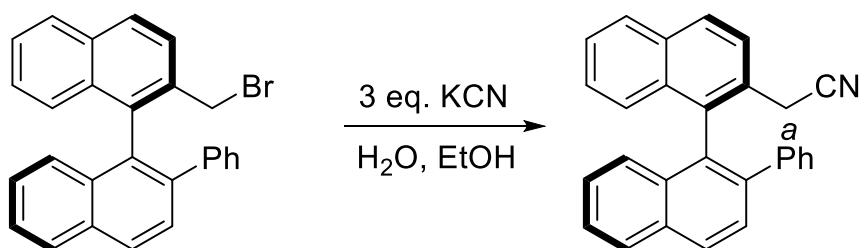
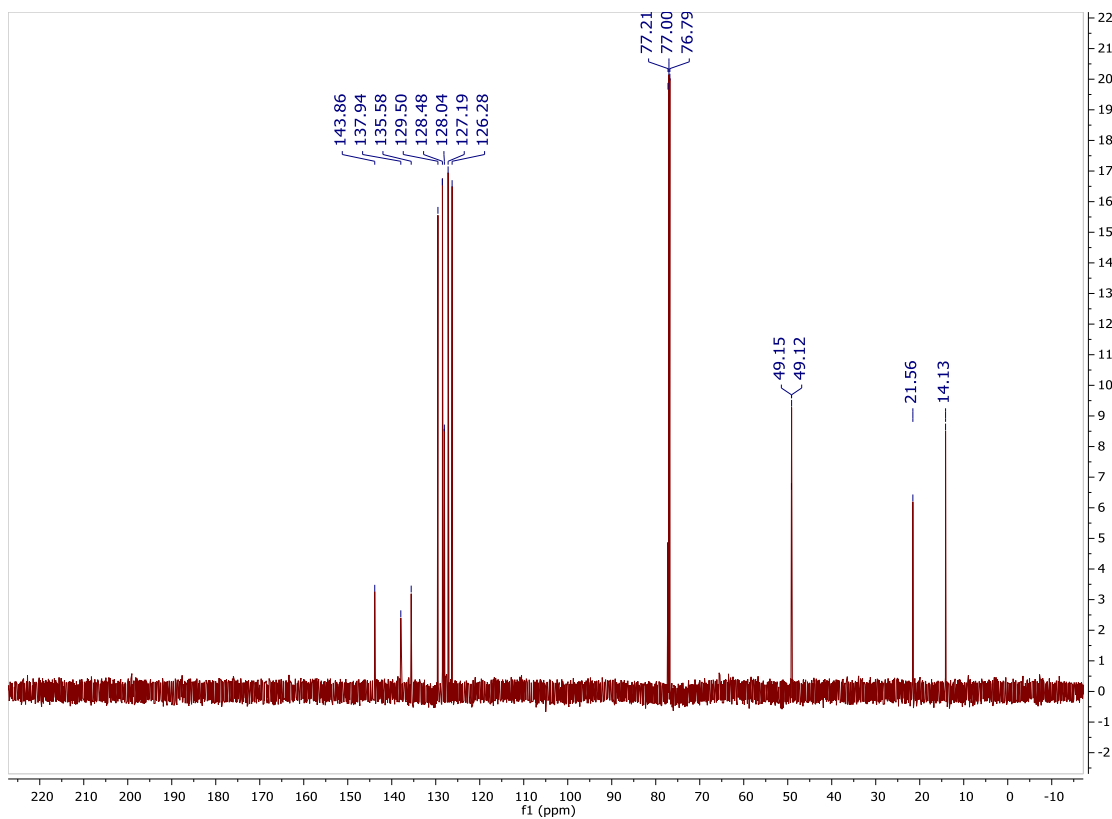


### ***trans*-2-methyl-3-phenyl-1-tosylaziridine (4.135)**

*trans*-b-methylstyrene (59 mg, 0.5 mmol) or *cis*-b-methylstyrene (59 mg, 0.5 mmol) were subjected to the general aziridination procedure. Purification by column chromatography (silica, 10% to 20% EtOAc/hexanes) gave product as a clear oil (34.5 mg, 0.12 mmol, 24%). <sup>1</sup>H NMR (598 MHz, CDCl<sub>3</sub>) δ 7.82 (d, *J* = 8.0 Hz, 2H), 7.25 (m, 5H), 7.14 (d, *J* = 7.5 Hz, 2H), 3.79 (H<sub>a</sub>, d, *J* = 4.3 Hz, 1H), 2.91 (H<sub>b</sub>, p, *J* = 5.4 Hz, 1H), 2.39 (H<sub>d</sub>, s, 3H), 1.84 (H<sub>c</sub>, d, *J* = 5.9 Hz, 3H). <sup>13</sup>C NMR (150 MHz, CDCl<sub>3</sub>) δ 143.86, 137.94, 135.58, 129.50, 128.48, 128.04, 127.19, 126.28, 77.21, 77.00, 76.79, 49.15, 49.12, 21.56, 14.13. Spectral data match literature reports.



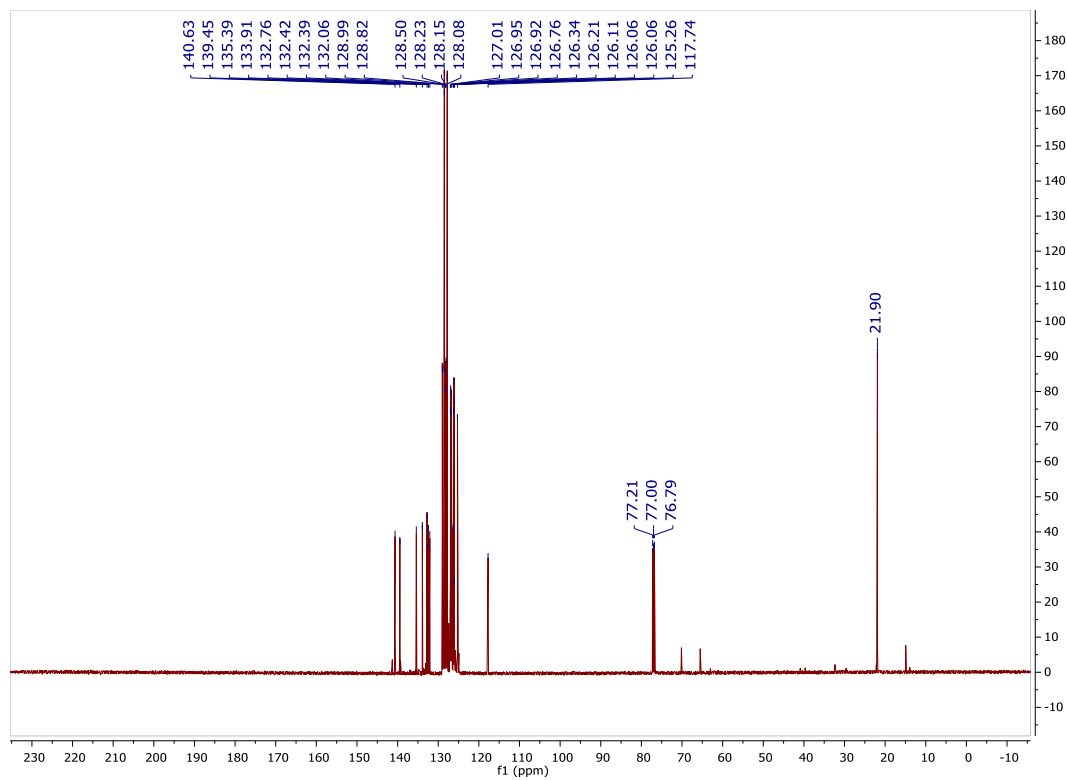
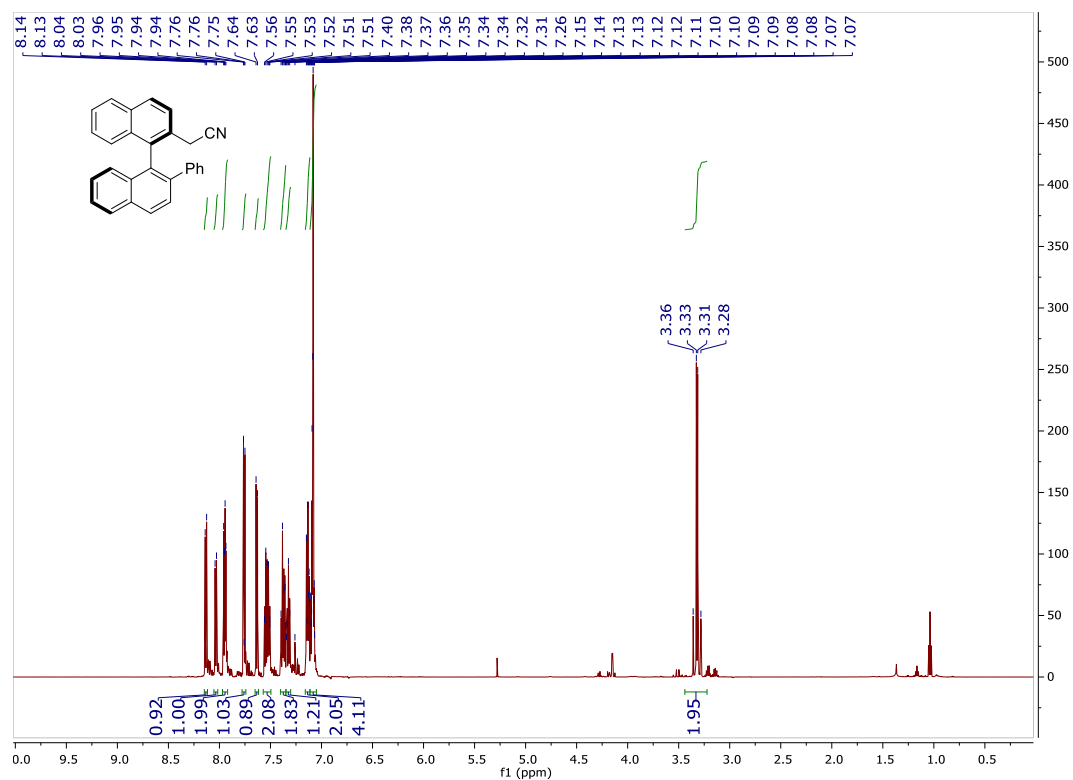


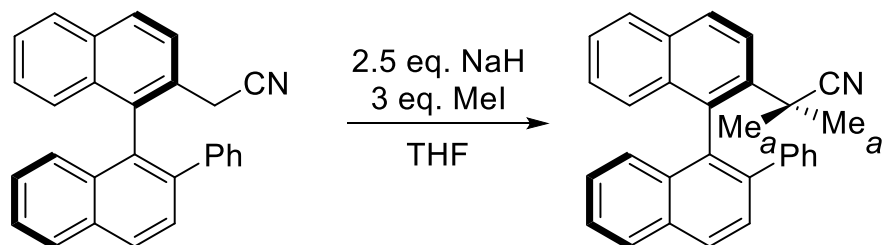


### 2-(2'-phenyl-[1,1'-binaphthalen]-2-yl)acetonitrile (4.137)

2-(bromomethyl)-2'-phenyl-1,1'-binaphthalene (930 mg, 2.2 mmol) was dissolved in hot ethanol (50 mL). To the heated solution was added KCN (430 mg, 6.6 mmol, 3 eq.) in 2 mL H<sub>2</sub>O dropwise. The suspension was held at reflux for 19 h, during which time a homogenous light-yellow solution was formed. The reaction was

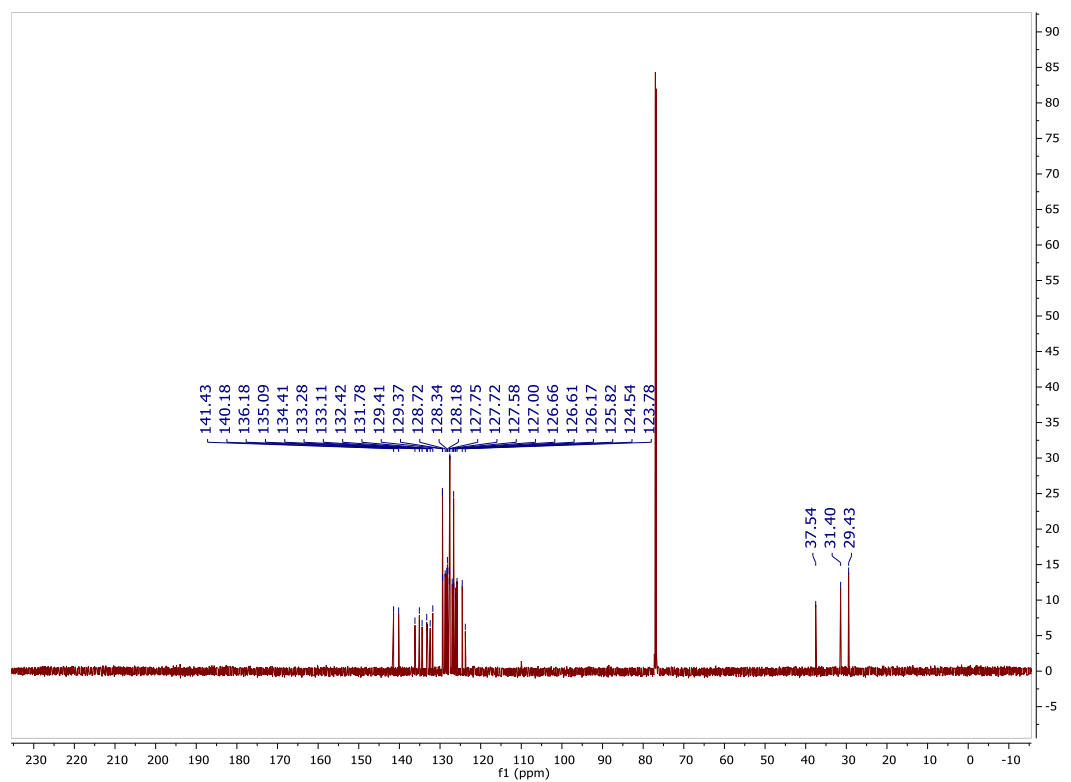
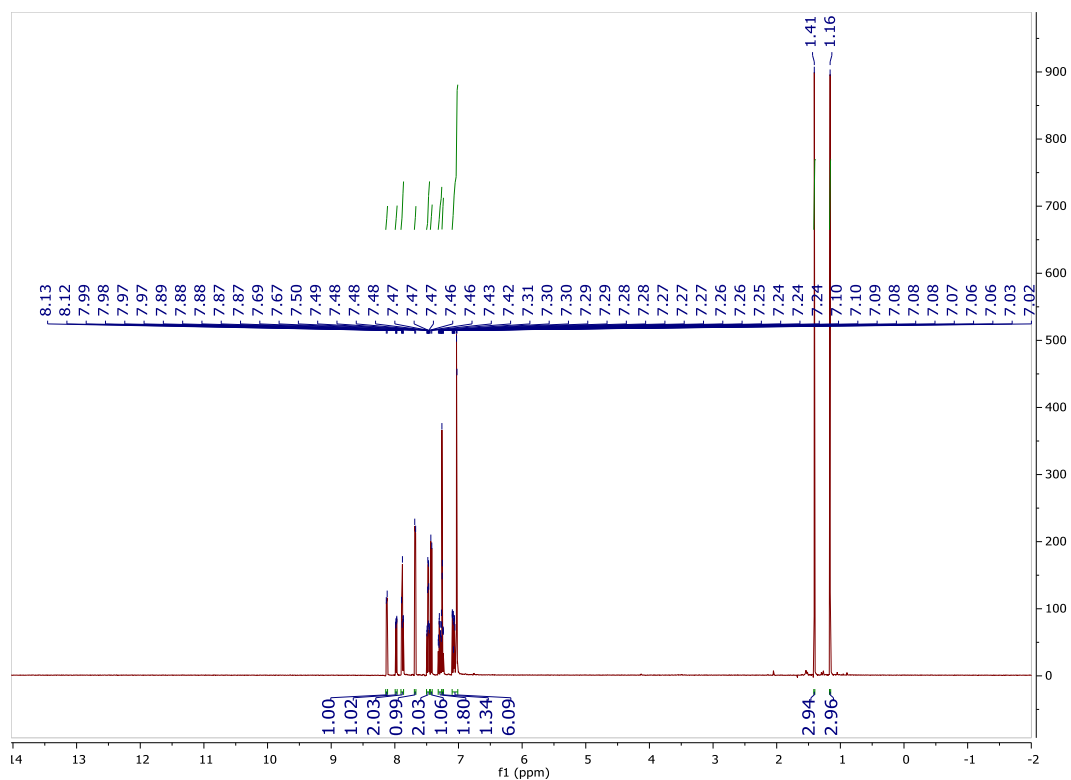
cooled to room temperature and diluted by slow addition of an equal volume of H<sub>2</sub>O. The white solid which formed was filtered, washed with H<sub>2</sub>O, and dissolved in DCM. The product containing solution was dried over Na<sub>2</sub>SO<sub>4</sub> and concentrated to give product as a white solid (749.3 mg, 2.0 mmol, 92%). <sup>1</sup>H NMR (600 MHz, CDCl<sub>3</sub>) δ 8.13 (d, *J* = 8.4 Hz, 1H), 8.04 (d, *J* = 8.2 Hz, 1H), 7.95 (dd, *J* = 8.4, 5.1 Hz, 2H), 7.76 (d, *J* = 8.5 Hz, 1H), 7.63 (d, *J* = 8.6 Hz, 1H), 7.53 (dt, *J* = 15.0, 7.5 Hz, 2H), 7.40 – 7.35 (m, 2H), 7.35 – 7.30 (m, 1H), 7.16 – 7.11 (m, 2H), 7.11 – 7.05 (m, 4H), 3.44 – 3.22 (H<sub>a</sub>, m, 2H). <sup>13</sup>C NMR (151 MHz, CDCl<sub>3</sub>) δ 140.63, 139.45, 135.39, 133.91, 132.76, 132.42, 132.39, 132.06, 128.99, 128.82, 128.50, 128.50, 128.23, 128.15, 128.08, 127.79, 127.01, 126.95, 126.92, 126.76, 126.34, 126.21, 126.11, 126.06, 126.06, 125.26, 117.74, 21.90. IR: 3055 (w), 1593 (w), 813 (s), 761 (s), 700 (s). Optical Rotation (0.5% w/v, CHCl<sub>3</sub>): 101.98°. HRMS, calc'd for C<sub>28</sub>H<sub>19</sub>N: 370.1596, found: 370.1587.

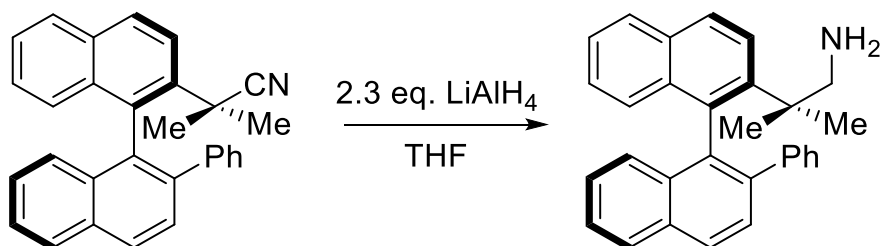




### 2-methyl-2-(2'-phenyl-[1,1'-binaphthalen]-2-yl)propanenitrile (4.138)

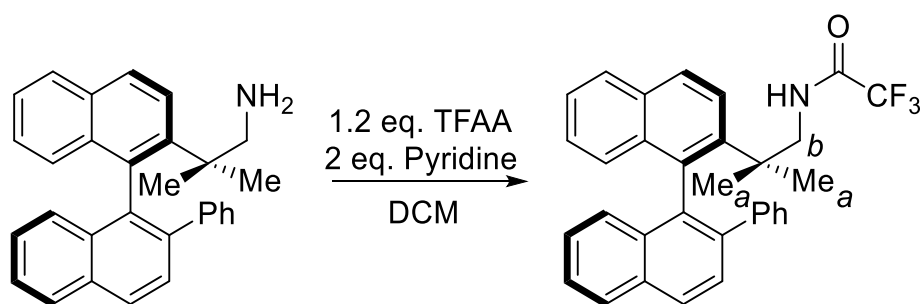
Chiral acetonitrile (1.59 g, 4.3 mmol) was dissolved in THF (30 mL). NaH (60% in mineral oil, 430 mg, 10.8 mmol, 2.5 eq.) was added forming a bright red suspension. The reaction mixture was heated to reflux, and methyl iodide (0.8 mL, 13 mmol, 3 eq.) was added dropwise. The mixture was refluxed overnight, cooled to room temperature, and quenched with 10 mL sat.  $\text{NH}_4\text{Cl}$ . The crude mixture was diluted with an equal volume of EtOAc. The layers were separated, washed with brine, and dried over  $\text{Na}_2\text{SO}_4$ . The crude mixture was adsorbed onto silica and purified on silica column (gradient, hexanes to 10% EtOAc/hexanes). Product was obtained as a white foam (1.5368 g, 3.87 mmol, 90%).  $^1\text{H}$  NMR (600 MHz,  $\text{CDCl}_3$ )  $\delta$  8.13 (d,  $J$  = 8.4 Hz, 1H), 7.98 (dd,  $J$  = 8.3, 1.2 Hz, 1H), 7.90 – 7.86 (m, 2H), 7.68 (d,  $J$  = 8.5 Hz, 1H), 7.48 (dtd,  $J$  = 8.1, 6.7, 1.3 Hz, 2H), 7.43 (d,  $J$  = 8.9 Hz, 1H), 7.32 – 7.26 (m, 2H), 7.25 (dd,  $J$  = 8.8, 1.3 Hz, 1H), 7.10 – 7.01 (m, 6H), 1.41 ( $\text{H}_a$ , s, 3H), 1.16 ( $\text{H}_a$ , s, 3H).  $^{13}\text{C}$  NMR (151 MHz,  $\text{CDCl}_3$ )  $\delta$  141.43, 140.18, 136.18, 135.09, 134.41, 133.28, 133.11, 132.42, 131.78, 129.41, 129.37, 128.72, 128.34, 128.18, 127.75, 127.72, 127.58, 127.00, 126.66, 126.61, 126.17, 125.82, 124.54, 123.78, 37.54, 31.40, 29.43. IR: 3043 (w), 810 (s), 758 (s), 705 (s). Optical Rotation (0.5% w/v,  $\text{CHCl}_3$ ): 145.44°. HRMS, calc'd for  $\text{C}_{30}\text{H}_{24}\text{N}$ : 398.1909, found: 398.1903.





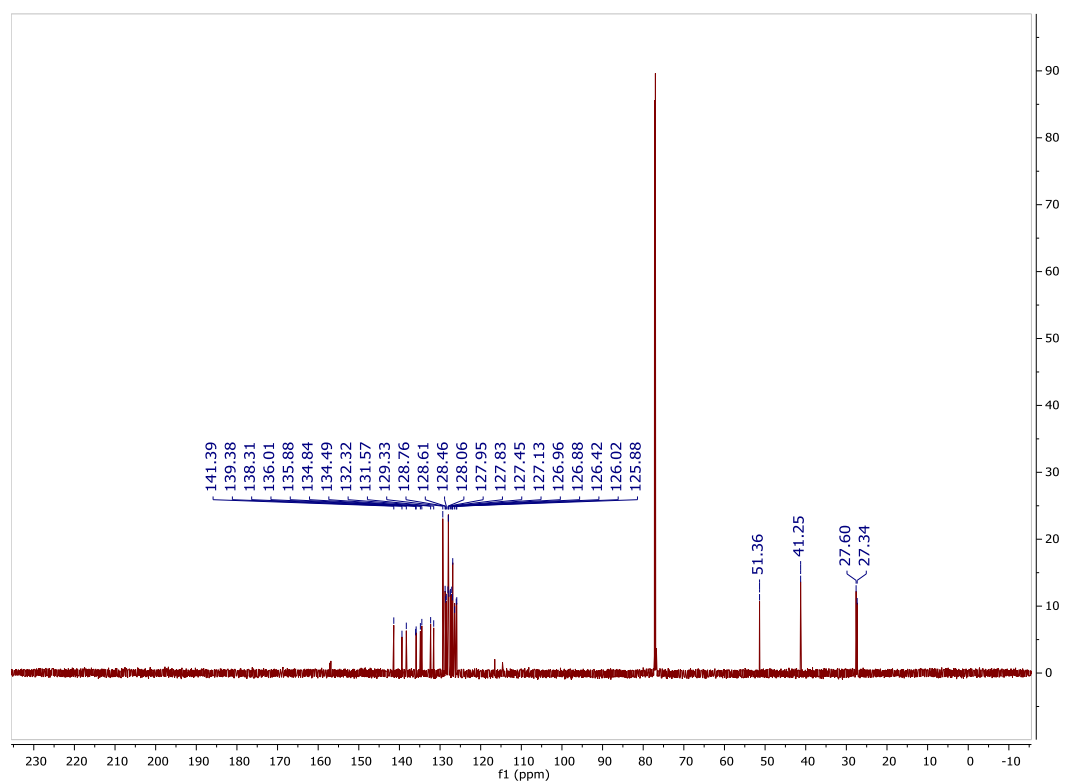
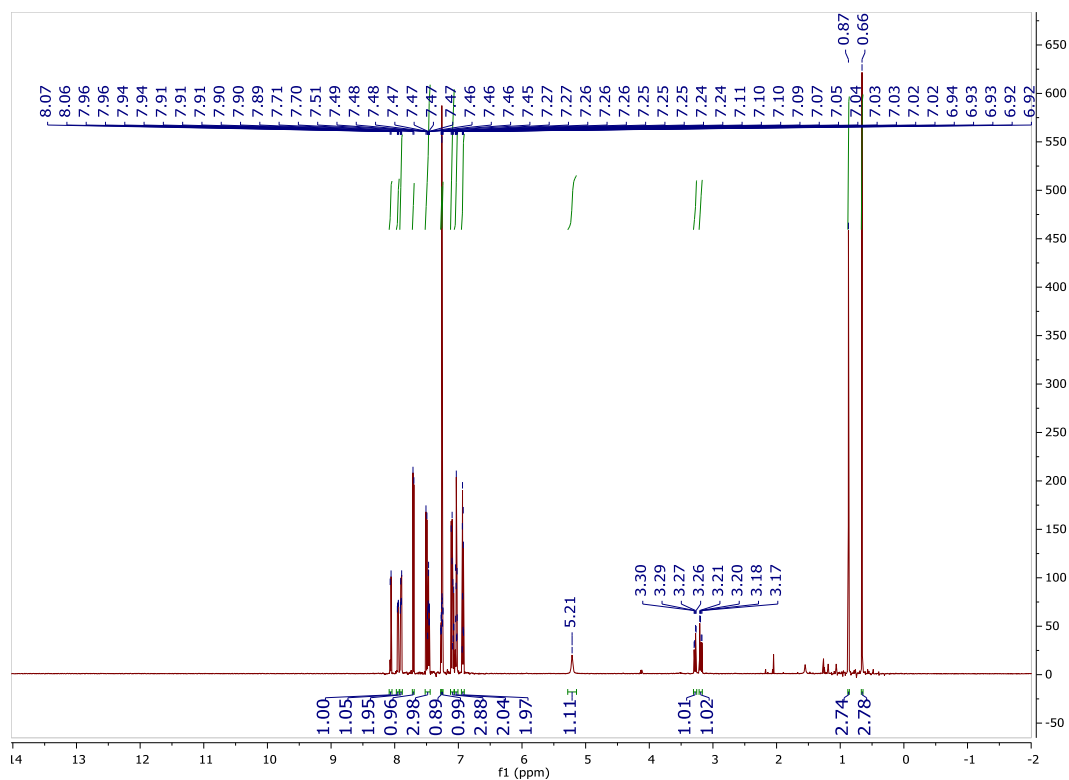
**2-methyl-2-(2'-phenyl-[1,1'-binaphthalen]-2-yl)propan-1-amine (4.139)**

Chiral acetonitrile (1.54 g, 3.87 mmol) was dissolved in THF (30 mL). LiAlH<sub>4</sub> (2.4 M in THF, 3.7 mL, 8.9 mmol, 2.3 eq.) was added dropwise forming an orange solution. The reaction was stirred at room temperature for 18 h, then cooled to 0 °C and quenched with 5 mL 10% NaOH. The suspension was filtered through celite, washed with brine, and dried over Na<sub>2</sub>SO<sub>4</sub>. The crude product was concentrated to give product as sufficiently pure material, confirmed by LCMS (1.311 g, 3.25 mmol, 84%).

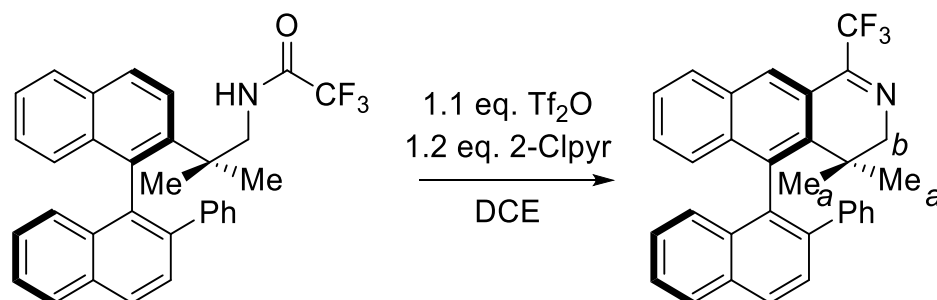


**2,2,2-trifluoro-N-(2-methyl-2-(2'-phenyl-[1,1'-binaphthalen]-2-yl)propyl)acetamide (4.140)**

Chiral amine (1.311 g, 3.25 mmol) was dissolved in DCM (35 mL) and cooled to 0 °C. Pyridine (0.53 mL, 6.6 mmol, 2 eq.) was added followed by TFAA dropwise (0.56 mL, 4.0 mmol, 1.2 eq.). The reaction was allowed to warm to room temperature overnight. After 19 h, the mixture was cooled to 0 °C and quenched with an equal volume of sat.  $\text{NH}_4\text{Cl}$ . The layers were separated, and the crude product was dried over  $\text{Na}_2\text{SO}_4$ . The crude product was adsorbed onto silica and purified by silica column (gradient, 5% to 20% EtOAc/hexanes). Product was obtained as a white foam (1.3701 g, 2.8 mmol, 85%).  $^1\text{H}$  NMR (600 MHz,  $\text{CDCl}_3$ )  $\delta$  8.06 (d,  $J$  = 8.5 Hz, 1H), 7.95 (dd,  $J$  = 8.2, 1.3 Hz, 1H), 7.92 – 7.88 (m, 2H), 7.71 (d,  $J$  = 8.5 Hz, 1H), 7.52 – 7.44 (m, 3H), 7.27 (td,  $J$  = 3.4, 1.4 Hz, 1H), 7.26 – 7.24 (m, 1H), 7.12 – 7.06 (m, 3H), 7.06 – 7.01 (m, 2H), 6.95 – 6.91 (m, 2H), 5.21 (s, 1H), 3.28 ( $\text{H}_b$ , dd,  $J$  = 13.7, 4.8 Hz, 1H), 3.19 ( $\text{H}_b$ , dd,  $J$  = 13.6, 7.6 Hz, 1H), 0.87 ( $\text{H}_a$ , s, 3H), 0.66 ( $\text{H}_a$ , s, 3H).  $^{13}\text{C}$  NMR (151 MHz,  $\text{CDCl}_3$ )  $\delta$  141.39, 139.38, 138.31, 136.01, 135.88, 134.84, 134.49, 132.32, 131.57, 129.33, 128.76, 128.61, 128.46, 128.06, 127.95, 127.83, 127.45, 127.13, 126.96, 126.88, 126.42, 126.02, 125.88, 51.36, 41.25, 27.60, 27.34. IR: 3057 (w), 1709 (s), 1153 (s), 819 (m), 764 (m), 700 (m). Optical Rotation (0.5% w/v,  $\text{CHCl}_3$ ): 180.56°. HRMS, calc'd for  $\text{C}_{32}\text{H}_{27}\text{NOF}_3$ : 498.2045, found: 498.2035.

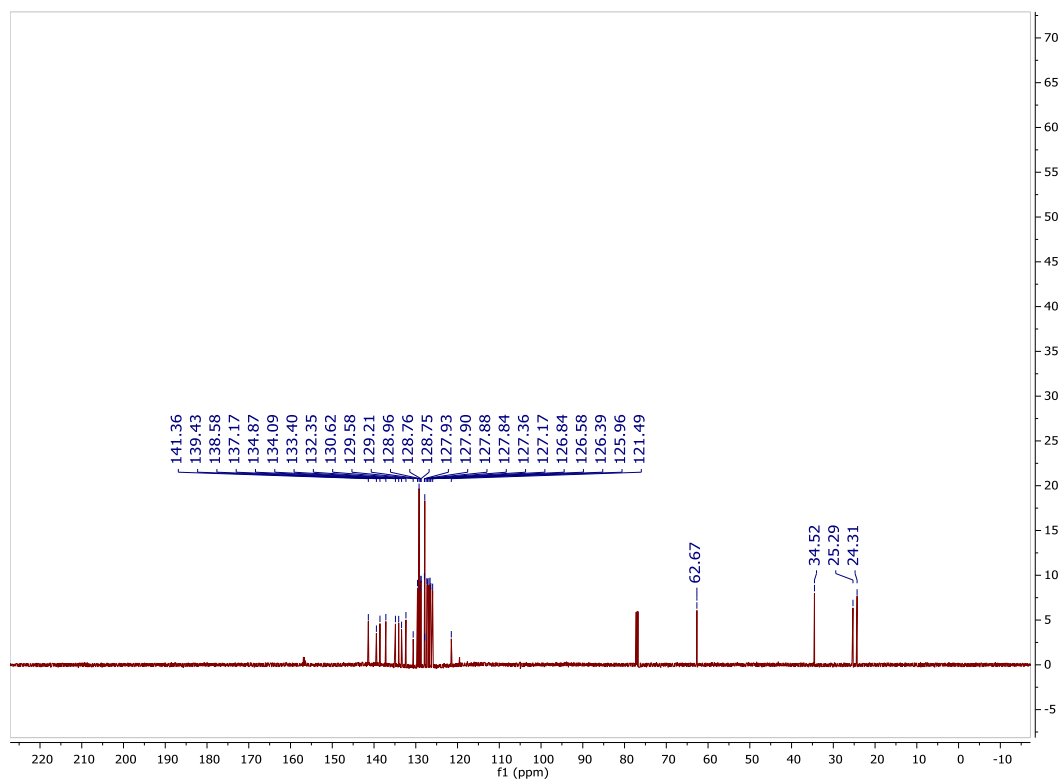
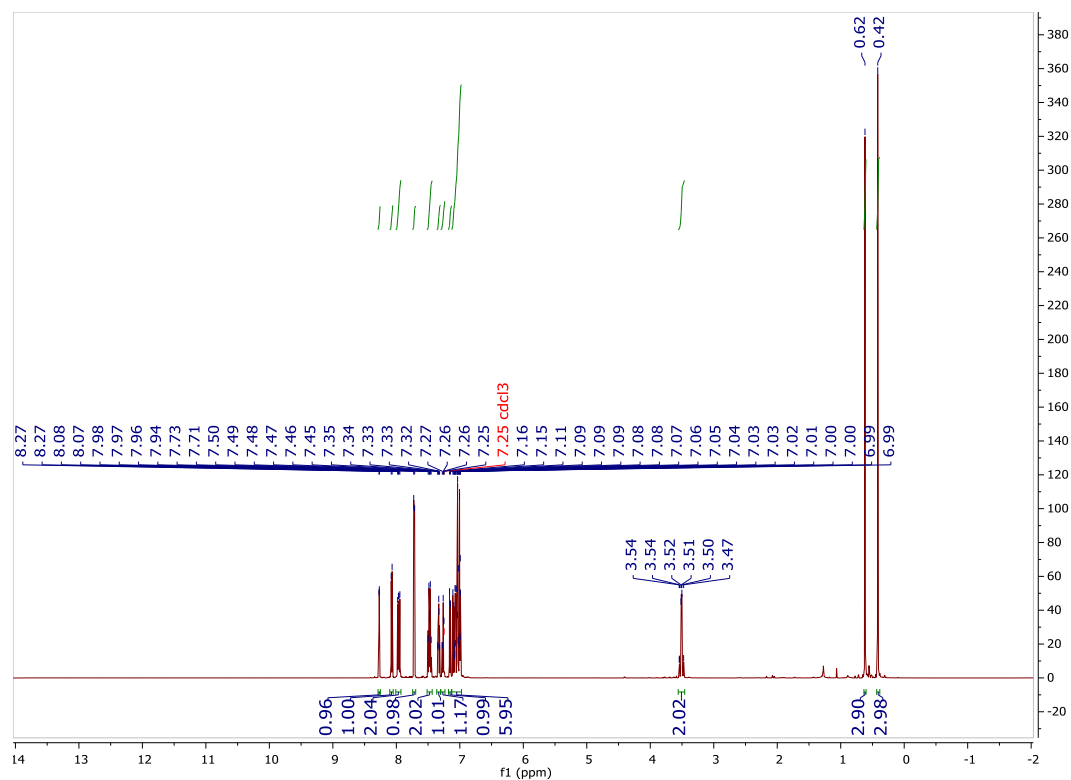


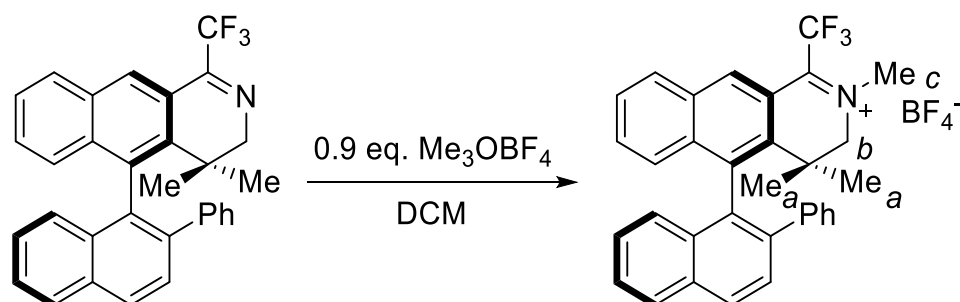




**4,4-dimethyl-5-(2-phenylnaphthalen-1-yl)-1-(trifluoromethyl)-3,4-dihydrobenzo[g]isoquinoline (4.141)**

Chiral amide (1.37 g, 2.8 mmol) was dissolved in DCE (25 mL) and cooled to  $-78^{\circ}\text{C}$ . 2-Chloropyridine (0.32 mL, 3.4 mmol, 1.2 eq.) was added followed by slow addition of  $\text{Tf}_2\text{O}$  (0.52 mL, 3.1 mmol, 1.1 eq.). The suspension was allowed to warm to room temperature overnight. After stirring at room temperature for 23 h, the mixture was heated to reflux for an additional 24 h. The now brown mixture was cooled to  $0^{\circ}\text{C}$  and quenched by slow dropwise addition of triethylamine (5 mL). The reaction mass was adsorbed directly on silica and purified on silica column (gradient, 5% to 10% EtOAc/hexanes). Product was obtained as a white foam (966 mg, 2.0 mmol, 71%).  $^1\text{H}$  NMR (598 MHz,  $\text{CDCl}_3$ )  $\delta$  8.27 (d,  $J = 1.9$  Hz, 1H), 8.07 (d,  $J = 8.6$  Hz, 1H), 7.96 (dd,  $J = 13.0, 8.1$  Hz, 2H), 7.72 (d,  $J = 8.5$  Hz, 1H), 7.52 – 7.44 (m, 2H), 7.36 – 7.30 (m, 1H), 7.26 (t,  $J = 7.4$  Hz, 1H), 7.15 (d,  $J = 8.7$  Hz, 1H), 7.13 – 6.97 (m, 6H), 3.56 – 3.46 ( $\text{H}_b$ , m, 2H), 0.62 ( $\text{H}_a$ , s, 3H), 0.42 ( $\text{H}_a$ , s, 3H).  $^{13}\text{C}$  NMR (150 MHz,  $\text{CDCl}_3$ )  $\delta$  141.36, 139.43, 138.58, 137.17, 134.87, 134.09, 133.40, 132.35, 130.62, 129.58, 129.21, 128.96, 128.76, 128.75, 127.93, 127.90, 127.88, 127.84, 127.36, 127.17, 126.84, 126.58, 126.39, 125.96, 121.49, 62.67, 34.52, 25.29, 24.31. IR: 3057 (w), 2930 (w), 1647 (m), 1184 (m), 1123 (s), 748 (s), 700 (s). Optical Rotation (0.5% w/v,  $\text{CHCl}_3$ ):  $160.80^{\circ}$ . HRMS, calc'd for  $\text{C}_{32}\text{H}_{25}\text{NF}_3$ : 480.1939, found: 480.1932.

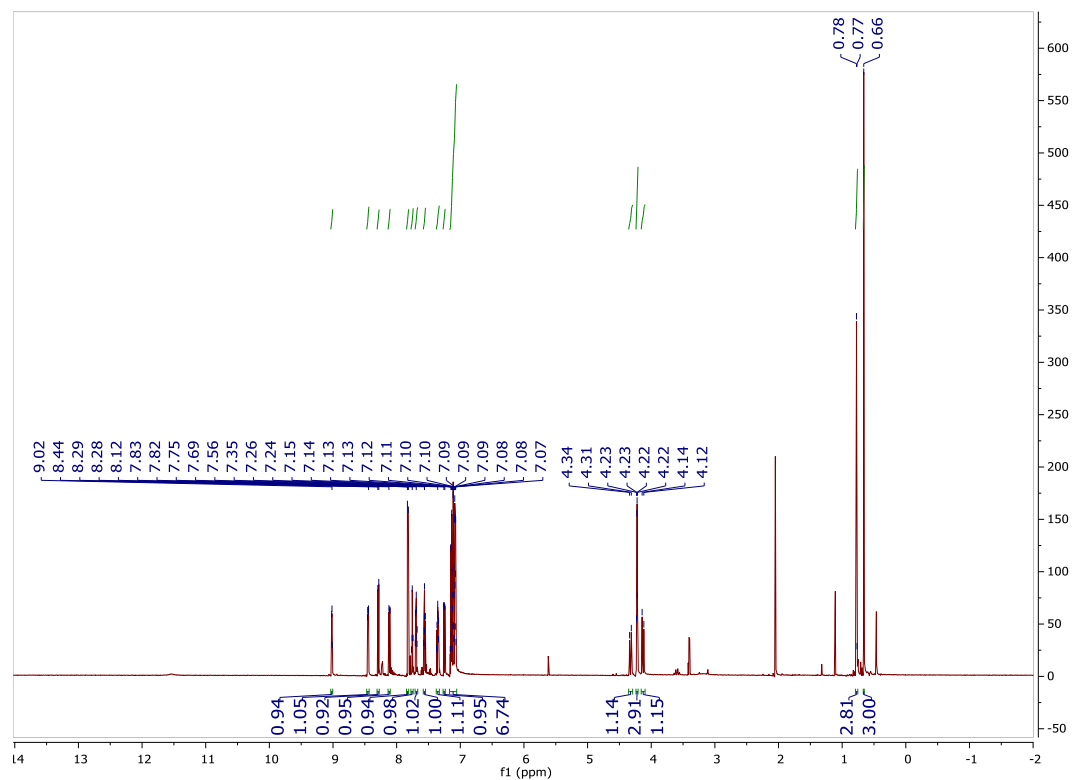


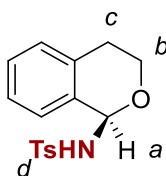
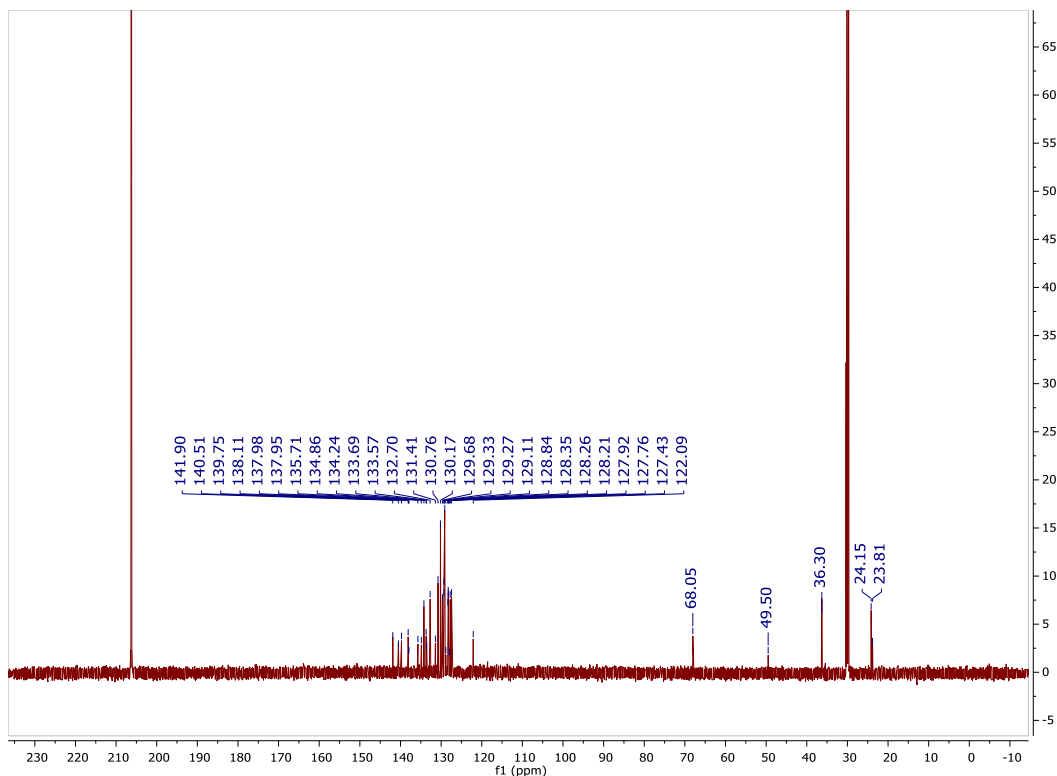


**2,4,4-trimethyl-5-(2-phenylnaphthalen-1-yl)-1-(trifluoromethyl)-3,4-dihydrobenzo[*g*]isoquinolin-2-ium tetrafluoroborate (4.130)**

Chiral imine **5** (966 mg, 2 mmol) was dissolved in DCM (5 mL). Trimethyloxonium tetrafluoroborate (266 mg, 1.8 mmol, 0.9 eq) was added, and the reaction was stirred for 20 h. The reaction was concentrated to a brown oil. Sonication in diethyl ether and decantation of the organic layer gave the desired product as a bright yellow solid (988 mg, 1.7 mmol, 94%).  $^1\text{H}$  NMR (600 MHz, Acetone- $d_6$ )  $\delta$  9.02 (t,  $J$  = 2.6 Hz, 1H), 8.45 (dd,  $J$  = 8.2, 1.4 Hz, 1H), 8.29 (d,  $J$  = 8.6 Hz, 1H), 8.13 – 8.10 (m, 1H), 7.82 (d,  $J$  = 8.6 Hz, 1H), 7.78 – 7.74 (m, 1H), 7.69 (ddd,  $J$  = 8.5, 7.0, 1.7 Hz, 1H), 7.58 – 7.55 (m, 1H), 7.38 – 7.33 (m, 1H), 7.25 (d,  $J$  = 8.5 Hz, 1H), 7.17 – 7.06 (m, 7H), 4.33 ( $\text{H}_b$ , d,  $J$  = 16.4 Hz, 1H), 4.22 ( $\text{H}_c$ , q,  $J$  = 2.7 Hz, 3H), 4.13 ( $\text{H}_b$ , d,  $J$  = 16.2 Hz, 1H), 0.78 ( $\text{H}_a$ , s, 3H), 0.66 ( $\text{H}_a$ , s, 3H).  $^{13}\text{C}$  NMR (151 MHz, Acetone- $d_6$ )  $\delta$  141.90, 140.51, 139.75, 138.11, 137.98, 137.95, 135.71, 134.86, 134.24, 133.69, 133.57, 132.70, 131.41, 130.76, 130.17, 129.68, 129.33, 129.27, 129.11, 128.84, 128.35, 128.26, 128.21, 127.92, 127.76, 127.43, 122.09, 68.05, 49.50, 36.30, 24.15, 23.81. IR: 3059 (w), 1621 (m), 1265 (m), 1180 (m), 1063 (s), 731 (s),

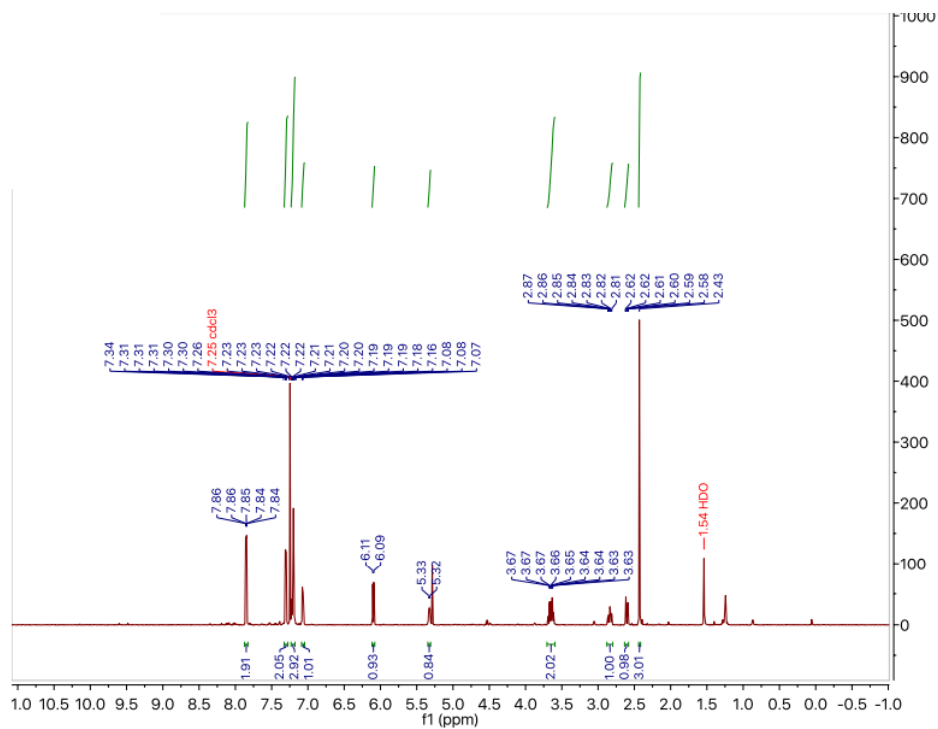
700 (s). Optical Rotation (0.5% w/v,  $\text{CHCl}_3$ ):  $254.8^\circ$ . HRMS, calc'd for  $\text{C}_{33}\text{H}_{27}\text{F}_3\text{N}$ : 494.2096, found: 494.2092.

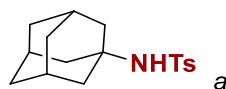
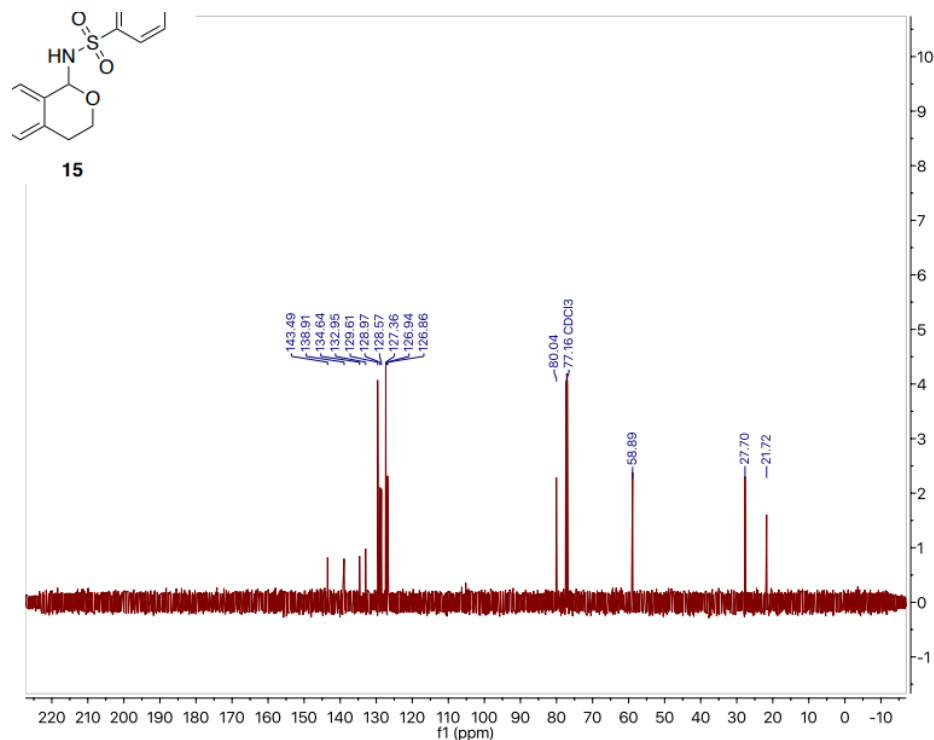




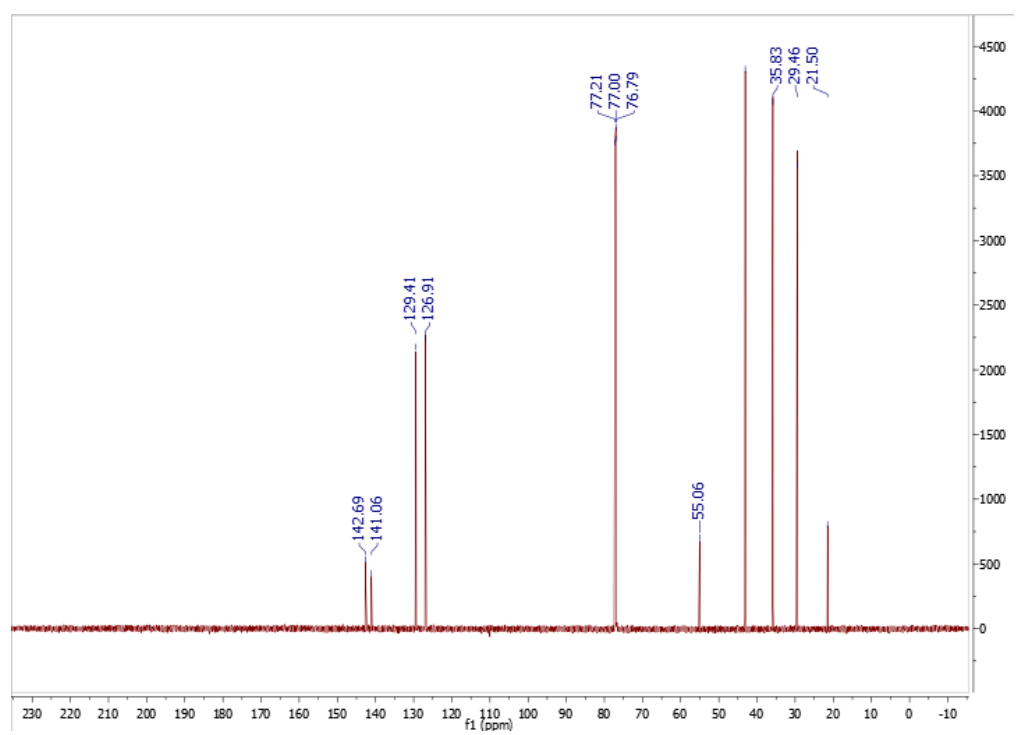
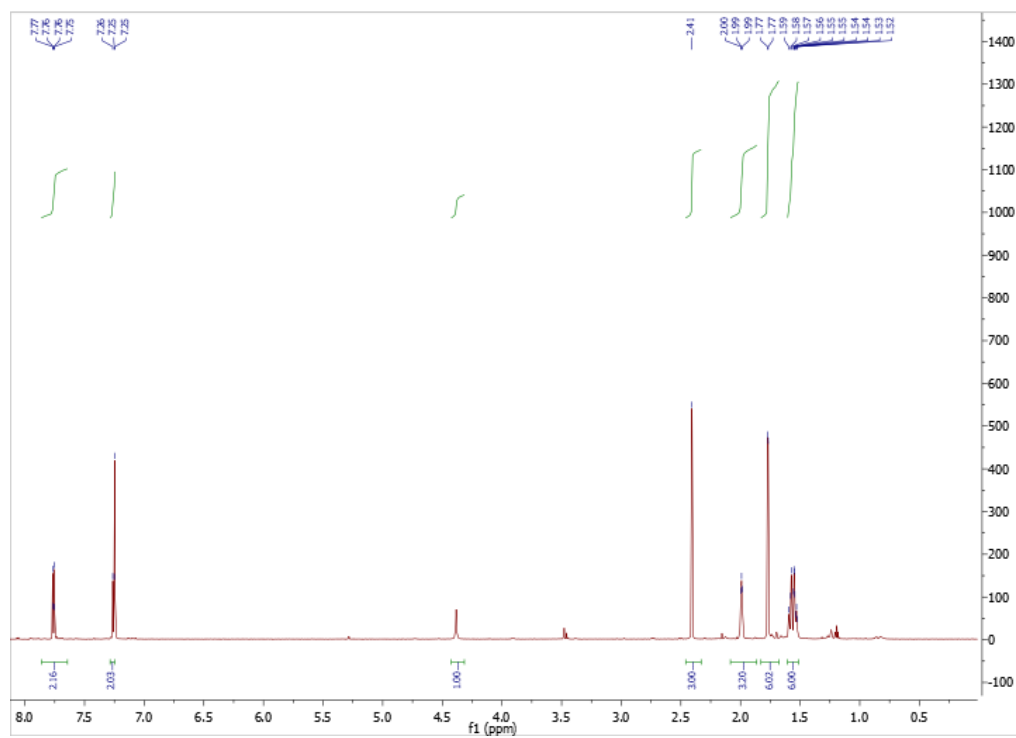
**N-(isochroman-1-yl)-4-methylbenzenesulfonamide (4.144)** Isochroman (63  $\mu$ L, 0.5 mmol) was aminated using the general procedure and purified by chromatography (silica gel, 10% to 20% EtOAc/hexanes) to give product (33.4 mg, 0.11 mmol, 22%).  $^1\text{H}$  NMR (600 MHz,  $\text{CDCl}_3$ )  $\delta$  7.85 (d,  $J$  = 8.3 Hz, 2H), 7.31 (d,  $J$  = 8.0 Hz, 2H), 7.24 – 7.18 (m, 3H), 7.08 (d,  $J$  = 7.2 Hz, 1H), 6.10 (d,  $J$  = 8.6 Hz, 1H), 5.41 ( $\text{H}_a$ , d,  $J$  = 8.6 Hz, 1H), 3.71 – 3.59 ( $\text{H}_b$ , m, 2H), 2.85 ( $\text{H}_c$ , ddd,  $J$  = 15.9, 9.7, 5.7 Hz, 1H), 2.61 ( $\text{H}_c$ , dt,  $J$  = 16.6, 3.8 Hz, 1H), 2.44 ( $\text{H}_d$ , s, 3H) ppm.  $^{13}\text{C}$  NMR (150 MHz,  $\text{CDCl}_3$ )  $\delta$  143.34, 138.73, 134.47, 132.77, 129.45, 128.80,

128.41, 127.19, 126.71, 126.44, 79.87, 58.73, 27.53, 21.55 ppm. NMR spectra are consistent with literature reports.<sup>15</sup>

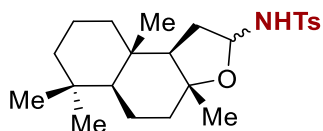




**N-(adamantan-1-yl)-4-methylbenzenesulfonamide (4.145)** Adamantane (68 mg, 0.5 mmol) was aminated using the general procedure and purified by chromatography (silica gel, 10% to 20% EtOAc/hexanes) to give product (57 mg, 0.19 mmol, 37%).  $^1\text{H}$  NMR (600 MHz,  $\text{CDCl}_3$ )  $\delta$  7.76 (d,  $J$  = 8.3 Hz, 2H), 7.26 (d,  $J$  = 8.3 Hz, 2H), 4.38 (s, 1H), 2.41 ( $\text{H}_a$ , s, 3H), 2.02 – 1.96 (m, 3H), 1.77 (d,  $J$  = 2.9 Hz, 6H), 1.60 – 1.53 (m, 6H) ppm.  $^{13}\text{C}$  NMR (150 MHz,  $\text{CDCl}_3$ )  $\delta$  142.68, 141.05, 129.39, 126.89, 55.05, 43.06, 35.82, 29.45, 21.48 ppm. NMR spectra are consistent with literature reports.<sup>15</sup>

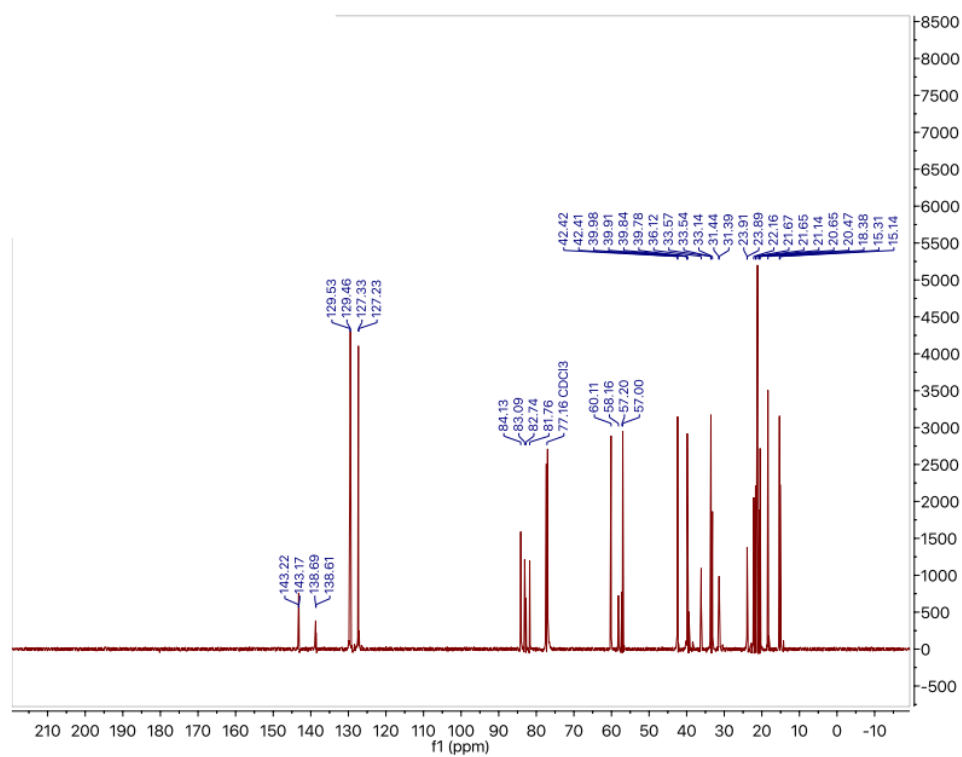


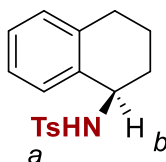




**4-methyl-N-((3aR,5aS,9aS,9bR)-3a,6,6,9a-tetramethyldodecahydronaphtho[2,1-b]furan-2-yl)benzenesulfonamide**

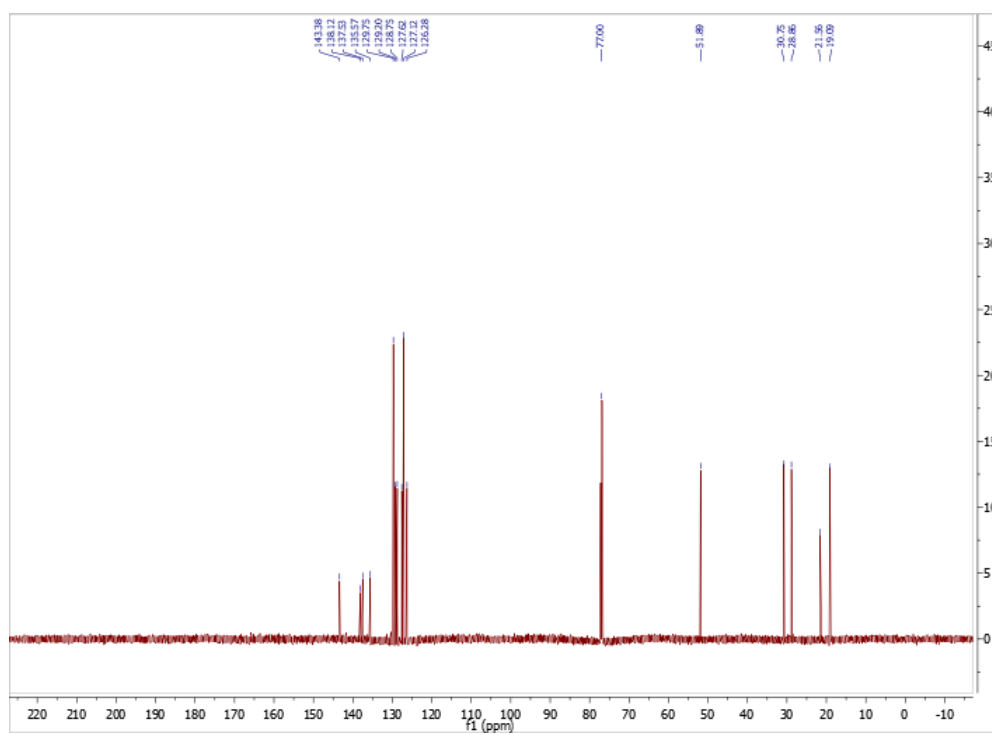
**(4.146)** Ambroxide (118mg, 0.5 mmol) was aminated using the general procedure and purified by chromatography (silica gel, 10% to 20% EtOAc/hexanes) to give product (32.4 mg, 0.08 mmol, 16%).  $^1\text{H}$  NMR (600 MHz,  $\text{CDCl}_3$ )  $\delta$  7.79 (d,  $J$  = 8.3 Hz, 2H), 7.26 (d,  $J$  = 7.8 Hz, 2H), 5.31 – 5.24 (m, 1H), 5.19 (d,  $J$  = 9.4 Hz, 1H), 2.41 (s, 3H), 1.76 (dt,  $J$  = 11.7, 3.2 Hz, 1H), 1.72 – 1.51 (m, 3H), 1.45 – 1.35 (m, 3H), 1.32 – 1.09 (m, 4H), 1.01 (s, 3H), 0.98 – 0.85 (m, 3H), 0.83 (s, 3H), 0.78 (s, 3H) ppm.  $^{13}\text{C}$  NMR (201 MHz,  $\text{CDCl}_3$ )  $\delta$  143.22, 143.17, 138.69, 138.61, 129.53, 129.46, 127.33, 127.23, 84.13, 83.09, 82.74, 81.76, 77.16, 60.11, 58.16, 57.20, 57.00, 42.42, 42.41, 39.98, 39.91, 39.84, 39.78, 36.12, 33.57, 33.54, 33.14, 31.44, 31.39, 23.91, 23.89, 22.16, 21.67, 21.65, 21.14, 20.65, 20.47, 18.38, 15.31, 15.14 ppm. NMR spectra are consistent with literature reports.<sup>15</sup>





**4-methyl-N-(1,2,3,4-tetrahydronaphthalen-1-yl)benzenesulfonamide (4.90)**

Tetralin (66 mg, 0.5 mmol) was aminated using the general procedure and purified by chromatography (silica gel, 10% to 20% EtOAc/hexanes) to give product (24 mg, 0.08 mmol, 16%).  $^1\text{H}$  NMR (600 MHz,  $\text{CDCl}_3$ )  $\delta$  7.83 (d,  $J$  = 7.9 Hz, 2H), 7.35 (d,  $J$  = 7.9 Hz, 2H), 7.14 (t,  $J$  = 7.4 Hz, 1H), 7.08 – 7.01 (m, 2H), 6.94 (d,  $J$  = 7.7 Hz, 1H), 4.62 (d,  $J$  = 7.8 Hz, 1H), 4.45 ( $\text{H}_b$ , q,  $J$  = 5.7 Hz, 1H), 2.78 – 2.73 (m, 1H), 2.70 – 2.63 (m, 1H), 2.46 (s, 1H), 1.87 – 1.79 (m, 3H), 1.77 – 1.68 (m, 1H) ppm.  $^{13}\text{C}$  NMR (150 MHz,  $\text{CDCl}_3$ )  $\delta$  143.38, 138.12, 137.53, 135.57, 129.75, 129.20, 128.75, 127.62, 127.12, 126.28, 51.89, 30.75, 28.86, 21.56, 19.09 ppm. NMR spectra are consistent with literature reports.<sup>15</sup>



## 4.9 References

1. DesMarteau, D. D.; Montanari, V.; Petrov, V.; Donadelli, A.; Resnati, G.; *J. Am. Chem. Soc.*, **1993**, *115*, 4897-4898.
2. Arnone, A.; Cavicchioli, M.; Montanari, V.; Resnati, G.; *J. Org. Chem.*, **1994**, *59*, 5511-5513. Arnone, A.; Foletto, S.; Metrangolo, P.; Resnati, G.; *Org. Lett.*, **1999**, *1*, 281-284.
3. Brodsky, B. H.; Du Bois, J.; *J. Am. Chem. Soc.*, **2005**, *127*, 15391-15393. Litvinas, N.; Brodsky, B.; Du Bois, J.; *Angew. Chem. Int. Ed.*; **2009**, *48*, 4513-4516. Adams, A.; Du Bois, J.; *Chem. Sci.*, **2014**, *5*, 656-659.
4. For reviews of oxaziridinium chemistry, see: Xia, Q. H.; Ge, H. Q.; Ye, C. P.; Liu, Z. M.; Su, K. X.; *Chem. Rev.*, **2005**, *105*, 1603-1662. Wong, O. A.; Shi, Y.; *Chem. Rev.*, **2008**, *108*, 3958-3987. Zhu, Y.; Wang, Q.; Cornwall, R.; Shi, Y.; *Chem. Rev.*, **2014**, *114*, 8199-8256.
5. Hanquet, G.; Lusinch, X.; *Tetrahedron*, **1994**, *50*, 12185-12200.
6. Chen, M. S.; White, M. C.; *Science*, **2007**, *318*, 783-787.
7. Murray, R.; Jeyaraman, R.; *J. Org. Chem.*, **1985**, *50*, 2847-2853.
8. Biscoe, M. R.; Breslow, R.; *J. Am. Chem. Soc.*, **2005**, *127*, 10812-10813.
9. Breslow, R.; *Acc. Chem. Res.*, **1991**, *24*, 159-164.
10. Fung, Y.; Yan, S.; Wong, M.; *Org. Biomol. Chem.*, **2012**, *10*, 3122-3130.

11. Jeffrey, J. L.; Terrett, J. A.; MacMillan, D. W. C.; *Science*, **2015**, *349*, 1532-1536.
12. Dantignana, V.; Milan, M.; Cusso, O.; Company, A.; Bietti, M.; Costas, M.; *ACS Cent. Sci.*, **2017**, *3*, 1350-1358.
13. Wong, M. K.; Ho, L. M.; Zheng, Y. S.; Ho, C. Y.; Yang, D.; *Org. Lett.*, **2001**, *3*, 2587-2590.
14. M. F. A., Adamo; Aggarwal, V. K.; Sage, M. A.; *J. Am. Chem. Soc.*, **2000**, *122*, 8317-8318. M. F. A., Adamo; Aggarwal, V. K.; Sage, M. A.; *J. Am. Chem. Soc.*, **2002**, *124*, 11223-11223.
15. Bohe, L.; Hanquet, G.; Lusinchi, M.; Lusinchi, X.; *Tetrahedron Letters*, **1993**, *34*, 7271-7274.
16. For reviews: Wong, O. A.; Shi, Y.; *Chem. Rev.*, **2008**, *108*, 3958-3987. Zhu, Y.; Wang, Q.; Cornwall, R. G.; Shi, Y.; *Chem. Rev.*, **2014**, *114*, 8199-8256.
17. Bohé, L.; Lusinchi, M.; Lusinchi, X.; *Tetrahedron*, **1999**, *55*, 141-154.
18. Hanquet, G.; Lusinchi, X.; Milliet, P.; *Tet. Lett.*, **1987**, *28*, 6061-6064.
19. Page, P. C. B.; Rassias, G. A.; Bethell, D.; Schilling, M. B.; *J. Org. Chem.*, **1998**, *63*, 2774-2777.

20. Bulman Page, P. C.; Rassias, G. A.; Barros, D.; Bethell, D.; Schilling, M. B.; *J. Chem. Soc., Perk. Trans. 1*, **2000**, 2, 3325–3334.
21. Bulman Page, P. C.; Chan, Y.; Liddle, J.; Elsegood, M. R. J.; *Tetrahedron*, **2014**, 70, 7283–7305.
22. Bulman Page, P. C.; Buckley, B. R.; Barros, D.; Blacker, A. J.; Heaney, H.; Marples, B. A.; *Tetrahedron*, **2006**, 62, 6607–6613.
23. Page, P. C. B.; Buckley, B. R.; Heaney, H.; Blacker, A. J.; *Org. Lett.*, **2005**, 7, 375–377.
24. Bulman Page, P. C.; Buckley, B. R.; Rassias, G. A.; Blacker, A. J.; *Eur. J. Org. Chem.*, **2006**, 803–813.
25. Bulman Page, P. C.; Appleby, L. F.; Chan, Y.; Day, D. P.; Buckley, B. R.; Slawin, A. M. Z.; McKenzie, M. J.; *J. of Org. Chem.*, **2013**, 78(16), 8074–8082.
26. Aggarwal, V. K.; Wang, M. F.; *Chem. Commun.*, **1996**, 191–192.
27. Page, P. C. B.; Buckley, B. R.; Barros, D.; Blacker, A. J.; Marples, B. A.; Elsegood, M. R. J.; *Tetrahedron*, **2007**, 63, 5386–5393.
28. Novikov, R.; Bernardinelli, G.; Lacour, J.; *Adv. Synth. Cat.*, **2008**, 350(7–8), 1113–1124.

29. Bulman Page, P. C.; Bartlett, C. J.; Chan, Y.; Allin, S. M.; McKenzie, M. J.; Lacour, J.; Jones, G. A.; *Organic and Biomolecular Chemistry*, **2016**, *14*, 4220–4232.
30. Bulman Page, P. C.; Parker, P.; Rassias, G. A.; Buckley, B. R.; Bethell, D.; *Adv. Synth. Cat.*, **2008**, *350*(11–12), 1867–1874.
31. Page, P. C. B.; Parker, P.; Buckley, B. R.; Rassias, G. A.; Bethell, D.; *Tetrahedron*, **2009**, *65*, 2910–2915.
32. Washington, I.; Houk, K. N.; Armstrong, A.; *J. Org. Chem.*, **2003**, *68*, 6497–6501.
33. Visco, M. D.; Wieting, J. M.; Mattson, A. E.; *Org. Lett.*, **2016**, *18*, 2883–2885.
34. For an overview, see: Du Bois, J.; *Org. Process Res. Dev.*, **2011**, *15*, 758–762.
35. Saito, T.; Nishimoto, Y.; Yasuda, M.; Baba, A.; *J. Org. Chem.*, **2007**, *72*, 8588–8590.
36. Nishimoto, Y.; Yasuda, M.; Baba, A.; *Org. Lett.*, **2007**, *9*, 4931–4934.
37. Leggans, E. K.; Barker, T. J.; Duncan, K. K.; Boger, D. L.; *Org. Lett.*, **2012**, *14*, 1428–1431.
38. Hashimoto, T.; Hirose, D.; Taniguchi, T.; *Angew. Chem. Int. Ed.*, **2014**, *53*, 2730–2734.



39. Mori, K. and Senda, S.; *Tetrahedron*, **1985**, *41*, 541-546.
40. Combee, L. A.; Raya, B.; Wang, D.; Hilinski, M. K.; *Chem. Sci.*, **2018**, *9*, 935-939.